Liliana Raquel Simões Marques

TAPERED STEEL MEMBERS:
FLEXURAL AND LATERAL-TORSIONAL BUCKLING

Dissertação apresentada para o grau de Doutor
na Especialidade de Construção Metálica e Mista

2012

· U C ·

UNIVERSIDADE DE COIMBRA

Tapered steel members:
Flexural and lateral-torsional buckling

Dissertação científica na especialidade de Construção Metálica e Mista

Autor
Liliana Raquel Simões Marques

Orientador
Prof. Doutor Luís Alberto Proença Simões da Silva

Co-orientador
Prof. Richard Greiner

ISISE, Departamento de Engenharia Civil – Universidade de Coimbra
Colaboração institucional da Fundação para a Ciência e Tecnologia

Coimbra, 2012

RESUMO

Elementos de secção variável em aço são geralmente utilizados devido à sua eficiência estrutural relativamente a elementos prismáticos, uma vez que a utilização de cada secção é optimizada.

O EC3 – parte 1-1 (CEN, 2005) fornece várias metodologias para a verificação de elementos e pórticos. Relativamente a elementos não uniformes, i.e., com secção variável, distribuição irregular de contraventamentos, eixo não recto, etc, surgem diversas dificuldades não existindo orientações para as contornar. Assim, a verificação acaba por não tirar partido das vantagens associadas a estes elementos, tornando-se conservativa. Neste trabalho de investigação analisam-se as metodologias de verificação para elementos de secção variável.

Hoje em dia, o projectista possui ferramentas numéricas sofisticadas que lhe permitem estudar a estrutura como um todo, de um modo seguro e fiável. No entanto, não existe ainda orientação suficiente para proceder à verificação de estruturas através desta via.

Assim, a verificação da estabilidade é geralmente feita através de fórmulas existentes nos regulamentos. O EC3-1-1 apresenta um conjunto de fórmulas para verificação da estabilidade de colunas, vigas e vigas-coluna. No entanto, a aplicabilidade das mesmas abrange apenas os casos mais simples: elementos simplesmente apoiados; com contraventamentos intermédios simétricos e regulares; ou secções duplamente simétricas e não variáveis.

Assim, o EC3-1-1 inclui um método geral para verificação da encurvadura por flexão e da encurvadura lateral, especificamente desenvolvido para verificar estruturas que se encontram fora do âmbito das equações de interacção, nomeadamente elementos de secção variável. No entanto, a aplicação directa das imperfeições codificadas para elementos prismáticos, além de ser mecanicamente inconsistente, conduz a uma verificação que poderá ser demasiado segura para alguns casos ou insegura para outros casos.

Pelas razões mencionadas e porque elementos não uniformes em aço conduzem a soluções estruturais competitivas, esta dissertação tem como principal objectivo desenvolver novas regras de estabilidade para a verificação da encurvadura por flexão e lateral de elementos de alma variável, na qual o fenómeno de instabilidade é considerado através de um factor de imperfeição adequado. Pretendeu-se atingir simplicidade de aplicação e ao mesmo tempo transparência mecânica. Finalmente, as propostas são consistentes com as actuais regras existentes para elementos prismáticos, contribuindo assim para a harmonização das regras de verificação da estabilidade de elementos do Eurocódigo 3.

Palavras-Chave

Aço | Eurocódigo 3 | Secção variável | Verificação da estabilidade | Elementos não uniformes

ABSTRACT

Tapered steel members are usually adopted in order to optimize the load capacity at each cross section taking into account the respective distribution of stresses.

Eurocode 3 – part 1-1 (CEN, 2005) provides several methodologies for the stability verification of members and frames. However, regarding non-uniform members in general, with tapered cross section, irregular distribution of restraints, non-linear axis, castellated, etc., several difficulties are noted. There are yet no guidelines to overcome any of these issues and, as a result, safety verification is conservative, not accounting for the advantages non-uniform members provide. This research deals with the stability design of tapered members.

The designer has nowadays sophisticated numerical tools which allow him to study any of the above-mentioned structures. However, there is not yet enough guidance to safely perform fully non-linear numerical verification.

Therefore, approaches based on structural analysis followed by design checks are usually preferred. EC3-1-1 provides a set of design formulae for member design, covering column and/or lateral-torsional buckling. However, these formulae are related to standard conditions of structural members, such as simply supported members, with double-symmetric and constant sections and with intermediate regular lateral restraints.

As a consequence, EC3-1-1 includes a general method for lateral and lateral-torsional buckling of structural components, specifically developed to verify the structures that lie outside the validation range of the interaction formulae, namely tapered members. However, considering the coded buckling curves for application of this method is not only inconsistent from a mechanical point of view but also may lead to an over-conservative or even unconservative level of resistance.

For all of the referred reasons, and because tapered steel members lead to competitive structural solutions, this dissertation focus on developing new stability rules for lateral and lateral-torsional buckling of web-tapered members in which the buckling phenomena is accounted for by a proper buckling coefficient related to realistic imperfections. The objective is to have a straight forward procedure, nevertheless with mechanical consistency. The outcomes of this research are consistent with existing rules for prismatic members and aim at contributing to the harmonization of stability member verification procedures of Eurocode 3.

Kewords

Steel | Eurocode 3 | Tapered | Stability verification | Non-uniform members

ACKNOWLEDGMENTS

During the past years I have focused on the thesis I am presenting. Yet, if I were to ask all of those who contributed to it in one or another way, a piece of paper would simply not be enough to include all the names. I hope this text can fairly express my gratitude to them.

First of all, this thesis would not have been possible to do without the support of my supervisor, Professor Luís Simões da Silva, not only professionally but also personally. His expertise in this research field gave this work a valuable output and his guidance was incalculable. From my first years as a researcher he always made sure I was going in the right direction by providing me with constructive criticism and encouraging me to believe in my own ideas.

During the last year I had the opportunity to spend some time in the city of Graz, in Austria, to develop some of my work at the Institute for Steel Structures of the Technical University of Graz where I always felt welcomed. The attention, advice and broad perception that my co-supervisor Professor Richard Greiner always provided me cannot be thanked enough.

The work in this thesis has been discussed several times in the ECCS Technical Committee 8 – Stability. To all the members of TC8, who always listened attentively to what I had to present. The advice and outcomes of these meetings and presentations helped to keep my work in the correct and meaningful path.

As for my Colleagues and Professors in the research team of Steel and Mixed Construction Technologies in Coimbra, I cannot distinguish each of them in their effort in helping me, with my work when necessary, and emotionally at other times. Also, to Cristina and Nuno for the attention and prompt help they were always willing to provide. I must say I am grateful to be working in such a team.

The harmonization and mechanical consistency of steel member design rules was a goal to achieve in this thesis. I express here my gratitude to the research team of Graz, who has a valuable past in this research field. In one of the recent works of this team Dr. Andreas Taras made his contribution to prismatic members and I hereby add my brick to tapered members and thank him for the advice he has given me during the times I spent in Graz.

Last but not least I give my attention to all the ones who are not part of my professional life but always helped me carry on, smile, and cheer up when I felt most unsure of myself. To all my friends which have accompanied me during these years and who had often to take a "raincheck", especially during the last months. I need to thank them for understanding my lack of patience and providing me with the necessary energy to keep on.

I know that the ones who suffered more from my absence were my dear family, my Mother, my Father, my Sister Inês, João and his family too.

To my father who always made sure I was well, I must thank him for everything and apologize to him for not always being there in the past months.

My little sister, Inês, for the past years has been such a nice and comforting listener. I therefore wish to offer her my loving gratitude.

To João, who genuinely cared for me, although sometimes I misinterpreted his sincere constructive criticism and support. Thank you for being there, always and no matter what.

And finally, I dedicate this to my special one, my mother. She raised me to be the person I am today and I look up to her as my ideal of a perfect mother, friend, person. Without her unconditional love I would never be writing this piece of work I am presenting today.

TABLE OF CONTENTS

6 On the Verification of tapered members and frames under axial compression and uniaxial bending

7 Conclusions and further work

NOTATIONS

Lowercases

a, A	Auxiliary terms for application of proposed formula for $N_{cr,Tap}$
a, b	Auxiliary terms for application of the design method for tapered columns
a_0, a, b, c, d	Class indexes for buckling curves according to EC3-1-1
a_γ	Auxiliary term to the taper ratio for application of LTB proposed methodology
b	Cross section width
b_{max}	Maximum cross section width
b_{min}	Minimum cross section width
c, t	Cross section dimensions for class determination acc. to EC3-1-1
e_0	Maximum amplitude of a member imperfection
$e_{0,aux}$	Amplitude of the beam at $h=h_{min}$
f	Function for the displacement
f	Modification factor for χ_{LT}
f_y	Yield stress
h	Cross section height
h_{max}	Maximum cross section height
h_{min}	Minimum cross section height
$h_{xcII,lim}$	cross section height at $x_{c,lim}^{II}$
i	Radius of gyration
i_s	Polar radius of gyration
k_c	Correction factor for moment distribution
k_{GMNIA}	Calibration factor to be applied to the results of the finite element analysis
k_{yy}, k_{zy}, k_{yz}, k_{zz}	Interaction factors dependent of the phenomena of instability and plasticity involved
$k_{yy}^{in\_pl}$	Interaction factor for in-plane instability

k_σ	Buckling factor corresponding to the stress ratio ψ and boundary conditions
m_x	Acting torque per unit length
n	Number of cases
n	Ratio of design normal force to design plastic resistance to normal forces of the gross cross section
n(x)	Distributed axial force
$n_{Ed}(x)$	Design distributed axial force
p_y, p_z	distributed loading, *y-y* direction and *z-z* direction
t_f	Flange thickness
t_f'	Flange thickness of a tapered member projected in a vertical plane
t_w	Web thickness
v, w	maximum deformation, out-of-plane and in-plane
v_0, w_0	maximum initial imperfection, out-of-plane and in-plane
$x_{c,lim}^{II}$	Second order failure cross section for a high slenderness level
$x_{c,N}^{i}$, $x_{c,M}^{i}$, $x_{c,MN}^{i}$	Denomination of the failure cross section in Chapter 6 (to differentiate from the type of loading it refers to): N – do to axial force only; M – due to bending moment only; MN – due to the combined action of bending moment and axial force
x_c^{I}	First order failure cross section
x_c^{II}	Second order failure cross section
$x_{cr,max}$	Location corresponding to the maximum deflection
x_{min}	Location corresponding to the smallest cross section
x-x	Axis along the member
y-y	Cross section axis parallel to the flanges
z-z	Cross section axis perpendicular to the flanges

Uppercases

A	Cross section area
A_c	Gross cross sectional area of the plate
$A_{c,eff}$	Effective cross sectional area of the plate

A_{eff} — Effective cross sectional area

A_{min} — Cross section area of the smallest cross section in of a tapered member

A_v — Shear area

C_1 — Equivalent uniform moment factor for critical moment determination

C_m — Equivalent moment factor according to clause 6.3.3

CoV — Coefficient of variation

E — Modulus of elasticity

FEM — Finite Element Method

G — Shear modulus

GM — General Method

GMNIA — Geometrical and Material Non-linear Analysis with Imperfections

I — 2nd moment of area

$I_{fl,z}$ — Flange inertia relatively to zz axis

I_T — Torsional constant

I_y, I_z — Second moment of area, y-y axis and z-z axis

$I_{y,eq}$ — Equivalent 2nd moment of area, y-y axis

$I_{y,max}$ — Maximum 2nd moment of area, y-y axis

$I_{y,min}$ — Minimum 2nd moment of area, y-y axis

I_{ω} — Warping constant

L — Member length

$L_{cr,z}, L_{cr,y}$ — Member buckling length regarding flexural buckling, minor and major axis

L_{LT} — Member buckling length regarding lateral-torsional buckling

F_{Ed} — Design load

F_{Rk} — Characteristic value of resistance

F_{cr} — Elastic critical buckling load for global instability mode based on initial elastic stiffnesses

LBA — Linear Buckling Analysis

L_{eq} — Equivalent member length

LTB — Lateral Torsional-Buckling

M — Bending moment

$M_{3,y,Rd}$	Design value of the interpolated resistance to bending moments about y-y axis for class 3 cross-sections, according to Greiner et. al (2011)
$M_{3,z,Rd}$	Design value of the interpolated resistance to bending moments about z-z axis for class 3 cross-sections, according to Greiner et al. (2011)
$M_{b,Rd}$	Design buckling resistance moment
M_{cr}	Elastic moment for lateral-torsional buckling
$M_{cr,tap}$	Elastic critical moment of the tapered column
$M_{cr,y,N}$	Critical moment of a beam-column subject to axial force N and uniform bending moment M_y
M_{Ed}	Design bending moment
$M_{f,Rd}$	Cross section resistance to bending considering the area of the flanges only
$M_{n,3,y,Rd}$; $M_{n,3,z,Rd}$	Reduced design value of the resistance to bending moments making allowance for the presence of normal forces, y-y axis and z-z axis, for class 3 cross-sections according to Greiner et al. (2011)
$M_{n,y,Rd}$; $M_{n,z,Rd}$	Reduced design value of the resistance to bending moments making allowance for the presence of normal forces, y-y axis and z-z axis
MNA	Materially Non-linear Analysis
$M_{pl,y,Rd}$	Design value of the plastic resistance to bending moments about y-y axis
$M_{pl,z,Rd}$	Design value of the plastic resistance to bending moments about z-z axis
M_R	Resistant bending moment
M_{sup}, M_{inf}	Flange bi-moment
M_w	Warping moment
M_y, M_z	Bending moments, y-y axis and z-z axis
$M_{y,cr,MN}$	Critical moment of a beam-column subject to $N+M_y$
$M_{y,Ed}$, $M_{z,Ed}$	Design bending moment, y-y axis and z-z axis
$M_{y,max,cs}$	Resistance to bending moments making allowance for the presence of normal forces, y-y axis
$M_{y,max}^{Method}$	Maximum bending moment for the given method, y-y axis
$M_{y,Rd}$	Design bending moment resistance, y-y axis
M_y^{II}	Second order strong axis bending moment
M_z^{II}	Second order weak axis bending moment

M_ω^{II}	Second order warping moment
N	Normal force
$N_{b,Rd}$	Design buckling resistance of a compression member
$N_{b,Rd,min}$	Design buckling resistance of a tapered compression member with the smallest cross-section
$N_{b,Rd,tap}$	Design buckling resistance of a tapered compression member
$N_{b,y,Rd}$	Design buckling resistance of a compression member, y-y axis
$N_{b,z,Rd}$	Design buckling resistance of a compression member, z-z axis
N_{conc}	Concentrated axial force
$N_{cr,MN}$	Critical axial force of a beam-column subject to $N+M_y$
$N_{cr,T}$	Elastic torsional buckling force
$N_{cr,tap}$	Elastic critical force of a tapered column
$N_{cr,tap}$	Elastic critical force of the tapered column
$N_{cr,tap}^{LBA}$	Elastic critical force of a tapered column obtained by a LBA analysis
$N_{cr,tap}^{Method}$	Elastic critical force of a tapered column for a given method
$N_{cr,y}$	Elastic critical force for in-plane buckling
$N_{cr,z}$	Elastic critical force for out-of-plane buckling
$N_{cr,z,tap}$	Elastic critical force of the tapered column about the weak axis
N_{Ed}	Design normal force
$N_{max,cs}$	Maximum axial force making allowance for the presence of bending moment acting about y-y axis
N_{max}^{Method}	Maximum normal force for the given method
N_{pl}	Plastic resistance to normal force at a given cross section
$N_{pl,Rd}$	Design plastic resistance to normal forces of the gross cross section
N_R	Resistant normal force
N_{Rd}	Design resistance to normal forces
Q	Shear force
T	Torsion
T_T	Uniform torsional component
T_w	Non-uniform torsional component
U, U_b	Strain energy, due to bending

UDL	Uniformly distributed loading
V	Shear force
V, V_b	Potential energy, due to bending
V_{Ed}	Design Shear force
V_{Ed}	Vertical applied load on the structure
H_{Ed}	Horizontal applied load on the structure
V_{inf}, V_{sup}	Flange shear
$V_{pl,Rd}$	Design resistance to shear
$W_{pl,y}$, $W_{pl,z}$	Plastic section modulus, weak and strong axis
$W_{y,el}$, $W_{z,el}$	Elastic bending modulus, weak and strong axis

Lowercase Greek letters

α	Angle of taper
α, α_{EC3}	Imperfection factor according to EC3-1-1
α_1	Factor related to the uncertainty that results of the modeling by finite elements
α_2	Factor related to the uncertainty that results of the spreading of models of actions and resistances
$\alpha_b^{(Method)}$	Load multiplier which leads to the resistance for a given method
α_{cr}	Load multiplier which leads to the elastic critical resistance
α_{cr}	Load multiplier which leads to the elastic critical resistance
$\alpha_{cr,op}$	Minimum amplifier for the in-plane design loads to reach the elastic critical resistance with regard to lateral or lateral-torsional buckling
$\alpha_{pl}^{cs,ends}$	Cross section resistance multiplier regarding both member ends, for class 1 and 2 cross sections
α_{pl}^M	Load amplifier defined with respect to the plastic cross section bending Moment
α_{pl}^N	Load amplifier defined with respect to the plastic cross section axial force
α_u	Load factor corresponding to the maximum load of the structure
α_u^{cs}	Cross section resistance multiplier

$\alpha_{ult,k}$	Minimum load amplifier of the design loads to reach the characteristic resistance of the most critical cross section
β	Correction factor for the lateral torsional buckling curves for rolled sections;
β	Generalized imperfection factor accounting for non-uniform force/moment and/or cross section
β	Reliability index
β_{lim}	Value of the generalized imperfection factor β for a sufficient high slenderness
γ_i	Taper ratio: γ_w – according to bending modulus; γ_I – according to inertia; γ_h – according to height; γ_b – according to witdh
γ_{M0}	Partial factor for resistance of cross sections whatever the class is
γ_{M1}	Partial safety factor for resistance of members to instability assessed by member checks
γ_{M2}	Partial factor for resistance of cross-sections in tension to fracture
γ_{Rd}	Partial factor associated with the uncertainty of the resistance model
$\delta''_{cr,max}$	Curvature at the critical cross section, acc. to equation (5.9) of EC3-1-1
δ_0	General displacement of the imperfect shape
δ_{cr}	General displacement of the critical mode
$\delta_{cr,hmin}$	Lateral displacement of the critical mode at $h=h_{min}$
δ_x	Longitudinal displacement
δ_y	Displacement about y-y axis
δ_z	Displacement about z-z axis
ε	Coefficient depending on f_y
ε	Utilization ratio at a given cross section
ε_M	Utilization ratio regarding the bending moment M
ε_{M+V}	Utilization ratio regarding bending and shear interaction
ε_M^{I}	Utilization ratio regarding first order bending moment M
ε_M^{II}	Utilization ratio regarding the second order bending moment
ε_N	Utilization ratio regarding the axial force N
ε_V	Utilization ratio regarding shear

η	Generalized imperfection
η*	Generalized imperfection for lateral-torsional buckling from the Ayrton-Perry type formulation
η''$_{cr}$	Curvature of the buckling mode shape at the critical cross section
η$_{cr}$	Buckling mode shape
η$_{EC3}$, η$_{uniform}$	Generalized imperfection for the prismatic member (considering cross section properties at the critical position)
η$_{init}$	Initial equivalent imperfection
η$_{non-uniform}$	Generalized imperfection for the tapered member
η$_{num}$	Generalized imperfection (numerical)
$\overline{\lambda}_{op}$	Global non-dimensional slenderness of a structural component for out-of-plane buckling according to the general method of clause 6.3.4
$\overline{\lambda}$	Non-dimensional slenderness
$\overline{\lambda}(x)$	Non-dimensional slenderness at a given position
$\overline{\lambda}_y$	Non-dimensional slenderness for flexural buckling, *y-y* axis
$\overline{\lambda}_z$	Non-dimensional slenderness for flexural buckling, *z-z* axis
$\overline{\lambda}_{LT}$	Non-dimensional slenderness for lateral-torsional buckling
$\overline{\lambda}_{LT,0}$	Plateau length of the lateral torsional buckling curves for rolled sections
$\overline{\lambda}_0$	Plateau relative slenderness
$\overline{\lambda}_p$	Relative slenderness of the plate subject to local buckling
ξ. η	Rectangular coordinates, longitudinal and transversal
ρ	Reduction factor for local plate buckling
σ	Normal stress
φ	Over-strength factor
ϕ	Global initial sway imperfection
ϕ	Maximum angle of twist
ϕ	Ratio between $\alpha_{pl}{}^{M}$ and $\alpha_{pl}{}^{N}$
ϕ$_0$	Maximum initial angle of twist
$\overline{\phi}_0$	Amplitude of the initial angle of twist

ϕ_{cr}	Rotation of the critical mode
ϕ_x	Rotation about *x-x* axis
φ_y, φ_z	Over-strength factor for in-plane buckling, out-of-plane buckling
χ	Reduction factor
χ_{LT}	Reduction factor to lateral-torsional buckling
$\chi_{LT,mod}$	Modified reduction factor for lateral-torsional buckling
χ_{num}	Reduction factor (numerical)
χ_{op}	Reduction factor for the non-dimensional slenderness $\bar{\lambda}_{op}$
χ_{ov}	Reduction factor for the non-dimensional slenderness $\bar{\lambda}_{ov}$
χ_y	Reduction factor due to flexural buckling, *y-y* axis
χ_z	Reduction factor due to flexural buckling, *z-z* axis
χ_z	Reduction factor to weak axis flexural buckling
ψ	Stress ratio
ψ	Ratio between the maximum and minimum bending moment, for a linear bending moment distribution
ψ_{lim}	Auxiliary term for application of LTB proposed methodology

Uppercase Greek letters

$\Delta M_{y,Ed}$	Moments due to the shift of the centroidal *y-y* axis
$\Delta M_{z,ed}$	Moments due to the shift of the centroidal *z-z* axis

Chapter 1

1 INTRODUCTION

1.1 Motivation and objectives

EC3 provides several methodologies for the stability verification of members and frames. The stability of uniform members in EC3-1-1 (CEN, 2005) is checked by the application of clauses 6.3.1 – stability of columns; clause 6.3.2 – stability of beams and clause 6.3.3 – interaction formulae for beam-columns. Regarding the stability of a non-uniform member, clauses 6.3.1 to 6.3.3 do not apply.

Figure 1.1(a) and *Figure 1.1(b)* illustrate recent examples of the use of curved and tapered members or members with polygonal centroidal axis. The evaluation of the buckling resistance of such members lies outside the range of application of the interaction formulae of EC3-1-1 and raises some new problems to be solved.

(a) Curved and tapered elements – Barajas Airport, Madrid, Spain

(b) Members with polygonal centroidal axis (stairs) – Italy pavilion, World Expo 2010 – Shanghai

Figure 1.1 Non-uniform members. Pictures obtained from (Steel Construct, no date [online])

For those cases, verification should be performed according to clause 6.3.4 (general method). Alternatively, if a second order analysis in which both in-plane and out-of-plane second order effects and imperfections (local and global) are considered, the obtained second order forces shall be considered and only cross sectional checks apply, see EC3-1-1, clauses 5.2.2 (3) a) and (7) a), and Greiner *et al.* (2010). Alternatively, the strength capacity may also be checked by a numerical analysis that accounts for geometrical and/or material imperfections and material and/or geometrical nonlinearities, henceforth denoted as GMNIA. However, for any of these methodologies, several difficulties are noted for the verification of a non-uniform member.

Firstly, taking as an example the case of beam-columns (uniform or not) with varying ratios of $M_{y,Ed}$ to N_{Ed} over the member length, the cross sectional classification changes from cross section to cross section, see the example of *Figure 1.2*. For such a case, an exhaustive (and iterative) evaluation of the stresses (1st and 2nd order) along the member is required to identify the design cross section and, as a result, the cross section class. As this is not practical, the highest class is adopted which may result in over-conservative design. A qualitative analysis of the example shows that the stresses in the interval corresponding to class 3 cross section are not critical compared to the stresses in the remainder of the member.
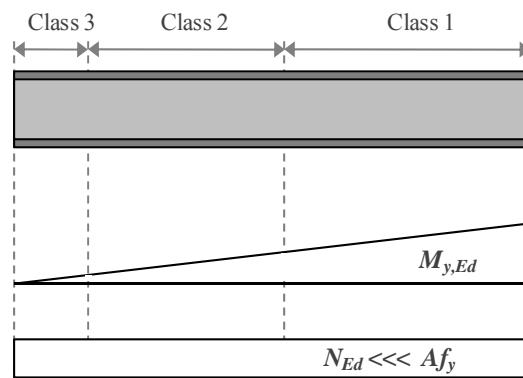
Figure 1.2 Uniform beam-column with non-uniform loading

Regarding non-uniform members in general, as mentioned, there is not a simple procedure available for evaluation of the critical cross section, i.e., critical design location. Alternatively,

equivalent cross section property formulae for the calculation of elastic critical forces of tapered members are available, either by calculation of, for example, an equivalent length (Galambos, 1998); depht (Galéa, 1986) or moment of inertia (Hirt and Crisinel, 2001). However, the introduction of these formulae in the buckling design formulae is not validated nor these equivalent properties were calibrated to be considered for the calculation of cross sectional properties associated to the stability resistance of the real member, but only for the term in the verification procedure concerning the critical load calculation.

Secondly, the determination of an adequate buckling curve is also necessary and leads to inconsistencies, such as:

(i)   The buckling curves in the code were derived for uniform columns with a sinusoidal imperfection with one wave length. When dealing with non-uniform members (either with varying cross section, axis or loading), the direct use of such curves may over predict the resistance level as the buckling mode is usually not a sine function;

(ii) The buckling curves in the code are geared towards specific buckling cases. That is why the interaction formulae and coefficients for uniform members have to take into account the transitions from one failure mode to the other (flexural buckling to lateral-torsional buckling, etc.) The "general method" can only treat these transitions in a very superficial way, by interpolation (not recommended by (ECCS TC8, 2006)) or, on the other hand, by a time-consuming specific calibration, not practical;

(iii) If the General Method is applied to a tapered member, the question also arises of how to categorize the member in terms of buckling curves as the main parameter h/b (height/width) changes continuously, see *Figure 1.3*. Because of this, the more restrictive buckling curve is most likely to be chosen, leading to over conservative results. In fact, this aspect can be further generalized to the application of the method to structural components. The method is supposed to establish the safety level of "plane frames or sub-frames composed of such *[single]* members". However, if the same structural system is characterized by single members, each one with distinct buckling curves, again the application of the method becomes unclear.
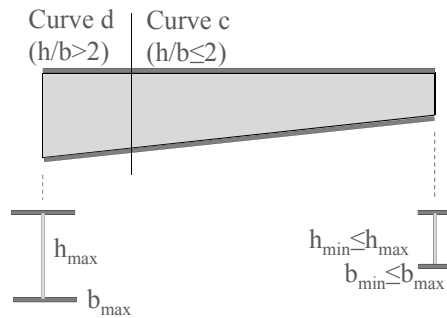
Figure 1.3 Change of buckling curve in a tapered member

If a second order analysis/verification is to be considered the correct shape and magnitude of the imperfection must also be considered. In EC3-1-1, as an alternative to Table 5.1 of clause 5.3.2 (6) which gives amplitudes for bow imperfections (see *Table 1.1*), clause 5.3.2 (11) may be used for determination of the amplitude of the imperfection with the relevant buckling mode shape, η_{cr}, see Eq. (1.1). Again, a critical cross section is necessary for application of this expression. In addition, the curvature η'' needs to be explicitly considered by the designer.

Table 1.1 Design values of initial bow imperfection e_0/L (Table 5.1 of EC3-1-1)

Buckling curve acc. to EC3-1-1, Table 6.1	Elastic analysis e_0/L	Plastic analysis e_0/L
a_0	1/350	1/300
a	1/300	1/250
b	1/250	1/200
c	1/200	1/150
d	1/150	1/100

$$\eta_{init}(x) = e_0 \eta_{cr}(x) \cdot \frac{N_{cr}}{EI\eta''_{cr,\max}} \tag{1.1}$$

In Eq. (1.1), N_{cr} is the axial critical load and $EI\,\eta''_{cr,max}$ is the bending moment due to η_{cr} at the critical cross section.

Finally, on one hand the General Method requires sophisticated global FEM models but on the other hand it contains so many simplifications that one must wonder if it is worth to apply it when compared to a "full" non-linear second-order analysis of the system. The latter is not

really more complicated but more precise and "readable" for the designer. Therefore it nowadays makes sense to develop simple rules for the basic cases and to include as much knowledge as possible of the "real" behavior of members in these rules.

Tapered steel members are commonly used over prismatic members because of their structural efficiency: by optimizing cross section utilization, significant material can be saved. However, if proper rules and guidance are not developed for these types of members, safety verification will lead to an over prediction of the material to be used. The main objective of this research is to provide stability verification procedures for linearly web-tapered members giving answer to the above-mentioned issues. For this, several goals will be fulfilled:

- Overview of existing methodologies for elastic and inelastic buckling of tapered members;

- Assessment and validation of the general methodology of EC3-1-1 for stability checking of non-uniform members. The General Method is given in clause 6.3.4 to give answer to the cases that cannot be verified by using clauses 6.3.1 to 6.3.3 and, as a result, tapered members. Results of the General Method are computed for a range of prismatic members, for which solutions of the same code exist and, in a second step, tapered members are verified and discussed;

- Development of analytical formulations for web-tapered steel columns subject to flexural buckling and beams subject to lateral-torsional buckling based on an Ayrton-Perry formulation. It is then possible to maintain consistency with EC3-1-1 flexural buckling verification procedure, clause 6.3.1, by extending it with adequate modifications. Columns and beams with fork conditions, subject to constant axial force and to linearly varying bending moments or uniformly distributed load, respectively, are treated;

- Based on the above, proper parameters for establishment of verification procedures that take into account the relevant instability modes of in-plane and out-of-plane flexural buckling of columns and lateral-torsional buckling of beams are calibrated;

- Development of a simple procedure for major axis critical axial force determination of tapered columns, based on the critical axial force of the smallest cross section;

- The codified imperfection of clause 6.3.1 in EC3-1-1 for welded sections is modified and re-calibrated as it is shown that current provisions do not follow accurately the residual stress pattern adopted for such cases. A similar modification is also proposed for lateral-torsional buckling verification of beams;

- Discussion of the possible approaches for the stability verification of portal frames with tapered members. This is evaluated on the basis of future development of member buckling design rules for tapered beam-columns subject to flexural and lateral-torsional buckling.

Finally, all the recommendations and proposals are in line with one of the main goals of TC8 – Stability to achieve consistency and harmonized levels of safety within the checking procedures for any stability phenomena in EC3.

1.2 The use of tapered members in steel structures

Tapered members are used in structures mainly due to their structural efficiency, providing at the same time aesthetical appearance. Examples of the application of tapered steel members in various structures are given in *Figure 1.4* to *Figure 1.9*.

(a)   (b)

Figure 1.4 Multi-sport complex – Coimbra, Portugal

(a) Dragão Stadium, Porto, Portugal (Picture obtained from (Steel Construct, no date [online]))

(b) "Cidade de Coimbra" stadium, Coimbra, Portugal (Tal Projecto, no date [online])

Figure 1.5 Stadium rooftops

(a) Exterior of the building (MIMOA, no date [online])

(b) Interior of the building (Veer, no date [online])

Figure 1.6 Bilbao exhibition center, Bilbao, Spain

Figure 1.7 Building entrance, near Porto Alegre airport, Porto Alegre, Brazil (CBCA, no date [online])

Figure 1.8 Construction site in front of the Central Station, Europaplatz, Graz, Austria (Nahverkehrsdrehscheibe Graz-Hauptbahnhof, 02-02-2012 [online])

Figure 1.9 Three bridges over the Hoofdvaart Haarlemmermeer, the Netherlands (Steel Construct (no date) [online])

Tapered members are commonly applied in steel frames, namely industrial halls, warehouses, exhibition centers, etc. Adequate verification procedures are then required for these types of structures. Some structural configurations are illustrated in *Figure 1.10*, see also Optima Cube (no date) [online] for other examples of multiple span frames or even asymmetrical frames with unequal column heights.
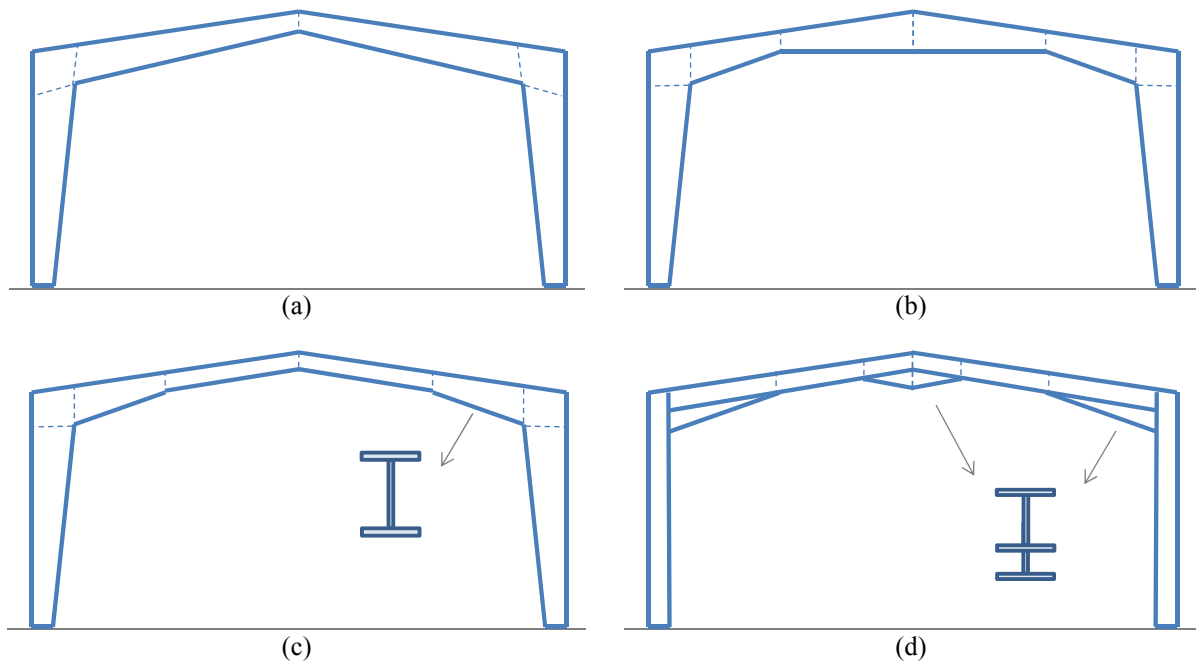
Figure 1.10 Different portal frame configurations with tapered members (not to scale)

In the scope of member design, maximum taper ratios (defined as the ratio between the maximum and the minimum height of the tapered member – $\gamma_{h=}h_{max}/h_{min}$) of $\gamma_h=4$ may be assumed to be of practical application. *Figure 1.10(b), (c)* and *(d)* illustrate this even for the shorter members. The rafter of *Figure 1.10(d)* presents a different configuration for the cross section of the haunches. The latter is not considered in this thesis.

If the General Method (clause 6.3.4) is considered for verification of structural systems composed of non-uniform members, the imperfection factors to apply in the buckling check are mechanically inconsistent, of unclear choice, and may lead to over safe or even unsafe levels of resistance. On the other hand, if global (P-Δ) and local (P-δ) effects and global (ϕ) and local (e_0) imperfections are considered for a second order analysis of the structure, the number of combinations and definition of the relevant in-plane (global and local) and out-of-plane imperfections may not be simple to define.

In this thesis, the flexural and lateral-torsional buckling verification of linearly web-tapered I-section columns and beams with fork conditions respectively is treated, such that an answer is provided regarding adequate imperfection factors for each of those buckling modes. Possible

approaches for treatment of isolated beam-columns and members in the context of framed structures are then analyzed.

1.3 Outline of the dissertation

This thesis is divided in 7 chapters.

- In **Chapter 1** existing problems related to the stability verification of non-uniform members in general are presented and the objectives of this research are drawn;

- In **Chapter 2** existing stability verification procedures for tapered members are presented and discussed. Firstly, a general literature review is made. In a second step, the analytical background for prismatic members is presented as it will be the benchmark and starting point for the varying cross section case to be developed. The General Method in EC3-1-1 is then presented and results are analyzed for a range of prismatic members. Specifically for the case of prismatic members analytical derivations of the method are carried out to be compared to the interaction formulae. The available procedures in EC3-1-1 for the stability verification of structures are described and finally general issues regarding the analysis of structures by FEM are pointed;

- In **Chapter 3** assumptions and simplifications for the numerical models are also presented and discussed;

- **Chapter 4** deals with the stability verification of tapered columns. Firstly, the analytical background for tapered columns is presented. Regarding the elastic in-plane flexural buckling of web-tapered columns subject to constant axial force, a simplified formula for calculation of the critical load is presented based on Raleigh-Ritz method. Introducing nonlinearities in the analytical model, an Ayrton-Perry model is developed and validated for tapered columns, with varying web and/or flange, subject to out-of-plane or in-plane buckling, and to constant or uniformly distributed axial force. Adequate parameters are then calibrated for web-tapered columns with constant axial force and discussed. Throughout this chapter specific issues such as the cross section class or the codified imperfections for welded cross sections are brought in and taken into account;

- In **Chapter 5**, lateral-torsional buckling of tapered beams is considered. Here, an analytical model is also developed and verified. Presence of shear and shear buckling is analyzed. For calibration of relevant parameters many decisions are taken especially due to the complexity brought in by the combination of non-uniform loading and cross section properties. Again, the codified imperfections for welded cross sections are analyzed and reevaluated;

- **Chapter 6** the proposed methodologies are applied for the stability verification of beam-columns and possible methodologies based either on an interaction approach and generalized slenderness approach are evaluated. Out-of-plane verification is performed. These are then brought into the structural level, regarding the stability verification of portal frames;

- Finally, **Chapter 7** points the main conclusions of this research and important subjects to be further developed.

Chapter 2

2 SAFETY VERIFICATION OF STEEL MEMBERS – THEORETICAL BACKGROUND AND DESIGN PROCEDURES

2.1 Scope

There are many alternatives to study stability aspects. The designer will choose which method to adopt according to the complexity of the problem; the precision of results; the level of safety to be achieved or even the simplicity of application of the method to the problem itself. *Figure 2.1* describes the available possibilities for the analysis of a structure according to EC3 part 1-1.
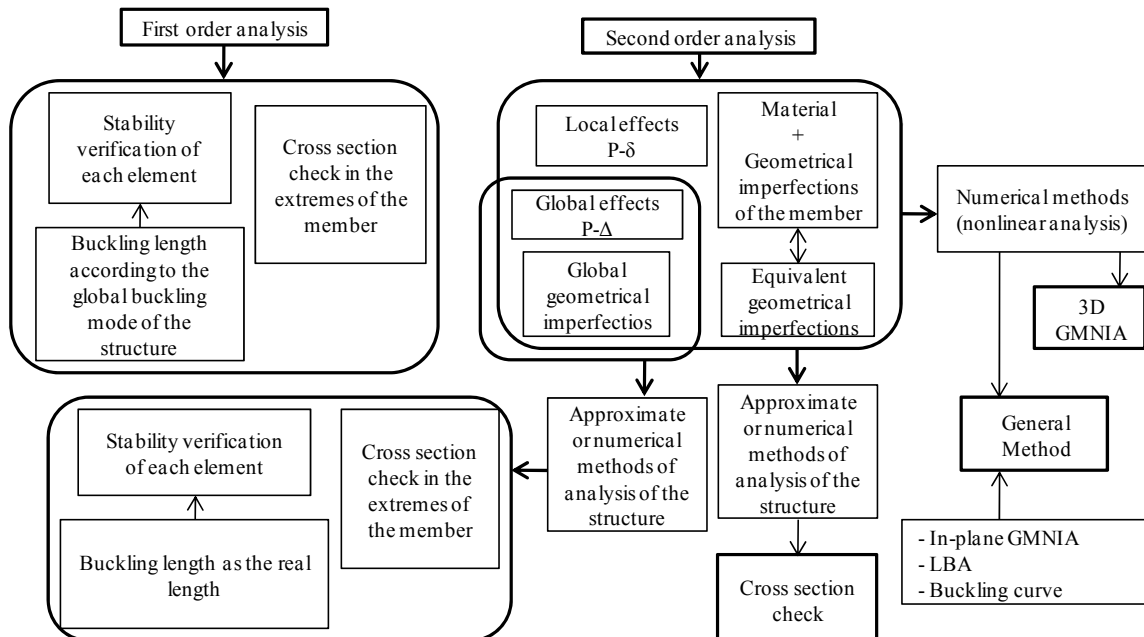
Figure 2.1: Methods of analysis

Tapered steel construction leads to competitive solutions and, as a result, a great deal of attention has been given to this subject. Many studies focusing on the elastic behavior and on elastic or inelastic stability issues have been carried out, either by analytical, numerical or experimental approaches. Nevertheless, the present research work is motivated by the fact that, for the time being, EC3-1-1 does not present satisfactory solutions for the stability verification of this type of members.

In this chapter a literature review of relevant studies in the field of tapered members is firstly presented. Subsequently, the Eurocode methodologies for stability verification of members are described:

(i) The analytical background for prismatic members is presented. Second order beam theory and Ayrton-Perry formulations adopted in EC3-1-1 for the stability verification of prismatic members are given as this is the basis for the developments of Chapters 4 and 5, respectively, regarding tapered columns and beams;

(ii) The General Method in EC3-1-1, suitable for the stability verification of tapered members, is analyzed and discussed. A parallel study regarding its application to prismatic members is performed in order to validate the method against well-known solutions;

The structural analysis procedures summarized in *Figure 2.1* are then described and illustrated in Section 2.5.

Finally, in the context of numerical analysis and verification of members and structures, the highest level of numerical analysis is generally introduced, i.e. non-linear analysis by FEM.

2.2 Studies and solutions on tapered members

A general review regarding the analysis and verification of tapered members is given in this section. It is worth mentioning that in Galambos (1988) a chapter is dedicated to this type of steel members. In addition, a very well documented overview may be found in the PhD thesis of Boissonnade (Boissonnade, 2002).

Firstly, the variation of the depth of the cross section in a tapered member relatively to a prismatic member leads to differences in the stress determination if the Bernoulli-Euler theory for prismatic bars is used. Additional normal stresses and/or shear stresses occur and this error increases with the angle of taper, α. Analytical solutions for determination of these stresses may be found in the literature (Timoshenko and Goodier, 1970). In reality, the surface in which normal stresses are developed is a circular surface that develops perpendicularly to the inclination of the flange and not vertical, see the red line in *Figure 2.2(a)*. As a result, in order to achieve vertical equilibrium, shear stresses in the web must develop. For practical reasons, Bleich (1931) illustrates that the circular surface may be quite accurately replaced by a "bi-linear" surface (see green line) of *Figure 2.2(b)*, for evaluation of the elastic shear capacity.
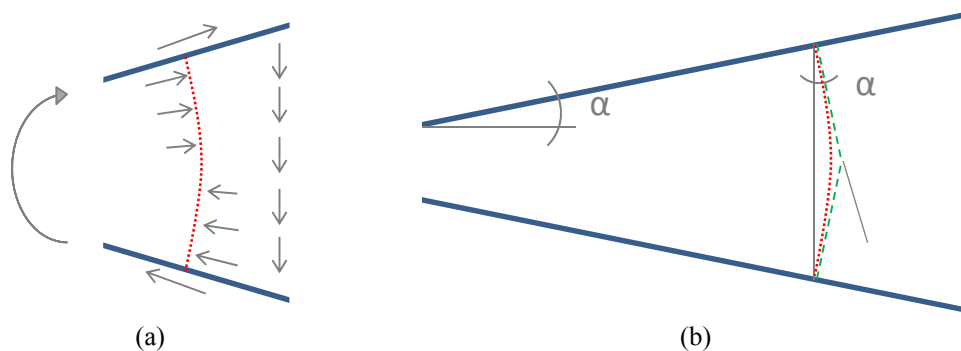
(a)   (b)
Figure 2.2: Direction and equilibrium of forces in a tapered segment

However, it has been established that, for small tapering angles (<15º) this difference is negligible and, as a result, regarding member design, the design formulae for prismatic have been extended for the case of tapered members (Galambos, 1988).

Experimental programs can be found reported in Butler and Anderson (1963) and in Prawel *et al.* (1974). The first deal with the elastic stability of web and flange tapered beams. Here, bracing requirements were investigated. Regarding the latter, inelastic stability was analyzed. Here, the measured residual stresses showed a similar distribution to the residual stresses of prismatic members with welded cross sections. The effect of material nonlinearity was also considered in Horne *et al.* (1979) and Salter *et al.* (1980).

Regarding expressions concerning the stability of tapered columns, it is mainly formulae for the calculation of the elastic critical forces that are available in the literature. For example, Hirt and Crisinel (2001) present an expression for determination of the equivalent inertia of tapered columns, I_{eq}, with I-shaped cross sections, depending on the type of web variation. Lee (1972) (see also Galambos, 1998) present an expression for a modification factor g of the tapered member length. The critical load is then calculated based on the smallest cross section. In Petersen (1980), design charts for extraction of a factor β to be applied to the critical load of a column with the same length and the smallest cross section are available for different boundary conditions and cross section shapes.

Ermopoulos (1997) presents the non-linear equilibrium equations of non-uniform members in frames under compression for non-sway and sway mode. Equivalent length factors are calibrated for both cases based and presented in forms of tables and graphs similar to the ones presented in Annex E of ENV1993-1-1 (1992).

Nevertheless, the consideration of a critical position is still undefined, which, on the safe side, requires the consideration of the smallest cross section and as a result leads to over-conservative design.

Regarding design rules, a design proposal for stability verification of tapered columns can be found in Baptista and Muzeau (1998), in which an additional coefficient K, calibrated numerically and presented in the form of an abacus, is applied to the reduction factor of a column with the smallest cross section (see Eq. (2.1)):

$$N_{b,rd,Tap} = K \times N_{b,rd,Min} \qquad (2.1)$$

In addition, some analytical formulations are available: in Raftoyiannis and Ermopoulos (2005) the differential equation of a tapered column subject to flexural buckling is derived, considering a parabolic shape for the imperfection; in Naumes (2009), the equilibrium

equation is also derived, considering the eigenmode shape. However, these expressions are not applicable for practical verification, as adequate factors for a design rule were not calibrated for this purpose.

In AISC (Kim, 2010; Kaehler *et al.*, 2010) an equivalent prismatic member which shall have the same critical load and the same first order resistance is defined. Such member is then to be verified considering the rules for prismatic columns.

Considering now tapered beams, Kitipornchai and Trahair (1972) give an analytical solution for the elastic critical moment, covering any type of tapered I-beam and loading.

Expressions for the elastic critical moment are given, for example, by Galéa (1986) in which the elastic critical load of a web-tapered beam subject to a uniform bending moment distribution is obtained by determination of an equivalent height and moments of inertia.

Another procedure for the computation of the elastic critical moment based on equivalent moment C_1 factors was presented by Ibañez and Serna (2010). Here, the tapered beam is replaced by an equivalent uniform beam by modification of the bending moment diagram. For application of the "Equivalent Moment Approach", in a first step, the tapered beam subject to $M(x)$ is replaced by a prismatic beam with the smallest cross section. The new moment $M^*(x)$ acting at each cross section of this equivalent beam is given by considering the critical moment which would be obtained at each cross section of the tapered beam, $M_{cr}(x)$, such that $M^*(x)=M(x).[M_{cr,0}/M_{cr}(x)]$, in which $M_{cr,0}$ is the critical moment obtained by the smallest cross section. With this, an equivalent prismatic beam with a distribution of moments given by $M^*(x)$ is obtained. Finally, considering the adequate factor C_1 for that moment distribution and the formula for prismatic beams, the critical moment of the tapered beam may be determined.

In Andrade *et al.* (2005), an expression for the calculation of M_{cr} based in the Rayleigh-Ritz method is developed. Equivalent moment factors C_1 are calibrated for the case of tapered beams with fork conditions subject to end moments. Similarly, Andrade *et al.* (2007b) develop expressions for critical moment determination of tapered beams subject to a concentrated load (the depth of the beam increases from the supports ($x/L=0$ and $x/L=1$) to the

middle (*x/L*=0.5)). Expressions for cantilevers subject to a tip load are presented in Andrade *et al.* (2006).

For the case of tapered or haunched members with partial bracing near the tension flange, Horne *et al.* (1979) also present expressions for the calculation of the critical moment.

If numerical analysis is to be performed, Boissonnade (2002) and Andrade *et al.* (2007a) refer the inadequacy of using stepped prismatic finite beam elements for the analysis of tapered members stability, as the inclination of the flange is not taken into account. In these studies, adequate elements to account for the torsional behavior of tapered members were developed. In Andrade *et al.* (2010a) the model is extended to discretely restrained tapered beams.

Finally, when material and geometric non-linearity is taken into account, some studies, proposals and code rules are summarized:

- In AISC, see Ziemian (2010), Kim (2010) and Kaehler *et al.* (2010), the mapping of the elastic buckling strength of tapered members to the design strength of equivalent prismatic members is performed, i.e., an equivalent prismatic beam with the same first order resistance and the same elastic critical load is determined and, afterwards, the rules for prismatic members are applied to the equivalent beam;

- Bradford (1988) derives a finite element for the elastic buckling resistance of tapered double symmetric I-beams loaded by end moments or uniformly distributed load. Solutions are presented in graphical form and may be considered in the Australian (Standards Australia, 1998) or British (British Standard Institution, 1985) codes. When the new critical moment approach is applied to those standards more accurate design curves are achieved;

- Andrade *et al.* (2007a, 2007c, 2010b) carried out numerical studies for the computation of the lateral-torsional buckling resistance of web-tapered I-beams subject to linear bending moment distribution and subject to concentrated loading. Results are plotted in a buckling curve format following the provisions of the General Method in EC3-1-1: for the tapered beam case the in-plane resistance multiplier is given by the first order

resistance multiplier here defined by a moment envelope; and the critical load multiplier is obtained numerically. The nonlinear resistance of the beam is also obtained by means of numerical analysis. With this information, it is possible to compute the overall reduction factor as a function of the overall slenderness (see Section 2.4). This study shows the inadequacy and high conservatism of considering curves *c* or *d* for application of the General Method as currently recommended. Moreover, the influence of the cross section flange/web proportions is also observed. It is shown that stockier cross sections (*h/b*<2 along the beam) present higher lateral-torsional buckling resistance than the narrow flange cross sections.

- In Vandermeulen (2007), solutions for a "plateau" slenderness $\bar{\lambda}_0$ (i.e., the limit slenderness for which instability effects will influence the resistance of the beam) and adequate imperfection factors α are given for analyzed cases with linear bending moment distributions. If general expressions for $\bar{\lambda}_0$ and α were then to be calibrated for a range of tapering and loading situations, the given rules in EC3-1-1 could be applied.

- Braham and Hanikenne (1993) present a Merchant-Rankine formula for determination of the reduction factor of the tapered beam based on the generalized slenderness given by the squared root of the ratio between the plastic load and the critical load multipliers. For the elastic critical moment, at first, the equivalent height is given by the mid height of the beam. Because this is very limiting and does not account for the proper torsional behavior due to the flange inclination, a new definition for the equivalent height was derived and proposed in Braham (1997).

However, most of these approaches treat the tapered member only by considering the correct value of the critical load (either by analytical formulae or numerically). The ultimate resistance is then brought into the prismatic member verification.

Regarding beam-columns (Kim, 2010; Kaehler *et al.*, 2010), the stability verification is performed on the basis of the interaction formulae for prismatic members with the provisions for the tapered beams and columns. Alternatively, in EC3-1-1, the generalized slenderness concept is considered and the out-of-plane stability of non-uniform members may be verified

with the General Method, clause 6.3.4, in which a generalized slenderness is applied in the Ayrton-Perry equation, considering the most restrictive buckling curve for flexural or lateral-torsional buckling of clauses 6.3.1 or 6.3.2, respectively (or an interpolation between the two). Note however that, when plastic design is performed, in Clause 6.3.5 of EC3-1-1 lateral-torsional buckling is prevented by limiting the length between the plastic hinge and proper restraining in the compression flange. Annex BB.3 of EC3-1-1 provides guidelines for determination of the stable length of tapered members.

With increasing complexity, a second order analysis in which all global and local second order effects and imperfections may be considered such that only cross sectional checks (in a sufficient number of sections) need to be performed, see *Figure 2.1*. This is required because there are currently no satisfactory member stability verification procedures for non-uniform members, giving over-conservative results most of the times. Furthermore, regarding the General Method in EC3-1-1, it will be seen throughout this thesis that the consideration of certain buckling curves assumed to be adequate may even lead to unsafe results. As a result, all second order effects and imperfections need to be accounted for in the structural analysis such that only cross section checks need to be performed, see also Greiner *et al.*, (2011).

Finally, for a more complex analysis, a full non-linear analysis taking into account nonlinear geometrical and plasticity effects shall be performed. Provided that modeling and nonlinearities are correctly considered this alternative leads to the actual failure load of the structure. Code guidance for this approach is given in Eurocode 3, part 1-5 (CEN, 2006).

In summary, although formula for the elastic critical loads or even finite element analysis may be considered for the elastic buckling resistance, the main problem lies in the further verification of the imperfect member with material nonlinearities. On the other hand, member verification may be avoided if the structural analysis accounts for all the relevant geometrical nonlinearities or, even more precisely, for all the geometrical and material nonlinearities. Because several difficulties are still present when considering the latter approaches (even for prismatic members), member stability verification procedures are preferred and developed in this thesis. Section 2.3 and Section 2.4 present and review EC3-1-1 background

methodologies for stability verification of members. The stability verification procedures to be developed have the same analytical background of the procedures for prismatic members adopted in EC3-1-1 and are therefore consistent with those, which are already familiar to the designer. Straight forward and mode conform design buckling rules are then provided, leading to a simple but at the same time efficient design.

2.3 Ayrton-Perry approach for prismatic beams and columns and interaction formulae format – analytical background

2.3.1 Introduction

Eurocode 3 – EN 1993 for the design of steel structures has been developed with respect to member stability verification since its first edition in 1992 thanks to extensive research dedicated to the subject coordinated by ECCS (European Convention for Constructional Steelwork) – Technical Committee 8 (TC8). However, there are still many issues to solve.

EC3 provides two distinct methodologies to verify the stability of beam-columns in buildings developed by different European teams. The existing interaction formulae for beam-columns in ENV 1993-1-1 (1992) needed to be improved as they gave either over-conservative or unconservative results for some cases and, therefore, two sets of new design formulae with different background have been derived by TC8 (Boissonade *et al.* 2006, Kaim, 2004). One is a mainly theoretically derived set of formulae called Method 1 (Boissonade et al, 2003) and the other is a simpler set of formulae for quick manual applications, calibrated with numerical simulations and it is called Method 2 (Greiner and Lindner, 2006). The interaction formulae in EC3-1-1 have reduction factors for pure axial force and for pure bending moment; the interaction between these effects is then taken into account by proper interaction factors attached to the bending terms. Method 1 consists of two sets of formulae in which the in-plane stability and out-of-plane stability are evaluated. For both these formulae, torsional deformations may be included or not. Regarding Method 2, it is necessary to choose between

the two categories "susceptible" or "not susceptible" to torsional deformations. The method consists, therefore, of 4 formulae: out-of-plane stability (i) with and (ii) without torsional effects; and in-plane stability (iii) with and (iv) without torsional effects.

However, there are still many aspects to be solved; some are highlighted here:

- The formulation of the interaction formulae is oriented to isolated members which are assumed to be pinned at their extremities and subject to a well-defined transverse and end loading. Therefore, several parameters shall be determined, such as the buckling length, the equivalent moment factors and the maximum bending moment. Sometimes, this is not a clear procedure. Thus, each designer will evaluate a different level of safety, as there are limited guidelines for these procedures, e.g. the extraction of a member from a framed system;

- While the buckling curves for flexural buckling were derived based on a mechanical model (Beer and Schulz, 1970) with equivalent geometric imperfections fulfilling the reliability requirements of 2 standard deviations away from the mean value for a normal distribution (Taras, 2010), the buckling curves for all other phenomena in EC3-1-1 are simply based on the column buckling curves. For example, regarding lateral-torsional buckling of beams, the derived buckling curves for flexural buckling of columns were simply adapted to best fit the results for beams concerning the General Case of clause 6.3.2.2 (for the Special Case of clause 6.3.2.3 the existing buckling curves were calibrated to best fit the numerical results). Similarly, in the case of members with torsional restraints which are not symmetrical relatively to the center of gravity, the buckling mode might not be sinusoidal. Using the buckling curves for flexural buckling as a basis is clearly inconsistent. Moreover, numerical calculations for torsional-flexural buckling (Taras, 2010) show these procedures are very conservative for sections which activate torsional rigidity within the buckling process;

- Within a member, the classification of a cross section may vary. Moreover, discontinuities may be observed in the utilization ratios corresponding to the limits from class 2 to class 3 for cross sections in bending. To overcome this problem, in the European Project RFCS Semi-Comp, see Greiner *et al.* (2011), an interpolation between

the plastic and elastic capacity of the cross section is performed. This interpolation is carried out by achieving the resistance for limit c/t of the analyzed cross section, taking as reference the c/t values of the plastic limit (for example, c/t=83 for major axis bending) and of the elastic limit (c/t =124 for major axis bending), see *Figure 2.3*. After establishing the interpolated resistant moments, cross section interaction verification shall be performed. Finally, for the determination of the "equivalent" member cross section class, a simplified procedure was established based on the determination of the utilization ratio along a satisfactory number of locations along the beam (e.g. 10 locations), considering the adequate cross section resistance at each position (elastic, plastic, or elasto-plastic, i.e., following the Semi-Comp approach). The position with the maximum utilization leads to first order failure cross section and is then used for specifying the equivalent class of the whole member.
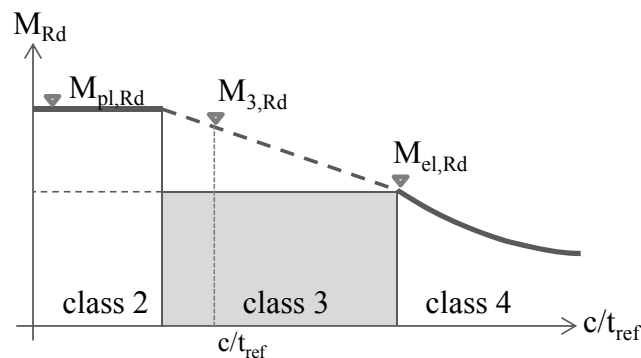
Figure 2.3: Resistant moment determination for I- and H-sections according to Semi-Comp (Greiner *et al.*, 2011)

In the past years, several studies have been carried out and proposals were made in order to analyze and overcome several problems in the rules for the stability verification of prismatic members and provide harmonization and consistency within the existing rules in EC3-1-1. Extensive parametric studies (more than 20000 beam-element models) have been carried out in Graz University of Technology and provided by Ofner (1997) to study the interaction factors between axial force and bending moment. For the same purpose, Kaim (2004) has carried out numerical studies. Within the goals of the 2 research teams in TC8 that developed Method 1 and Method 2, extensive research was done (Boissonade *et al.*, 2003; Greiner and Lindner, 2006). More recently, Taras (2010) has developed consistent buckling curves for

torsional and lateral-torsional buckling, based on the Ayrton-Perry formulation. The same author has also investigated the effect of laterally restrained I-sections along the weak-axis flange and, on a same logic, has developed buckling curves for this type of buckling mode. In addition a consistent design procedure was developed for in-plane stability verification of beam-columns by making use of a generalized slenderness definition.

Section 2.3.2 to Section 2.3.4 present the analytical background for the stability verification of columns, beams and beam-columns according to EC3-1-1.

Firstly, the second order theory formulae is presented for simply supported beam-columns with bi-symmetrical cross section subject to bending in both planes and axial force and with initial bow in-plane, out-of-plane and torsional imperfections. Note that this derivation can be found in detail in the PhD thesis of Kaim (2004). Following this procedure, simplifications are carried out in order to be applied to the cases of columns, beams and beam-columns. Parallel to this, the stability verification rules in EC3-1-1 are presented.

The required notations are the following:
- $v(x), w(x), \phi(x)$ – function of the deformations;
- $v_0(x), w_0(x), \phi_0(x)$ – function of the imperfections;
- v, w, ϕ – maximum deformations (midspan – considering a sinusoidal function);
- v_0, w_0, ϕ_0 – maximum initial imperfections (midspan – considering a sinusoidal function);
- N, M_y, M_z – uniform first order forces of the cross section;
- p_y, p_z, m_x – distributed external loading;
- $A, i_s, I_T, I_y, I_z, I_\omega$ – cross section properties;

Note that, in accordance with the plane of loading of the beam-column, buckling about major axis and buckling about minor axis will be commonly referred by in-plane and out-of-plane buckling, respectively. This notation is also adopted for the case of flexural buckling of columns.

The elastic buckling axial loads are given by:

$$N_{cr,z} = \frac{EI_z \pi^2}{L^2} \quad N_{cr,y} = \frac{EI_y \pi^2}{L^2} \quad N_{cr,T} = \left(\frac{EI_\omega \pi^2}{L^2} + GI_T \right)\frac{1}{i_s^{\,2}} \quad N_{cr,\omega} = \frac{EI_\omega \pi^2}{i_s^{\,2} L^2} \quad (2.2)$$

The elastic critical moment of a beam and also of a beam-column subject to axial force and uniform bending moment is given by (Trahair, 1993):

$$M_{cr}^2 = N_{cr,z} N_{cr,T} i_s^{\,2} \qquad M_{cr,y,N}^2 = N_{cr,z} N_{cr,T}\left(1 - \frac{N}{N_{cr,z}} \right)\left(1 - \frac{N}{N_{cr,T}} \right)i_s^{\,2} \qquad (2.3)$$

Imperfections and deflections are assumed to be sinusoidal. For example, regarding the out-of-plane deflection, v, it is given by

$$v(x) = v \sin\left(\frac{\pi x}{L} \right) \qquad (2.4)$$

The amplification factors for $N_{cr,z}, N_{cr,y}, M_{cr,y,N}$ will be named as

$$D_z = 1 - \frac{N}{N_{cr,z}} \qquad D_y = 1 - \frac{N}{N_{cr,y}} \qquad D_M = 1 - \frac{M_y^2}{M_{cr,y,N}^2} \qquad (2.5)$$

Compressive stresses are assumed to be positive. The remaining sign conventions are illustrated in *Figure 2.4*.
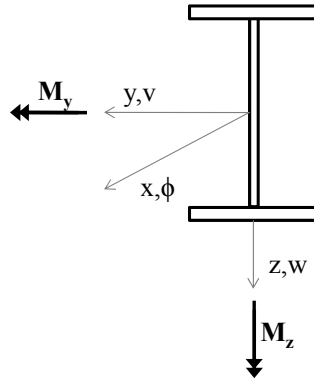
Figure 2.4: Sign convention

2.3.2 Second-order beam theory for flexural and lateral-torsional buckling of beam-columns

The differential equations for flexural and lateral-torsional buckling of prismatic members with double symmetric cross sections are given by Eq. (2.6). The first and second rows of the matrix deal, respectively with out-of-plane and in-plane flexural buckling. The third row is the differential equation for torsion.

$$\begin{bmatrix} EI_z v''''+Nv'' \\ 0 \\ M_y v'' \end{bmatrix} + \begin{bmatrix} 0 \\ EI_y w''''+Nw'' \\ M_z w'' \end{bmatrix} + \begin{bmatrix} M_y \phi'' \\ M_z \phi'' \\ EI_\omega \phi''''-(GI_T \phi''-Ni_s^2 \phi'') \end{bmatrix} = \begin{bmatrix} p_y \\ p_z \\ m_x \end{bmatrix} \qquad (2.6)$$

Considering $m_x=0$ and

- Neglecting the differences between the uniform first order bending moments M_y and M_z and the sinusoidal moments resultant from p_z and p_y, respectively;

- Neglecting the stiffness terms due to the curvature of the imperfect member;

and introducing the imperfections $v_0(x)$, $w_0(x)$, and $\phi_0(x)$, Eq. (2.6) becomes

$$\left(\begin{bmatrix} N_{cr,z} & 0 & 0 \\ 0 & N_{cr,y} & 0 \\ 0 & 0_z & i_s^2 N_{cr,T} \end{bmatrix} - \begin{bmatrix} N & 0 & M_y \\ 0 & N & M_z \\ M_y & M_z & i_s^2 N \end{bmatrix}\right)\begin{bmatrix} v \\ w \\ \phi \end{bmatrix} = \begin{bmatrix} -M_z \\ M_y \\ 0 \end{bmatrix} + \begin{bmatrix} N & 0 & M_y \\ 0 & N & M_z \\ M_y & M_z & Ni_s^2 \end{bmatrix}\begin{bmatrix} v_0 \\ w_0 \\ \phi_0 \end{bmatrix} \quad (2.7)$$

Eq. (2.7) can be expressed as

$$(K_{mat} - K_{geo})u = F^I + K_{geo}u_0 \quad (2.8)$$

in which K_{mat} is the first order material stiffness matrix; K_{geo} is the geometrical stiffness matrix; u and u_0 are vectors containing respectively the second order deformations and imperfections at mid-span ; and F^I is the first order load vector.

The solution of Eq. (2.7) is

$$\begin{bmatrix} v \\ w \\ \phi \end{bmatrix} = \frac{1}{D_M M_{cr,y,N}^2} \begin{bmatrix} \dfrac{M_{cr,y,N}^2}{D_z N_{cr,z}} & \dfrac{M_y M_z}{D_y N_{cr,y}} & M_y \\[3mm] \dfrac{M_y M_z}{D_y N_{cr,y}} & \dfrac{D_M M_{cr,y,N}^2}{D_y N_{cr,y}} & \dfrac{M_z D_z N_{cr,z}}{D_y N_{cr,y}} \\[3mm] M_y & \dfrac{M_z D_z N_{cr,z}}{D_y N_{cr,y}} & D_z N_{cr,z} \end{bmatrix} \times$$

$$\times \left(\begin{bmatrix} -M_z \\ M_y \\ 0 \end{bmatrix} + \begin{bmatrix} N & 0 & M_y \\ 0 & N & M_z \\ M_y & M_z & Ni_s^2 \end{bmatrix}\begin{bmatrix} v_0 \\ w_0 \\ \phi_0 \end{bmatrix}\right) \quad (2.9)$$

In Eq. (2.9), $M^2_{cr,y,N} \gg M^2_z$ for simplification (Kaim, 2004).

Second order forces are obtained by multiplying the cross section stiffness (*EI*) with the curvatures, as expressed in Eq. (2.10). Shear deformations are neglected. If it is assumed that $sin \approx sin^2$, second order forces lead to the second set of equations in Eq. (2.10), see also Salzgeber (2000a).

$$\begin{cases} M_y^{II} = EI_y(-w''(x) + v_0''(x)\phi(x) - v(x)\phi_0''(x)) \\ M_z^{II} = EI_z(v''(x) + w_0''(x)\phi(x) + w''(x)\phi_0(x)) \\ M_\omega^{II} = -EI_\varpi\phi'' \end{cases} \rightarrow \begin{cases} M_y^{II} = N_{cr,y}(w - v_0\phi - v\phi_0) \\ M_z^{II} = -N_{cr,z}(v + w_0\phi + w\phi_0) \quad (2.10) \\ M_\omega^{II} = -i_s^2 N_{cr,\omega}\phi \end{cases}$$

Finally, applying a first yield criterion in which a linear distribution of stresses σ due to the applied (first and second order) forces is considered, failure occurs for $\sigma = f_y$.

$$\frac{\sigma}{f_y} = \frac{N}{Af_y} + \frac{M_y^{II}}{W_y f_y} - \frac{M_z^{II}}{W_z f_y} - \frac{M_\omega^{II}}{I_\varpi/\varpi_{\max} f_y} \leq 1 \qquad (2.11)$$

2.3.3 Flexural buckling of columns

2.3.3.1 Derivation

Consider a simply supported column subject to axial force N with lateral imperfection v_0, only. Eq. (2.9) becomes:

$$\begin{bmatrix} v \\ w \\ \phi \end{bmatrix} = \frac{1}{M_{cr,y,N}^2} \begin{bmatrix} \dfrac{M_{cr,y,N}^2}{D_z N_{cr,z}} & 0 & 0 \\ 0 & \dfrac{M_{cr,y,N}^2}{D_y N_{cr,y}} & 0 \\ 0 & 0 & D_z N_{cr,z} \end{bmatrix} \cdot \begin{bmatrix} Nv_0 \\ 0 \\ 0 \end{bmatrix} \rightarrow v = \frac{Nv_0}{\left(1 - \dfrac{N}{N_{cr,z}}\right)N_{cr,z}} \qquad (2.12)$$

Applying the first yield criterion of Eq. (2.11),

$$\frac{\sigma}{f_y} = \frac{N}{N_{pl}} + \frac{M_y^{II}}{M_{y,el}} - \frac{M_z^{II}}{M_{z,el}} - \frac{M_\omega^{II}}{M_{\omega,el}} = \frac{N}{Af_y} + 0 - \frac{-N_{cr,z}(v+0+0)}{W_{z,el}f_y} - 0 \quad \rightarrow$$

$$\rightarrow \quad \frac{N}{Af_y} + \frac{Nv_0}{\left(1 - \dfrac{N}{N_{cr,z}}\right)W_{z,el}f_y} \leq 1 \tag{2.13}$$

Note that, for the case of in-plane flexural buckling of the column, i.e., considering an in-plane imperfection w_0, only, Eq. (2.13) would be

$$\frac{N}{Af_y} + \frac{Nw_0}{\left(1 - \dfrac{N}{N_{cr,y}}\right)W_{y,el}f_y} \leq 1 \tag{2.14}$$

Defining now the quantity $\chi_z N_{pl}$ as the value of N which makes $\sigma=f_y$ and introducing the non-dimensional slenderness $\overline{\lambda}_z = \sqrt{N_{pl}/N_{cr,z}}$, the Ayrton-Perry equation (Ayrton and Perry, 1886) for flexural buckling about the weak axis is obtained, which is also the background to the current EC3-1-1 rules:

$$\chi_z + \frac{v_0 A}{W_{z,el}}\frac{\chi_z}{1 - \chi_z \overline{\lambda}_z^{\,2}} = 1 \quad (=) \quad (1 - \chi_z)(1 - \chi_z \overline{\lambda}_z^{\,2}) = \frac{v_0 A}{W_{z,el}}\chi_z \tag{2.15}$$

2.3.3.2 Application in EC3-1-1

If the flexural instability mode (in-plane or out-of-plane) is kept undefined, Eq. (2.15) can be rewritten as

$$(1 - \chi)(1 - \chi\overline{\lambda}^{\,2}) = \frac{e_0 A}{W_{el}}\chi = \eta\chi \tag{2.16}$$

e_0 is the amplitude of the imperfection regarding the respective buckling mode. The terms e_0A/W_{el} may be defined as a generalized imperfection η. Representing η as a function of the relative slenderness $\bar{\lambda} = \sqrt{Af_y / N_{cr}}$, yields

$$\eta = \frac{e_0 A}{W_{el}} = \frac{e_0}{L} \frac{L \cdot A}{I/v} = \frac{e_0}{L} \frac{1}{i/v} \frac{L}{i} = \frac{e_0}{L} \frac{1}{i/v} \lambda = \frac{e_0}{L} \left[\frac{1}{i/v} \pi \sqrt{E/f_y} \right] \bar{\lambda} \qquad (2.17)$$

η includes the effect of several imperfections such as residual stresses, initial out of straightness or eccentrically applied forces. Considering a plateau non-dimensional slenderness of $\bar{\lambda}_z = 0.2$ for which flexural buckling is negligible, Eq. (2.17) becomes

$$\eta = \underbrace{\frac{e_0}{L} \left[\frac{1}{i/v} \pi \sqrt{E/f_y} \right]}_{\alpha} (\bar{\lambda} - 0.2) = \alpha(\bar{\lambda} - 0.2) \qquad (2.18)$$

The solution of Eq. (2.16) is given by

$$\chi = \frac{1}{\phi - \sqrt{\phi^2 - \bar{\lambda}^2}} \leq 1 \quad \text{with} \quad \phi = 0.5(1 + \eta + \bar{\lambda}^2) \qquad (2.19)$$

Or, taking into account the new definition of η,

$$\chi = \frac{1}{\phi - \sqrt{\phi^2 - \bar{\lambda}^2}} \leq 1 \quad \text{with} \quad \phi = 0.5\left(1 + \alpha(\bar{\lambda} - 0.2) + \bar{\lambda}^2\right) \qquad (2.20)$$

The design buckling resistance of the column is given by

$$N_{b,Rd} = Min\left(N_{b,y,Rd}; N_{b,z,Rd}\right) = Min\left(\chi_y; \chi_z\right) N_{Rd} \qquad (2.21)$$

From which N_{Rd} shall be determined considering adequate section properties according to the respective cross-section class.

In Eq. (2.18) α is an imperfection factor calibrated both by extensive numerical and experimental parametric tests (Beer and Schulz, 1970). It was later adopted in the codes in the Ayrton-Perry format (ECCS, 1978; Rondal and Maquoi, 1979). The values for the imperfection factor α and the corresponding buckling curves in EC3-1-1 (a_0, a, b, c and d) are represented in *Figure 2.5* and *Table 2.1*.
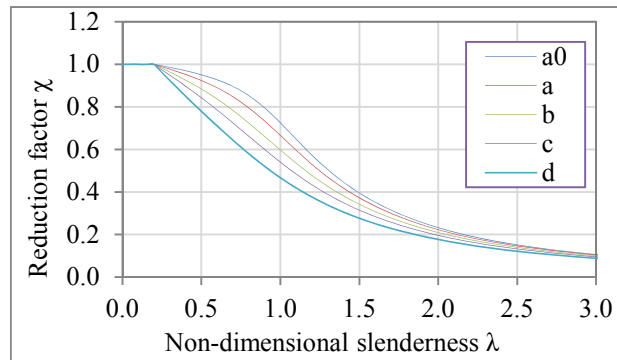
Figure 2.5: Imperfection factors α and corresponding buckling curves in EC3-1-1

Table 2.1: Imperfection factors α and corresponding buckling curves in EC3-1-1

Buckling curve	a_0	a	b	c	d
Imperfection factor α	0.13	0.21	0.34	0.49	0.76

For the cases analyzed in this thesis, the classification of the buckling curve for a given cross section is summarized in *Table 2.2*.

Table 2.2: Selection of buckling curve for a given cross section and buckling mode

Fabrication procedure	h/b	Buckling about axis	Buckling curve
Rolled I-sections	>1.2	y-y	a
		z-z	b
	≤1.2	y-y	b
		z-z	c
Welded I-sections		y-y	b
		z-z	c

Finally, for the case of welded I-sections, the generalized imperfection η and corresponding imperfection factor α are reassessed in Chapter 4 as, for these cases, the given buckling curves in EC3-1-1 seem not to represent accurately the influence of the residual stress distribution. This has been discussed in Greiner *et al.* (2000) and in Taras (2010) for the case of lateral-torsional buckling of welded beams. In fact, for welded columns, the buckling curve overestimates the resistance of the numerical model up to 8%. Note that the adopted magnitude of the compressive residual stresses in the flange (all most of the flange is subject to an initial stress of $0.25f_y$) may not be a truthful representation of reality, leading to restrictive resistance levels (Greiner *et al.*, 2000). Nevertheless, in Taras (2010) modifications for welded cross-sections are proposed in line with the current residual stress definition for the case of lateral-torsional buckling of beams.

2.3.4 Lateral-torsional buckling of beams

2.3.4.1 Derivation

Consider a simply supported beam with fork conditions, I-shaped cross section and initial imperfections v_0 and ϕ_0. Assuming small displacements, the two degrees of freedom may be coupled according to the following criteria (Taras, 2010):

$$v_0 = \frac{M_{cr}}{N_{cr,z}} \phi_0 \qquad (2.22)$$

The differential equations for lateral-torsional buckling (beam under uniform bending moment) are given by (see Eq. (2.6)):

$$\begin{bmatrix} EI_z v''''+0 \\ 0 \\ M_y v'' \end{bmatrix} + \begin{bmatrix} 0 \\ EI_y w''''+0 \\ 0 \end{bmatrix} + \begin{bmatrix} M_y \phi'' \\ 0 \\ EI_\omega \phi''''-(GI_T \phi''-0) \end{bmatrix} = \begin{bmatrix} 0 \\ 0 \\ 0 \end{bmatrix} \rightarrow$$

(2.23)

$$\rightarrow \begin{cases} EI_z v''+M_y \phi = 0 \\ M_y v''+EI_\omega \phi''''-GI_T \phi''= 0 \end{cases} \rightarrow v''=-\frac{M_y \phi}{EI_z} \rightarrow -M_y \frac{M_y \phi}{EI_z}+EI_\omega \phi''''-GI_T \phi''= 0$$

In Eq. (2.23), $v(x)$ and $\phi(x)$ are sinusoidal functions. It is known that M_{cr} is the nontrivial solution to this equation. Therefore, considering $M_y=M_{cr}$ the first equation leads to:

$$EI_z v''+M_y \phi = 0 \rightarrow EI_z\left[-v\frac{\pi^2}{L^2}\sin(\frac{\pi}{L}x)\right]+M_{cr}\left[\phi\sin(\frac{\pi}{L}x)\right]=0 \rightarrow v=\frac{M_{cr}}{N_{cr,z}}\phi \quad (2.24)$$

which has a similar format to Eq. (2.22).

Eq. (2.9) becomes

$$\begin{bmatrix} v \\ w \\ \phi \end{bmatrix} = \frac{1}{D_M M_{cr}^2}\begin{bmatrix} \dfrac{M_{cr}^2}{N_{cr,z}} & 0 & M_y \\ 0 & \dfrac{D_M M_{cr}^2}{N_{cr,y}} & 0 \\ M_y & 0 & N_{cr,z} \end{bmatrix}\cdot\left(\begin{bmatrix} 0 \\ M_y \\ 0 \end{bmatrix}+\begin{bmatrix} 0 & 0 & M_y \\ 0 & 0 & 0 \\ M_y & 0 & 0 \end{bmatrix}\begin{bmatrix} v_0 \\ 0 \\ \phi_0 \end{bmatrix}\right) \quad (2.25)$$

The second equation (in-plane) is independent from the other two. Introducing Eq. (2.22), the solution for v and ϕ is reached.

$$\begin{bmatrix} v \\ \phi \end{bmatrix} = \frac{1}{\left(1 - \dfrac{M_y^2}{M_{cr}^2}\right) M_{cr}^2} \begin{bmatrix} \dfrac{M_{cr}^2}{N_{cr,z}} M_y \phi_0 + M_y^2 v_0 \\[2mm] M_y^2 \phi_0 + N_{cr,z} M_y v_0 \end{bmatrix} \rightarrow \begin{cases} v = v_0 \dfrac{M_{cr}}{N_{cr,z}} \dfrac{M_y}{M_{cr} - M_y} \\[4mm] \phi = \phi_0 \dfrac{M_y}{M_{cr} - M_y} \end{cases} \tag{2.26}$$

Consider now the following relationship between the initial imperfections ϕ_0 and v_0 given by *Figure 2.6* and Eq.(2.27):
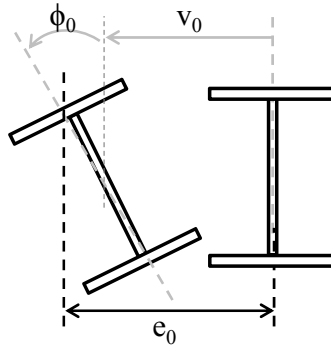
Figure 2.6: Relationship between ϕ_0 and v_0

$$e_0 = v_0 + \frac{h}{2}\phi_0 = \frac{M_{cr}}{N_{cr,z}}\phi_0 + \frac{h}{2}\phi_0 \rightarrow \phi_0 = \frac{e_0}{h/2 + M_{cr}/N_{cr,z}} \tag{2.27}$$

Applying again a first yield criterion (Eq. (2.11)) in which terms containing v_0^2 are neglected due to their minor significance (Salzgeber, 2000a); replacing M_y by $\chi_{LT} W_{y,el} f_y$; introducing the non-dimensional slenderness $\bar{\lambda}_{LT} = \sqrt{W_{y,el} f_y / M_{cr}}$ and $\bar{\lambda}_z = \sqrt{A f_y / N_{cr,z}}$; considering $\omega_{max} = bh/4$; and replacing Eq. (2.27) and Eq. (2.22) in the expressions for v and ϕ (Eq. (2.26)); a similar equation to Eq. (2.19) for flexural buckling is obtained (the complete derivation of this can be found in Taras (2010)):

$$\chi_{LT} = \frac{1}{\phi_{LT} - \sqrt{\phi_{LT}^2 - \overline{\lambda}_{LT}^2}} \leq 1 \quad \text{with} \quad \begin{cases} \phi = 0.5(1 + \eta* + \overline{\lambda}_{LT}^2) \\ \eta* = \dfrac{\overline{\lambda}_{LT}^2}{\overline{\lambda}_z^2} \dfrac{Ae_0}{W_{el,z}} = \dfrac{\overline{\lambda}_{LT}^2}{\overline{\lambda}_z^2} \eta_z \end{cases} \qquad (2.28)$$

2.3.4.2 Application in EC3-1-1

Lateral-torsional buckling verification of beams is performed according to clause 6.3.2 of EC3-1-1. The buckling resistance is calculated using the buckling curves for flexural buckling. Whereas Eq. (2.28) leads to a consistent approach for lateral-torsional buckling of beams (if η_z is replaced by a similar expression to Eq. (2.18) with adequate imperfection factor α for the lateral-torsional buckling case), in EC3-1-1 the values of the imperfection factors α for flexural buckling are adapted to the lateral-torsional buckling of beams, according to numerical based-GMNIA calibrations.

The reduction factor for lateral-torsional buckling is given by

$$\chi_{LT} = \frac{1}{\phi_{LT} - \sqrt{\phi_{LT}^2 - \overline{\lambda}_{LT}^2}} \leq 1 \quad \text{with} \quad \phi_{LT} = 0.5\left(1 + \alpha_{LT}(\overline{\lambda}_{LT} - 0.2) + \overline{\lambda}_{LT}^2\right) \quad (2.29)$$

The design buckling resistance of the beam is given by

$$M_{b,Rd} = \chi_{LT} M_{y,Rd} \qquad (2.30)$$

From which $M_{y,Rd}$ shall be determined considering adequate section properties according to the respective cross-section class.

The imperfection factors α_{LT} are categorized differently than the factors for flexural buckling – the height to width ratio limit is given by $h/b=2$ while for flexural buckling is given by $h/b=1.2$. Here, more slender cross sections lead to higher imperfection factors, unlike for

flexural buckling. As a result, the lower torsional resistance that slender cross sections provide is accounted for by a higher imperfection. This categorization is however inconsistent with the residual stress definition of I-sections which is differentiated at the limit *h/b*=1.2.

EC3-1-1 presents two approaches for the design check of lateral-torsional buckling effects of I-beams. One is denoted the "General Case" (clause 6.3.2.2). The other procedure, "Special Case" (clause 6.3.2.3) is intended for use for hot rolled or equivalent welded sections. This procedure introduces a correction factor *f*, which takes into account the effect of the bending moment diagram and considers new buckling curves that take into account the torsional stiffness of the beam (Rebelo et al, 2009). The reduction factor for lateral-torsional buckling according to the "Special Case" is given by

$$\chi_{LT} = \frac{1}{\phi_{LT} - \sqrt{\phi_{LT}^2 - \beta \overline{\lambda}_{LT}^2}} \leq \begin{cases} 1 \\ 1/\overline{\lambda}_{LT}^2 \end{cases}$$

$$\text{with} \quad \phi_{LT} = 0.5\left(1 + \alpha_{LT}(\overline{\lambda}_{LT} - \overline{\lambda}_{LT,0}) + \beta \overline{\lambda}_{LT}^2\right)$$

(2.31)

Recommended values in Eq. (2.31) for *β* and $\overline{\lambda}_{LT,0}$ are β=0.75 and $\overline{\lambda}_{LT,0} = 0.4$. Finally, for consideration of the bending moment distribution, χ_{LT} must be modified by a factor *f* (and respective correction factor k_c) such that a modified reduction factor $\chi_{LT,mod}$ is obtained by

$$\chi_{LT,\text{mod}} = \frac{\chi_{LT}}{f} \leq 1 \quad \text{with} \quad f = 1 - 0.5(1 - k_c)\left[1 - 2(\overline{\lambda}_{LT} - 0.8)^2\right] \leq 1 \qquad (2.32)$$

k_c is a factor that takes into account the type bending moment distribution. The values of α_{LT} in clause 6.3.2 of EC3-1-1 are given in *Table 2.3*.

For the determination of the design buckling resistance of the beam, χ_{LT} in Eq. (2.30) must be replaced by $\chi_{LT,mod}$.

Table 2.3: Buckling curves for lateral-torsional buckling

Fabrication procedure	h/b	General Case	Special Case
Rolled I-sections	≤2	a	b
	>2	b	c
Welded I-sections	≤2	c	c
	>2	d	d

To assess the accuracy of the alternative design formulae for the verification of lateral-torsional buckling, a statistical analysis of the results was performed on the basis of EN 1990-Annex D (Rebelo et al, 2009). A proposal for the definition of the partial safety factor γ_{rd} (uncertanties in the resistance model) is presented for the various methods, in line with the target failure probability of EN 1990. In order to compare the influence of the load parameter f together with the "General Case" procedure, the use of the f-factor together with the "General Case" procedure is there addressed as "General Case/f". The 1331 studied cases covered several parameters: non-dimensional slenderness; bending moment diagrams; fabrication processes; cross section shapes; and yield stress of steel, representative of practical situations. It was seen that the General Case gives good results on the safe side, however with a great amount of spreading, especially for the low slenderness range. The scatter relatively to the "Special Case" is much lower, however the values do not remain exclusively on the safe side. In a second step of that study (Simões da Silva et al, 2009), the evaluation of the influence of the variability of steel properties on the lateral-torsional resistance of steel beams was performed in order to establish γ_m (uncertainties for the material product) by analyzing the results of a range of coupon tests. These two partial safety factors lead to the establishment of γ_{MI} between $\gamma_{MI} = 1.0$ up to $\gamma_{MI} = 1.2$ for the special case and S460 steel grade.

2.3.4.3 Ayrton-Perry based proposal (literature)

In Taras (2010) a consistent formulation (see Section 2.3.4.1) based on the Ayrton-Perry format is derived. This formulation adjusts significantly better to the GMNIA results. A new format for the generalized imperfection is obtained from the Ayrton-Perry derivation and kept for a design proposal.

$$\eta^* = \frac{\overline{\lambda}_{LT}^{\,2}}{\overline{\lambda}_z^{\,2}} \frac{Ae_0}{W_{el,z}} = \frac{\overline{\lambda}_{LT}^{\,2}}{\overline{\lambda}_z^{\,2}} \eta = \frac{\overline{\lambda}_{LT}^{\,2}}{\overline{\lambda}_z^{\,2}} \alpha_{LT} (\overline{\lambda}_z - 0.2) \tag{2.33}$$

The factor $\overline{\lambda}_{LT}^{\,2} / \overline{\lambda}_z^{\,2}$ provides a correct consideration of the cross section torsional rigidity and as a result, it is possible to maintain the limits h/b=1.2, consistent with the residual stress definition. Calibrated imperfection factors α_{LT} are given in *Table 2.4*.

Table 2.4: Imperfection factors by Taras (2010)

Fabrication procedure	h/b	α_{LT}
Rolled I-sections	>1.2	$0.12\sqrt{W_{y,el}/W_{z,el}} \leq 0.34$
	≤1.2	$0.16\sqrt{W_{y,el}/W_{z,el}} \leq 0.49$
Welded I-sections		$0.21\sqrt{W_{y,el}/W_{z,el}} \leq 0.64$

Furthermore, the correction factor $\sqrt{W_{y,el}/W_{z,el}}$ of *Table 2.4* is able to accurately reflect the change of residual stresses at the frontier h/b=1.2. To overcome excessive high values of $\sqrt{W_{y,el}/W_{z,el}}$ for cross sections with extreme geometry (low torsion rigidity), a limit value of α corresponding to the weak axis flexural buckling imperfection factor is established. In fact, the limiting value of α_{LT}≤0.64 for welded cross sections coincides with the calibrated imperfection factor for weak axis flexural buckling of welded columns (to be further discussed and developed in Chapter 5).

For beams subject to non-uniform bending moment distribution, an "over-strength" factor φ was developed. Finally, the reduction factor for lateral-torsional buckling of beams is given by

$$\chi_{LT} = \frac{\varphi}{\phi_{LT} - \sqrt{\phi_{LT}^{\,2} - \varphi\overline{\lambda}_{LT}^{\,2}}} \leq 1$$

$$\tag{2.34}$$

$$\text{with} \quad \phi_{LT} = 0.5\left(1 + \varphi\left(\alpha_{LT}(\overline{\lambda}_z - 0.2)\frac{\overline{\lambda}_{LT}^{\,2}}{\overline{\lambda}_z^{\,2}} + \overline{\lambda}_{LT}^{\,2}\right)\right)$$

from which α_{LT} is given in *Table 2.4* and $\varphi=1.05$ for parabolic bending moment distribution and $\varphi = 1.25 - 0.1\psi - 0.15\psi^2$ for linear bending moment distribution (ψ is the ratio between the maximum and minimum bending moment applied in the beam).

A similar approach is adopted for lateral-torsional buckling verification of tapered beams in Chapter 5.

2.3.5 Bending and axial force interaction

2.3.5.1 Analytical solution for the relevant modes

Analogous to EC3-1-1 – clause 6.3.3, the in-plane and out-of-plane failure modes are presented here. The case of beam-columns under uniaxial bending and axial force ($N+M_y$) is studied. The procedure is based on Section 2.3.2 – second order theory for beam-columns and first yield criterion, considering lateral imperfections. Again, further information is given in Kaim (2004). In EC3-1-1 the interaction formulae for stability verification of beam-columns are based on these derivations considering a second-order in-plane theory. In order to account for the spatial or elastic-plastic behavior specific concepts are considered afterwards (Boissonade *et al.* 2006).

The solution regarding in-plane flexural buckling without lateral-torsional buckling (w_0) is given by

$$\frac{N}{N_{pl}} + \frac{Nw_0}{D_y M_{y,el}} + \frac{M_y}{D_y M_{y,el}} = 1 \qquad (2.35)$$

Similarly, for out-of-plane flexural buckling without lateral-torsional buckling (v_0; $I_T=\infty$) Eq. (2.10) leads to

$$\frac{N}{N_{pl}} + \frac{Nv_0}{D_z M_{z,el}} + \frac{M_y}{D_y M_{y,el}} = 1 \tag{2.36}$$

In Eq. (2.35) and Eq. (2.36), M_y may be replaced by $C_m M_y$ such that the actual bending moment distribution M_y is replaced by an equivalent sinusoidal bending moment distribution therefore avoiding the determination of the critical second order cross section. Further manipulations lead to the well-known adopted format in EC3-1-1, see also Boissonade *et al.* (2006) and Lindner (2004).

$$\frac{N}{\chi N_{pl}} + \underbrace{\frac{1 - N/N_{cr}}{1 - \chi N/N_{cr}}}_{\mu} \frac{C_m M_y}{(1 - N/N_{cr})M_{y,el}} = 1 \tag{2.37}$$

The consideration of torsional effects for the case of out-of-plane flexural buckling considering lateral imperfections v_0 is given by Kaim (2004)

$$\frac{N}{N_{pl}} + \frac{M_y}{D_y M_{y,el}} + \frac{v_0}{D_M M_{z,el}} \left(\frac{N}{D_z} + \frac{M^2{}_y N_{cr,z}}{M^2_{cr,y,N}} \right) + \frac{i_s^2 N_{cr,\omega} M_y N_{cr,z} v_0}{M^2_{cr,y,N} D_M M_{\omega,el}} = 1 \tag{2.38}$$

Or, rewritten in another format (see also Boissonade *et al.*, 2006)

$$\frac{N}{N_{pl}} + \frac{M_y}{D_y M_{y,el}} + \frac{v_0}{D_M} \left(\frac{N}{D_z M_{z,el}} + \frac{M^2{}_y N_{cr,z}}{M^2_{cr,y,N} M_{z,el}} + \frac{N_{cr,z}{}^2 \frac{h}{2} M_y}{M_{z,el} M^2_{cr,y,N}} \right) = 1 \tag{2.39}$$

provided that

$$i_s{}^2 N_{cr,\omega} = \frac{\pi^2 E I_\varpi}{L^2} \tag{2.40}$$

and, for I-sections, that

$$I_\varpi = I_z \frac{h^2}{4} \quad \text{and} \quad M_{\varpi,el} = M_{z,el} \frac{h}{2} \tag{2.41}$$

In Eq. (2.38), terms with v_0^2 were neglected.

The case of in-plane buckling subject to torsional deformations is discussed in the following.

2.3.5.2 EC3-1-1 interaction formulae

There are two different formats of the interaction formulae in EC3-1-1 which were derived for uniform beam-columns with double-symmetric cross sections. Method 1 was derived such that each physical phenomenon is accounted for through a well-defined factor, it is a theory-based approach (Boissonnade et al, 2006) although coefficients were still calibrated to numerical benchmarks; In Method 2, simplicity prevails. The latter is a method calibrated with numerical simulations.

The two stability interaction formulae of clause 6.3.3 in EC3-1-1 are given by

$$\frac{N_{Ed}}{\chi_y\, N_{Rk}/\gamma_{M1}} + k_{yy} \frac{M_{y,Ed} + \Delta M_{y,Ed}}{\chi_{LT}\, M_{y,Rk}/\gamma_{M1}} + k_{yz} \frac{M_{zEd} + \Delta M_{z,Ed}}{M_{z,Rk}/\gamma_{M1}} \le 1.0 \tag{2.42}$$

$$\frac{N_{Ed}}{\chi_z\, N_{Rk}/\gamma_{M1}} + k_{zy} \frac{M_{y,Ed} + \Delta M_{y,Ed}}{\chi_{LT}\, M_{y,Rk}/\gamma_{M1}} + k_{zz} \frac{M_{z,Ed} + \Delta M_{z,Ed}}{M_{z,Rk}/\gamma_{M1}} \le 1.0 \tag{2.43}$$

where:

- N_{Ed}, $M_{y,Ed}$ and $M_{z,Ed}$ are the calculation values of the axial force and bending moments around y and z, respectively;

- $\Delta M_{y,Ed}$ and $\Delta M_{z,Ed}$ are the moments due to the variation of the centroid for class 4 sections;

- χ_y and χ_z are the reduction factors due to buckling by bending around y and z, respectively, evaluated according to clause 6.3.1;

- χ_{LT} is the reduction factor due to lateral buckling, evaluated according to clause 6.3.2 (χ_{LT} = 1.0 for elements that are nor susceptible of buckling laterally);

- k_{yy}, k_{yz}, k_{zy}, and k_{zz} are interaction factors dependent on the relevant instability and plasticity phenomena, obtained according to Annex A of EC3 (Method 1) or Annex B (Method 2);

The several parameters of the interaction formulae of clause 6.3.3 are now briefly explained:

- Firstly, the interaction formulae describe the stability behavior of a beam-column under axial force and bending moments – acting in-plane; out-of-plane; or in both planes. Each force is analyzed separately and then coupled together by the interaction factors k_{yy}, k_{yz}, k_{zy}, and k_{zz} above-mentioned. The detailed description and calculation of the interaction factors of Method 1 and Method 2 are given in Annexes A and B of EC3-1-1 respectively; they include many of the effects of the beam-column such as the bending moment distribution or the plasticity of the cross section;

- There are two formulae to check the stability of a member – in Method 2 Eq. (2.42) describes the in-plane behavior and Eq. (2.43) describes the out-of-plane behavior; in Method 1 the two equations are not separately bound to the in-plane and out-of-plane buckling modes and as a result both equations must be fulfilled for the check. If the member is susceptible to lateral-torsional buckling, it should be accounted for in each of these equations;

- The interaction formulae are based on a second order theory and, therefore, they are based on second order forces and amplification factors (Boissonade et al, 2006). Due to lateral imperfections, the axial force N will produce second order bending moments. When the bending moment distribution or the structure is not symmetrical, it becomes necessary to know the position of the critical cross section in order to perform a safe evaluation. Regarding Method 1, the equivalent moment factors, C_m (see Eq. (2.37)),

replace the first order bending system by an "equivalent sinusoidal" first order bending moment which will produce the same amplified bending moment in the span of the member (Boissonade et al, 2006). Regarding Method 2, equivalent uniform moment factors C_m were calibrated based on GMNIA calculations with non-uniform bending moment distributions which were compared to calculations with uniform bending moment. Finally, it is then enough to verify the buckling resistance in span with the applied moment affected by C_m. For this reason, additional to the application of the interaction formulae, a cross section verification of the extremes of the member is needed;

- The interaction formulae are based on an in-plane second order theory. Spatial behavior is extended afterwards, accounting for the existence of out-of-plane forces;

- The elastic-plastic behavior is not considered in the analytical format of the formulae. In Method 1, for the cases of class 1 and 2 cross section, the plasticity coefficients "C_{ij}" are then defined and $M_{el,Rd}$ is replaced by $C_{ij}.M_{pl,Rd}$. In Method 2, this is accounted for in the the interaction factors k_{ij};

- The susceptibility of the member to have torsional deformations or not is considered differently in Method 1 and Method 2. The solution considering lateral-torsional buckling is based on a second order theory, see Eq.(2.38), but considering only lateral imperfection v_0 (Boissonade et al, 2006). Here, twist will produce additional second order bending and warping moments. In Method 1, there are only two formulae whereas in Method 2 the two formulae to be considered are chosen according to the susceptibility of the member to exhibit torsional deformations or not – this is evaluated according to the type of cross section or the restraining against torsional deformations along the member;

- Finally, in Salzgeber (2000b) it was found that in-plane buckling deformations combined with torsional effects needed to be accounted for – particularly for the case of members between lateral restraints, i.e., with an in-plane buckling length significantly higher than the out-of-plane buckling length, see also Boissonnade *et al.* (2006). As a result, if relevant, torsional effects shall be included in the in-plane verification formula. For this case, a combination of initial twist ϕ_0 and in-plane w_0 imperfections were considered. Torsional effects are accounted for by the inclusion of the reduction factor χ_{LT} to the

resistant bending moment $M_{y,Rk}$. Additionally, Method 1 includes factor C_{mLT} which accounts for the influence of torsional deformations and modifies the interaction factor k_{yy} (for the case of in-plane buckling).

In addition, as already referred, clause 6.3.3 of EN 1993-1-1 states that the safety of a beam-column requires the verification of the cross section capacity at the member ends using an appropriate interaction expression. The cross sectional resistance is checked using Section 6.2 of EC3-1-1. Cross section resistance verifications considered in this thesis are described in the following, namely regarding bending and axial force interaction and shear.

a) Bending and axial force interaction

For the verification of bending and axial force interaction, clause 6.2.9 should be considered. Regarding I and H cross sections, these expressions are:

$$M_{N,y,Rd} = M_{pl,y,Rd} \frac{1-n}{1-0.5a} \quad \text{but} \quad M_{N,y,Rd} \leq M_{pl,y,Rd} \; ; \tag{2.44a}$$

$$M_{N,z,Rd} = M_{pl,z,Rd} \quad \text{if} \quad n \leq a \; ; \tag{2.44b}$$

$$M_{N,z,Rd} = M_{pl,z,Rd} \left[1 - \left(\frac{n-a}{1-a} \right)^2 \right] \quad \text{if} \quad n > a \tag{2.44c}$$

where $n = N_{Ed}/N_{pl,Rd}$ and $a = \left(A - 2bt_f \right)/A \leq 0.5$.

For a cross section of class 1 or 2 subject to axial force and uniaxial bending moment, the interaction diagram for the resistance of the cross section is illustrated in *Figure 2.7*:
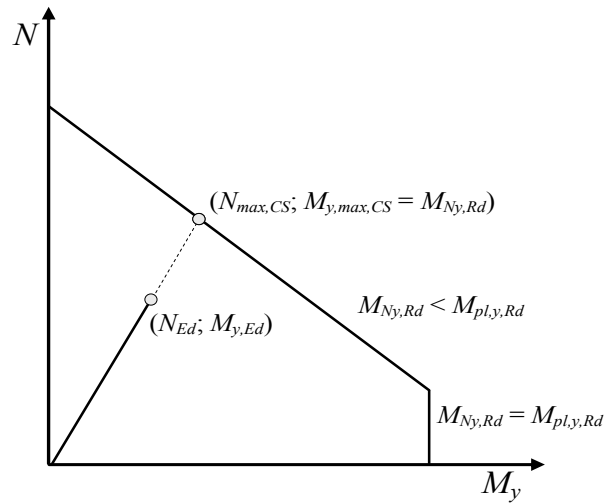
Figure 2.7: Cross section plastic interaction diagram ($N+M_y$)

The pair of forces ($N_{max,CS}$; $M_{y,max.CS}$) in *Figure 2.7* are obtained by solving the following system of equations:

$$\begin{cases} M_{y,\max} = M_{N,y,Rd} = M_{pl,y,Rd} \dfrac{1 - N_{\max}/N_{pl}}{1 - 0.5a} \le M_{pl,y,Rd}; \\ \dfrac{N_{\max,CS}}{M_{y,\max,CS}} = \dfrac{N_{Ed}}{M_{y,Ed}}. \end{cases} \tag{2.45}$$

The utilization ratio of the cross section (or the inverse of the cross section resistance multiplier) is given by the ratio between the vector norm of the applied internal forces and the vector norm of the bending and axial force resistance along the same load vector (*Figure 2.7*):

$$\frac{1}{\alpha_u^{cs}} = \frac{\sqrt{N_{Ed}^2 + M_{y,Ed}^2}}{\sqrt{N_{\max,CS}^2 + M_{y,\max,CS}^2}} \le 1 \tag{2.46}$$

For a class 3 cross section, the utilization ratio of the cross sections is given by

$$\frac{N_{Ed}}{A f_y} + \frac{M_{y,Ed}}{W_{el,y} f_y} \leq 1 \tag{2.47}$$

Finally, in Greiner *et al.* (2011) (Semi-Comp project) the verification to mono-axial bending and axial force interaction for cross section class 3 is given by

$$M_{N,3,y,Rd} = M_{3,y,Rd}(1-n) \tag{2.48a}$$

$$M_{N,3,z,Rd} = M_{3,z,Rd}(1-n^2) \tag{2.48b}$$

b) Shear

If shear stresses are present, Eq. (2.49) and Eq. (2.50) should be satisfied. For elastic verification the Von-Mises criterion may be used.

- Shear resistance, clause 6.2.6 of EC3-1-1:

$$\frac{V_{Ed}}{V_{pl,Rd}} \leq 1; \qquad V_{pl,Rd} = A_v \frac{f_y / \sqrt{3}}{\gamma_{M0}} \tag{2.49}$$

in which A_v is the shear area.

- Shear and bending interaction, clause 6.2.8 of EC3-1-1 or clause 7.1 of EC3-1-5 (CEN, 2006):

$$\varepsilon_{M+V} = \begin{cases} \dfrac{M_{y,Ed}}{M_{pl,y,Rd}} \leq 1, & if \quad \dfrac{V_{Ed}}{V_{pl,Rd}} \leq 0.5 \\[4mm] \dfrac{M_{y,Ed}}{M_{pl,y,Rd}} + \left(1 - \dfrac{M_{f,Rd}}{M_{pl,y,Rd}}\right)\left(2\dfrac{V_{Ed}}{V_{pl,Rd}} - 1\right)^2 \leq 1, & if \quad \dfrac{V_{Ed}}{V_{pl,Rd}} > 0.5 \end{cases} \tag{2.50}$$

in which $M_{f,Rd}$ is the cross section resistance to bending considering the area of the flanges only.

2.4 Analysis of the General Method in EC3-1-1

2.4.1 Introduction and scope

Part 1-1 of Eurocode 3 includes a so called "general method" for lateral and lateral-torsional buckling of structural components such as: (i) single members, built-up or not, with complex support conditions or not; or (ii) plane frames or sub-frames composed of such members which are subject to compression and/or mono-axial main axis bending in the plane, but which do not contain rotative plastic hinges. The method uses a Merchant-Rankine type of empirical interaction expression to uncouple the in-plane effects and the out-of-plane effects. Conceptually, the method is an interesting approach because it deals with the whole structural component for the evaluation of the stability with respect to the various buckling modes (Müller, 2003). In addition, for more sophisticated design situations that are not covered by code rules but need finite element analysis, the method simplifies this task. It is noted that EN 1993-1-6 (CEN, 2007) specifies a similar approach, the MNA/LBA approach known as the "Overall Method", that may be seen as a generalization of the stability reduction factor approach used throughout many parts of Eurocode 3, see Rotter and Schmidt (2008).

It is, however, questionable that the application of the general method results in a lower bound estimate of the safety of the structural component for the target probability of failure that is specified in EN 1990 (1992). In addition, the method specifies two alternative criteria for the evaluation of the out-of-plane effects, leading to different levels of safety.

Apart from the doctoral thesis of Müller (2003), this method was not widely validated and there is scarce published background documentation to establish its level of safety. Within Technical Committee 8 of ECCS, the need to explore deeply the field and limits of the application of the General Method was consensually recognized (Snijder et al, 2006; ECCS TC8, 2006). In particular, several examples have been carried out at the University of Graz (Greiner and Ofner, 2007; Greiner and Lechner, 2007), comparing advanced finite element analyses (GMNIA) using beam elements with the General Method.

In this section the theoretical background of this method is firstly discussed. Analytical derivations of the method in line with clauses 6.3.1 to 6.3.3 for the stability verification of prismatic members are performed. It is seen that, even for prismatic members with double symmetric cross section, the method deviates from the buckling design rules although the existing buckling curves are to be considered (as stated in clause 6.3.4). More detail may be found in Simões da Silva *et al.* (2010a) in which a comprehensive analysis of the General Method when applied to prismatic simply supported members is carried out.

Finally, application of the method to non-uniform members is then analysed. Detailed description of the numerical assumptions is given in Chapter 3, as a basis for the main developments of this thesis.

2.4.2 Theoretical background – analogy to rules for prismatic members

2.4.2.1 Description of the method

The General Method, as given in EN 1993-1-1 in clause 6.3.4 states that the overall resistance to out-of-plane buckling for any structural component conforming to the scope defined in the introduction can be verified by ensuring that:

$$\chi_{op}\alpha_{ult,k} / \gamma_{M1} \geq 1 \qquad (2.51)$$

where $\alpha_{ult,k}$ is the minimum load amplifier of the design loads to reach the characteristic resistance of the most critical cross section of the structural component, considering its in-plane behavior without taking lateral or lateral-torsional buckling into account however accounting for all effects due to in-plane geometrical deformation and imperfections, global and local, where relevant. χ_{op} is the reduction factor for the non-dimensional slenderness to take into account lateral and lateral-torsional buckling and γ_{M1} is the partial safety factor for instability effects (adopted as 1.0 in most National Annexes).

The global non dimensional slenderness $\bar{\lambda}_{op}$ for the structural component, used to find the reduction factor χ_{op} in the usual way using an appropriate buckling curve, should be determined from

$$\bar{\lambda}_{op} = \sqrt{\alpha_{ult,k} / \alpha_{cr,op}} \qquad (2.52)$$

where $\alpha_{cr,op}$ is the minimum amplifier for the in-plane design loads to reach the elastic critical resistance of the structural component with respect to lateral or lateral-torsional buckling without accounting for in-plane flexural buckling. In the determination of $\alpha_{cr,op}$ and $\alpha_{ult,k}$, finite element analysis may be used.

According to EC3-1-1, χ_{op} may be taken either as: (i) the minimum value of χ_z (for flexural buckling, according to clause 6.3.1 of EC3-1-1) or χ_{LT} (for lateral-torsional buckling, according to clause 6.3.2); or (ii) an interpolated value between χ and χ_{LT} (determined as in (i)), by using the formula for $\alpha_{ult,k}$ corresponding to the critical cross section. It is noted that ECCS TC8 (2006) recommends the use of the first option only.

Finally, in EC3-1-6 (CEN, 2007) the Overall Method considers for the in-plane behavior a materially non-linear analysis, instead of (in the General Method) an in-plane analysis with the account of in-plane imperfections. Moreover, the Overall Method requires the use of a problem-specific buckling reduction factor χ, which is calibrated to the given conditions of loading and structural behaviour.

2.4.2.2 Application to flexural column buckling

In order to illustrate the application of the General Method to a trivial example, consider the pinned column of Figure 2.8 subject to an arbitrary axial force N_{Ed}. Let also assume that the in-plane direction corresponds to the cross-section major axis in bending. Let also assume, for simplicity, that buckling in a torsional mode is not relevant.
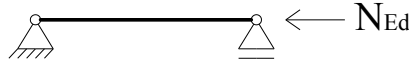
Figure 2.8: Pinned column

The application of clause 6.3.1 of EC3-1-1 leads, in succession, to:

$$\begin{cases} \overline{\lambda}_y = \sqrt{\dfrac{Af_y}{N_{cr,y}}} = \sqrt{\dfrac{N_{pl}}{N_{cr,y}}} \xrightarrow{\substack{buckling\\curve}} \chi_y \quad \Rightarrow \quad N_{b,y,Rd} = \chi_y \dfrac{N_{pl}}{\gamma_{M1}} = \chi_y N_{pl,Rd} \quad \geq N_{Ed} \\[2em] \overline{\lambda}_z = \sqrt{\dfrac{Af_y}{N_{cr,z}}} = \sqrt{\dfrac{N_{pl}}{N_{cr,z}}} \xrightarrow{\substack{buckling\\curve}} \chi_z \quad \Rightarrow \quad N_{b,z,Rd} = \chi_z \dfrac{N_{pl}}{\gamma_{M1}} = \chi_z N_{pl,Rd} \quad \geq N_{Ed} \end{cases} \tag{2.53}$$

and

$$N_{b,Rd} = \min\{N_{b,y,Rd}; N_{b,z,Rd}\} \quad \geq N_{Ed} \tag{2.54}$$

or, defining α_b as the ultimate load multiplier with respect to the applied axial force,

$$\alpha_b^{6.3.1} = \min\left\{\dfrac{N_{b,y,Rd}}{N_{Ed}}; \dfrac{N_{b,z,Rd}}{N_{Ed}}\right\} \quad \geq 1.0 \tag{2.55}$$

Alternatively, the application of the General Method for the same reference applied axial force yields, successively:

$$\begin{cases} \alpha_{ult,k} = \dfrac{N_{b,y,Rd}}{N_{Ed}} \\[1.5em] \alpha_{cr,op} = \dfrac{N_{cr,z}}{N_{Ed}} \end{cases} \rightarrow \quad \overline{\lambda}_{op} = \sqrt{\dfrac{\alpha_{ult,k}}{\alpha_{cr,op}}} = \sqrt{\dfrac{N_{b,y,Rd}}{N_{cr,z}}} = \sqrt{\dfrac{\chi_y N_{pl,Rd}}{N_{cr,z}}} = \overline{\lambda}_z \sqrt{\chi_y} \tag{2.56}$$

Since

$$\chi_y \leq 1.0 \Rightarrow \overline{\lambda}_{op} \leq \overline{\lambda}_z \Rightarrow \chi_{op} \geq \chi_z \qquad (2.57)$$

it follows that

$$N_{b,Rd} = \chi_{op}\alpha_{ult,k}N_{Ed} = \chi_{op}\chi_y N_{pl,Rd} \geq N_{Ed} \qquad (2.58)$$

or

$$\alpha_b^{GM} = \chi_{op}\chi_y \frac{N_{pl,Rd}}{N_{Ed}} \geq 1.0 \qquad (2.59)$$

Comparing Eq. (2.55) and Eq. (2.59) for this trivial example shows that the General Method does not exactly give the same result as the application of clause 6.3.1 even whenever the same column buckling curves are used. Assuming that flexural buckling around the minor axis is critical ($\chi_z \leq \chi_y$), yields

$$\frac{\alpha_b^{GM}}{\alpha_b^{6.3.1}} = \frac{\chi_{op}\chi_y}{\chi_z} \qquad (2.60)$$

Considering the case of pin-ended columns first, *Figure 2.9* plots Eq. (2.60) for a range of profiles and lengths, with the aim to compare the results from General Method with clause 6.3.1.
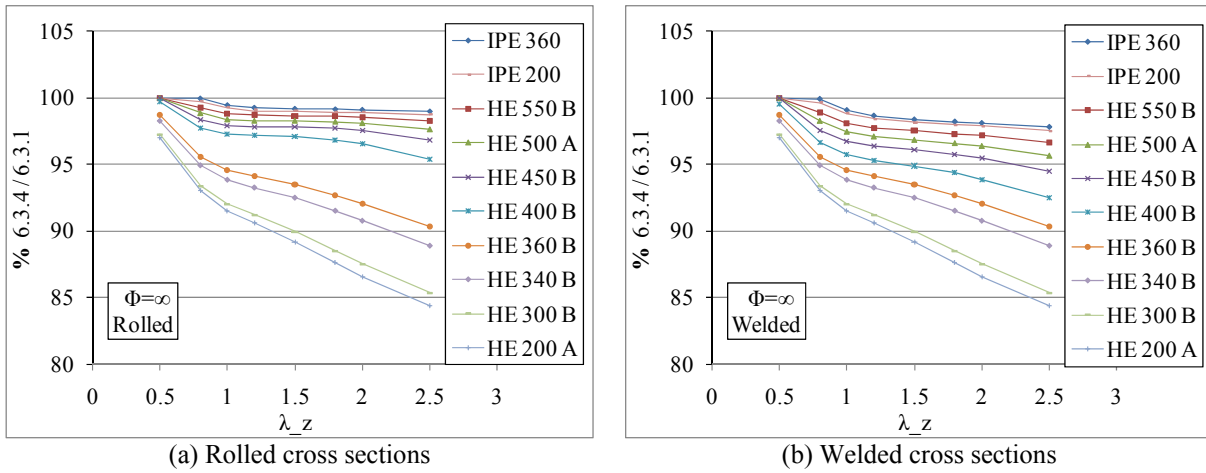
(a) Rolled cross sections   (b) Welded cross sections
Figure 2.9: Results of Eq. (2.60) – pin-ended columns

The ratio between the ultimate load multipliers for the General Method and for clause 6.3.1 decreases as the slenderness of the column increases. This can be explained by the fact that slender columns have lower reduction factors χ_y, leading to an increased difference between $\overline{\lambda}_z$ and $\overline{\lambda}_{op}$. The same reason is given for the higher differences illustrated in stocky cross-sections relatively to slender cross-sections, see also Taras (2010). The latter present a high in-plane stiffness relatively to the out-of-plane stiffness and as a result $\overline{\lambda}_{op}$ is closer to $\overline{\lambda}_z$. It can also be noticed that the results concentrate in groups according to the chosen buckling curve (see *Table 2.5*) or, in other words, curve *b* (higher imperfection) leads to a higher relative decrease in the ultimate resistance.

Table 2.5: Buckling curves for Flexural Buckling about zz, (acc. *Figure 2.9*)

Cross sections	h/b	Rolled	Welded
IPE 360 – IPE 200	>1.2	b	c
HEB 550 – HEB 400			
HEB 360 – HEA 200	≤1.2	c	c

The fact that the column resistance to out-of-plane flexural buckling needs to be reduced by the in-plane second order effects, when the given curves in the code were calibrated considering only one direction for the imperfection, leads to a deviation from the start. In fact, even if both directions are considered for the imperfection, the reduction felt by the in-plane imperfection is not as restrictive as the reduction provided by the consideration of the full in-

plane reduction in the resistance load multiplier $\alpha_{ult,k}$. The example of *Figure 2.10* supports this. Resistance is compared considering the following cases:

- Nonlinear numerical analysis considering imperfections in both directions (*GMNIA_yz*);

- Nonlinear numerical analysis considering imperfection in weak axis direction (*GMNIA_z*);

- General Method considering an in-plane GMNIA analysis for $\alpha_{ult,k}$ and the well-known Euler critical load multiplier for $\alpha_{cr,op}$ (*GM*);

- Clause 6.3.1 of EC3-1-1 (*6.3.1*);

- Eq. (2.60) (*EQU*).

In *Figure 2.10(a)* results are presented relatively to a nonlinear numerical analysis considering imperfections in weak axis direction (*GMNIA_z*); in *Figure 2.10(b)* results are illustrated in a buckling curve format. If a slender cross section were to be illustrated, e.g. IPE200 (*h/b*=2), results would practically coincide, see Simões da Silva *et al.* (2010a). The numerical model accounting for imperfection in directions *z-z* and *y-y* presents slightly lower resistance than the reference model with out-of-plane imperfections only. Nevertheless, if compared to the General Method cases (numerical or analytical), differences can still reach 25%, confirming the above discussed. Numerical assumptions are described in detail in Chapter 3.
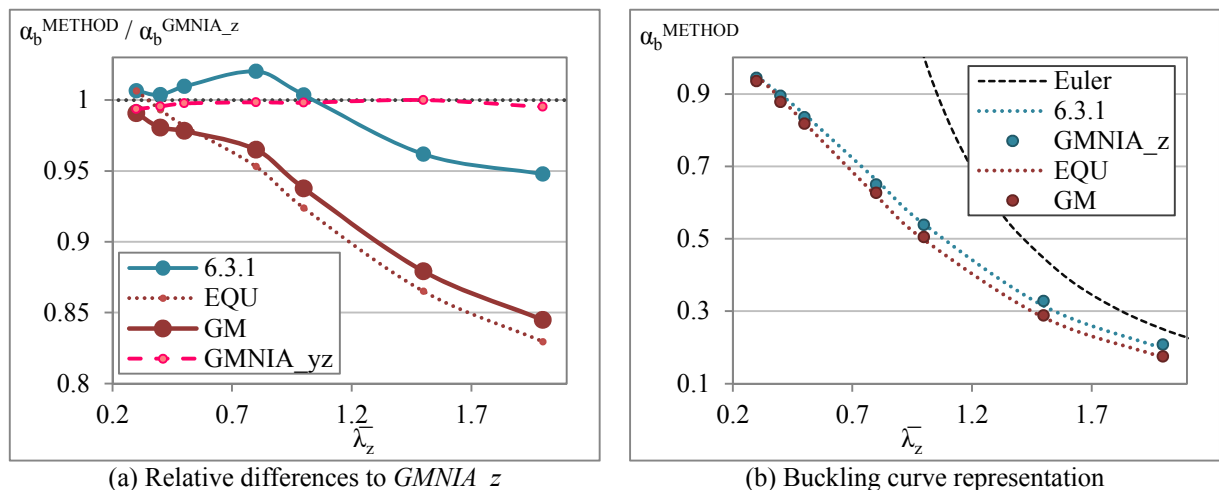

(a) Relative differences to *GMNIA_z*   (b) Buckling curve representation
Figure 2.10: Evaluation of the General Method applied to prismatic columns (HEB300, *h/b*=1; Hot-rolled; S235)

The same applies to beam-columns, in which the consideration of the second order in-plane effects should not be as severe (Taras, 2010). Actually, most codes that consider this concept of generalized imperfection, consider for $\alpha_{ult,k}$ the cross section resistance without in-plane 2nd order effects. This is further discussed in Section 2.4.2.5. Finally note that if, for the case of columns, in the definition of $\alpha_{ult,k}$, N_{pl} is considered in Eq. (2.56) instead of $N_{b,y,rd}$, the general method yields exacly the same result as clause 6.3.1 of EC3-1-1.

2.4.2.3 Application to lateral-torsional buckling

For an unrestrained beam, let $\alpha_{ult,k}$ denote the load level that corresponds to the attainment of the flexural resistance at the critical cross-section. Application of the General Method gives

$$\begin{cases} \alpha_{ult,k} = \dfrac{M_{pl,y,Rd}}{M_{max,Ed}} \\ \\ \alpha_{cr,op} = \dfrac{M_{cr}}{M_{max,Ed}} \end{cases} \rightarrow \quad \overline{\lambda}_{op} = \sqrt{\dfrac{\alpha_{ult,k}}{\alpha_{cr,op}}} = \sqrt{\dfrac{M_{pl,y,Rd}}{M_{cr}}} = \overline{\lambda}_{LT} \quad \rightarrow \quad \chi_{op} = \chi_{LT} \qquad (2.61)$$

and, in this case, the General Method exactly coincides with the application of clause 6.3.2 of EC3. Note also, that for the case of beams, the in-plane second order effects do not affect the in-plane resistance $\alpha_{ult,k}$ and therefore cross-section resistance is attained. As a result, both methods coincide.

2.4.2.4 Application to bending and axial force interaction

Consider the pin-ended beam-column of *Figure 2.11* subjected to an arbitrary axial force N_{Ed} and a uniform major axis bending moment $M_{y,Ed}$
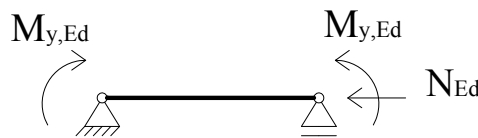
Figure 2.11: Pin-ended beam-column

Let

$$\alpha_{pl}^{N} = \frac{N_{pl,Rd}}{N_{Ed}} \qquad \alpha_{pl}^{My} = \frac{M_{pl,y,Rd}}{M_{y,Ed}} \qquad \phi = \frac{\alpha_{pl}^{My}}{\alpha_{pl}^{N}} \qquad (2.62)$$

Clause 6.3.3 of EN 1993-1-1 states that the safety of a beam-column requires the verification of the cross-section capacity at the member ends using an appropriate interaction expression such as Eq. (2.44) for I and H cross-sections, and the verification of the stability interaction formulae Eq. (2.42) and Eq. (2.43), see Section 2.3.5.2.

Assuming proportional loading (ϕ=constant) and class 1 or 2 cross sections ($N_{Rk}=N_{pl,Rd}$ and $M_{y,Rk}=M_{pl,y,Rd}$), an ultimate load multiplier can be defined with respect to the applied loading, given by

$$\frac{1}{\alpha_{b}^{6.3.3}} = \max\left(\frac{N_{Ed}}{\chi_z N_{pl,Rd}} + k_{zy} \frac{M_{y,Ed}}{\chi_{LT} M_{pl,y,Rd}} ; \frac{N_{Ed}}{\chi_y N_{pl,Rd}} + k_{yy} \frac{M_{y,Ed}}{\chi_{LT} M_{pl,y,Rd}} ; \frac{1}{\alpha_{pl}^{cs,ends}} \right) (2.63)$$

In Eq. (2.63), $\alpha_{pl}^{cs,ends}$ denotes for the cross section resistance multiplier regarding both member ends (see Eq.(2.46)). The application of the General Method leads to

$$\alpha_{b}^{GM} = \chi_{op}\alpha_{ult,k} \qquad (2.64)$$

Assuming the same applied loading N_{Ed} and $M_{y,Ed}$ and evaluating $\alpha_{ult,k}$ according to 6.3.3 gives

$$\frac{1}{\alpha_{ult,k}} = \max\left(\frac{N_{Ed}}{\chi_y N_{pl,Rd}} + k_{yy}^{in-pl} \frac{M_{y,Ed}}{M_{pl,y,Rd}} ; \frac{1}{\alpha_{pl}^{cs,ends}} \right) \qquad (2.65)$$

Note that Eq. (2.65) can only be considered for evaluation of the in-plane resistance if Method 2 (Annex B of EC3-1-1) is applied. As referred previously, only in Method 2 the in-plane and

out-of-plane behavior are separately considered in the both sets of equations of clause 6.3.3 of EC3-1-1. Comparing Eq. (2.63) and Eq. (2.64), gives:

$$\frac{\alpha_b^{GM}}{\alpha_b^{6.3.3}} = \chi_{op}\alpha_{ult,k}\max\left(\frac{N_{Ed}}{\chi_z N_{pl,Rd}} + k_{zy}\frac{M_{y,Ed}}{\chi_{LT}M_{pl,y,Rd}}; \frac{N_{Ed}}{\chi_y N_{pl,Rd}} + k_{yy}\frac{M_{y,Ed}}{\chi_{LT}M_{pl,y,Rd}}; \frac{1}{\alpha_{pl}^{cs,ends}}\right)$$
(2.66)

Or, considering also Eq. (2.65),

$$\frac{\alpha_b^{GM}}{\alpha_b^{6.3.3}} = \chi_{op}\frac{\max\left(\dfrac{1}{\chi_z} + \dfrac{k_{zy}}{\chi_{LT}\phi}; \dfrac{1}{\chi_y} + \dfrac{k_{yy}}{\chi_{LT}\phi}; \dfrac{\alpha_{pl}^N}{\alpha_{pl}^{cs,ends}}\right)}{\max\left(\dfrac{1}{\chi_y} + \dfrac{k_{yy}^{in\_pl}}{\phi}; \dfrac{\alpha_{pl}^N}{\alpha_{pl}^{cs,ends}}\right)}$$
(2.67)

According to clause 6.3.4(4) of EN 1993-1-1, the reduction factor χ_{op} may be determined from either of the following methods: (i) the minimum value of χ (for lateral buckling, according to clause 6.3.1 of EC3-1-1) or χ_{LT} (for lateral-torsional buckling, according to clause 6.3.2); (ii) an interpolated value between χ and χ_{LT} (determined as in (i)). In EC3-1-1, it is suggested that the formula for $\alpha_{ult,k}$ corresponding to the critical cross section is used. This leads to:

$$\begin{cases} \dfrac{N_{Ed}}{N_{Rk}} + \dfrac{M_{y,Ed}}{M_{y,Rk}} \le \chi_{op} \\ \dfrac{N_{Ed}}{\chi N_{Rk}} + \dfrac{M_{y,Ed}}{\chi_{Lt}M_{y,Rk}} \le 1 \end{cases} \Rightarrow \chi_{op} = \frac{\phi + 1}{\dfrac{\phi}{\chi} + \dfrac{1}{\chi_{Lt}}}$$
(2.68)

The values of χ and χ_{LT} considered for the reduction factor χ_{op}, are calculated with the global non dimensional slenderness $\overline{\lambda}_{op}$ of the structural component, determined from Eq.(2.52). According to Trahair (1993), the elastic critical bending moment and axial force are given by

$$\left(\frac{M_{y,cr,MN}}{M_{cr}}\right)^2 = \left(1 - \frac{N_{cr,MN}}{N_{cr,z}}\right)\left(1 - \frac{N_{cr,MN}}{N_{cr,T}}\right) \qquad (2.69)$$

where M_{cr} is the elastic critical bending moment, $N_{cr,z}$ is elastic critical compressive buckling force in a bending mode about the z-z axis and $N_{cr,T}$ is the elastic critical compressive buckling force in a torsional mode. Eq. (2.69) is valid for beam-columns with constant bending moment distribution. To adapt the equation to other types of bending moment distribution, see Trahair (1993). Finally, introducing $\phi = \dfrac{N_{pl,Rd}/N_{\max}}{M_{pl,y,Rd}/M_{y,\max}}$ in Eq. (2.69) leads to ($N_{cr,MN}$, $M_{y,cr,MN}$), so that $\alpha_{cr,op}$ is given by:

$$\alpha_{cr,op} = \frac{N_{cr,MN}}{N_{Ed}} = \frac{M_{y,cr,MN}}{M_{y,Ed}} \qquad (2.70)$$

Results of Eq. (2.67) are now analysed for a range of profiles, loading and lengths, with the aim to compare the results from General Method with clause 6.3.3, and find any trends. The cross sections were chosen in order to enclose a range of profiles with several depth/width ratios, and consist of class 1 or 2 cross sections.

Concerning all results, comparing the General Method with Method 2 (for determination of $\alpha_{ult,k}$) using Eq. (2.67) leads to a variation of results between 81% and 113%, as shown in *Table 2.6*:

Table 2.6: All results of Eq. (2.67) for $\phi=1$ – n=80 for each case ; $\chi_{op}= \min(\chi_z;\chi_{LT})$

Fabrication Process	Bending Moment	EC3 Method 2	
		Min.	Max.
Hot Rolled	All	84.4	112.3
	$\Psi=1$	87.7	109.8
	$\Psi=0$	87.0	108.2
	$\Psi=-1$	84.4	101.2
	Conc.	90.0	111.1
	Dist.	89.0	112.3
Welded	$\Psi=1$	94.4	110.3

Figure 2.12 illustrates the results for rolled cross sections. Results are plotted for a range of member lengths between $\overline{\lambda}_z$=0.5 and $\overline{\lambda}_z$=2.5 for ϕ=1. χ_{LT} is calculated according to the General Case from EC3-1-1, and $\chi_{op}= min\ (\chi_z;\chi_{LT})$.

(a) Constant bending moment   (b) Triangular bending moment
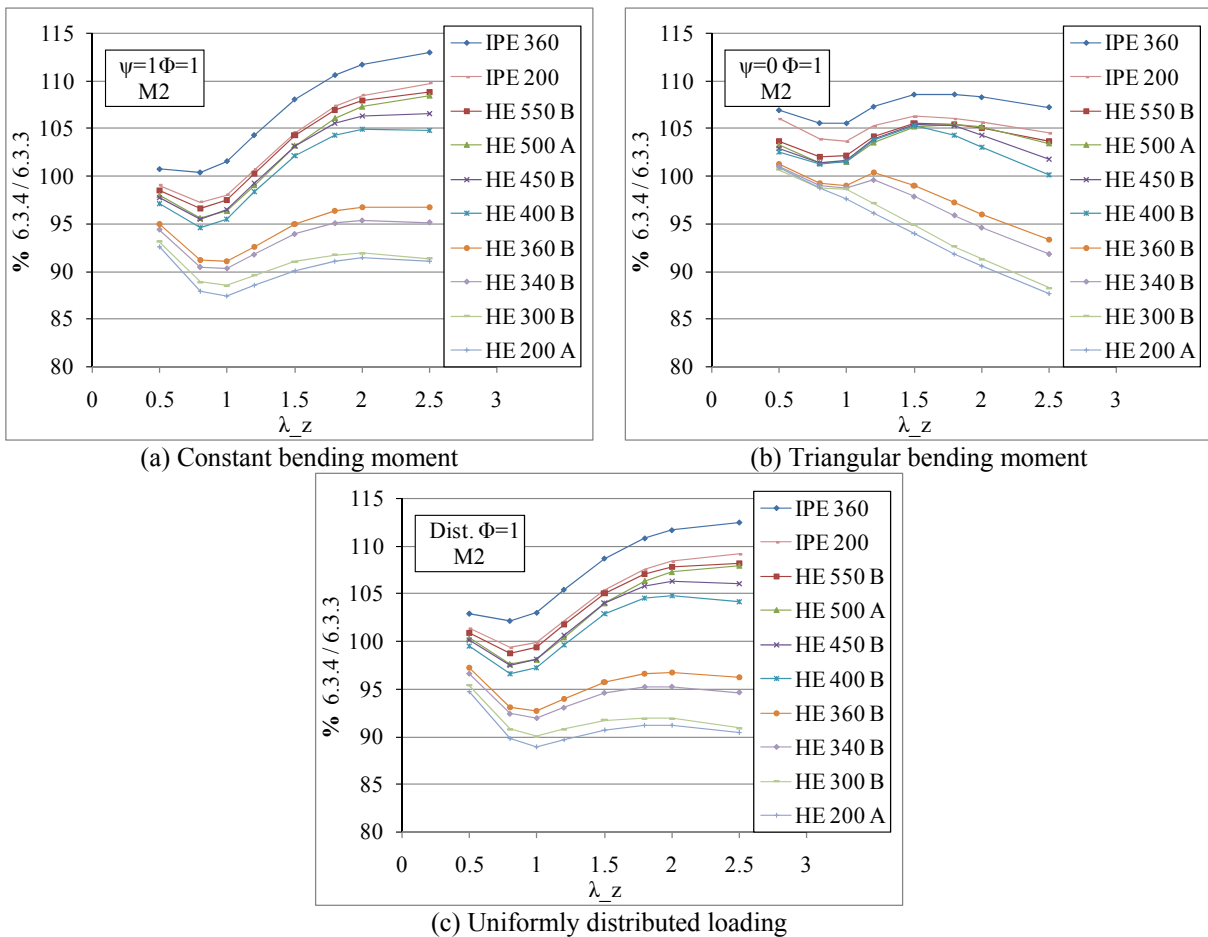
(c) Uniformly distributed loading
Figure 2.12: Fig. 9 Results of Eq. (2.69)

When *Figure 2.12* is analyzed, it is seen that for more slender cross sections (larger *h/b*), the General Method is less conservative. Again, the results also tend to concentrate in groups according to the buckling curve, see *Table 2.7*.

Table 2.7:Buckling curves for rolled cross sections (General Case for LTB)

Cross sections	Buckling curve – FBzz	Buckling curve - LTB
IPE 360	b	b
IPE 200 HEB 550 – HEB 400	b	a
HEB 360 – HEA 200	c	a

Consider now *Figure 2.13* which represents the results for a HEB 300 for uniform moment (Ψ=1), with different ratios of $\phi=\alpha_{pl}{}^{M}/\alpha_{pl}{}^{N}$:
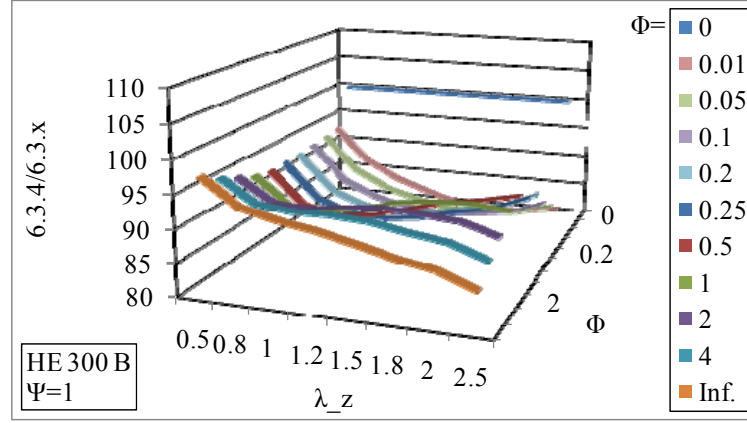
Figure 2.13: Results of Eq. (2.67) – beam-columns; Eq. (2.60) – columns; or Eq. (2.61) – beams; Ψ=1; HEB 300; Method 2

An inconsistency around $\phi=0$, i.e., high bending moment relatively to the axial force is observed: for $\phi=0$ (lateral torsional buckling), the results are calculated using Eq. (2.61), that is, $\chi_{op}=\chi_{LT}$ while for $\phi>0$ Eq. (2.67) is used whereby $\chi_{op}= min(\chi_z, \chi_{LT})= \chi_z$ in this case of a HEB 300 profile.

In general, taking χ_{op} as the minimum value between χ_z or χ_{LT}, for $\phi=0$, in case the reduction factor χ_z is smaller than χ_{LT}, the above discontinuity will be observed. For $\phi=\infty$, i.e., high axial force relatively to bending moment and in case reduction factor χ_{LT} is smaller than χ_z the same inconsistency is observed. However, if χ_{op} is calculated with Eq. (2.68) (interpolated value between χ_z and χ_{LT}), the discontinuity in the interaction curve disappears, as

$$\chi_{op} = \frac{\phi+1}{\dfrac{\phi}{\chi}+\dfrac{1}{\chi_{Lt}}} \Rightarrow \begin{cases} \lim\limits_{\phi \to 0} \chi_{op} = \chi_{Lt} \\ \lim\limits_{\phi \to \infty} \chi_{op} = \chi \end{cases} \tag{2.71}$$

To illustrate this, two cases are chosen such that: (a) $\chi_z < \chi_{LT}$ and (b) $\chi_{LT} < \chi_z$. The results are plotted in the interaction curves of *Figure 2.14*, considering the results of Eq. (2.64) – clause

6.3.4 for beam-columns. For comparison, results of Eq. (2.59) – clause 6.3.4 for columns; Eq. (2.61) – clause 6.3.4 for beams; and Eq. (2.63) – clause 6.3.3, are also plotted.

$$\text{(a)} \quad \chi_z < \chi_{LT} \qquad\qquad \text{(b)} \quad \chi_{Lt} < \chi_z$$

Figure 2.14:Interaction curves regarding the value of χ_{op}
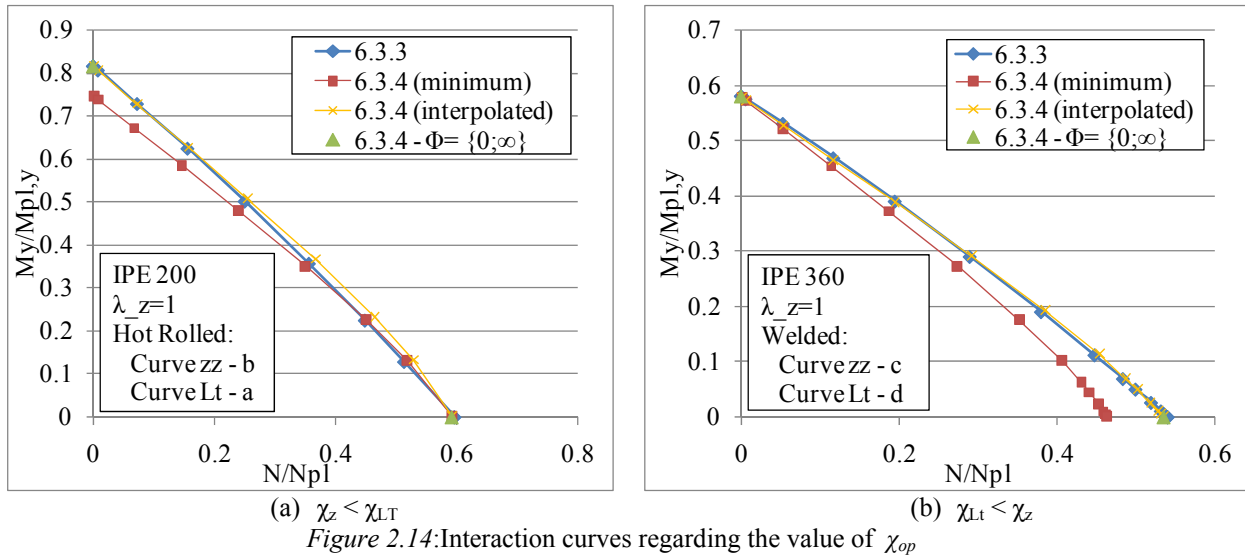
Using an interpolated value of χ and χ_{LT} leads to more accurate results in a way that the referred discontinuities are avoided. Nevertheless, if such an interpolation is to be proposed in the future, a more detailed study is needed in order to establish the limits of the application of the reduction factor χ_{op} along the interaction curve, as also pointed out by Taras (2010): whereas the interpolation curve χ_{op} provides a smooth transition between the curve χ_{LT} and χ_z (with varying ϕ), the real curve (i.e. GMNIA curve) does not vary continuously between the extremes $\phi=0$ and $\phi=\infty$, as it may seem by analyzing results in the interaction curve representation (instead of in a buckling curve representation). This means that although the interpolation in Eq. (2.71) may solve the discontinuities in the limits of the interaction curve ($\phi=0$ and $\phi=\infty$), it still does not describe with sufficient accuracy the mechanical behavior of the beam-column with varying ratios of $N_{Ed}/M_{y,Ed}$, i.e., in intermediate ϕ. This will be explored in Chapter 6 for the case of tapered members.

To illustrate this, a IPE200 with $\bar{\lambda}_z=0.5$ and varying ϕ is given in *Figure 2.15*. In *Figure 2.15(a)* results are represented in the buckling curve format, whereas in *Figure 2.15(b)* results are represented in the interaction curve format, such that the curve regarding the interpolation

is given by $(\overline{\lambda}_{op}; \chi_{op})$. For the general method results, Eq. (2.64) is solved with the derived formula for the interpolated value of χ_{op}, Eq.(2.68). The GMNIA curve is given by

$$\overline{\lambda}_{op} = \sqrt{\alpha_{ult,k}^{6.3.3} / \alpha_{cr}^{LBA}} \qquad \text{and} \qquad \chi_{op} = \alpha_b^{GMNIA} / \alpha_{ult,k}^{6.3.3} \qquad (2.72)$$

from which $\alpha_{ult,k}^{6.3.3}$ is given by Eq. (2.65) (i.e., evaluation of the in-plane buckling resistance according to clause 6.3.3).
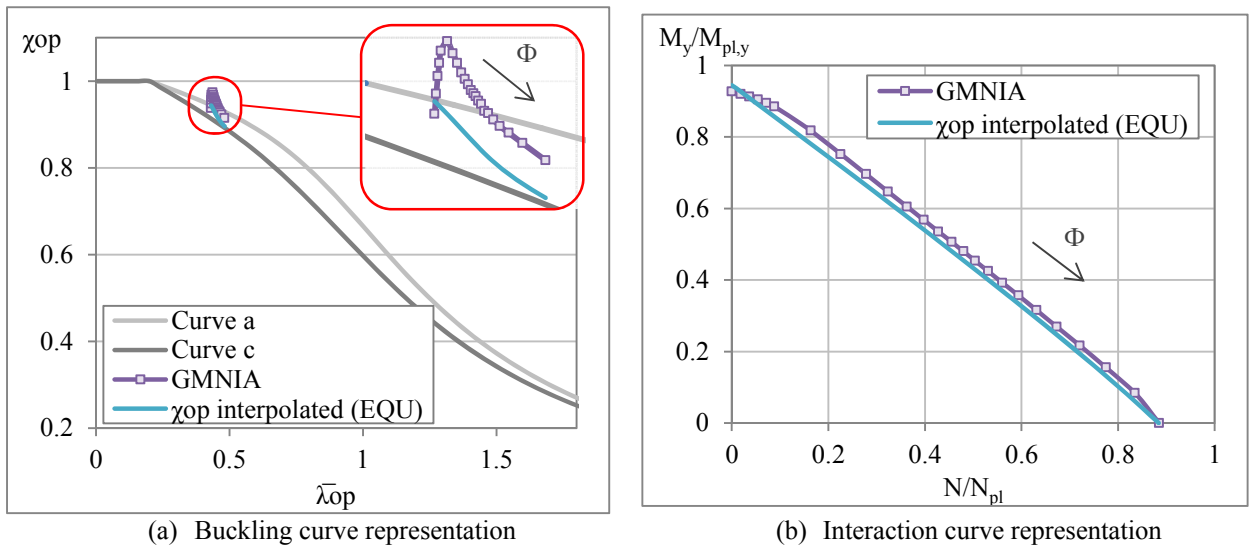
(a) Buckling curve representation   (b) Interaction curve representation
Figure 2.15:Analysis of the interpolation of χ_{op}

It is shown in *Figure 2.16* that considering Eq. (2.71) does not lead to unsafe levels of resistance. *Figure 2.16* illustrates the mean values ±1 standard deviation of the ratio $\alpha_b^{GMNIA}/\alpha_b^{Method}$ for several intervals of ϕ, regarding 606 beam element simulations from the PhD thesis of Ofner (1997), see Simões da Silva *et al.* (2010a) for details. It is here visible that the interpolation of χ gives less conservative results than the minimum. Although it also leads to higher resistance than clause 6.3.3, it is always on the safe side relatively to GMNIA analysis. However, the conservatism associated to these results will be discussed in Section 2.4.2.5.
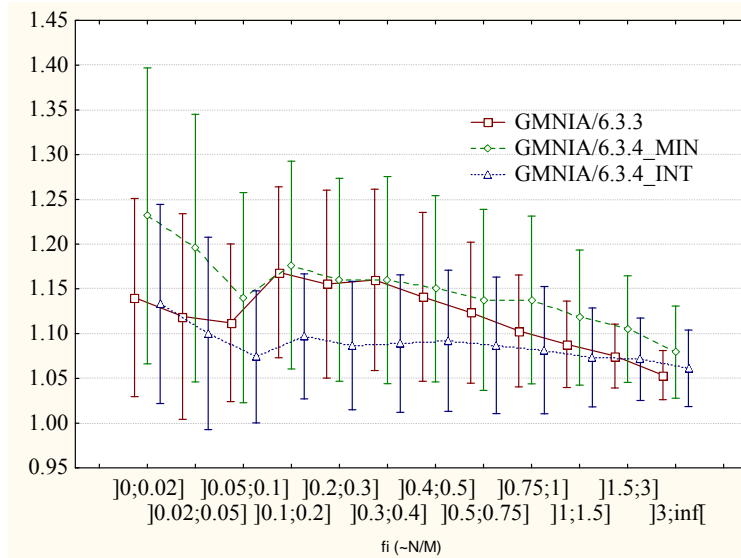
Figure 2.16:Mean values with vertical bars denoting ±1 standard deviation of the ratio $\alpha_b^{GMNIA}/\alpha_b^{Method}$ cases plotted against the defined sub-sets of Φ

Finally, in terms of numerical results, a full 3D GMNIA analysis yields the highest resistance, see Simões da Silva *et al.* (2010). A statistical evaluation was also carried out in the referred study. The evaluation of the safety factor γ_{Rd} according to Annex D of EN 1990 (2002) demonstrates that the General Method becomes more conservative with the increase of the length of the member (*Figure 2.17*). Finally, as also observed previously, more slender cross sections lead to higher safety factors. The evaluation of the partial safety factor, γ_{Rd}, is carried out according to the procedure described in detail by Rebelo *et al.* (2009).
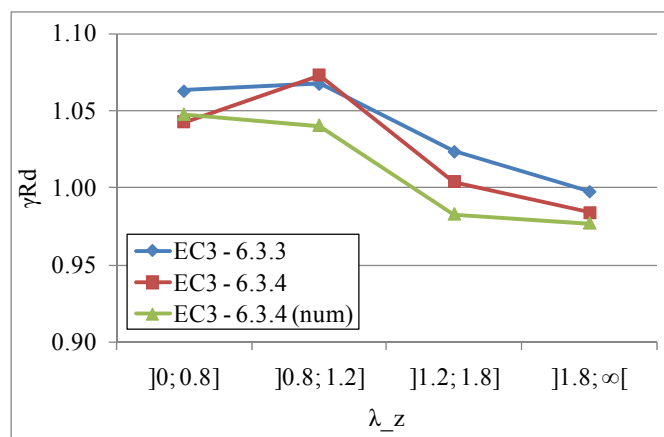
Figure 2.17:Variation of safety factor γ_{rd} with slenderness, χ_{op}=min(χ; χ_{LT}); χ_{LT} evaluated according to the General Case of clause 6.3.2; and $\alpha_{ult,k}$ evaluated according to Method 1 of EC3-1-1.

2.4.2.5 Some comments on the value of $\alpha_{ult,k}$

It was shown in Section 2.4.2.2 that the consideration in-plane local imperfections in the multiplier $\alpha_{ult,k}$ for the out-of-plane flexural buckling verification of columns gives inconsistent results with clause 6.3.1.

This definition was adopted in clause 6.3.4 because the consideration of the cross section resistance load multiplier (with no local imperfections) may sometimes lead to unsafe results for the stability verification of beam-columns, even if the minimum between χ_z and χ_{LT} is considered (Ofner and Greiner, 2005).

To differentiate the two alternatives, the following nomenclature is considered in the thesis:

- General Method in its current format, in which $\alpha_{ult,k}$ is evaluated considering in-plane local imperfections $- \bar{\lambda}_{op}$ and χ_{op} are considered for illustration of results;

- Modification of the General Method, in which $\alpha_{ult,k}$ is evaluated excluding second order local effects. For a simply supported member, this corresponds to the cross section capacity. The subscript "op" (*out-of-plane*) is then replaced by "ov" (*overall*) (in the more general format of generalized slenderness procedures).

Figure 2.18 reproduces one example given in Taras and Greiner (2006) for a simply supported beam-column with $\bar{\lambda}_z = 0.75$ subject to constant bending moment and axial force with a hot-rolled cross section IPE500. From *Figure 2.18(b)*, it is seen that the minimum reduction factor χ_{ov} is given by the minimum ratio between the distances to the origin of the cross section resistance interaction curve and the GMNIA curve. For this case, it is achieved at ϕ=0.2. In *Figure 2.18(a)*, $\chi_{ov,GMNIA}=\alpha_{b,GMNIA}/\alpha_{ult,k}$. Note that for the lateral-torsional buckling curve, the more adequate developed buckling curves for lateral-torsional buckling (Taras, 2010) are adopted.

(a) Buckling curve representation   (b) Interaction curve representation
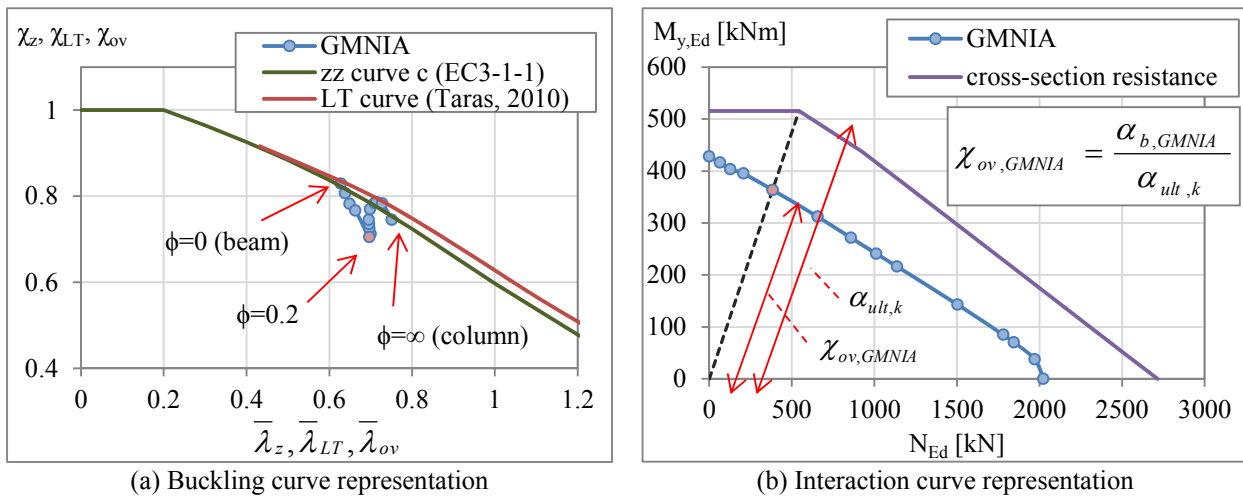
Figure 2.18 Example of a member which χ_{ov} is lower than both χ_z and χ_{LT}

As a result, if the upper bound of the member resistance is then reduced, it may avoid the existence of unconservative cases in which the in-plane bending moment significantly reduces the out-of-plane resistance of the beam-column. Another possibility was given in Ofner and Greiner (2005), in which $\alpha_{ult,k}$ is determined considering the cross section capacity. Here, an amplification of the flexural buckling imperfection factor α is performed, which accounts for the bending moment deflection of the respective bending moment distribution. The resultant buckling curve χ_{ov} is then determined considering this imperfection. This proposal leads to fairly accurate results for the case of in-plane flexural buckling or out-of-plane flexural buckling. However, if lateral-torsional buckling is a potential mode, the method becomes less accurate.

Regarding the given approach in EC3-1-1 (in which $\alpha_{utl,k}$ is decreased), it leads to over conservative resistance if the in-plane effects are of the same magnitude as the out-of-plane effects (for example, RHS sections), see Greiner and Ofner (2005); Ofner and Greiner (2005); Taras and Greiner (2006); or Taras (2010). Although this definition aims at accounting for the destabilizing effect of the in-plane bending moment on the out-of-plane resistance (Greiner and Ofner, 2005), this is not significant for all cases – for example, an in-plane bending moment distribution $\psi=-1$ will have a much lower destabilizing effect on the out-of-plane instability than a bending moment distribution $\psi=1$. As a result, for the first case, the reduction of the cross section capacity will be too restrictive.

As a result, the fact that safe results are obtained either for the minimum or for the interpolation given in Section 2.4.2.4 may be purely due to the fact that a lower estimate of the maximum capacity is set. Because this assumption does not truly correspond to the main reason of the generalized reduction factor being smaller than the minimum of χ_z and χ_{LT}, it is possible that this approach may, at some point, give unsafe levels of resistance.

In the given parametric study of Section 2.4.2.4 note that, for the determination of χ_z and χ_{LT}, EC3-1-1 rules were considered, which are already a safe assumption relatively to the real χ_z and χ_{LT} *GMNIA* results. If the latter would have been considered, surely lower $\alpha_b^{GMNIA}/\alpha_b^{Method}$ (*Figure 2.16*) values would be achieved.

In summary, to be mechanically consistent, this buckling resistance reduction should not be accounted for by such a restriction of the cross section capacity especially considering local in-plane effects that in reality do not have such high effect in the out-of-plane buckling resistance all the times. In other words, the resistance reduction should be considered afterwards in the generalized reduction factor and not applied to $\alpha_{ult,k}$. These aspects concerning a generalized slenderness concept are analyzed more in detail in Chapter 6, considering tapered beam-columns as case of study.

2.4.3 Treatment of non-uniform members

In the verification of the resistance of a non-uniform member, several assumptions have to be considered, which are not clear for the designer, as they are neither defined nor explained in the codes. These have been previously discussed in Section 1.1 and are: (i) evaluation of the design cross-section; (ii) definition of the cross-section class; and (iii) definition of the buckling curve. In Simões da Silva *et al.* (2010b) the stability verification of a web-tapered beam-column subject to uniformly distributed bending moment and constant axial force is performed, covering these aspects.

Given that there are various options for the application of the General Method, *Figure 2.19* summarizes the procedures for the calculation of the ultimate load factor, for the more general

case of beam-columns. Although for a tapered member $\alpha_{ult,k}$ should be evaluated numerically (as there are currently no guidelines to determine $\alpha_{ult,k}$ analytically – as defined in the code i.e. accounting for in-plane <u>local</u> and global second order effects and imperfections), the theoretical approach of the General Method is also considered for verification of resistance.
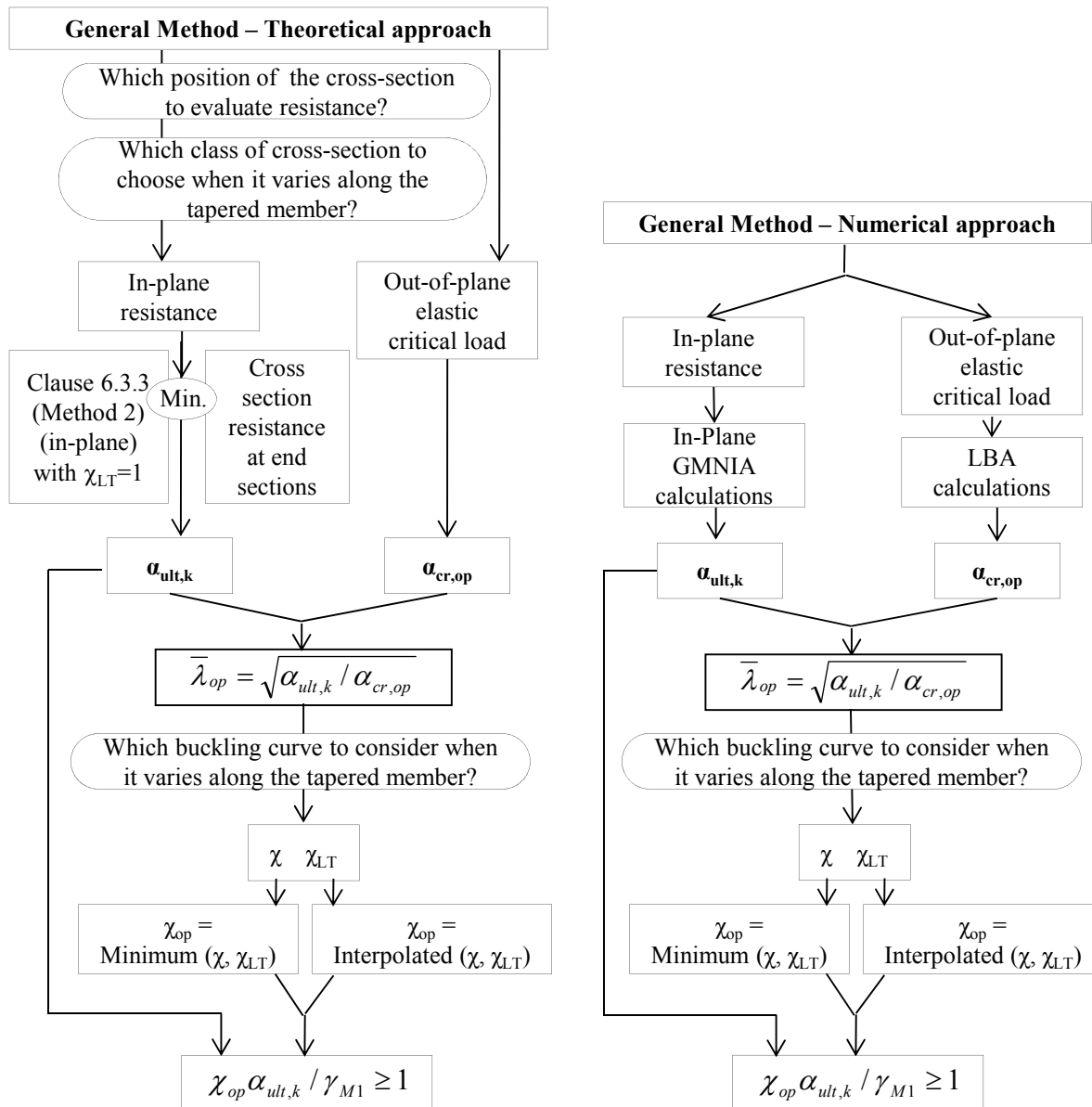
(a) According to clause 6.3.4 – analytical expressions   (b) According to clause 6.3.4 – numerical calculations
Figure 2.19: Stability verification of the member according to the General Method

Numerical evaluation of the General Method should simplify the procedure regarding all the questions which arise when verifying the buckling resistance of a tapered member. However,

when analyzing *Figure 2.19* it seems that the main problem of its application lies in the correct definition of the buckling curve as already discussed. Throughout Chapters 4 to 6 application of EC3-1-1 buckling curves is shown not to be proper.

2.4.4 Final remarks

For prismatic members, it is possible to directly evaluate the resistance using the General Method (6.3.4) evaluating $\alpha_{ult,k}$ according to 6.3.1 to 6.3.3 and $\alpha_{cr,op}$ according to Eq. (2.70), leading to similar results, except for the extremes of the interaction curve. In such regions of the interaction curve, the minimum value of χ and χ_{LT} might not correspond to the real type of buckling mode. Using an interpolated value of χ and χ_{LT}, see Eq. (2.68), solves at least this problem. However, a more detailed parametric study is needed in order to establish the limits of the application of the reduction factor χ_{op}. The definition of $\alpha_{ult,k}$ was also seen to be inconsistent from the mechanical point of view. In addition, concerning the "generality" of the general method there is no clear definition given, however it becomes obvious that it is restricted to open sections and hollow sections are excluded. For those aspects and limitations the generality is mainly based on general forms of open cross sections and with out-of-plane behaviour, so that the term "general" method is questionable.

Regarding non-uniform members, when in-plane GMNIA and LBA numerical simulations are considered to evaluate resistance according to the General Method, it is possible to avoid the difficult task of classifying the cross-section and knowing the position of the critical cross-section for use of its properties in the verification of stability. On the other hand, the definition of the buckling curve is still unclear.

As a result, in Chapter 4 and 5, adequate analytically based procedures for stability verification of web-tapered members are developed. These are further applied to beam-columns in Chapter 6 in which the application of the General Method is again analyzed.

2.5 Possible methods for the structural analysis

2.5.1 Introduction

The structural analysis methods described in *Figure 2.1* are analyzed in the following. Firstly, second order analysis may or may not be necessary depending on the relevance of the internal forces caused by deformations. In EC3-1-1, this condition may be assumed to be fulfilled if the following is satisfied:

$$\alpha_{cr} = \frac{F_{cr}}{F_{Ed}} \geq 10 \quad \text{for elastic analysis}$$
$$\alpha_{cr} = \frac{F_{cr}}{F_{Ed}} \geq 15 \quad \text{for plastic analysis}$$

(2.73)

where α_{cr} is the multiplier of the design loading which causes elastic instability in a global mode; F_{Ed} is the design loading on the structure; F_{cr} is the elastic critical buckling load for global instability mode based on initial elastic stiffnesses.

If second order analysis is required, second order internal forces may be determined either by a precise second order analysis including step-by-step or other iterative procedures, or by the amplification of the first order internal forces (several approximate procedures may be found in the literature, see for example Simões da Silva *et al.* (2010b)).

Regarding imperfections, global and local imperfections shall be taken into account according to clause 5.3 of EC3-1-1, respectively for frames and bracing systems and for individual members. The shape of imperfections may be derived from an elastic buckling analysis considering the relevant modes. Also, the most unfavorable direction and form should be considered.

Regarding the member imperfection, individual bow imperfection shall be considered (by an amplitude of the bow imperfection e_0, see also *Table 1.1* of this thesis). For frames sensitive

to buckling in a sway mode, global imperfections shall be accounted for in form of an initial sway imperfection (on the structure level – global imperfection ϕ, see EC3-1-1).

In a simplified way, imperfections may be replaced by equivalent forces, see *Figure 2.20*.
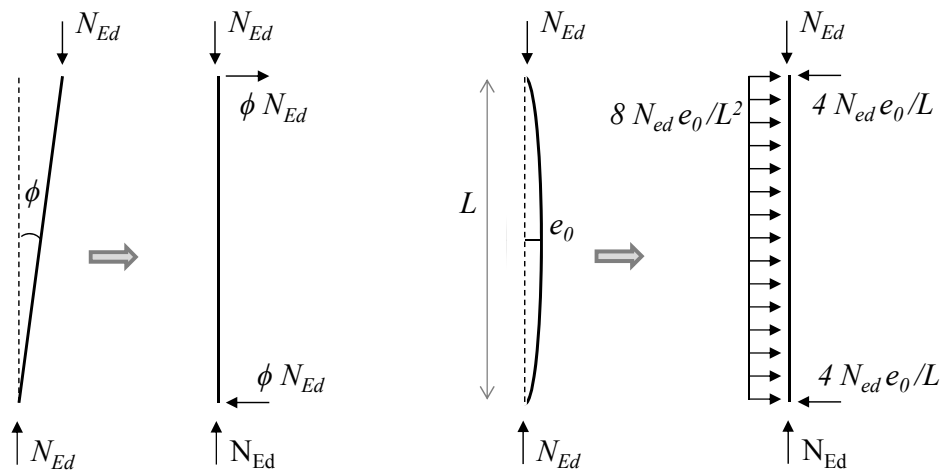
Figure 2.20: Imperfections and corresponding equivalent horizontal forces

Following EC3-1-1, there are mainly three levels of analysis.

- Level 1: Second order analysis accounting for all the effects and imperfections – global and local (clause 5.2.2 a) of EC3-1-1). It becomes only necessary to check the cross-section resistance of the member;

- Level 2: Second order analysis considering only global effects and global geometrical imperfections (clause 5.2.2 b) of EC3-1-1). This method is the most commonly used. The stability verification of the members according to clauses 6.3.1 to 6.3.3 is carried out considering the buckling length of the member as the non-sway buckling length;

- Level 3: First order analysis of the structure (clause 5.2.2 c) of EC3-1-1). Neither imperfections nor second order effects are included in the analysis of the structure and, as a result clauses 6.3.1 to 6.3.3 of EC3-1-1 must be verified considering the buckling length of the member defined according to the global buckling mode of the structure.

In Section 2.5.2, an example is given in order to illustrate the implementation of the several approaches (or even combination of those). Sections 2.5.2.2, 2.5.2.3 and 2.5.2.4 respectively correspond to the above-defined levels of analysis 1, 2 and 3. Because many times it is practical to mix the described methods of analysis, in Section 2.5.2.5 possible combinations are described.

2.5.2 Example

2.5.2.1 Introduction

Consider the frame of *Figure 2.21* with a similar configuration as in the frames presented in *Figure 1.10* of Chapter 1 – a typical configuration for frames with tapered members. For illustration of the problem (verification is focused at the structural level and not at the member level), the frame is assumed to be composed of prismatic members such that member stability verification formulae are applicable.

Consider also that the frame is unrestrained with respect to out-of-plane displacements at the top of the left column but braced at the apex and top of right column. Second order local and global effects and imperfections shall be considered in both directions (*y-y* and *z-z* are respectively the in-plane and out-of-plane member axis; LT stands for lateral-torsional) and are illustrated in *Figure 2.21* and *Figure 2.22*. The frame is also assumed to be sensitive to buckling in a sway mode. In *Figure 2.21* and throughout Section 2.5.2, red illustrates in-plane global imperfections; green illustrates out-of-plane global imperfections and yellow illustrates local member imperfections (in-plane, out-of-plane or both, depending on type of analysis).
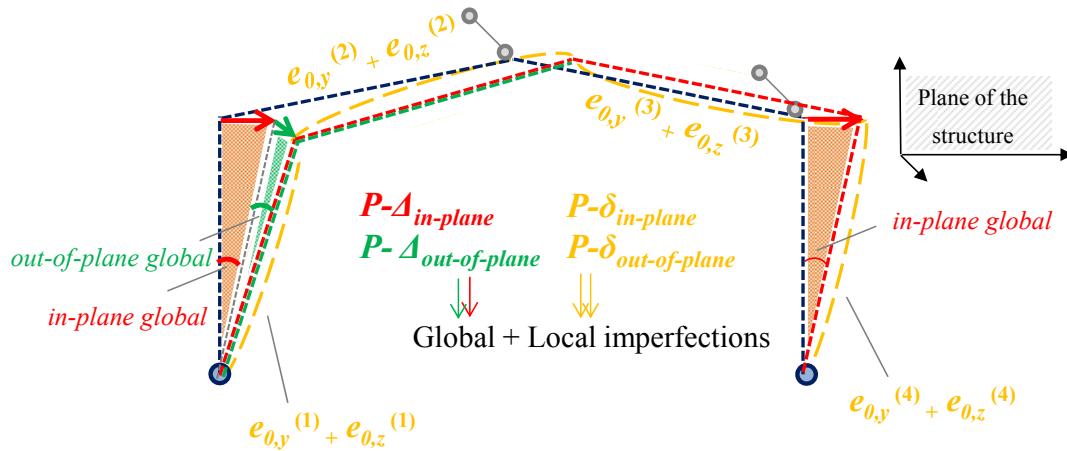
Figure 2.21: Frame subject to in-plane and out-of-plane second order effects
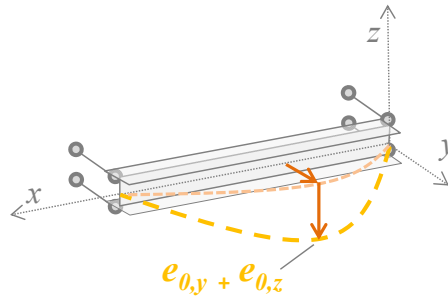
Figure 2.22: In-plane and out-of-plane bow imperfections

2.5.2.2 Second order analysis accounting for all the effects and imperfections

Level 1 corresponds to the case in which second order analysis accounting for all the effects and imperfections – global and local (illustrated in *Figure 2.21*) – is performed. It becomes only necessary to check the cross-section resistance of the member at a sufficient number of cross sections, as all stability effects are already included in the structural analysis. The consideration of local effects and imperfections in the analysis of the structure might not be simple if it is done analytically (by approximate methods) and, therefore, if this method is chosen, numerical analysis is preferred.

2.5.2.3 Second order analysis considering only global effects and global geometrical imperfections

The second level may be defined as a second order analysis considering only the global effects and global geometrical imperfections. This method is the most commonly used. As the global effects are already considered in the analysis of the structure, the stability verification of the members according to clauses 6.3.1 to 6.3.3 is much simpler. For this alternative, the buckling length of each member may be considered as the non-sway buckling length or, on the safe side, as the real length (Boissonnade et al, 2006). For example, assume that the column was fixed at the base – $L_{cr,column}$ shall be safely considered as L_{column}. In fact, note that the buckling length is never exactly the same as the member length because the restraining provided by the adjacent parts of the structure does not exactly coincide with the idealized fork conditions.
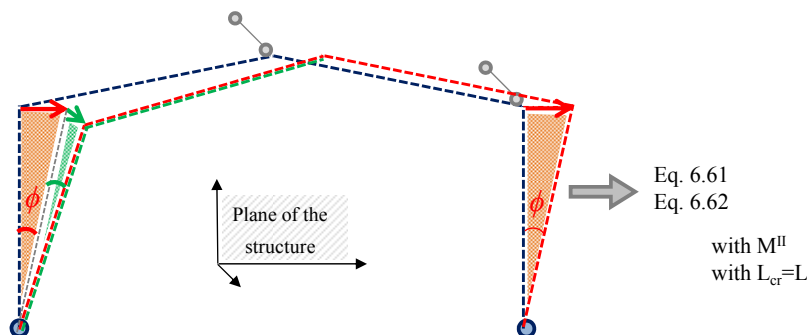
Figure 2.23: Verification according to a second order analysis with global effects

2.5.2.4 First order analysis of the structure

The third level may be defined by a first order analysis of the structure. Neither imperfections nor second order effects are included in the analysis of the structure, i.e., first order bending moments are considered for the verification. In order to account for these effects, a stability verification of each member has to be performed. In EC3-1-1, for the case of prismatic members this is done by applying the interaction formulae of clauses 6.3.1 to 6.3.3 of EC3-1-1 (members in bending and/or axial compression). Regarding clause 6.3.3 (beam-columns), equations 6.61 and 6.62 of EC3-1-1 shall be verified (respectively Eq. (2.42) and Eq. (2.43) of

this thesis). The difficulty of this method lies in the determination of the buckling length of the member which has to be defined according to the global buckling mode of the structure. In the example of *Figure 2.21*, see now *Figure 2.24*, the stability verification has to be performed for each member considering for each case the global buckling lengths. In Greiner and Lechner (2007), an example of a frame illustrates the determination of in-plane and out-of-plane global buckling lengths.
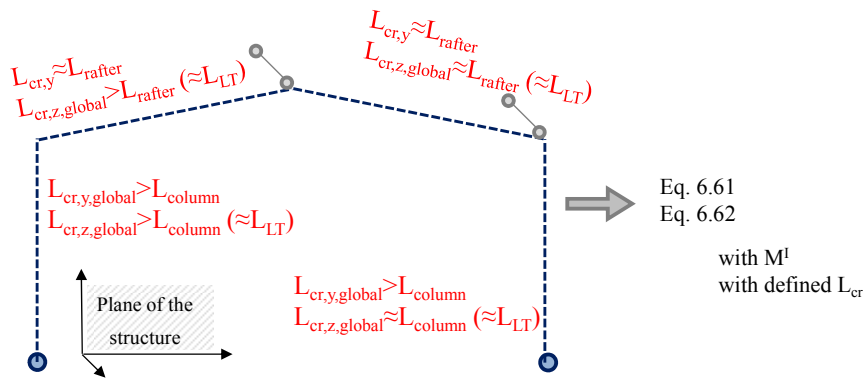
Figure 2.24: Verification according to first order analysis of the structure

2.5.2.5 Combination between the methods of analysis

For practical reasons the described methods may be combined in order to lead to more simple verification. In this section, the following is considered:

a) Level 1 and Level 3: In-plane global and local imperfections are considered in the structural analysis (level 1) such that no in-plane stability member verification needs to be carried out. On the other hand, out-of-plane (global and local) stability verification is performed by member design formulae considering adequate out-of-plane buckling lengths (level 3);

b) Level 2 and Level 3: only global effects and imperfections are considered in the structural analysis and stability must be checked individually for each member (level 2). However, because global out-of-plane imperfections may not be simple to define, only in-plane global imperfections are considered in the structural analysis by ϕ. As a result, in the

member design formulae adequate out-of-plane buckling lengths must be considered (level 3).

a) Level 1 and Level 3

Because the difficulty in combining in-plane and out-of-plane imperfections increases with the complexity of the structure, and also because many available software provide more reliable in-plane (than 3-D) second order calculations (see also Greiner and Lechner, 2007), a combination between the described methods of analysis – 1 (global and local second order effects in the structural analysis) and 2 (only global effects in the structural analysis) may be considered.

For example, when only in-plane effects and imperfections are considered (global and local), only <u>out-of-plane</u> stability verification procedures from clauses 6.3.1 to 6.3.3 need to be considered as all in-plane instability effects are already contemplated in the structural analysis. However, if this alternative is chosen, the second order moments to be considered in the stability verification formulae should only account for the global in-plane imperfections as considering the local imperfections may be too restrictive for the required <u>out-of-plane</u> check, this was discussed in Section 2.4.2 concerning the consideration of in-plane local imperfections in the definition of $\alpha_{ult,k}$.

Out-of-plane member verification may be verified as follows:

- If Method 1 of Annex A is used, both equations 6.61 and 6.62 shall be verified as in-plane and out-of-plane behavior is not considered separately by the interaction factors of those equations. The reduction factor χ_y, however, is considered as 1;

- On the other hand, if Method 2 of Annex B is used, the interaction factors equations 6.61 and 6.62 were calibrated such that in-plane and out-of-plane member effects are represented separately in each of the equations, respectively. The question arises now on another possibility regarding the inclusion of the lateral-torsional buckling effect in the in-plane resistance (i.e. replacing the check by equation 6.61) – should the resistant moment in the cross section check (from the in-plane global and local structural analysis)

be reduced by χ_{LT}? This latter alternative may be useful for the verification of tapered members in structures, as will be discussed in Chapter 6.

Illustration of the latter procedure is given in *Figure 2.25*, both for Method 1 and Method 2 of clause 6.3.3.
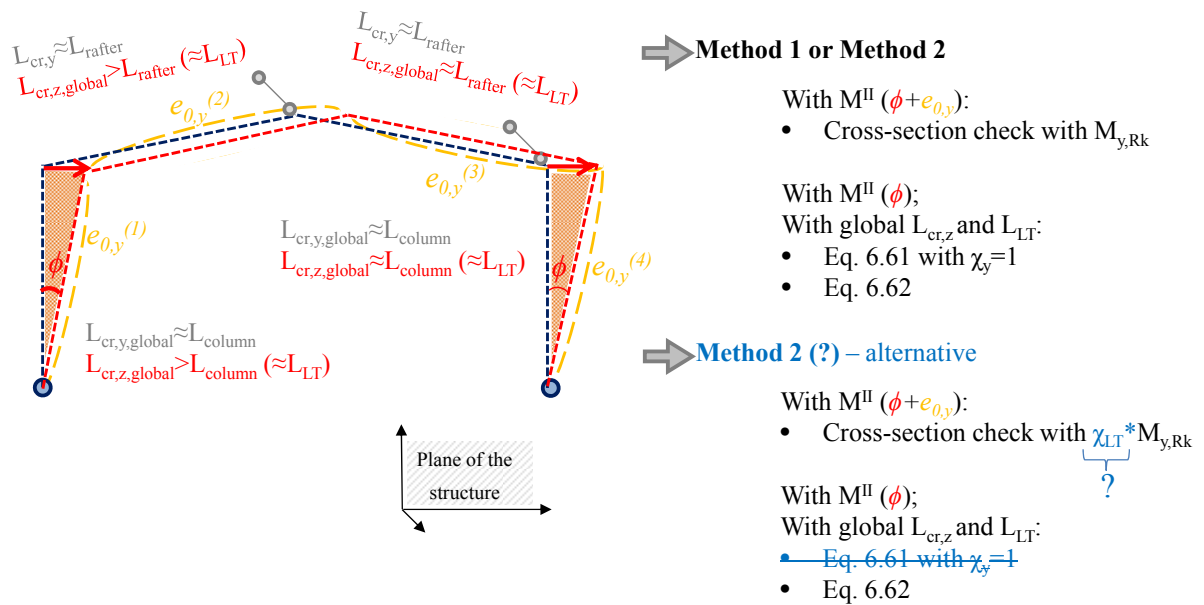
Figure 2.25: Verification according to a second order analysis with in-plane global and local effects only

b) Level 2 and Level 3

In EC3-1-1, in-plane global imperfections are determined by ϕ. Out-of-plane global imperfections are not as simple to define and to separate from the local (zz or LT) imperfections. Because of this, a combination between the second and third procedures above described can be adopted in which, for the out-of-plane behavior, the global buckling critical length shall be determined (level 3). As a result, for the structural analysis, only in-plane global imperfections are considered, see *Figure 2.26*.
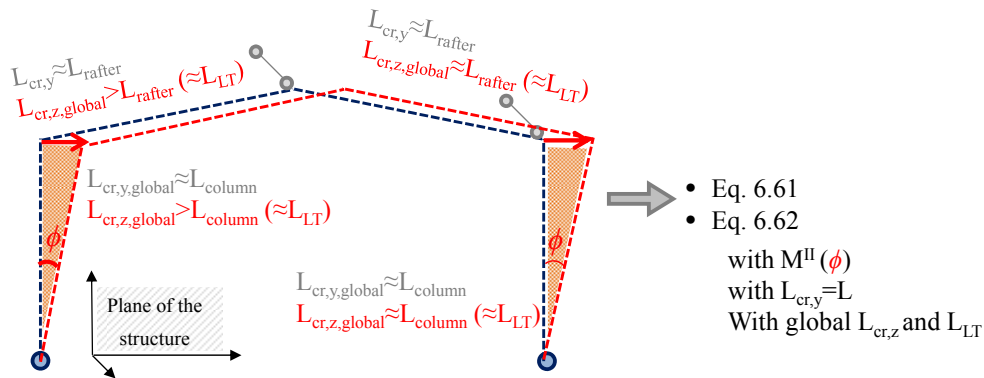
Figure 2.26: Verification according to a second order analysis with in-plane global effects only

2.6 Non-linear analysis of structures by FEM

2.6.1 Introduction

Design of steel structures by FEM allows for a more accurate representation of the physical phenomena that dictate the ultimate limit states of these structures. However, the added accuracy in the estimation of the behavior of a steel structure or component leads to increased complexity (Simões da Silva *et al.*, 2011).

When checking the strength capacity by the so called GMNIA analysis, complex shaped structures are verified more directly, as the assumption of coefficients regarding bending moment distributions, boundary conditions or properties of the cross-section are not necessary to be defined. However, the preparation of the data files is difficult and time-consuming; required data is missing or uncertain; and the physical interpretation and validation of results is not easy (Simões da Silva and Gervásio, 2007; Rebelo *et al.*, 2009).

Many aspects have to be carefully taken into account such as:

(i) modeling of the structure or structural component and their respective boundary conditions;

(ii) choice of software and its respective documentation;

(iii) modeling of the materials' properties;

(iv) use of imperfections;

(v) modeling of loads;

(vi) specification of the criteria for limit states;

(vii) selection of partial coefficients to adopt.

Moreover, a full calculation is needed for each load combination because of structural non-linearity.

2.6.2 Modeling

2.6.2.1 General aspects

The modeling of the structure is of major importance to characterize its real behavior. Features like the material law, imperfections, boundary conditions, or loading shall be correctly included in the model. One of the advantages that the analysis by FEM provides is the possibility of modeling only a component of the structure (as long as the boundary conditions are chosen in order to lead to results on the safe side (CEN, 2006)). This reduces the calculation time and the computer effort. However, it requires a greater attention to the modeling of the boundary conditions, namely supports and loading.

Concerning the type of finite element, it must be chosen according to the type of problem. Shell elements are able to overcome certain limitations of beam elements, e.g.: in a class 4 cross-section the calculation of the effective cross-section becomes unnecessary (as long as proper local imperfections are considered); or the "shear lag" effect, which is not characterized if beam elements are used. In addition, attention must be paid to the formulation of the existing beam elements – some elements might not consider e.g. the warping of cross-sections. On the opposite extreme of beam elements, solid elements should only be considered for the modeling of complex situations such as connections, since the calculation effort and time is much higher than for shell elements.

2.6.2.2 Treatment of imperfections

At present, the consideration of imperfections is probably the biggest obstacle to the use of the finite element method as an everyday design tool. In fact, imperfections, by definition, must be considered in all their possible ways, in order to lead to the whole of the most adverse effects (Simões da Silva and Gervásio, 2007).

Firstly, relevant buckling modes shall be determined. Not always the most unfavorable mode is the first mode, but also many times the interaction between several modes shall be taken into account. For example, *Figure 2.27* illustrates slender I-section members subject both to local and global buckling.
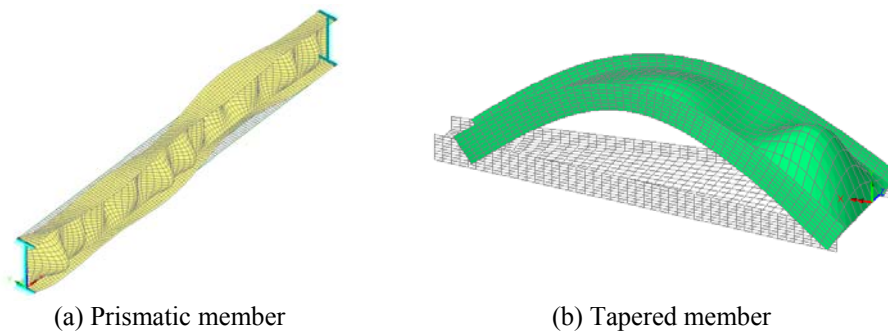
(a) Prismatic member   (b) Tapered member
Figure 2.27: Interaction of local and global buckling modes

Furthermore, three-dimensional modelling makes this task even more difficult as the combination of potential shapes increases exponentially (Simões da Silva and Gervásio, 2007). Besides the global geometrical imperfections, local imperfections such as the lack of linearity or the load eccentricity shall be considered. Material imperfections must also be considered. Finally, in case there is more than one relevant imperfection, a base imperfection must be defined, and the other imperfections may be reduced to 70% of their value.

2.6.3 Type of analysis

The type of analysis must be chosen according to the type of problem and the behavior of the structure. Material and/or geometrical nonlinearities may be considered. To trace the

structural response of problems, an iterative incremental procedure must be used (Rebelo *et al.*, 2006). Newton-Raphson procedure is one of most commonly used.

Besides adequate nonlinearities, geometrical and material imperfections may be included or not, leading to several combinations regarding the type of analysis: from a <u>L</u>inear <u>A</u>nalysis (LA) to a <u>G</u>eometrical and <u>M</u>aterially <u>N</u>onlinear <u>A</u>nalysis of the <u>I</u>mperfect structure (GMNIA).

For example, a linear elastic analysis is enough to verify the elastic resistance of a structure without considering the effects of imperfections. On the other hand, for the verification of the elastic-plastic resistance at ultimate limit states, a GMNIA analysis is needed (Simões da Silva and Gervásio, 2007). Finally, a <u>L</u>inear <u>B</u>ifurcation <u>A</u>nalysis (LBA) may be necessary to identify the relevant imperfections to be considered in a structure.

As a result, according to the type of analysis, numerical analysis of structures may be very complex and lead to the ultimate load of a structure, or may simply be used as an auxiliary tool associated to the existing verification formulae (for example, the second order analyses considered in Section 2.5).

2.6.4 Code guidance and safety verification

Part 1-1 of EC3 does not have yet codified guidance for the verification of structures by finite element analysis. For example, when an analysis in shell elements is performed, results are obtained as stresses. Therefore, in order to apply most verification formulae in EC3-1-1, forces have to be obtained, which is not always a simple procedure.

On the other hand, part 1-5 of EC3 for plated structures includes an Annex (Annex C) which is dedicated to this aspect. As well, due to complexity of shell structures, part 1-6 of EC3 was prepared having in mind the use of finite element software and advanced methods of analysis (Simões da Silva and Gervásio, 2007).

Nevertheless, part 1-1 of EC3 allows the use of this type of analysis, guiding the designer to Annex C of EC3-1-5.

Finally, whenever advanced numerical analysis by FEM is considered, the safety verification is performed as follows:

- In EC3-1-5, for safety verification, it is specified that the load factor α_u corresponding to the maximum load of the structure must correspond to the legal reliability index β (Rebelo *et al.*, 2006). The ultimate limit state is secured if

$$\alpha_u > \alpha_1 \alpha_2 \tag{2.74}$$

  where α_1 is a factor related to the uncertainty that results of the modeling by finite elements, which must be obtained from the evaluation of numeric calibrations, carried out in accordance with Annex D of EN 1990 (CEN, 2002); and α_2 is related to the uncertainty that results of the spreading of models of actions and resistances (can be taken as γ_{M1} or γ_{M2} depending on the phenomena of failure);

- In EC3-1-6, to ensure the reliability of the numerically determined resistance, a calibration factor k_{GMNIA} has to be applied to the results of the analysis, which serves as controlling parameter for the uncertainties associated to the modeled imperfections (Greiner, 2003).

There are however no guidelines to help the designer obtain these factors. In general, as the design of structures using full non-linear numerical analysis is time-consuming and, in addition there is not enough guidance, nearly all codes provide simple formulae for the buckling check as the previously mentioned for EC3-1-1. Similarly, buckling rules for stability verification of web-tapered members will be developed in the following chapters.

Chapter 3

3 NUMERICAL MODEL

3.1 Introduction

The evaluation of the accuracy and the safety of a design model requires reliable estimates of the real behaviour of some reference cases. Advanced numerical simulations contemplating geometrical and material nonlinearities with imperfections (GMNIA) were adopted for this purpose, as is nowadays widely accepted (Rebelo *et al*, 2009). In Section 3.2 the adopted structural model and the underlying assumptions are described. A large number of numerical simulations were carried out, these are described in the context of the respective chapter.

In addition, in order to develop a reliable numerical model, three well-detailed reference cases were taken from the literature to allow direct comparison with independent numerical simulations (Section 3.3).

3.2 Structural model

3.2.1 Finite element model

A finite element model was implemented using the commercial finite element package Abaqus (2010), version 6.10. Four-node linear shell elements (S4) with six degrees of freedom per node and finite strain formulation were used.

For the material nonlinearity, an elastic-plastic constitutive law based on the Von Mises yield criterion is adopted.

A load stepping routine is used in which the increment size follows from accuracy and convergence criteria. Within each increment, the equilibrium equations are solved by means of the Newton-Raphson iteration.

Besides GMNIA, LBA simulations are also carried out in order to obtain the numerical critical loads for tapered members.

The adopted mesh converged for the following discretization: 16 sub-divisions in the web and flanges; and 100 divisions along the axis of the member for every 10m of length.

3.2.2 Material properties

S235 steel grade was considered with a yield stress of 235 MPa (perfect elastic-plastic), a modulus of elasticity of 210 GPa, and a Poisson´s ratio of 0.3, see *Figure 3.1*. Strain hardening was noticed not to be of major importance for the analysed cases.
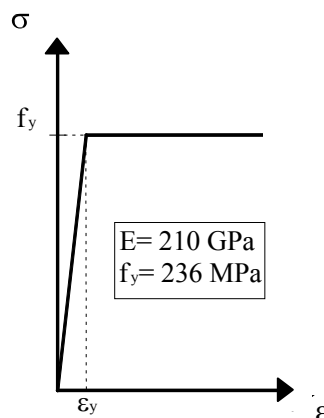
Figure 3.1: Modeling of steel behaviour, perfect elastic-plastic behaviour

3.2.3 Support conditions

Unless specified otherwise, the boundary conditions for a simply supported single span member with end fork conditions are implemented in the shell model as shown in *Figure 3.2*. The following restraints are imposed: (ii) vertical (δ_y) and transverse (δ_z) displacements and rotation about xx axis (ϕ_x) are prevented at nodes 1 and 2. In addition, longitudinal displacement (δ_x) is prevented in node 1. Cross-sections A and B are modeled to remain straight however allowing for warping, i.e., the flanges can move independently from the web.
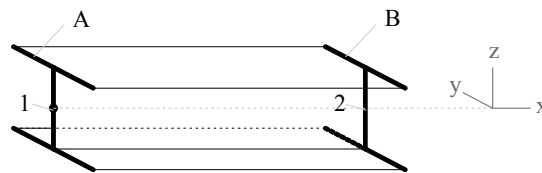
Figure 3.2: Support conditions

For other boundary conditions, the following is considered:

- In-plane behavior: δ_y is restrained at bottom and top of the web. In addition, cross-sections are modeled to remain straight against local displacements in the web;

- Regarding the LBA analysis, web is prevented from buckling and distortion.

3.2.4 Loading

The modelling of the various loads is represented in *Figure 3.3*. Concentrated loading and/or moment is applied at nodes 1 and 2 of *Figure 3.2*, whereas distributed loading is applied along the nodes of the centre of the web (*h/2*). The maximum reference load corresponds to the the plastic resistance of the smallest cross section – for example, for a parabolic bending moment distribution, $qL^2/8 = M_{pl,y,hmin}$.

(a) Concentrated forces / moments (b) UDL

Figure 3.3: Modelling of loads
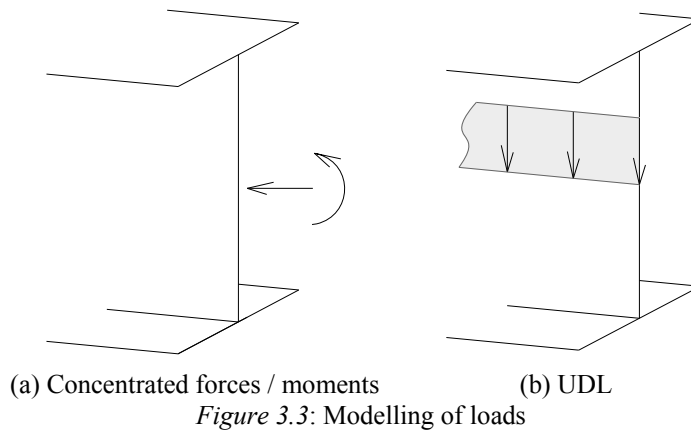
3.2.5 Imperfections

3.2.5.1 Geometrical global imperfections

Regarding global imperfections, a geometrical imperfection proportional to the eigenmode deflection is considered with a maximum value of $e_0=L/1000$, see *Figure 3.4*. This is consistent with the values considered during the development of the European column buckling curves (Beer and Schulz, 1969):

$$\delta_0(x) = \delta_{cr}(x)e_0 = \delta_{cr}(x)\frac{L}{1000} \tag{3.1}$$
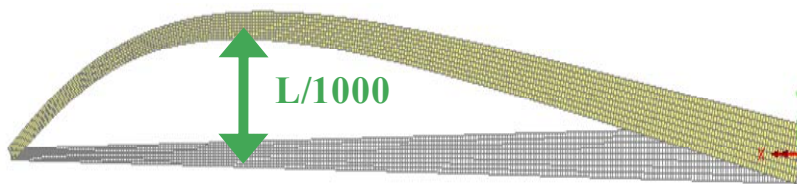
Figure 3.4: Shape and magnitude of the imperfection (in-plane buckling of a web-tapered column)

It was observed that the shape of the imperfections affected the results. The difference between considering either bow or eigenmode imperfections (see *Figure 3.5*) is analysed in *Table 3.1* for the case of tapered columns. It can be observed that the consideration of bow imperfections leads to an over-evaluation of resistance with the increase of the level of taper

and/or the shape of the normal force diagram relatively to a concentrated axial force. The taper ratio γ is defined as the ratio between the maximum height and the minimum height ($\gamma_h=h_{max}/h_{min}$), or the maximum width and the minimum width ($\gamma_b=b_{max}/b_{min}$).
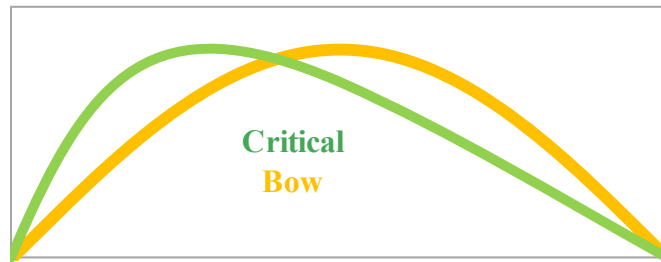
Figure 3.5: Critical load imperfection vs. Bow imperfection

Table 3.1: Analysis of the shape of the imperfection

Taper Ratio $\gamma_h=h_{max}/h_{min}$ ($\equiv\gamma_b=b_{max}/b_{min}$)	Axial force	$\alpha_{b,GMNIA}$		Diff (%)
		Critical	Bow	
1	Concentrated	0.0505		0
	Distributed	0.0935	0.0938	-0.32
3	Concentrated	0.2496	0.2522	-1.04
	Distributed	0.3495	0.3635	-4.01
5	Concentrated	0.5211	0.5462	-4.82
	Distributed	0.6454	0.7050	-9.23

Another example is the case of a prismatic beam with a bending moment distribution of $\psi=-1$, a numerical model with a sinusoidal imperfection can reach a resistance that is 30% higher than the corresponding model with the lateral-torsional buckling mode shape as the initial imperfection, see *Figure 3.6*. As the wave length of the buckling mode is half than wave length of the bow imperfection function, the latter will actually have a positive influence on half of the beam, leading to higher resistance.
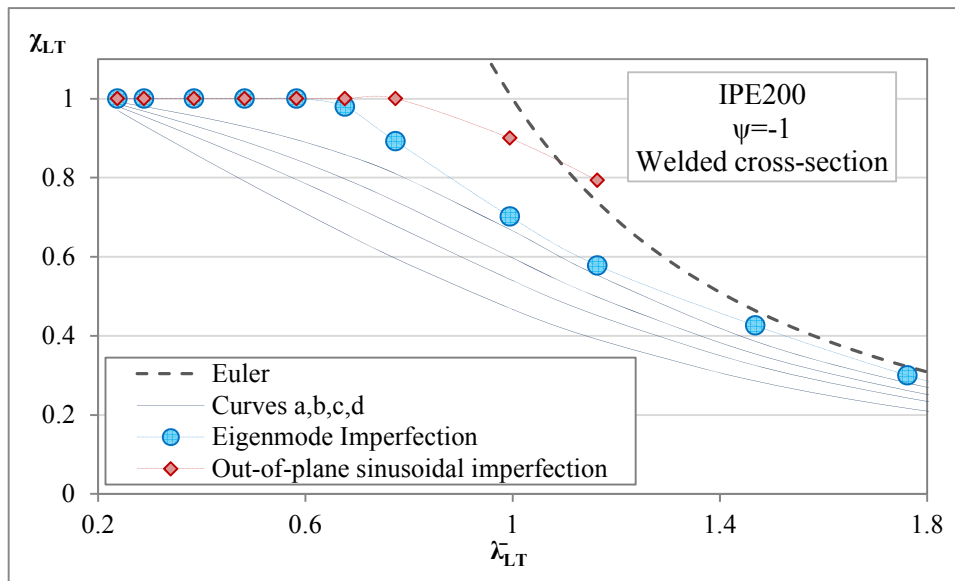
Figure 3.6: Influence of the imperfection

3.2.5.2 Geometrical local imperfections

Tapered members usually have slender webs and, as a result, web buckling should be allowed in the numerical model. However, shear may have an influence in local buckling as well. In order to isolate the different types of buckling modes, the numerical models are considered as follows:

- For computation of the elastic critical load, LBA models were carried out. In order to obtain the critical moment without considering local buckling, the web was prevented from buckling and distortion, as already mentioned;

- For the nonlinear models, two cases were considered:

  a) Unless specified, the web is prevented from buckling. In the absence of significant shear stresses, plastic load capacity should be attained.

  b) The web is unrestrained. In this study, cross-sections up to class 3 (semi-compact) are considered. Again, in the absence of significant shear stresses, a cross-sectional resistance between the elastic and plastic capacity should be met ($M_{3,Rd}$).

For each of these cases, the cross-section resistance of the design models is considered accordingly. Regarding the members with a semi-compact cross-section, unless specified, the

cross-section resistance is obtained according to the proposals of the European Project RFCS Semi-Comp, see Greiner *et al*. (2011).

Although the effects of shear buckling and local buckling due to bending cannot be detached, a qualitative analysis can be performed. The example of *Figure 3.7* illustrates the out-of-plane web deformations of a case in which the presence of shear leads to a decrease in the plastic resistance of the cross-sections. *Figure 3.7(b)* illustrates the presence of shear buckling in the unrestrained model.
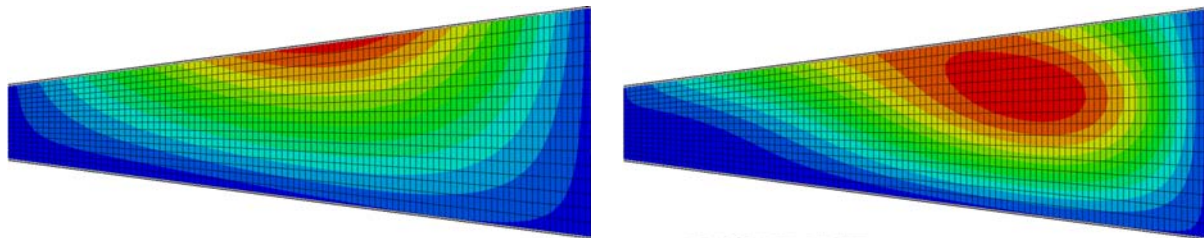
(a) Web prevented from buckling   (b) Web free to buckle – influence of shear stresses
Figure 3.7: Influence of local stresses in a tapered beam, out-of-plane displacement contours in the web –
$\psi=0.25$; $\gamma_h=3$

3.2.5.3 Material imperfections

For the material imperfections, residual stress patterns corresponding both to stocky hot-rolled (i.e. with a magnitude of $0.5f_y$ on the safe side) and welded cross-sections were considered. *Figure 3.8* shows the adopted residual stress pattern. If prismatic members with hot-rolled cross-sections and $h/b>1.2$ are studied, a magnitude of $0.3f_y$ for the residual stresses is considered.
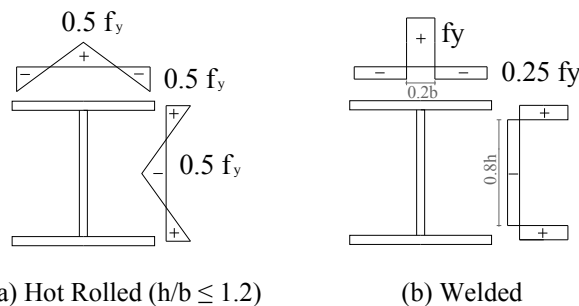
(a) Hot Rolled (h/b ≤ 1.2)   (b) Welded
Figure 3.8: Residual stresses adopted for the tapered members (+ Tension and – Compression)

In *Figure 3.9*, a possible fabrication procedure for the rolled case, which may exist for example in haunched beams, is illustrated (cutting of the web along the length of the column). This choice allowed the direct observation of the influence of the taper by comparing buckling curves for tapered members with curves for members without taper, but with otherwise the same residual stress distribution (*Figure 3.8(a)*).
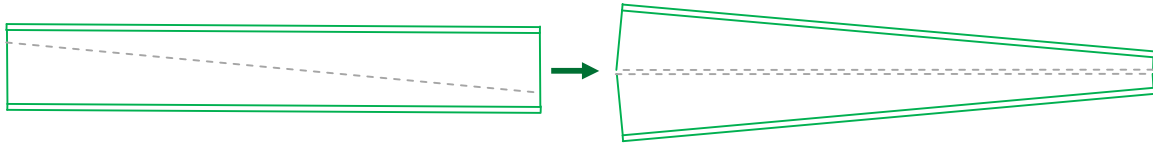
Figure 3.9: Fabrication procedure for hot-rolled tapered elements

3.2.6 Definition of the tapered members

Regarding tapered members, for the definition of the analytical models and development of design rules, the web was considered to vary symmetrically to its centroid axis, according to *Figure 3.10*.
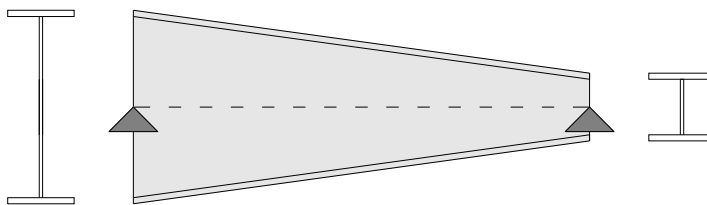
Figure 3.10: Tapered member with horizontal centroid axis

However, because in practice the variation of the flanges relatively to the centroid axis is usually not symmetrical, some cases considering the configuration of *Figure 3.11* are compared to *Figure 3.10*. In *Figure 3.11*, in which only the lower flange varies. Even that the supports are modeled to be at the center of the web, differences should be investigated as, for the same taper ratio, the taper angle of the lower flange is higher for the case of *Figure 3.11*.
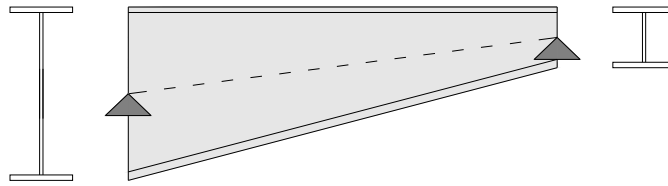
Figure 3.11: Tapered member with horizontal centroid axis

Figure 3.12 and *Figure 3.13* illustrate the differences between GMNIA results for some selected cases and as may be observed, results are almost coincident. In *Figure 3.12*, in-plane buckling of a tapered column was chosen and in *Figure 3.13(a)* and *Figure 3.13(b)*, lateral-torsional buckling of two beams is illustrated, respectively with negligible and significant shear for the shorter lengths (further discussion regarding the presence of shear in tapered beams is given in Chapter 5). The latter is the case in which a slight difference may be noticed for the low slenderness range. Although it is not illustrated, differences between those taper member configurations regarding LBA analysis were also shown to be negligible. Based on numerical results, it may be assumed that the proposals to be provided in Chapter 4 and Chapter 5 are applicable to tapered members in which only the position of one of the flanges varies, with no greater error.

The relative slenderness was obtained considering the elastic critical load of each numerical model and the first order failure load (not accounting for the influence of shear). In addition, the first order failure relative load considering the possible interaction of shear is also illustrated (see Section 2.3.5.2). In *Figure 3.12* and *Figure 3.13*, the denomination *2fl* and *1fl* is representative of *Figure 3.10* and *Figure 3.11*, respectively.
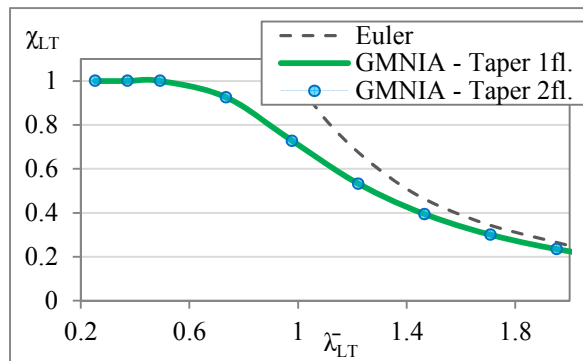
Figure 3.12: Buckling curve representation regarding in-plane flexural buckling – $h_i=b_i=100mm$ and $t_f=t_w=10mm$ (hot-rolled), $\gamma_h=4$
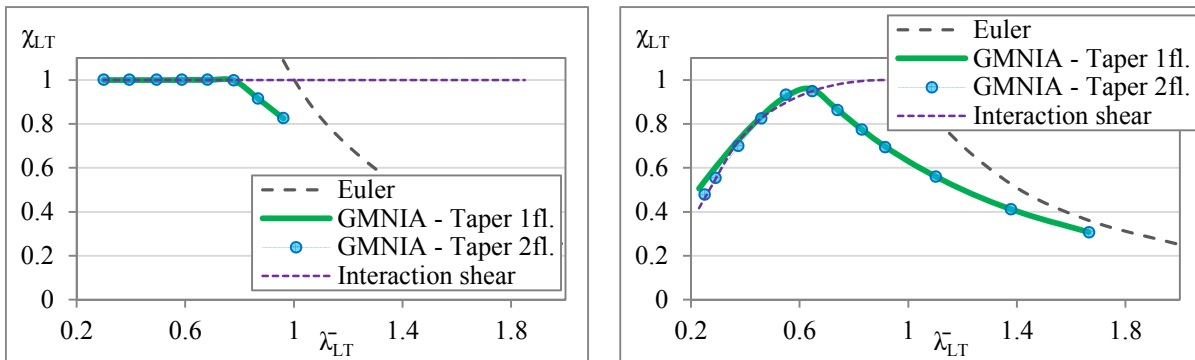
(a) *HEB300* (hot-rolled), $\gamma_h=3$, $\psi=0.75$ (b) *IPE200* (hot-rolled) – $\gamma_h=3$, $\psi=-0.25$

Figure 3.13: Buckling curve representation regarding lateral-torsional buckling

3.3 Validation of the model

In order to validate the model, some simulations were compared to the results obtained by Ofner (1997) for a HEB300. For the beam and the column, rotations about *xx* axis are restrained. Results are represented in *Figure 3.14*. Agreement is excellent, especially considering that a shell model is being compared with a beam model.
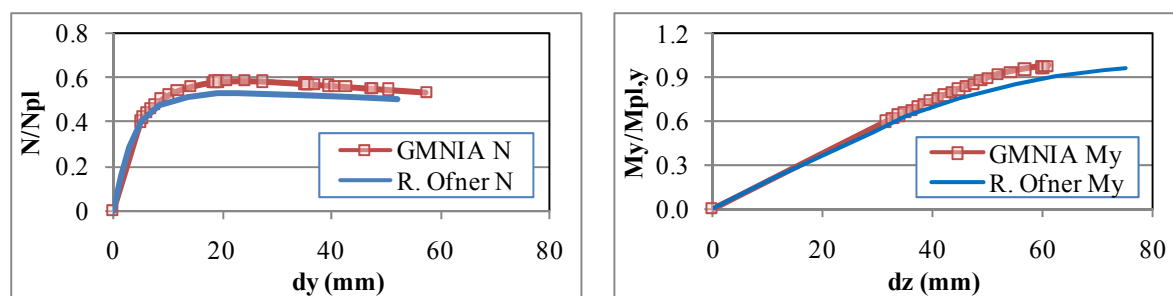
(a) *HEB 300;* L=7.27 m; δ_y (mm) vs. N/N$_{pl}$ (b) HEB 300; L=7.27 m; δ_z (mm) vs. M$_y$/M$_{pl,y}$

Figure 3.14: Validation of the model with cases from Ofner (1997)

Table 3.2 summarizes some results for a beam-column with length *L*=10.90 *m* and constant bending moment, good agreement being noted with the results from Ofner (1997).

Table 3.2: Beam-columns – L=10.9 m; HEB 300

$\Phi = \dfrac{\alpha_{pl}^{M}}{\alpha_{pl}^{N}}$	Ofner – beam – $1/\alpha_{pl}^{M}$	GMNIA – shell – $1/\alpha_{pl}^{M}$	Diff. (%)
2	0.144	**0.153**	5.9
1	0.246	**0.259**	5.0
0.5	0.372	**0.389**	4.4

Finally, performing an eigenvalue analysis for the three cases described in this section yields the results of *Table 3.3* that also shows, for comparison, theoretical predictions obtained from Trahair (1993).

Table 3.3: Critical load multiplier (M$_{y,cr,MN}$/M$_{pl,y}$ – beam-columns; M$_{cr}$/M$_{pl,y}$ – beams; N$_{cr}$/N$_{pl}$ – columns)

Case	$\overline{\lambda}_z = 1.0$	Trahair	LBA	Diff. (%)
Column	1	1.000	0.976	-2.40
Beam		1.880	1.827	-2.82
Beam-column – Φ=0.5	1.5	0.595	0.584	-1.85
Beam-column – Φ=1.0		0.381	0.374	-1.84
Beam-column – Φ=2.0		0.212	0.208	-1.89

3.4 Treatment of results

Both LBA (Linear Buckling Analysis) and GMNIA are carried out to provide data for the analyses in the subsequent chapters. Regarding the nonlinear numerical analysis, the failure load is considered to be the maximum load factor. In addition, the second order failure position x_c^{II} is also extracted from the numerical GMNIA model corresponding to the element with the maximum strain at the maximum load factor, α_b, see *Figure 3.15*.
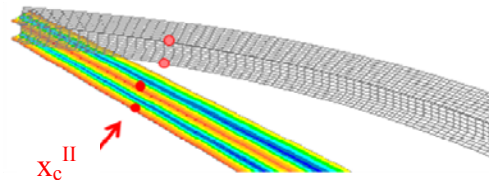
Figure 3.15: Critical position according to GMNIA analysis

Chapter 4

4   FLEXURAL BUCKLING OF TAPERED COLUMNS

4.1   Introduction

In this chapter, the case of columns subject to flexural buckling with varying cross-section is studied.

The differential equation for any boundary conditions; type of cross-section variation and loading is firstly presented. Eigenmode conform imperfections are then applied to the model and finally an Ayrton-Perry formula is derived.

Regarding the elastic range, the Rayleigh-Ritz method is applied and a formula for calculation of the elastic critical load of web-tapered columns subject to in-plane buckling is presented and compared to existing formulae from the literature.

For the inelastic range, design proposals are made for in-plane and out-of-plane flexural buckling of linearly web-tapered columns subject to constant axial force, followed by a numerical parametric study covering a range of slenderness, cross-sections and fabrication process. The proposal is consistent with current rules for uniform columns provided in EC3-1-1, i.e., clause 6.3.1. Some simplifications are analysed for the proposed model. At the end, an example is given, analysing current methodologies with the proposed one.

In addition, a proposal for modification of the generalized imperfection of prismatic welded columns is made, regarding both in-plane and out-of-plane flexural buckling. This is made in

order to accurately reflect the mechanical behaviour resulting from the adopted residual stress pattern for columns with welded cross-sections.

4.2 Elastic critical load of tapered columns

4.2.1 Differential equation

Figure 4.1 illustrates the equilibrium of a column segment for arbitrary boundary conditions in its deformed configuration:

(a) Non-uniform column
(simply supported)

(b) Equilibrium of forces

(c) Detail regarding
distributed force
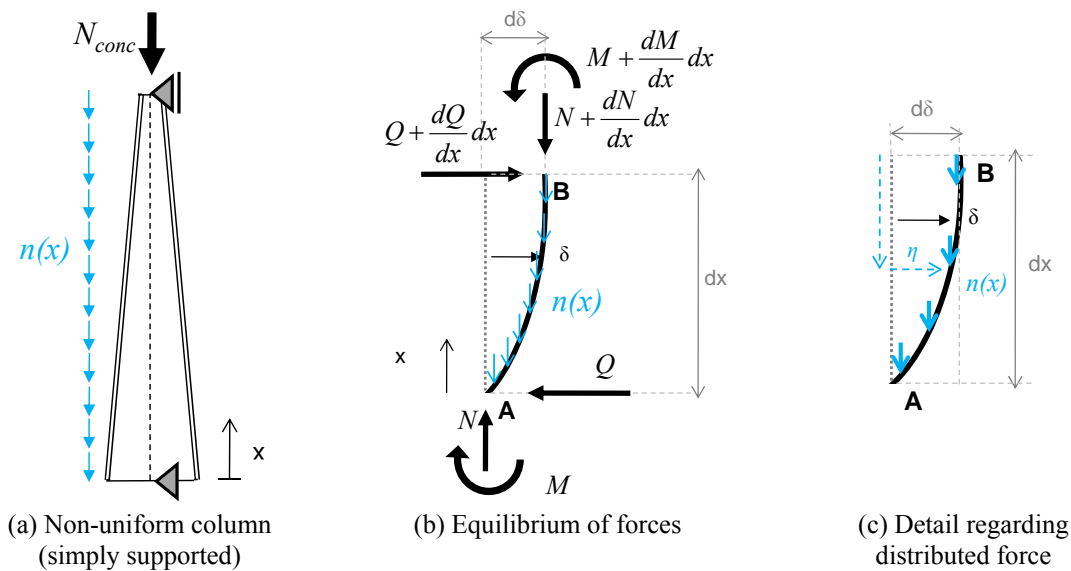
Figure 4.1: Equilibrium of a column segment

Considering the axial force as $N(x) = N_{conc} + \int_{x}^{L} n(\xi)d\xi$, neglecting second order terms and considering the internal moment given by $M(x) = -EI(x)\dfrac{d^2\delta}{dx^2}$, the differential equation is given in Eq. (4.1):

$$E\left(I(x)\cdot\delta''\right)'' + \left(N(x)\cdot\delta'\right)' = 0 \tag{4.1}$$

The solution of this equation leads to the elastic critical load, see (4.2). As it is not the purpose of this work to solve Eq. (4.1) analytically, numerical Linear Buckling Analysis (LBA) will be carried out and used to obtain the shape of the eigenmode as well as the critical load multiplier, α_{cr}.

$$\begin{cases} N(x) = \alpha_{cr} N_{Ed}(x) \\ n(x) = \alpha_{cr} n_{Ed}(x) \\ \delta(x) = \delta_{cr}(x) \end{cases} \tag{4.2}$$

$N_{Ed}(x)$ is the applied axial force and α_{cr} is the critical load multiplier, and $\delta_{cr}(x)$ is the critical eigenmode.

4.2.2 Determination of the elastic critical load of web-tapered columns (literature)

In Section 2.2 procedures for determination of the critical load of I-section tapered columns were briefly described. Two of the methods are now given in Table 4.1. These will also be considered throughout Chapter 4.

Table 4.1 Determination of the in-plane critical axial force from the literature

Source	Description
Hirt and Crisinel, (2001)	Expression for equivalent moment of inertia for the tapered column, I_{eq}, depending on the type of web variation. Suitable for I-shaped cross sections.
	$$N_{cr} = \frac{\pi^2 EI_{y,eq}}{L^2}, \quad I_{y,eq} = CI_{y,max}$$
[H&C]	$$C = 0.08 + 0.92r, \quad r = \sqrt{I_{y,min}/I_{y,max}}$$
Lee *et al*. (1972) Galambos (1998)	Expression for a modification factor of the tapered member length, g, i.e., calculation of the equivalent length of a prismatic column with the smallest cross section which leads to the same critical load. Suitable for I-shaped cross sections.
	$$N_{cr} = \frac{\pi^2 EI_{y,min}}{L_{eq}^2}, \quad L_{eq} = g \cdot L$$
[L&al.]	$$g = 1 - 0.375\gamma + 0.08\gamma^2(1 - 0.0775\gamma), \quad \gamma = h_{max}/h_{min} - 1$$

4.2.3 Rayleigh-Ritz method for the calculation of the elastic critical load

4.2.3.1 Introduction

The differential equation of a column in its deformed configuration is given by Eq. (4.1). For a simply supported column with constant axial force, it is simplified by

$$EI(x) \cdot \delta'' + N \cdot \delta = 0 \tag{4.3}$$

The solution for δ in Eq. (4.3) is not explicit and therefore, approximate or numerical methods are required to obtain the solution. Rayleigh-Ritz Method is presented here. If an adequate displacement function δ_{cr} (Eq. (4.4)) satisfying the geometric boundary conditions is considered to approximate the real displacement, the structural system is reduced to a system with finite degrees of freedom (Chen and Lui, 1987).

$$\delta_{cr} = a \cdot f \tag{4.4}$$

The total potential energy of the member is given by the sum of the strain U and potential V energy. Note that these are approximate, once the displacement function is also an approximation.

Considering the principle of stationary total potential energy, the solution for the critical load is obtained by solving Eq. (4.5), see e.g. Chen and Lui (1987) for more details.

$$\frac{\partial (U + V)}{\partial a} = 0 \tag{4.5}$$

For a simple supported column the strain energy U_b due to bending is given by

$$U_b = \frac{1}{2} \int_V \sigma \varepsilon \, dV = \frac{1}{2} \int_V \left(\frac{My}{EI} \right) \left(\frac{My}{I} \right) dV = \frac{1}{2} \int_0^L \frac{1}{E} \left(\frac{M}{I} \right)^2 \underbrace{\left(\int_A y^2 \, dA \right)}_{I} dx = \frac{1}{2} \int_0^L \frac{M^2}{EI} \, dx \tag{4.6}$$

Or, because $M = EI\delta_{cr}''$,

$$U_b = \frac{1}{2} \int_0^L EI \left(\delta_{cr}'' \right)^2 dx \tag{4.7}$$

And the potential energy V_b due to bending may be calculated by the work done on the system by the external forces

$$V_b = -N\Delta = -\int_0^L N \underbrace{\left(\frac{1}{2} \left(\delta_{cr}' \right)^2 \right)}_{d\Delta} dx = -\frac{1}{2} \int_0^L N \left(\delta_{cr}' \right)^2 dx \tag{4.8}$$

Eq. (4.5) finally becomes

$$\frac{\partial(U+V)}{\partial a} = 0 \rightarrow \frac{\partial\left(\frac{1}{2}\int_0^L \left(EI(\delta_{cr}'')^2 - N(\delta_{cr}')^2\right)dx\right)}{\partial a} = 0 \tag{4.9}$$

4.2.3.2 Adjustment of the displacement function

The displacement function δ_{cr} to be considered in Eq. (4.9) needs to satisfy the boundary conditions. For a simply supported column $\delta_{cr}(0)=\delta_{cr}(L)=0$ and $\delta_{cr}''(0)=\delta_{cr}''(L)=0$.

For a tapered column buckling in-plane with the smallest cross-section $h=b=100$ mm and $t_f=t_w=10$ mm (denoted as *100x10*), the following function was adjusted based on the critical mode displacement:

$$\delta_{cr} = a \times \begin{cases} \begin{aligned} &\cos\left(\frac{\pi(x - x_{cr,\max})}{2x_{cr,\max}}\right) - 0.058 \cdot \ln\gamma_h \sin\left(\frac{\pi(x - x_{cr,\max})}{x_{cr,\max}}\right) \\ &+ 0.024 \cdot \ln\gamma_h \sin\left(\frac{2\pi(x - x_{cr,\max})}{x_{cr,\max}}\right) \end{aligned} & ; \quad 0 \le x \le x_{cr,\max} \\[4mm] \cos\left(\frac{\pi(x - x_{cr,\max})}{2(L - x_{cr,\max})}\right) - 0.029 \cdot \ln\gamma_h \sin\left(\frac{\pi(x - x_{cr,\max})}{L - x_{cr,\max}}\right) & ; \quad x_{cr,\max} \le x \le L \end{cases} \tag{4.10}$$

In Eq. (4.10), $x_{cr,max}$ is the location corresponding to the maximum deflection and $\gamma_h=h_{max}/h_{min}$ is the taper ratio regarding the maximum and minimum depth. $x_{cr,max}$ may be given by

$$x_{cr,\max} = 0.5 \cdot \gamma_h^{-0.208} \cdot L \tag{4.11}$$

The fitted function for δ_{cr} given by Eq. (4.10) (δ_EQU) is illustrated in *Figure 4.2* and compared to the eigenmode deflection (δ_LBA). A small error is obtained and Eq. (4.10) will be considered for application of the Rayleigh-Ritz Method.
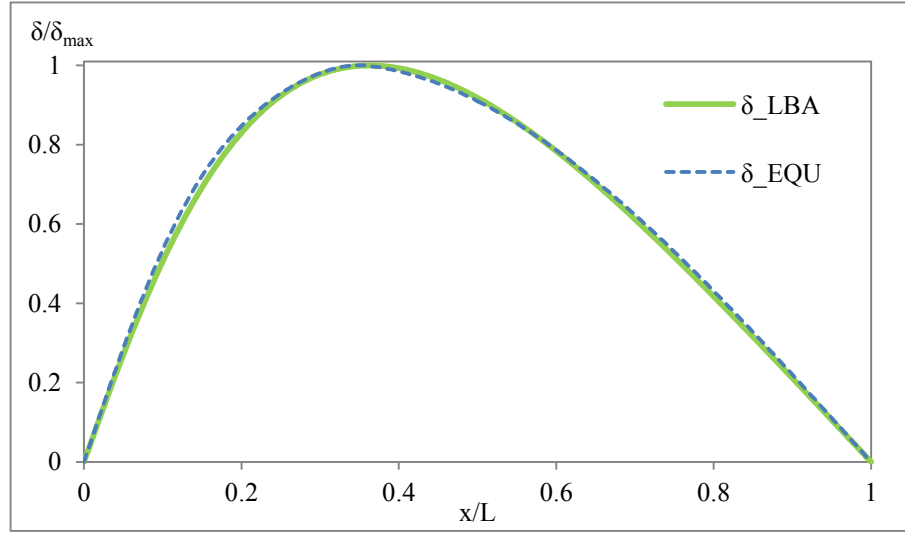
Figure 4.2: Displacement function for the in-plane critical mode of a web-tapered column (*100x10*; $\gamma_h=5$)

4.2.3.3 Results

Consider the cross section *100x10* for a range of taper ratios γ_h between 1 and 6. The solution of Eq. (4.10) is given in terms of $N_{cr,Tap}=K/L^2$, in which K is a constant, and can be represented as a function of the critical load of the smallest section, $N_{cr,min}$.

$$N_{cr,Tap} = A \cdot N_{cr,min} \rightarrow A = \frac{K}{\pi^2 EI_{y,min}} \tag{4.12}$$

Based on the values of K obtained by the Rayleigh-Ritz analysis for the several combinations of taper ratio and cross section type, an expression is now given for A.

$$N_{cr,Tap} = A \cdot N_{cr,min} \rightarrow A = \gamma_I^{0.56}\left(1 - 0.04 \cdot tan^{-1}\left(\gamma_I - 1\right)\right)$$
$$\gamma_I = I_{y.max} / I_{y.min} \tag{4.13}$$

Eq. (4.13) was calibrated to give results on the safe side as it can be observed in *Figure 4.3*. *EQU_RR* represents the results of A given by the Rayleigh-Ritz method, Eq. (4.12), whereas *EQU_Adjusted* represents Eq. (4.13).
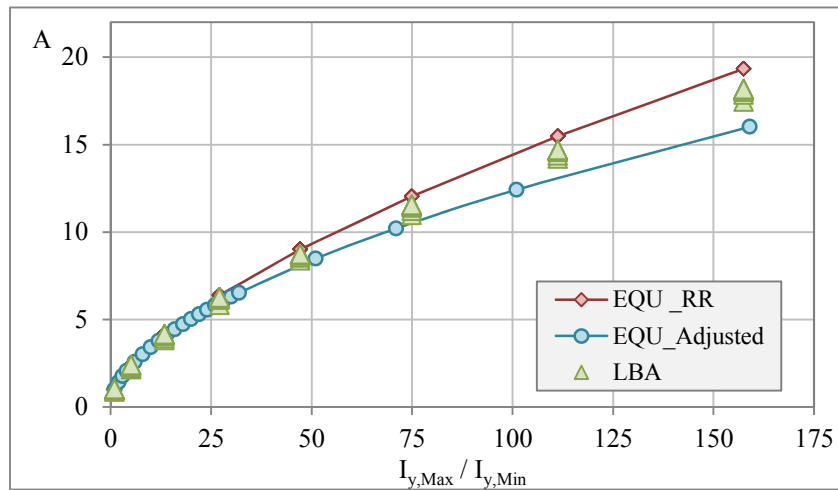
Figure 4.3: Calibration of factor *A*

Note that the taper ratio chosen for calculation of the critical load in Eq. (4.13) is represented in terms of the ratio between the maximum and minimum inertia, i.e., $\gamma_I = I_{max}/I_{min}$. This is the best parameter to characterize the elastic flexural buckling behavior of the tapered column. When analyzing other sections, e.g., a *HEB300* (smallest cross-section) that present the same γ_I, a very good agreement is noticed in the function for δ_{cr} and also in the function that characterizes the second moment of area along the column. As a result, the expression of Eq. (4.13) may be used for any section. For the member with a smallest cross section *100x10*, $\gamma_h = 1.9$ and for the *HEB300*, $\gamma_h = 2$. Both members present $\gamma_I = 4.62$.

In addition, the above-defined expression may be considered with not much increase in error on cross sections with varying flange buckling out-of-plane. The inertia of the flanges buckling out-of-plane can be compared to the inertia of the web buckling in-plane. The analyzed member is composed of a smallest cross section *100x10* with $\gamma_b = b_{max}/b_{min} = 1.67$ (and accordingly, a $\gamma_I = 4.62$, in which for this case I_y is replaced by I_z). The same however cannot be considered for flange-tapered columns buckling in-plane, as the inertia varies linearly. A similar Rayleigh-Ritz procedure could be adopted for the latter, it is however not the scope of this study.

Figure 4.4 illustrates the moment of inertia (I_z or I_y) variation and *Table 4.2* compares the analyzed cases with a Linear Buckling Analysis. Lengths of the columns were chosen in order to lead to similar (numerical) slenderness $\bar{\lambda} = \sqrt{N_{pl,\min} / N_{cr,tap}^{LBA}}$. The critical displacement δ_{cr} is not illustrated as results practically match.

Table 4.2: Analysis of the critcal load obtained by Eq. (4.13)

Ref. Section	γ_h	γ_b	Buckling Mode	N_{cr}^{LBA} [kN]	$N_{pl,\min}$ [kN] (S235)	$\bar{\lambda}_y$	$N_{cr,\min}$ [kN]	γ_I	A	$N_{cr,tap}$ [kN]	Diff (%)
100x10	1.9	-	In	248.5	658	1.63	110.6			246.9	0.64
HEB300	2.0	-	In	1242.6	3356.27	1.64	551.1	4.62	2.23	1231.0	0.94
100x10	-	1.67	Out	252.4	658	1.61	114.4			255.4	-1.22

*For HEB300 the fillet radius is not considered
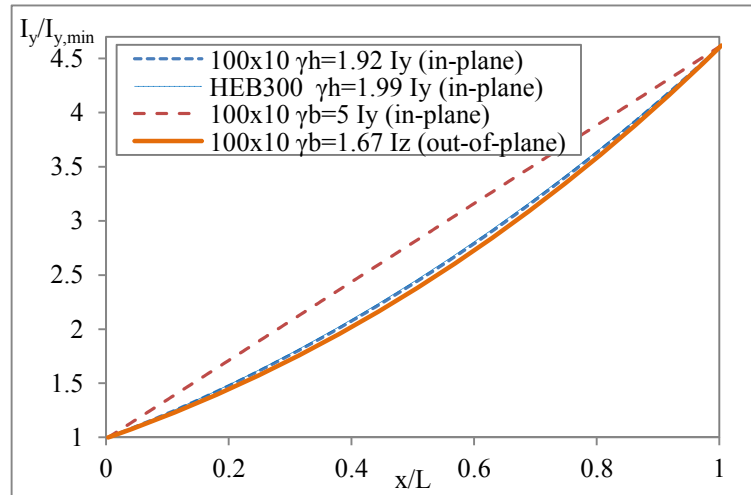
Figure 4.4: Variation of inertia along the member for distinct sections with the same $\gamma_{I=Imax/Imin}$

Finally, for a range of cross-sections with varying γ_h (or γ_I) the error is analyzed in *Figure 4.5*. For comparison, the procedures given in *Table 4.1* are also shown. Note that, because the taper ratio γ_h is an intuitive parameter to describe the tapered member, presentation of results relatively to that parameter γ_h is kept. The difference is given by Eq. (4.14), such that a positive difference illustrates a safe evaluation of N_{cr} by the given method. Maximum differences of 8% (on the safe side) are noted. It is measured relatively to the columns with higher slenderness, i.e., for which the numerical analysis does not present the effect of shear. For the low slenderness range this effect is higher and decreases asymptotically to the correct

critical load – this can be observed for the well-known solution of a simply supported column with prismatic cross-section (Euler load).

$$Diff\,(\%) = 100 \times \left(1 - \frac{N_{cr,tap}^{Method}}{N_{cr,tap}^{LBA}}\right)$$
(4.14)

(a) According to γ_h (b) According to γ_I
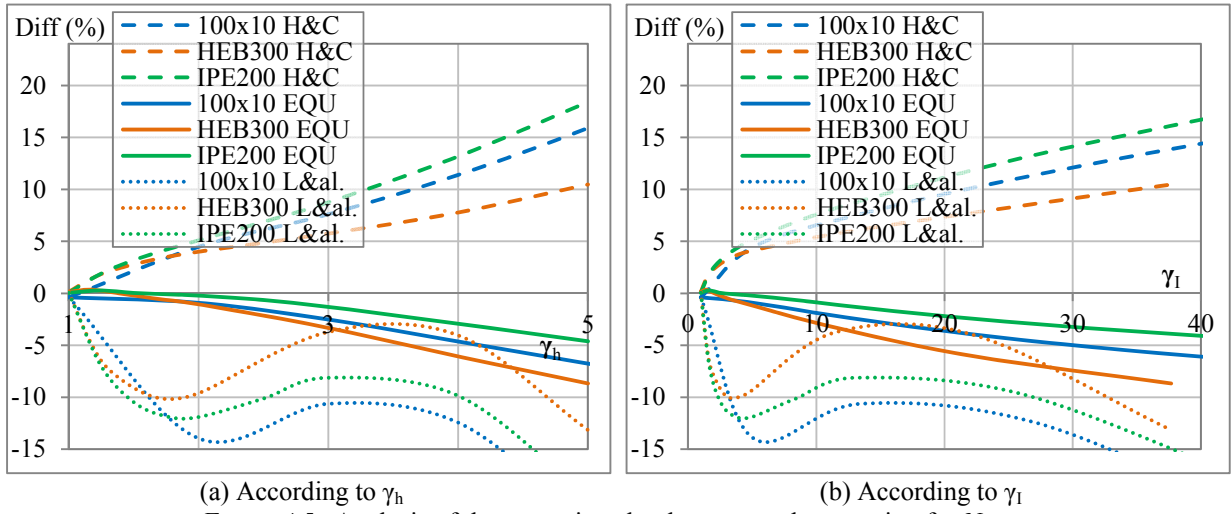
Figure 4.5: Analysis of the error given by the proposed expression for $N_{cr,tap}$

4.3 Imperfect column

4.3.1 Differential equation

Consider now an initial imperfection proportional to the shape of the eigenmode ($\delta_{cr}(x)$). Considering a similar approach to Section 4.2.1 and assuming that the internal forces are independent of the imperfection, the differential equation, Eq. (4.1), becomes

$$\left(EI(x)\,\delta''\right)'' + \left(N(x)\,\delta' + N(x)\,\delta_0'\right)' = 0$$
(4.15)

Defining $N(x)=\alpha_b N_{Ed}(x)$, where α_b is the load multiplier corresponding to the plastic resistance of the column, the solution to Eq. (4.15) is given by

$$\delta(x) = \frac{\alpha_b}{\alpha_{cr} - \alpha_b} \delta_0(x) \qquad (4.16)$$

This leads to a second order bending moment of

$$M(x) = -EI(x)\delta''(x) = -EI(x)\left[\frac{\alpha_b}{\alpha_{cr} - \alpha_b}\delta_0''(x)\right] \qquad (4.17)$$

Defining the utilization ratio ε as the ratio between the applied forces and the corresponding resistance, and considering a linear interaction between moment and axial force, the utilization ratio at each section of the column is given by

$$\varepsilon(x) = \frac{\alpha_b N_{Ed}(x)}{N_R(x)} + \frac{M(x)}{M_R(x)} = \frac{\alpha_b N_{Ed}(x)}{N_R(x)} + \frac{EI(x)\left[\dfrac{\alpha_b}{\alpha_{cr} - \alpha_b}(-\delta_0''(x))\right]}{M_R(x)} \qquad (4.18)$$

As a result, considering a first yield criterion, for a certain load multiplier α_b, the utilization ratio attains a maximum of $\varepsilon=1$ at the second order failure position of the column, x_c^{II}. As only one equation is given (Eq. (4.18)), but two variables are unknown (α_b and x_c^{II}), an iterative procedure is needed to obtain the solution.

4.3.2 Assumptions for the magnitude of the imperfection

As already mentioned, a similar derivation was carried out in Naumes (2009) applicable to flexural buckling in general, in which, for the magnitude of the initial imperfection, equation (5.9) of EC3-1-1 was considered. It will be shown in this section that this assumption leads to an expression matching clause 6.3.1 of EC3-1-1 for uniform columns at the critical position. This topic will be further discussed.

Two cases are then considered for the proportionality factor of the eigenmode deformed shape:

a) Imperfection consistent with the derivation of the column buckling curves – the amplitude of this deflection is given by e_0;

b) Imperfection according to equation (5.9) of EC3-1-1 (equivalent geometric imperfection) – the amplitude of the critical mode is given multiplied by e_0 and an additional factor. Again, this derivation may be found in Naumes (2009);

In the above, e_0 denotes the maximum amplitude of a member imperfection.

4.3.2.1 Imperfection consistent with European column buckling curves formulation

Following a similar approach as for the derivation of the European Column Buckling Curves, the imperfection is given by

$$\delta_0(x) = \delta_{cr}(x)e_0 \qquad (4.19)$$

The utilization ratio ε considering this imperfection can now be derived

$$\varepsilon(x) = \frac{\alpha_b N_{Ed}(x)}{N_R(x)} + \frac{M(x)}{M_R(x)} = \frac{\alpha_b N_{Ed}(x)}{N_R(x)} + \frac{EI(x)\left[\frac{\alpha_b}{\alpha_{cr}-\alpha_b} \cdot \overbrace{(-1)\left(\delta_{cr}''(x)e_0\right)}^{-\delta_0''}\right]}{M_R(x)} \qquad (4.20)$$

Considering

$$\overline{\lambda}(x) = \sqrt{\frac{N_R(x)/N_{Ed}(x)}{\alpha_{cr}}}; \quad \chi(x) = \frac{\alpha_b}{N_R(x)/N_{Ed}(x)} \qquad (4.21)$$

After some manipulations and reorganizing terms, the utilization ratio ε becomes

$$\varepsilon(x) = \chi(x) + \chi(x) \cdot \cfrac{1}{1 - \cfrac{\alpha_b}{\alpha_{cr}}} \left[e_0 \frac{N_R(x_c)}{M_R(x_c)} \right] \left[\frac{EI(x)\left(-\delta_{cr}''(x)\right)}{N_{Ed}(x)\alpha_{cr}} \right] \left[\frac{N_R(x)}{N_R(x_c)} \frac{M_R(x_c)}{M_R(x)} \right] \quad (4.22)$$

At the position $x = x_c^{II}$, $\varepsilon(x_c^{II}) = 1$,

$$\varepsilon(x_c^{II}) = 1 = \chi(x_c^{II}) + \frac{\chi(x_c^{II})}{1 - \overline{\lambda}^2(x_c^{II})\chi(x_c^{II})} \left[e_0 \frac{N_R(x_c^{II})}{M_R(x_c^{II})} \right] \left[\frac{EI(x_c^{II}).(-\delta_{cr}''(x_c^{II}))}{\alpha_{cr}.N_{Ed}(x_c^{II})} \right] \quad (4.23)$$

Considering

$$\left[e_0 \frac{N_R(x_c^{II})}{M_R(x_c^{II})} \right] = \alpha_{EC3} \left(\overline{\lambda}(x_c^{II}) - 0.2 \right) \quad (4.24)$$

where $\alpha_{EC3} = \alpha_{EC3}(x_c^{II})$. Eq. (4.23) becomes

$$1 = \chi(x_c^{II}) + \chi(x_c^{II}) \frac{1}{1 - \overline{\lambda}^2(x_c^{II})\chi(x_c^{II})} \underbrace{\underbrace{\alpha_{EC3}(x_c^{II})\left(\overline{\lambda}(x_c^{II}) - 0.2\right)}_{\eta_{uniform} \quad (x_c^{II})} \underbrace{\left[\frac{EI(x_c^{II}).(-\delta_{cr}''(x_c^{II}))}{\alpha_{cr}.N_{Ed}(x_c^{II})} \right]}_{\beta(x_c^{II})}}_{\eta_{non-uniform} \quad (x_c^{II})} \quad (4.25)$$

Eq. (4.25) is identical to the Ayrton-Perry formulation for uniform columns. It can be shown that, for prismatic columns with constant axial force, the factor $\beta(x_c^{II})$ is unity, see Eq. (4.26):

$$\begin{cases} I(x) = K = I \\ x_c^{II} = L/2 \end{cases}$$

$$\rightarrow \frac{EI(x_c^{II}).(-\delta_{cr}''(x_c^{II}))}{\alpha_{cr}.N_{Ed}(x_c^{II})} = \frac{EI.\left[-\left(\sin\left(\dfrac{\pi x}{L}\right)\right)_{x=L/2}''\right]}{\left(\dfrac{\pi^2 EI}{L^2}\middle/N_{Ed}\right)N_{Ed}} = \frac{EI.\dfrac{\pi^2}{L^2}}{\left(\dfrac{\pi^2 EI}{L^2}\middle/N_{Ed}\right)N_{Ed}} = 1 \quad (4.26)$$

$$\rightarrow \beta(x_c^{II}) = 1$$

Finally, this factor takes into account the non-uniformity of the column and leads to a modification of the current column buckling curves, i.e. of clause 6.3.1 of EC3-1-1.

4.3.2.2 Imperfection according to equation (5.9) of EC3-1-1

The equivalent imperfection of equation (5.9) of EC3-1-1 is given by (see also Eq. (1.1) of Chapter 1)

$$\delta_0(x) = e_0 \delta_{cr}(x) \cdot \frac{N_{cr}}{EI\delta_{cr,max}''} = e_0 \delta_{cr}(x) \frac{N_{Ed}.\alpha_{cr}}{E.I\delta_{cr,max}''} \quad (4.27)$$

The amplitude e_0 shall here be obtained by Table 5.1 of EC3-1-1 (or *Table 1.1* of this thesis).

For a prismatic column, the critical position is at mid-span and, therefore, $\delta''_{cr,max}= \delta''_{cr}(L/2)= \delta''_{cr}(x_c)$. Analogously, $N_{Ed}=constant= N_{Ed}(x_c^{II})$. Eq. (4.27) becomes

$$\delta_0(x) = \delta_{cr}(x)e_0\left[\frac{N_{Ed}(x_c^{II}).\alpha_{cr}}{E.I(x_c^{II}).\left(-\delta_{cr}''(x_c^{II})\right)}\right] \quad (4.28)$$

Note: The sign (-) in Eq. (4.28) leads to a positive value of the imperfection.

Analogous to 4.3.2.1, the utilization ratio ε becomes

$$\varepsilon(x) = \frac{\alpha_b N_{Ed}(x)}{N_R(x)} + \frac{M^{II}(x)}{M_R(x)} = \frac{\alpha_b N_{Ed}(x)}{N_R(x)} + \frac{EI(x)\left[\dfrac{\alpha_b}{\alpha_{cr}-\alpha_b}\delta_0''(x)\right]}{M_R(x)}$$

$$(...) \qquad\qquad\qquad\qquad\qquad\qquad\qquad\qquad\qquad\qquad\qquad\qquad\qquad\qquad\qquad (4.29)$$

$$= \chi(x) + \frac{\chi(x)}{1-\overline{\lambda}^2(x)\chi(x)}\left[e_0\,\frac{N_R(x_c^{II})}{M_R(x_c^{II})}\right]\left[\frac{EI(x)}{EI(x_c^{II})}\frac{\delta_{cr}''(x)}{\delta_{cr}''(x_c^{II})}\frac{N_{Ed}(x_c^{II})}{N_{Ed}(x)}\frac{N_R(x)}{N_R(x_c^{II})}\frac{M_R(x_c^{II})}{M_R(x)}\right]$$

At the position $x=x_c^{II}$, $\varepsilon(x_c^{II})=1$,

$$\varepsilon(x_c^{II}) = 1 = \chi(x_c^{II}) + \chi(x_c^{II})\frac{1}{1-\overline{\lambda}^2(x_c^{II})\chi(x_c^{II})}\underbrace{\left[e_0\,\frac{N_R(x_c^{II})}{M_R(x_c^{II})}\right]}_{\alpha\left(\overline{\lambda}(x_c^{II})-0.2\right)\equiv\eta_{EC3}} \qquad (4.30)$$

In this case, Eq. (4.30) coincides exactly with equation (6.49) of EC3-1-1 and leads to the application of clause 6.3.1 for columns if the cross-section properties at the position $x = x_c^{II}$ are considered.

4.3.3 Interpretation of the utilization ratio ε

x_c^{II} and α_b are obtained as follows:

- x_i $(0 \leq x_i \leq L)$ is assumed as x_c^{II} and Eq. (4.25) (or Eq. (4.30)) is solved for α_b (see Eq. (4.21) for the definition of α_b);
- After this, $\varepsilon(x)$ in Eq. (4.22) (or Eq. (4.29)) is obtained for all values of x. Here, the assumptions of Eq. (4.24) for the generalized imperfection according to EC3-1-1 are considered;
- If $\varepsilon(x_i) \geq \varepsilon(x)$, then $x_c^{II}=x_i$. If not, the procedure is repeated for $x=x_{i+1}$.

The variation of the utilization ratio ε of a non-uniform column ($L=10\ m$) with the smallest cross-section *100x10* is illustrated in *Figure 4.6*, concerning Eq. (4.22) for out-of-plane buckling. For this, a taper ratio of $\gamma_h=\gamma_b=5$ was considered. In addition, a distributed loading is considered. For the case of out-of-plane buckling the variation of the flanges and the

distributed loading will mainly influence the buckling resistance of the tapered member (and the second order failure location, x_c^{II}).

To obtain the utilization ε, α_{cr} and δ''_{cr} are obtained numerically from a LBA analysis. The utilization ratio ε is divided into 2 terms – ε_N concerns first order forces, i.e., axial force, and ε_{MII} concerns 2nd order forces, i.e., bending moment due to curvature of the member. The sum of these terms leads to the total utilization ratio ε. For short members, ε_N is much higher compared to ε_M as cross-sectional resistance is more significant, and vice-versa. It can be seen that the critical position x_c^{II} is located at about 10% of the member length, close to the smallest cross-section.
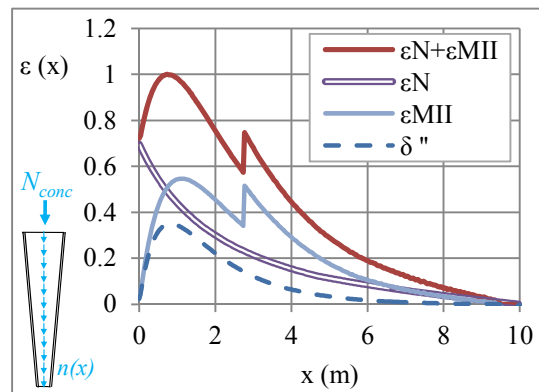
Figure 4.6: Curvature δ'' and utilization ratio ε (total, due to axial force only; due to 2nd order forces only)

Note that in *Figure 4.6* a discontinuity can be noticed at about *x=3m*. At this position, the class of the flanges in compression and <u>bending about zz</u> (out-of-plane buckling) changes from 2 (plastic verification) to 3 (elastic verification), which leads to a modification of the resistant moment M_r (according to the cross-section class definition in EC3-1-1) and, therefore, a discontinuity in the utilization ratio due to 2nd order forces. Again, if the interpolation of the Semi-Comp project (Greiner *et al.*, 2010) for semi-compact cross sections would be considered, this discontinuity would not be observed.

4.3.4 Parametric study

4.3.4.1 Definition and methodology

Table 4.3 summarizes the sub-set of cases to be compared with the advanced numerical simulations. Although focus is given to the relevant case of in-plane flexural buckling, out-of-plane buckling is also presented. Linearly web-tapered columns subject to uniform axial force are considered. More than 500 numerical simulations with shell elements were carried out. Both GMNIA numerical simulations constrained in-plane and LBA are carried out to provide data for application of the analytical formulations and for calibration of necessary parameters. *Table 4.3* summarizes the parametric study, whereas *Table 4.4* summarizes the alternative procedures to obtain the resistance of the tapered column.

Table 4.3: Parametric study

Taper Ratio γ_h	Reference Cross-section (i.e. with h_{min}, at $x=x_{min}$)	Reference Column Slenderness $\overline{\lambda}(x_{min}) = \sqrt{\dfrac{N_R(x_{min})/N_{Ed}}{\alpha_{cr}}}$	Fabrication Procedure
1 ... 6	IPE 200 HEB 300 100x10 ($h=b=100$ *mm*; $t_f=t_w=10$ *mm*)	0 ... 3	Welded Hot-rolled ($0.5 f_y$)

Table 4.4: Considered procedures for stability verification

Method	Description
Eq. (4.25) [a]	Solution of the equation by an iterative procedure
Eq. (4.30) [a]	Solution of the equation by an iterative procedure
Eq. (4.25) [b]	Direct application – x_c^{II} is extracted numerically
Eq. (4.30) [b]	Direct application – x_c^{II} is extracted numerically $\equiv$ Eq. (4.30) considering $\beta(x_c^{II})=1$
EC3-1-1	$\equiv$ Eq. (4.25) considering x_c^{II} at the smallest cross-section and $\beta(x_c^{II})=1$ or $\equiv$ Eq. (4.30) considering x_c^{II} at the smallest cross-section
GMNIA	-

The first two cases (*a*) were previously described. Regarding the other cases (*b*), no iteration procedure is needed because the critical location x_c^{II} is assumed to be known from the numerical model. The procedure is implemented as follows:

1. Extraction of x_c^{II} from GMNIA model and of the critical load multiplier α_{cr} from LBA model;

2. Calculation of $\overline{\lambda}(x_c^{II}) = \sqrt{\dfrac{N_R(x_c^{II})/N_{Ed}(x_c^{II})}{\alpha_{cr}}}$, see Eq. (4.21);

3. Calculation of the generalized imperfection $\eta_{non\text{-}uniform}(x_c^{II})$ (when applicable) defined in Eq. (4.25) as

$$\eta_{non-uniform}(x_c^{II}) = \underbrace{\eta_{uniform}(x_c^{II})}_{} \times \beta(x_c^{II}) = \underbrace{\underbrace{\alpha_{EC3}(x_c^{II})\left(\overline{\lambda}(x_c^{II}) - 0.2\right)}_{\eta_{uniform}(x_c^{II})}\underbrace{\left[\frac{EI(x_c^{II}).(-\delta_{cr}''(x_c^{II}))}{\alpha_{cr}.N_{Ed}(x_c^{II})}\right]}_{\beta(x_c^{II})}}_{\eta_{non-uniform}(x_c^{II})};$$

4. Calculation of the reduction factor $\chi(x_c^{II})$ and finally of α_b, given by $\alpha_b = \chi(x_c^{II}).N_R(x_c^{II})/N_{Ed}(x_c^{II})$, see Eq. (4.21).

Finally, concerning nonlinear numerical calculations, the maximum load factor of GMNIA analysis corresponds to α_b load multiplier. The critical position x_c^{II} is also extracted from the numerical model corresponding to the node with the maximum strain at the maximum load factor, α_b, see Chapter 3. The critical load multiplier α_{cr} is obtained numerically for the in-plane cases. For the out-of-plane cases α_{cr} was obtained from the Euler load of the smallest cross section with negligible error.

Results are represented relatively to the failure first order location, x_c^{I}. For the case of constant axial force, it coincides with the smallest cross section, x_{min}. Because $N_{Rk}(x_{min})=N_{Ed}$, Eq. (4.21) becomes:

$$\begin{cases} \overline{\lambda}(x_c^I) = \overline{\lambda}(x_{min}) = \sqrt{\dfrac{N_{Rk}(x_{min})/N_{Ed}(x_{min})}{\alpha_{cr}}} = \dfrac{1}{\sqrt{\alpha_{cr}}} \\ \chi(x_c^I) = \chi(x_{min}) = \dfrac{\alpha_b}{\underbrace{N_{Rk}(x_{min})/N_{Ed}(x_{min})}_{=1}} = \alpha_b \end{cases} \tag{4.31}$$

4.3.4.2 Accuracy of the analytical model

Figure 4.7 illustrates the numerical results from GMNIA analyses against results from Eq. (4.25) for different taper ratios γ_h, regarding the maximum load factor α_b and the relative critical position x_c^{II}/L. A column consisting of the hot-rolled cross-section *100x10* defined in *Table 3* is chosen for illustration. Although differences of -5% (unsafe) to 7% (safe) are noticed, it can be seen that the analytical model characterizes the behaviour of the tapered column well when compared to the numerical model. It is also noticeable an increase of up to 20% in terms of resistance with the increase of tapering at a slenderness range of $\overline{\lambda}(x_c^I) = 0.5$ to $\overline{\lambda}(x_c^I) = 1$, which shows the relevance of Eq. (4.25). Eq. (4.25) was solved considering an imperfection factor $\alpha_{EC3}=0.34$ (curve *b* of EC3-1-1), in agreement with the adopted residual stresses of $0.5f_y$. In *Figure 4.7(a)*, the taper ratio of $\gamma_h=1$, i.e., prismatic column, is shown for comparison. It is expected that the relative critical location is located at mid-span where the curvature is maximum and therefore $x_c/L=0.5$ (see *Figure 4.7(a.2)*). Moreover, Eq. (4.25) should give the same results as the EC3 curve *b*. This is visible in *Figure 4.7(a.1)*.
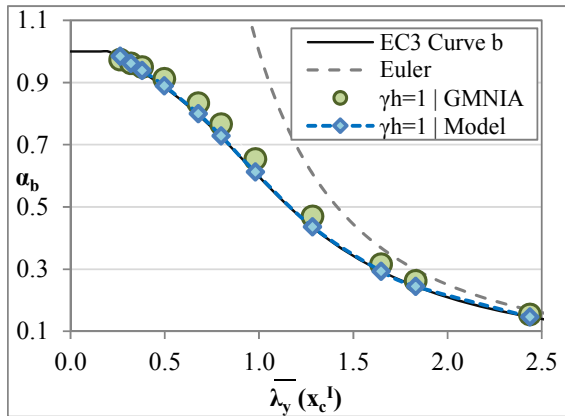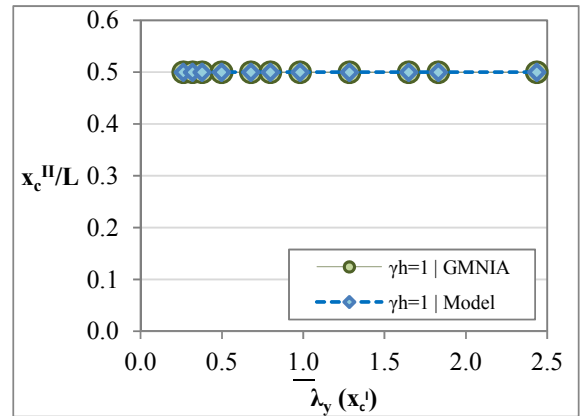
(a.1) $\gamma_h=1$ (a.2) $\gamma_h=1$
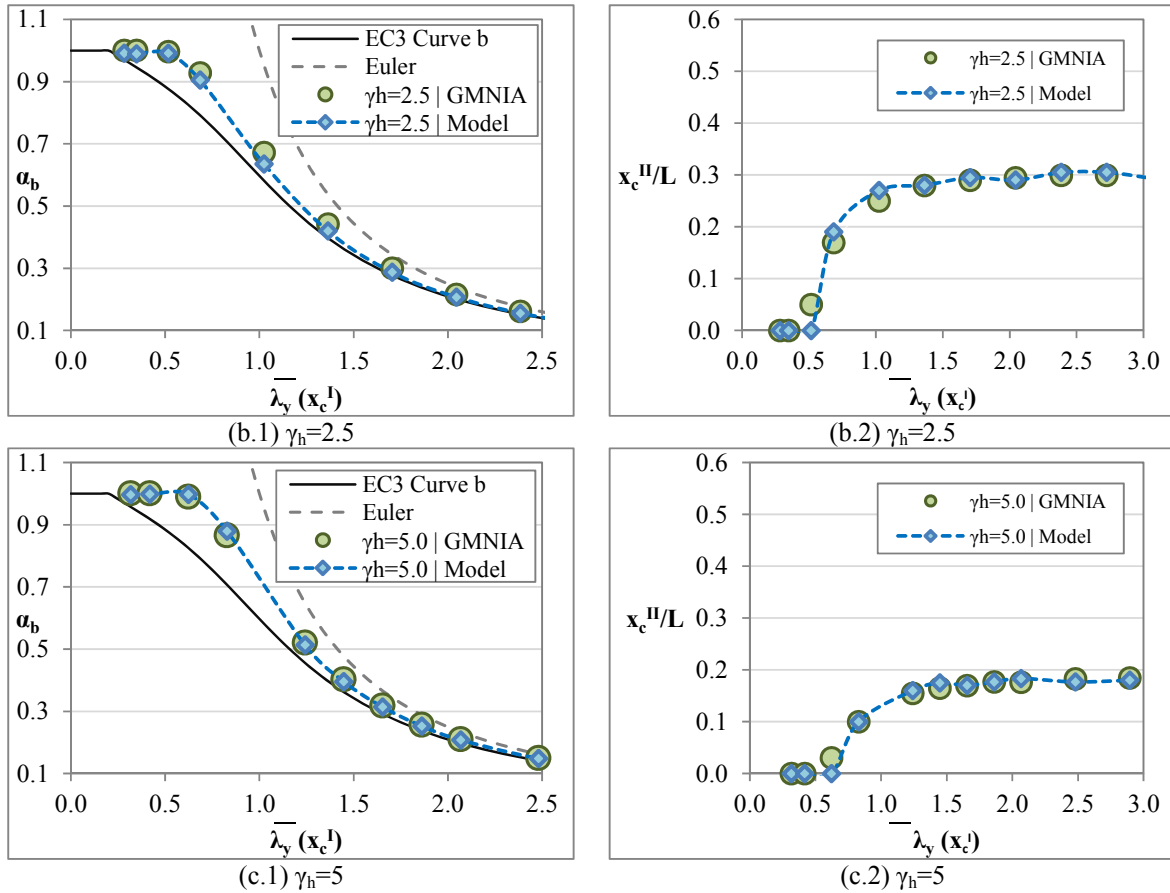
Figure 4.7: Analytical derivation; in-plane flexural buckling – Eq. (4.25) against GMNIA. (.1) Resistance $\alpha_b \equiv \chi(x_0)$ against slenderness $\bar{\lambda}(x_c^I)$; (.2) Critical position x_c^{II}/L against slenderness $\bar{\lambda}(x_c^I)$.

Figure 4.8 illustrates similar results for a web-tapered column buckling out-of-plane. Welded cross sections were chosen to illustrate this case. Although the increase in resistance is not as relevant (as the critical mode is practically not influenced by the variation of the web), an increase of 10% for the given taper ratio can still be noticed due to the variation of the cross section resistance along the column (i.e., due to the variation of the area *A* along the member). Again, Eq. (4.25) was solved considering an imperfection factor α_{EC3}=0.49 (curve *c* of EC3-1-1), in agreement with the adopted residual stress pattern for welded cross-sections subject to out-of-plane buckling.
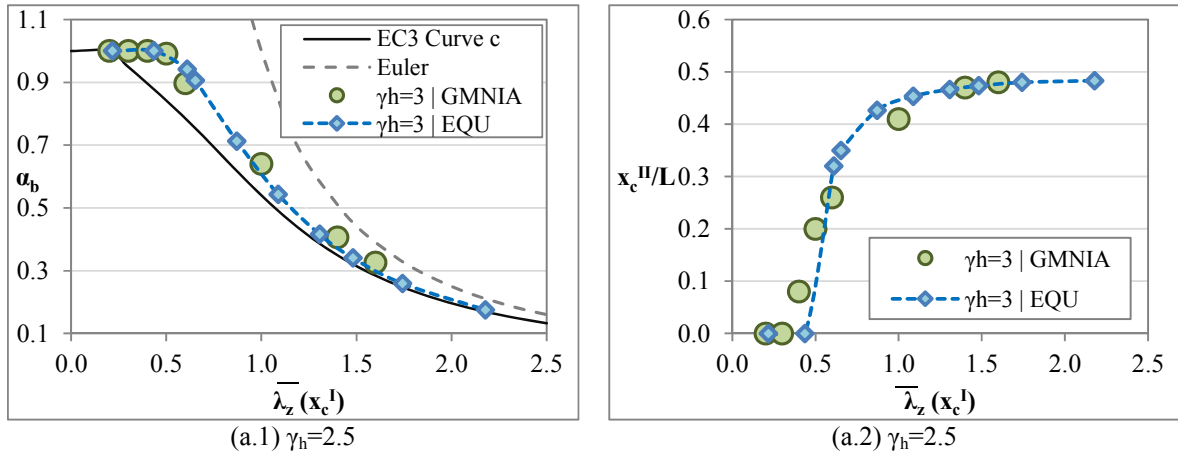
Figure 4.8: Analytical derivation; out-of-plane flexural buckling – Eq. (4.25) against GMNIA. (.1) Resistance $\alpha_b \equiv \chi(x_c^I)$ against slenderness $\bar{\lambda}(x_c^I)$; (.2) Critical position x_c^{II}/L against slenderness $\bar{\lambda}(x_c^I)$.

4.3.4.3 Influence of the taper ratio

In web-tapered members, the actual thickness of the flange to be taken into account is the projected thickness $t_f{'}$ in the vertical direction zz, i.e., higher than the plate thickness, t_f, see *Figure 4.9* and Eq. (4.32), leading to slightly different cross section resistance with the increase of member length.
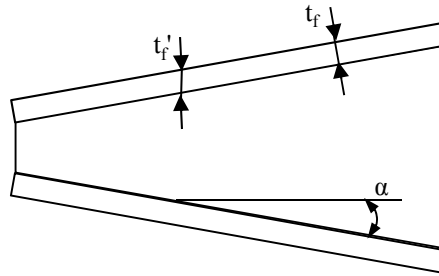
Figure 4.9: Projected thicknes $t_f{'}$ of the flange in a web-tapered member

$$t'_f = t_f / \cos(\arctan(\alpha)) = t_f / \cos\left(\arctan\left(0.5 \frac{h_{w,max} - h_{w,min}}{L}\right)\right) \quad (4.32)$$

Figure 4.10 illustrates results for in-plane buckling concerning the welded cross-section *100x10*, organized by taper angle *α*.

For higher angles it becomes unrealistic to compute values corresponding to higher slenderness. For example, for the taper angle $\alpha=2º$, a slenderness $\overline{\lambda}(x_0) = 0.65$ would already correspond to a tapering ratio of $\gamma_h=h_{max}/h_{min}\approx8$.
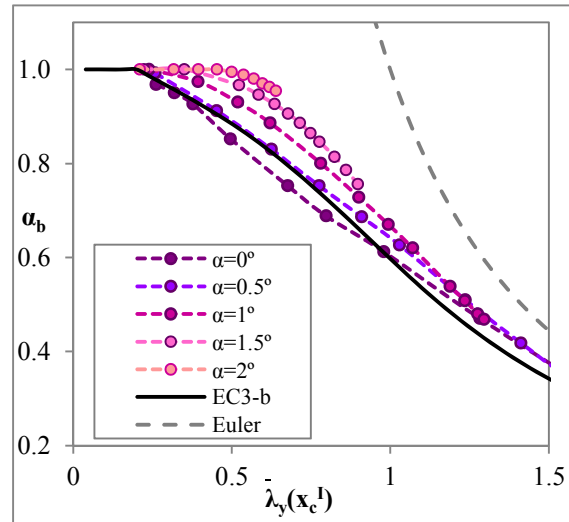
Figure 4.10: Numerical calculations GMNIA organized by α. Resistance $\alpha_b \equiv \chi(x_c^{II})$ against slenderness $\overline{\lambda}(x_c^{I})$. In-plane buckling

If the buckling curves are organized by $\gamma_h=h_{max}/h_{min}$ this will correspond to different angles α with increasing member length and, as a result, different plate thickness t_f' and different reference cross-section resistance. Nevertheless, the buckling curve is always represented in relative quantities. The representation of results according to γ_h along the slenderness range was shown to be adequate, see *Figure 4.11* in which GMNIA results are illustrated against the slenderness $\overline{\lambda}(x_c^{I})$ organized by taper ratio γ_h.

Curve *b* of EC3-1-1 is shown for comparison. Note that, for the welded cross-section cases, the numerical curve corresponding to the uniform element ($\gamma_h=1$) shows deviations that fall below the code curve results for the relevant slenderness range up to 1. This will be discussed in Section 4.4.2.

A smooth increase in the resistance with the increase of taper ratio γ_h along all slenderness ranges can be observed in all cases of *Figure 4.11*. It also shows to be less significant for higher levels of γ_h.
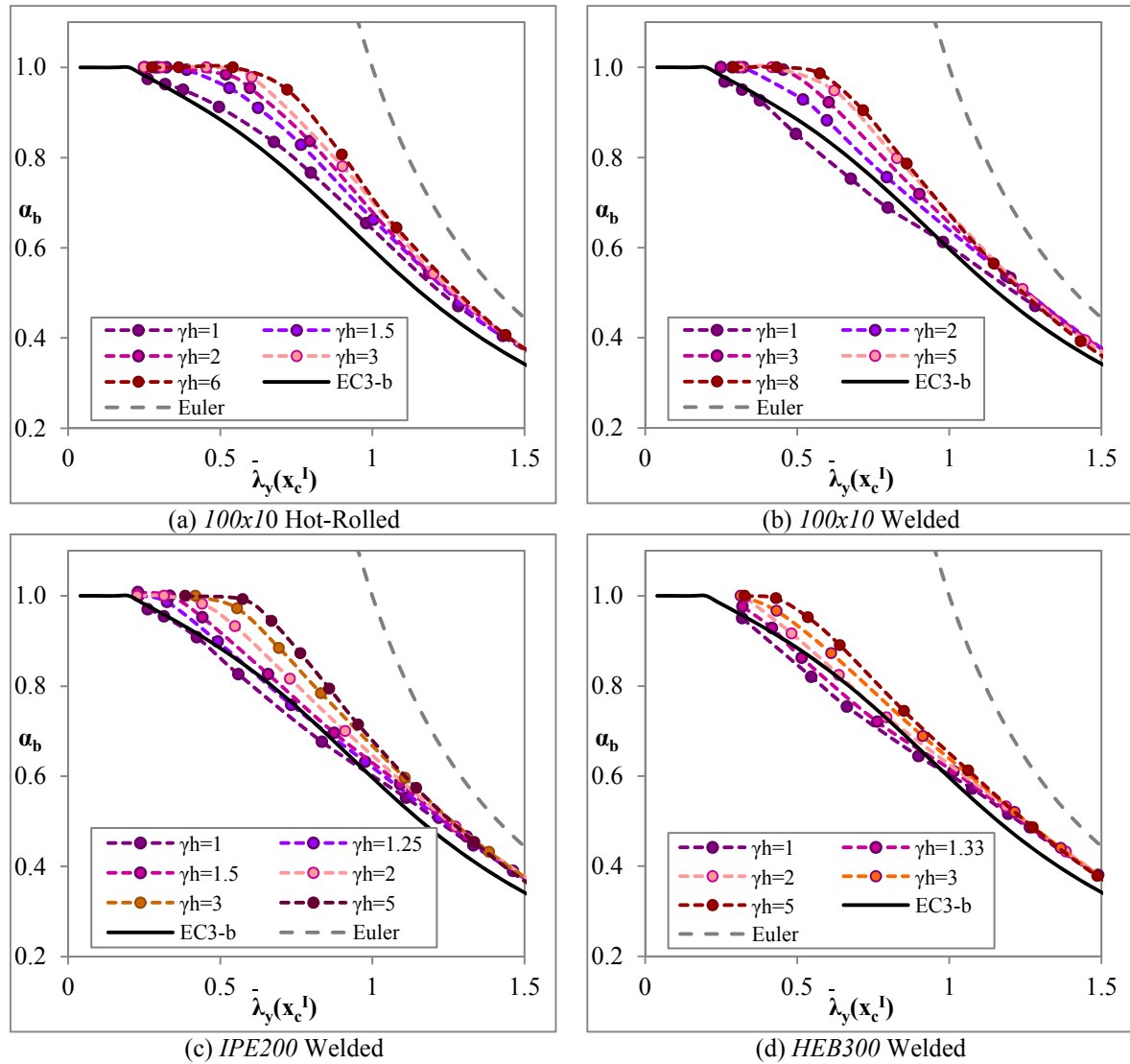
Figure 4.11: Numerical calculations GMNIA organized by γ_h. Resistance $\alpha_b \equiv \chi(x_c^{II})$ against slenderness $\overline{\lambda}(x_c^I)$. In-plane buckling

Finally, *Figure 4.12* illustrates similar results to *Figure 4.11* for out-of-plane buckling of *IPE200* case. The same conclusions are observed. The assumed residual stress pattern <u>for the hot-rolled tapered cases</u> was $0.5f_y$. Note that for the rolled cases, $\gamma_h=1$ is not considered as, for

a *IPE200* cross-section, the buckling curve should be *b* and the residual stress pattern should be *0.3f_y*.

(c) *IPE200* Hot-Rolled   (d) *IPE200* Welded
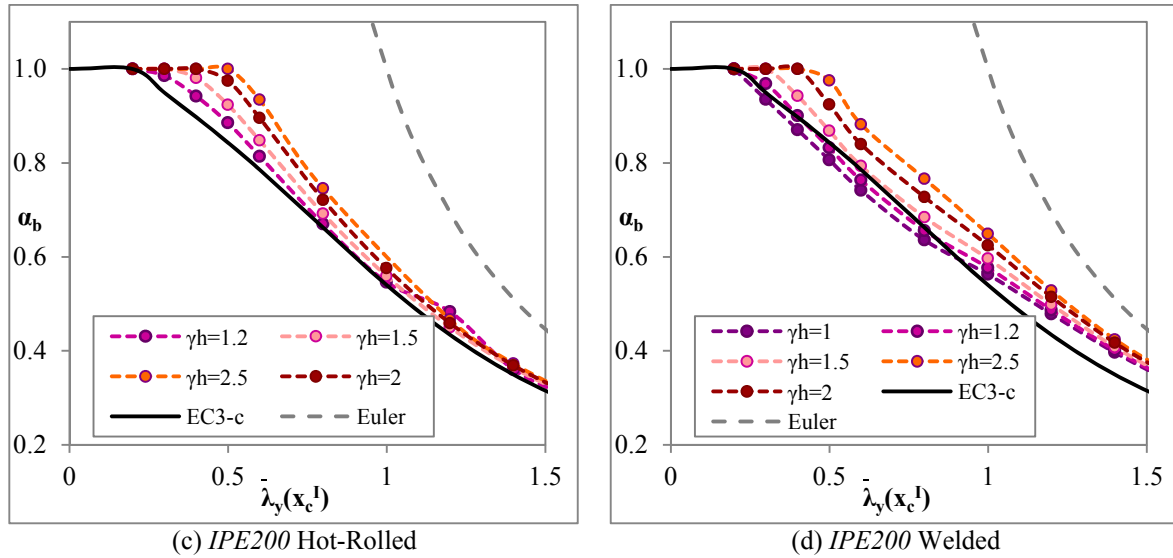
Figure 4.12: Numerical calculations GMNIA organized by γ_h. Resistance $\alpha_b \equiv \chi(x_c^{II})$ against slenderness $\overline{\lambda}(x_c^{I})$. Out-of-plane buckling

4.3.4.4 Analysis of the critical position x_c^{II} and of the imperfection factor β

The importance of identification of the critical location has already been discussed. Nowadays, there is no straight-forward procedure to obtain this location. Therefore, most designers in practice will use the smallest cross-section properties for verification according to clause 6.3.1 of EC3-1-1.

Moreover, an additional factor $\beta(x_c^{II})$ derived in Section 4.3.2.1 and given in Eq. (4.25) characterizes the increase of resistance of the tapered member relatively to the prismatic member. This factor attains a limit for prismatic members, reaching unity for those cases. When associated to the generalized imperfection of the uniform member $\eta_{uniform}$ to give a generalized imperfection of the tapered member $\eta_{non-uniform}$, see Eq. (4.25), the latter becomes lower and, as a consequence the resistance of the tapered member becomes higher.

$$\beta(x_c^{II}) = \frac{EI(x_c^{II}).(-\delta_{cr}''(x_c^{II}))}{\alpha_{cr}.N_{Ed}(x_c^{II})} \tag{4.33}$$

Figure 4.13 illustrates the influence of these two parameters for a member with an initial cross-section of *100x10* (hot-rolled) and $\gamma_h=4$, regarding in-plane buckling. *Table 4.5* shows results for the case of $\overline{\lambda}_y(x_c^I) = 0.74$. In order to obtain the resistance for the cases considering x_c^{II}, the numerical position was considered. Moreover, to calculate $\beta(x_c^{II})$, y_{cr} is extracted from LBA analysis. It can be seen that the factor β has a great influence in the resistance of the column. *Table 4.5* shows an imperfection decrease of more than 50% ($\beta(x_c^{II})$=0.48) for the analysed case of $\overline{\lambda}_y(x_c^I) = 0.74$.
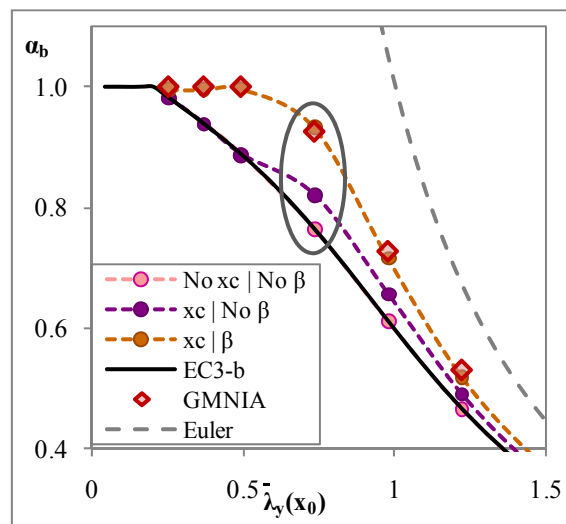
Figure 4.13: Influence of the critical position and of the imperfection in the resistance of the tapered column. In-plane buckling

Table 4.5: Influence of the critical position and of the imperfection in the resistance of the tapered column ($\overline{\lambda}_y(x_c^I) = 0.74$; α_{cr}=1.85). In-plane buckling.

Case	x_c^{II}/L	$\beta(x_c^{II})$	$\overline{\lambda}_y(x_c^I)$	$\chi(x_c^{II})$	$\alpha_b = \chi(x_c^{II})N_{Rk}(x_c^{II})/N_{Ed}$	Diff (%)
No x_c^{II} | No β	0	1	0.735	0.764	0.764	17.5
x_c^{II} | No β	0.10 (GMNIA)	1	0.773	0.741	0.820	11.5
x_c^{II} | β	0.10 (GMNIA)	0.48	0.773	0.842	0.932	-0.6
GMNIA	0.10	-	-	-	0.926	-

Finally, it can also be observed that the relative critical location x_c^{II}/L and the additional imperfection factor $\beta(x_c^{II})$ do not have a strong dependency of the fabrication process or of the initial cross-section proportions, see *Figure 4.14* and *Figure 4.15* computed for all the analysed cases. Note that here the relative critical location is higher.
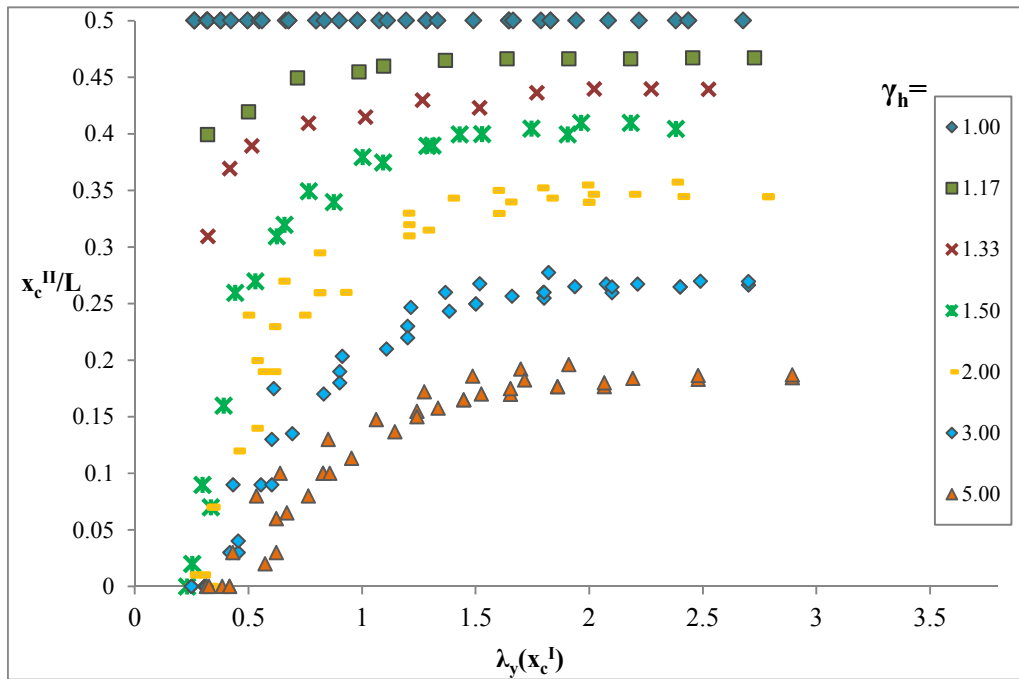
Figure 4.14: Relative critical position x_c^{II}/L against the relative slenderness $\overline{\lambda}_y(x_c^I)$, all cases (in-plane buckling)
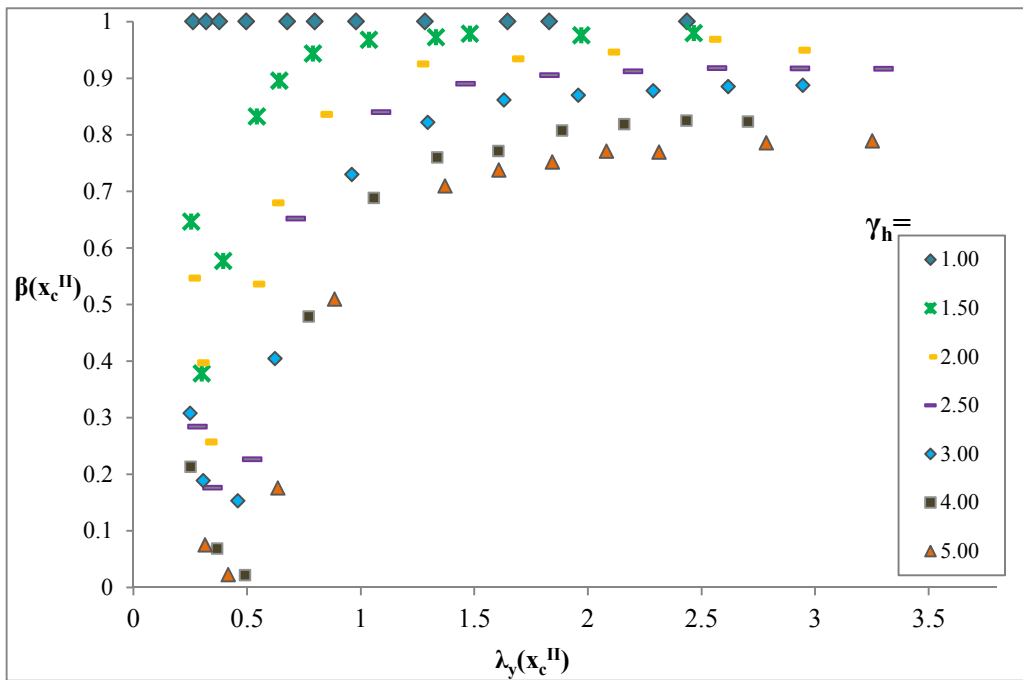
Figure 4.15: Additional imperfection factor $\beta(x_c^{II})$ against the relative slenderness $\overline{\lambda}_y\left(x_c^{II}\right)$, all cases (in-plane buckling)

The critical location x_c^{II}/L is also illustrated for the out-of-plane cases in *Figure 4.16*.
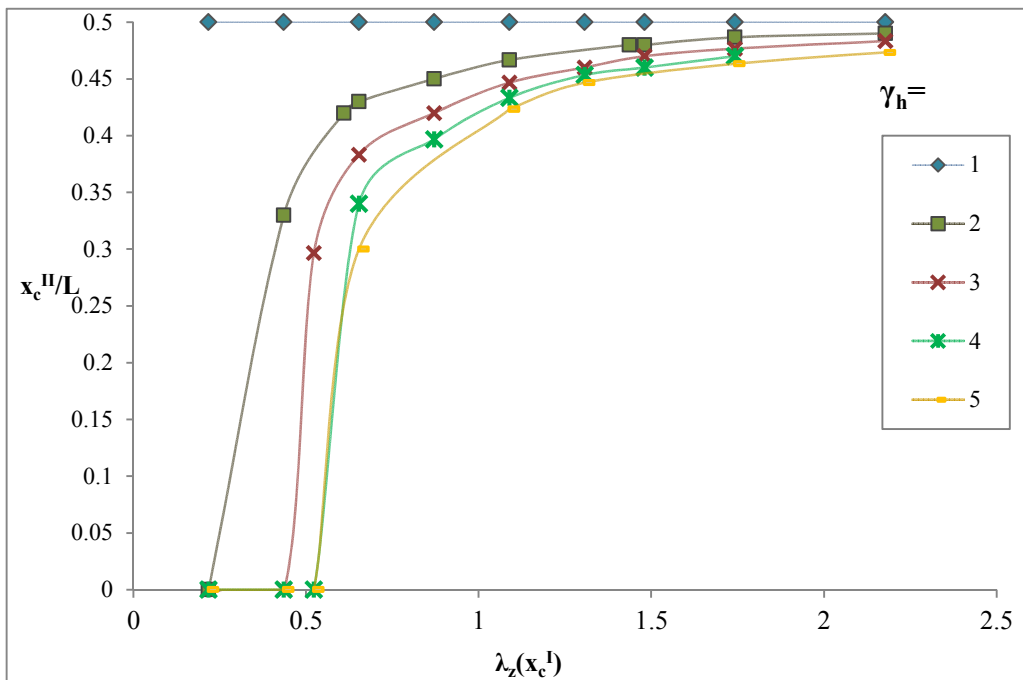
Figure 4.16: Relative critical position x_c^{II}/L against the relative slenderness $\overline{\lambda}_z\left(x_c^{I}\right)$, all cases (out-of-plane buckling)

Consider now the limit values of *Figure 4.14* to *Figure 4.16*. For high slenderness, x_c^{II} asymptotically reaches $x_{c,lim}^{II}$ and β reaches β_{lim}. Consider a tapered simply supported column subject to constant axial force. The differential equation is given by Eq. (4.34). For $N=\alpha_{cr}N_{Ed}$, $\delta=\delta_{cr}$ and Eq. (4.3) becomes

$$EI(x)\cdot\delta_{cr}'' + \alpha_{cr}N_{ED}\cdot\delta_{cr} = 0 \quad \rightarrow \quad -\delta_{cr}'' = \frac{\alpha_{cr}N_{ED}\cdot\delta_{cr}}{EI(x)} \tag{4.34}$$

Considering eigenmode conform imperfection and the imperfection given by Eq. (4.19), the utilization due to second order forces is given by (see Eq. (4.18))

$$\varepsilon_{M^{II}}(x) = \frac{M(x)}{M_R(x)} = \frac{EI(x)\left[\dfrac{\alpha_b}{\alpha_{cr}-\alpha_b}(-\delta_0''(x))\right]}{M_R(x)} = \frac{EI(x)\left[\dfrac{\alpha_b}{\alpha_{cr}-\alpha_b}e_0(-\delta_{cr}''(x))\right]}{M_R(x)} =$$

$$= \frac{EI(x)\left[\dfrac{\alpha_b}{\alpha_{cr}-\alpha_b}e_0\dfrac{\alpha_{cr}N_{ED}\cdot\delta_{cr}(x)}{EI(x)}\right]}{f_y I(x)/v(x)} = \left[\dfrac{\alpha_b}{\alpha_{cr}-\alpha_b}\dfrac{\alpha_{cr}N_{ED}e_0}{f_y}\right]\dfrac{\delta_{cr}(x)}{I(x)/v(x)} = \tag{4.35}$$

$$= K\frac{\delta_{cr}(x)}{I(x)/v(x)}$$

in which $v(x)=I(x)/W_{el}(x)$ is given by $h(x)/2$ for in-plane buckling and by $b/2$ for out-of-plane buckling.

For high slenderness, the weight of ε_M^{II} in the total utilization ratio ε is practically 100% and, as a result,

$$\varepsilon(x) = \varepsilon_N(x) + \varepsilon_{M^{II}}(x) \approx \varepsilon_{M^{II}}(x) = K\frac{\delta_{cr}(x)}{I(x)/v(x)} \tag{4.36}$$

The limit second order failure location, $x_{c,lim}^{II}$, may be obtained by determining the maximum of Eq. (4.36). The latter can be evaluated numerically.

Considering Eq. (4.34), the imperfection factor β given in Eq. (4.33), for $x=x_{c,lim}^{II}$ becomes

$$\beta_{\lim} = \beta(x_{c,\lim}^{II}) = \frac{EI(x_{c,\lim}^{II}).(-\delta_{cr}''(x_{c,\lim}^{II}))}{\alpha_{cr}.N_{Ed}} = \frac{EI(x_{c,\lim}^{II}).(\dfrac{\alpha_{cr} N_{ED} \cdot \delta_{cr}(x_{c,\lim}^{II})}{EI(x_{c,\lim}^{II})})}{\alpha_{cr}.N_{Ed}} = \delta_{cr}(x_{c,\lim}^{II}) \quad (4.37)$$

Eq. (4.36) and Eq. (4.37) are the general solution for flexural buckling of tapered columns. For the case of in-plane buckling of a web-tapered column, $x_{c,lim}^{II}$ and β_{lim} may be obtained by solving

$$\left(\frac{\delta_{cr}(x)}{I_y(x)/h(x)} \right)' = 0 \quad \rightarrow \quad x_{c,\lim}^{II} \quad \rightarrow \quad \beta_{\lim} = \delta_{cr}(x_{c,\lim}^{II}) \quad (4.38)$$

Figure 4.17 compares Eq. (4.38) with the numerical results of *Figure 4.14* and *Figure 4.15* for the *100x10* cross section.
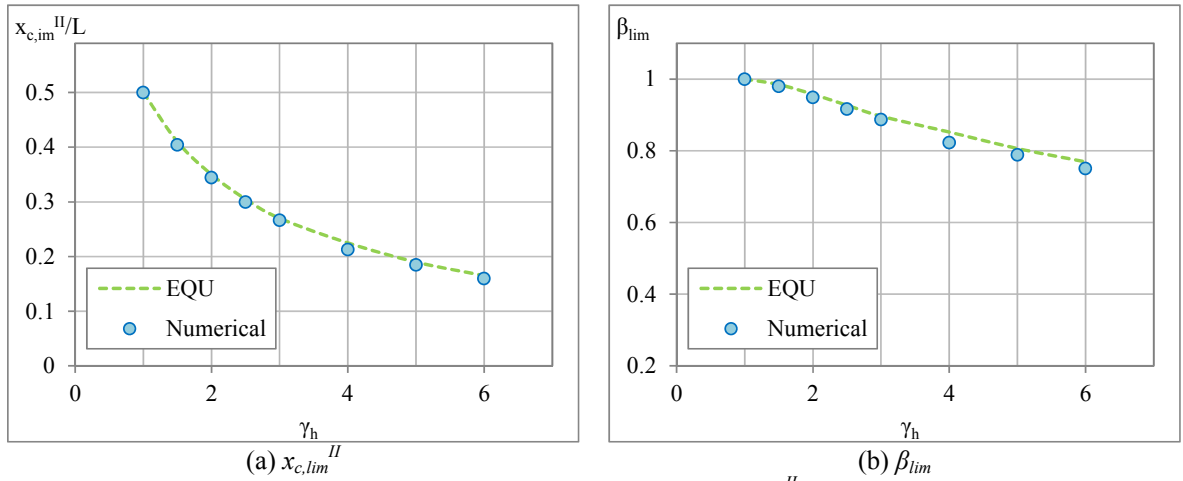
(a) $x_{c,lim}^{II}$ (b) β_{lim}
Figure 4.17: Analysis of the limit values for the critical location x_c^{II} and the imperfection factor β

For out-of-plane flexural buckling of web-tapered columns Eq. (4.36) and Eq. (4.37) may be further simplified considering that $I_z(x)$ is constant. The differential equation Eq. (4.3) leads to the Euler load with a sinusoidal shape for δ_{cr}. $x_{c,lim}^{II}$ and β_{lim} are then

$$\left(\frac{\delta_{cr}(x)}{I_z/b} \right)' = 0 \quad \rightarrow \quad x_{c,\text{lim}}^{II} \approx 0.5L \quad \rightarrow \quad \beta_{\text{lim}} \approx 1 \qquad (4.39)$$

The latter can be confirmed by analyzing *Figure 4.16* in which x_c^{II} in fact seems to approach *x=0.5L*.

4.3.4.5 Influence of the function for the magnitude of the imperfection

Results have been shown regarding the amplitude of the imperfection given by e_0 (Section 4.3.2), i.e., consistent with the derivation of the column buckling curves of EC3-1-1. *Figure 4.18* compares the solution of Eq. (4.25) and Eq. (4.30), in which for the latter, Eq. (4.28) (equation (5.9) of EC3-1-1) is considered for the imperfection. In the analyzed figures, the results of Eq. (4.25) and Eq. (4.30) are indicated as *EQU_e0* and *EQU_equiv*, respectively. Two representations of resistance are considered and illustrated concerning a taper ratio of $\gamma_h=4$ and the reference cross-section *100x10* (hot-rolled) for in-plane buckling: *Figure 4.18(a)* illustrates the reduction factor $\overline{\lambda}(x_c^I)$ as a function of the reduction factor $\chi(x_c^I) \equiv \alpha_b$, and, therefore, resistance can be directly compared; *Figure 4.18(b)* illustrates the reduction factor $\overline{\lambda}(x_c^{II})$ as a function of the reduction factor $\chi(x_c^{II})$ – it is stated in Naumes (2009) that when equation (5.9) of EC3-1-1 (Eq. (4.28)) is considered for the imperfection, results of the reduction factor $\chi(x_c^{II})$ coincide with current buckling curves for columns (see also *Figure 4.18(b)*) and that good agreement is achieved with numerical models. This is to be expected if the imperfections considered in the numerical models are also obtained from Eq. (4.28). However, the magnitude of the geometrical imperfection should only be dependent on the member length (Taras, 2010). Moreover, for the calibration of EC3 imperfection factors for columns, this magnitude was given by $e_0=L/1000$ (and additional residual stresses for the material imperfections). The same approach is considered in this study. Both *Figure 4.18(a)* and *(b)* show a better agreement with the EC3 consistent approach regarding Eq. (4.25). Note that the equivalent amplitudes of Table 5.1 of EC3-1-1 (or *Table 1.1* of this thesis) were in fact calibrated afterwards based on the column buckling curves.

In addition, concerning *Figure 4.18(b)*, GMNIA is also illustrated in terms of the reduction factor $\chi(x_c^{II})$, in which x_c^{II} is obtained from the numerical model. Finally, *Figure 4.19(a)* and *(b)* respectively illustrate the resistance α_b and relative critical location x_c^{II}/L regarding all taper ratios of the analyzed cross-section *100x10* (hot-rolled), for in-plane buckling. A higher spread is noticed for Eq. (4.30). Eq. (4.25) is therefore considered for development of the design methodology.

(a) Resistance $\alpha_b \equiv \chi(x_c^{II})$ against slenderness $\overline{\lambda}(x_c^{I})$ (b) Resistance $\chi(x_c^{II})$ against slenderness $\overline{\lambda}(x_c^{II})$
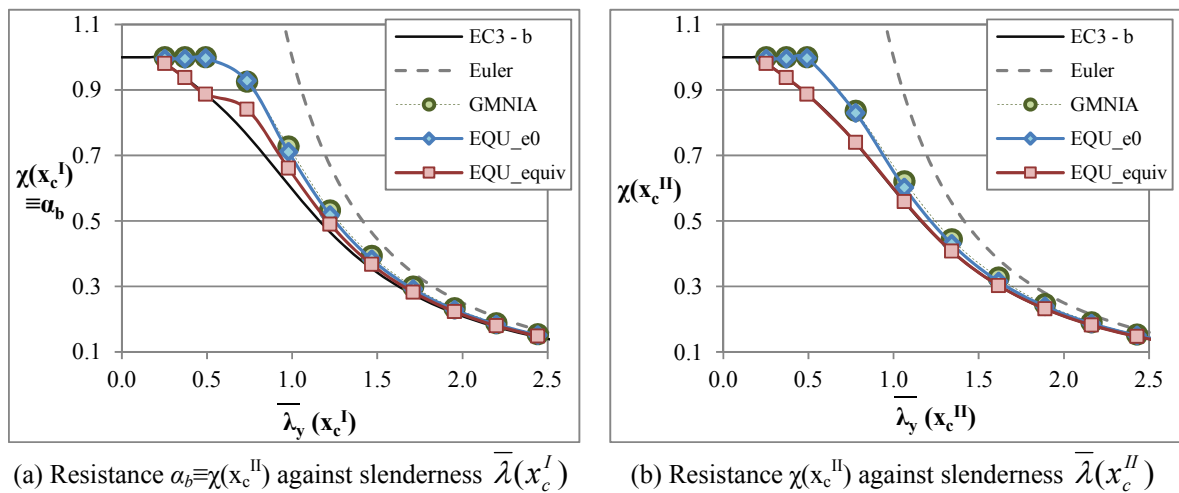
Figure 4.18: Influence of imperfection magnitude – buckling curve representation

(a) Resistance α_b (b) Critical location x_c^{II}/L
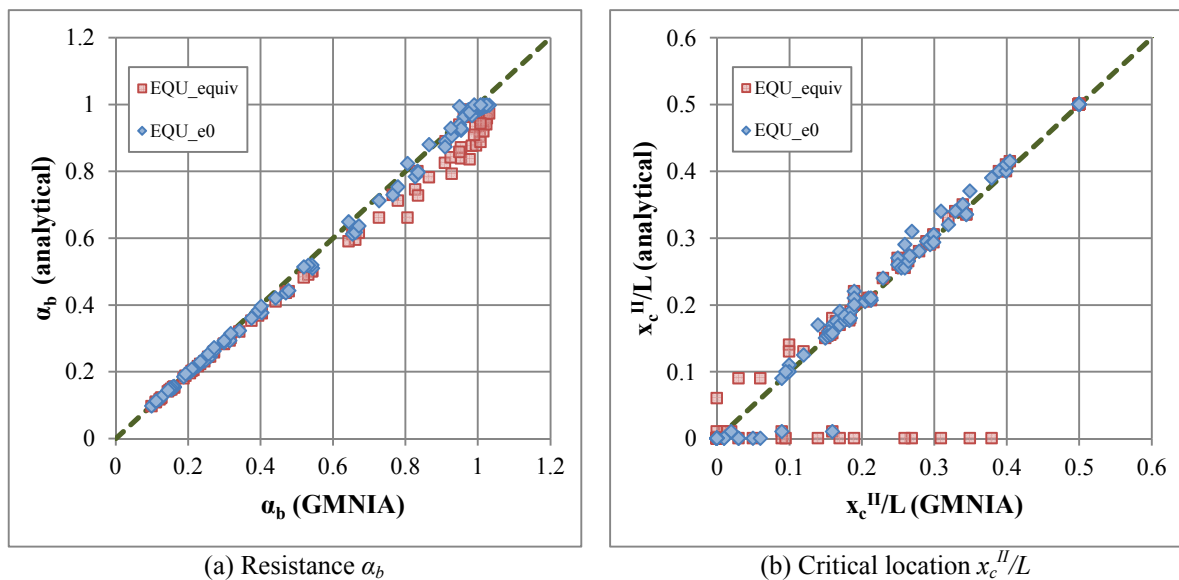
Figure 4.19: Influence of imperfection magnitude – *100x10* (hot rolled), all taper ratios

4.4 Design methodology

4.4.1 Introduction

Considering the developed analytical formulation and the numerical calculations, a verification procedure for the flexural buckling of tapered columns is now proposed.

In a first step, regarding the imperfection factor for prismatic welded cross-sections it was noticed that, for I-sections, the imperfection factors $\alpha=0.34$ and $\alpha=0.49$, respectively for in-plane and out-of-plane buckling, provide unsafe results for slenderness up to approximately 1 (differences of 8% were observed, see Section 4.4.2). Because this proposal has, as a reference limit, the case of prismatic members ($\gamma_h=1$), new imperfection factors for prismatic welded cross-sections are calibrated.

In a second step, the development of a verification procedure for tapered columns is carried out. Here, expressions for the critical location x_c^{II} and the additional imperfection factor $\beta(x_c^{II})$ are calibrated against numerical results of Section 4.3.4.4. Simplifications of the proposed method then are carried out leading to an equivalent safety level.

4.4.2 Generalized imperfection for flexural buckling prismatic columns with welded I-section

Ayrton-Perry formulation for prismatic columns is given by

$$1 = \chi + \chi \frac{1}{1-\bar{\lambda}^2\chi}\underbrace{\left[e_0\frac{N_R}{M_R}\right]}_{\alpha\left(\bar{\lambda}-0.2\right)\equiv\eta_{EC3}} \rightarrow (...) \rightarrow \eta_{EC3} = \alpha\left(\bar{\lambda}-0.2\right)=\left(1-\bar{\lambda}^2\chi\right)\left(1-\frac{1}{\chi}\right) \quad (4.40)$$

The generalized imperfection η_{EC3} of prismatic welded columns is given by Eq. (4.41), for a flange thickness $t_f \leq 40\ mm$

$$\eta_{EC3} = \alpha\left(\overline{\lambda} - 0.2\right) = \begin{cases} \alpha = 0.34, & \text{In-plane buckling} \\ \alpha = 0.49, & \text{Out-of-plane buckling} \end{cases} \tag{4.41}$$

Figure 4.20(a) and *Figure 4.21(a)* illustrate the generalized imperfection of EC3-1-1 η_{EC3}, respectively for in-plane and out-of-plane buckling, compared to the generalized imperfection η_{num} of about 100 numerical calculations covering a range of uniform columns with different h/b ratios varying from 0.95 (*HEA200*) to 2.5 (*IPE500*) and slenderness varying from $\overline{\lambda} = 0.1$ to $\overline{\lambda} = 2.0$. The value η_{num} is calculated according to Eq. (4.42), see also Taras (2010), in which χ is extracted numerically and corresponds to the maximum load factor of GMNIA calculation, α_b:

$$\eta_{num} = \left(1 - \overline{\lambda}^2 \chi_{num}\right)\left(1 - \frac{1}{\chi_{num}}\right) \tag{4.42}$$

Figure 4.20(a) shows the difference, on the unsafe side, in considering for the in-plane imperfection factor α the value of 0.34. A value of α=0.45 was shown to fit the reduction factor χ_y very accurately up to slenderness of 1. However, in order not to get too conservative for slenderness above 1 and to take into account the buckling behaviour of columns with a welded residual stress pattern for that slenderness range, a cut-off of $\eta = \alpha(\overline{\lambda} - 0.2) \leq 0.27$ was also shown to be adequate. If the cut-off of 0.27 is applied, for higher slenderness of about $\overline{\lambda}_y = 1.5$, imperfection becomes unsafe again. However, for high slenderness range, the column is not so sensitive to the imperfection level and resistance converges to the Euler load. *Figure 4.20(b)* illustrates the reduction factor χ_y against the relative slenderness $\overline{\lambda}_y$. An analogous study is illustrated in *Figure 4.21* for the case of out-of-plane buckling. Here, a value of α=0.64 (instead of currently adopted α=0.49) and a cut-off of the generalized imperfection of $\eta = \alpha(\overline{\lambda} - 0.2) \leq 0.34$ was shown to give accurate results. Finally, it is interesting to notice that α=0.64 was also given in Taras (2010) as the limit imperfection factor for lateral-torsional buckling of welded beams, see *Table 2.4* of Chapter 2.
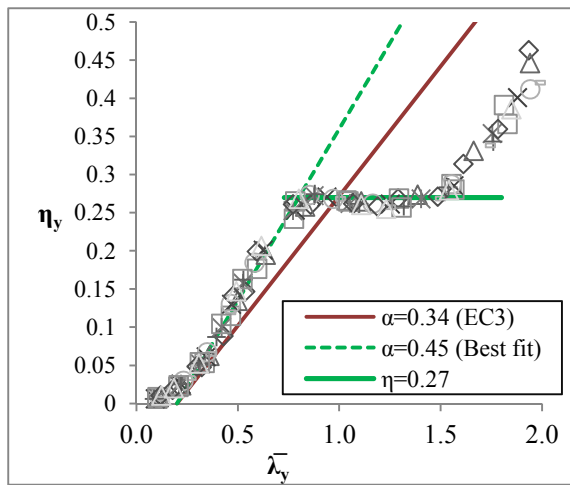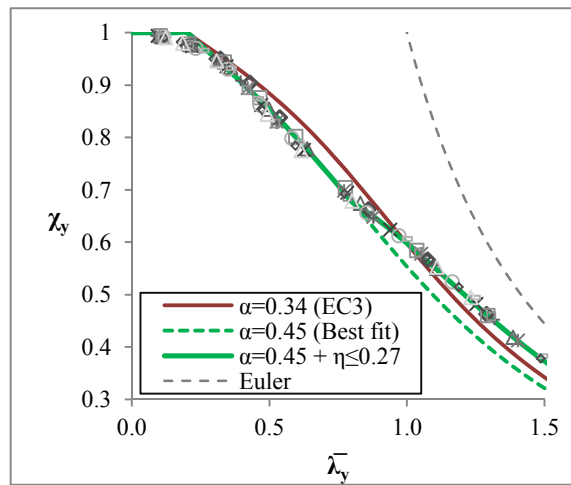
(a) Generalized imperfection η against $\overline{\lambda}_y$ (b) Resistance χ_y against $\overline{\lambda}_y$

Figure 4.20: Generalized imperfection of in-plane flexural buckling of welded columns
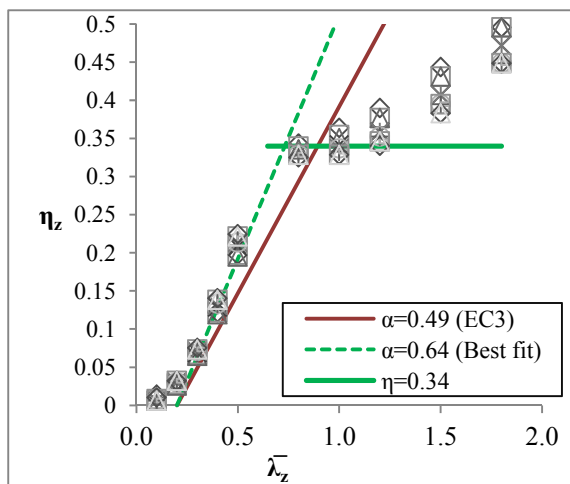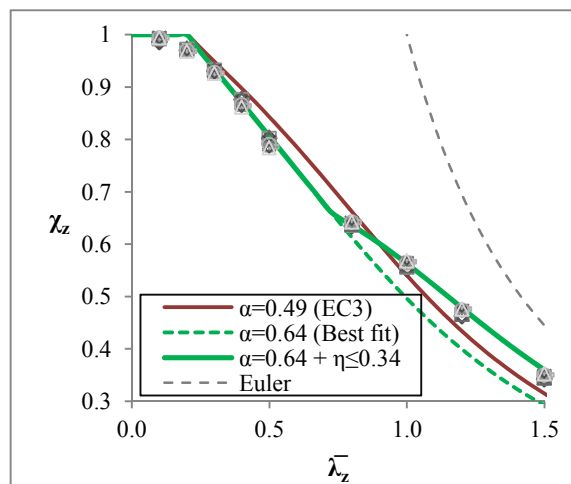
(a) Generalized imperfection η against $\overline{\lambda}_z$ (b) Resistance χ_z against $\overline{\lambda}_z$

Figure 4.21: Generalized imperfection of out-of-plane flexural buckling of welded columns

4.4.3 Possible approaches and calibration

4.4.3.1 The "real" behavior

a) Definition

Eq. (4.25) was shown to follow accurately the buckling behavior of a tapered column. However, the application of this expression is not straight forward:

- The critical location x_c^{II} is needed throughout the application of Eq. (4.25) and for this an iterative procedure is required;

- Once x_c^{II} is known, the additional imperfection factor $\beta(x_c^{II})$ can be calculated. However, to obtain it, the function for the critical curvature is needed – this is not a direct procedure.

x_c^{II} and $\beta(x_c^{II})$ vary with increasing slenderness, from a "plateau" slenderness in which $\beta(x_c^{II})=0$ (no imperfection) and $x_c^{II}= x_c^{I}$ ($=x_{min}$) (cross section resistance governs) up to a limit slenderness $x_{c,lim}^{II}$ and β_{lim} which may be determined by solving Eq. (4.38).

Assuming that the critical load multiplier, α_{cr}, is obtained from a numerical analysis, LBA, expressions regarding x_c^{II} and $\beta(x_c^{II})$ are still needed for the direct calculation of resistance. Elliptical expressions were shown to give good approximation for both these parameters.

b.1) Flexural buckling in-plane

Fitting equations for x_c^{II} and $\beta(x_c^{II})$ regarding in-plane buckling are illustrated in *Figure 4.22* and *Figure 4.23* respectively. Corresponding expressions are shown in *Figure 4.24* which illustrates the complete procedure for in-plane stability verification of tapered columns. Note that, for higher Taper Ratios, β could be lower as derived in Eq. (4.37). However, for safety reasons concerning the resistance multiplier α_b, the limit of $\beta_{lim}=1$ for all tapered ratios was chosen.
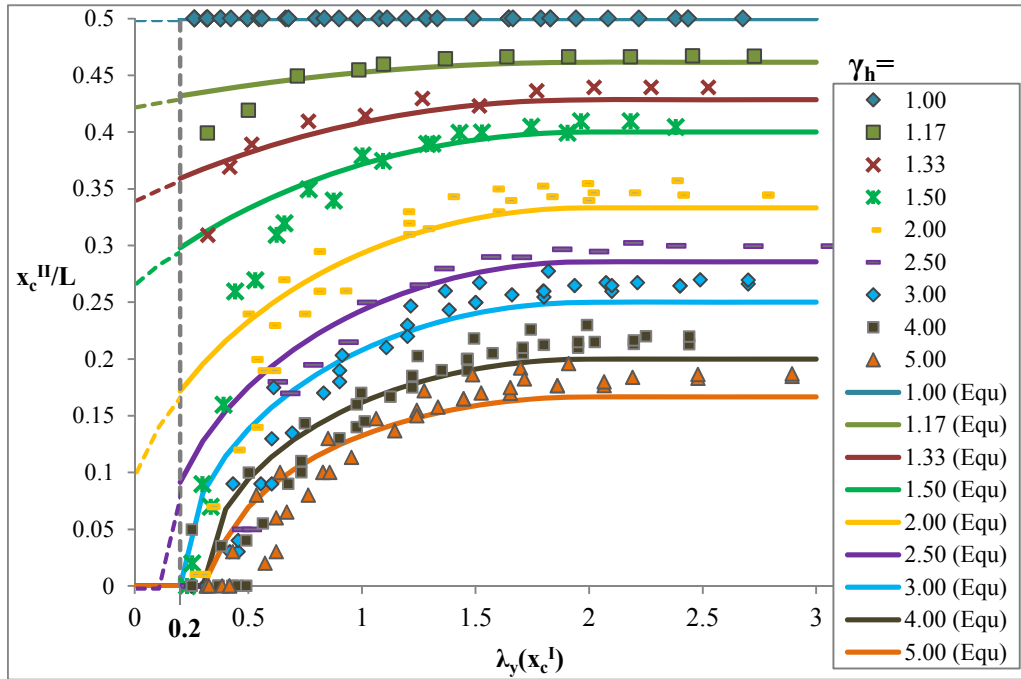
Figure 4.22: Fitting elliptical expression for the critical position, x_c^{II}
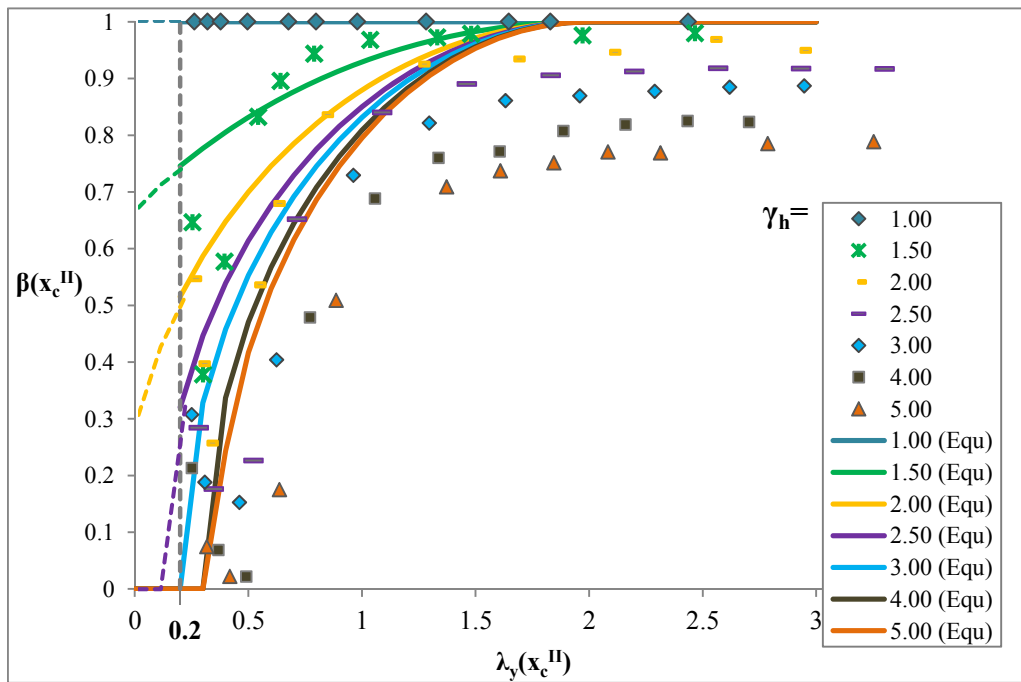
Figure 4.23: Fitting elliptical expression for the additional imperfection factor $\beta(x_c^{II})$

Figure 4.24 illustrates the steps to be followed. Firstly, the critical position x_c^{II} is determined based on the reference relative slenderness of the smallest cross-section. α_{cr} shall be calculated numerically. Note that from this step, geometrical properties of x_c^{II} are considered,

including slenderness calculation for the determined position. Imperfection can now be calculated by combining the imperfection effects of the uniform member ($\eta_{uniform}$) and of the non-uniform member (β). With this, the reduction factor at x_c^{II} is determined and the verification is finally made.

Required data

$$\bar{\lambda}(x_c^I) = \sqrt{\frac{N_{Rk}(x_c^I)/N_{Ed}}{\alpha_{cr}}}; \qquad \gamma_h = h_{max}/h_{min}; \qquad a = 1.5 + \frac{0.6}{\gamma_h - 1}; \qquad b = \frac{1}{\gamma_h + 1}$$

Critical Position, x_c^{II} ↓

$$x_c^{II}/L = \begin{cases} 0, & \bar{\lambda}(x_c^I) < 2-a \quad or \quad \bar{\lambda}(x_c^I) \le 0.2 \\[2mm] b\sqrt{1 - \frac{\left(\bar{\lambda}(x_c^I)-2\right)^2}{a^2}}, & 2-a \le \bar{\lambda}(x_c^I) \le 2 \\[2mm] b, & \bar{\lambda}(x_0) > 2 \end{cases}$$

Slenderness at x_c ↓

$$\bar{\lambda}(x_c^{II}) = \sqrt{\frac{N_{Rk}(x_c^{II})/N_{Ed}}{\alpha_{cr}}}$$

Account for Imperfection

$$\beta(x_c^{II}) = \begin{cases} 0, & \bar{\lambda}(x_c^{II}) < 2-a \quad or \quad \bar{\lambda}(x_c^{II}) \le 0.2 \\[2mm] \sqrt{1 - \frac{\left(\bar{\lambda}(x_c^{II})-2\right)^2}{a^2}}, & 2-a \le \bar{\lambda}(x_c^{II}) \le 2 \\[2mm] 1, & \bar{\lambda}(x_c^{II}) > 2 \end{cases}$$

$$\eta_{Uniform} = \alpha_{Uniform}\left(\bar{\lambda}(x_c^{II}) - 0.2\right)$$

	Hot $-$ Rolled	Welded
where $\alpha_{Uniform}$	0.34	0.45
$\eta_{Uniform}$	$-$	≤ 0.27

Reduction factor ↓

$$\chi(x_c^{II}) = \frac{1}{\phi(x_c^{II}) + \sqrt{\phi^2(x_c^{II}) - \bar{\lambda}^2(x_c^{II})}} \le 1, \qquad with \quad \begin{cases} \phi(x_c^{II}) = 0.5\left(1 + \eta(x_c^{II}) + \bar{\lambda}^2(x_c^{II})\right) \\[2mm] \eta(x_c^{II}) = \eta_{Uniform}\,\beta(x_c^{II}) \end{cases}$$

Verification ↓

$$N_{Ed} \le \chi(x_c^{II})N_{Rk}(x_c^{II}) \le N_{Rk}(x_c^I)$$

Figure 4.24: Design proposal for in-plane buckling

In *Figure 4.24*, the parameter a is associated to the referred "plateau" slenderness, and the parameter b is equivalent to $x_{c,lim}^{II}$.

b.2) Flexural buckling out-of-plane

For the case of out-of-plane buckling, the same procedure as in *Figure 4.24* is adopted with some modifications:

- The parameter b (or $x_{c,lim}^{II}/L$) can be replaced by $b=0.5$, as derived in Eq. (4.39). However, on the safe side the following expression (varying between $x_{c,lim}^{II}/L=0.5$ and 0.4) is proposed:

$$b = \frac{1 + 4\gamma_h}{10\gamma_h} \quad \left(= x_{c,\lim}^{II} / L\right);$$

- The generalized imperfection $\eta_{uniform}$ is replaced by

$$\eta_{uniform} = \alpha\left(\overline{\lambda}(x_c^{II}) - 0.2\right), \text{ where } \begin{cases} \alpha = 0.49, & \text{Hot} - \text{Rolled} \\ \alpha = 0.64 \wedge \eta \leq 0.34, & \text{Welded} \end{cases};$$

- Finally, the parameter a, associated to the "plateau" slenderness may be kept.

c) Results

Figure 4.25 illustrates the resistance of the numerical results $\chi(x_c^I)\equiv\alpha_b$ as a function of the relative slenderness $\overline{\lambda}(x_c^I)$, concerning GMNIA analysis as well as the proposed formulation for in-plane buckling. The current EC3 curve for uniform members that would be applied is also illustrated (i.e. $\alpha=0.34$; $\beta=1$; and considering x_c^{II} as the minimum cross-section as no guidelines exist at the moment). Good agreement is noted with the proposed methodology.
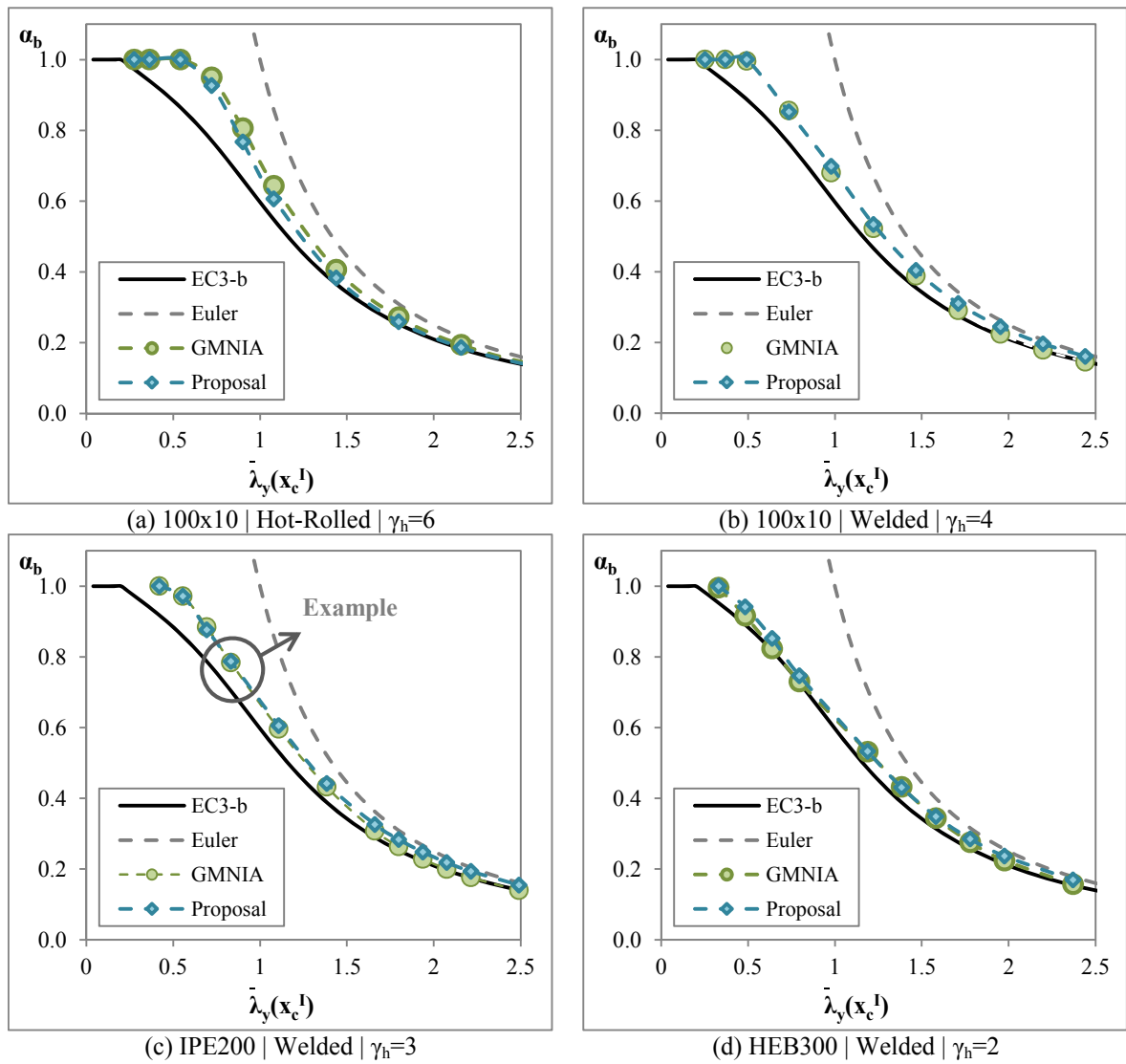
Figure 4.25: Resistance α_b against $\overline{\lambda}_y\left(x_c^I\right)$. Evaluation of the proposed method, in-plane buckling

Note that *Figure 4.25(b)* highlights a case which will be considered for the application example of Section 4.5.

Finally, *Figure 4.26* illustrates the results for the out-of-plane buckling verification proposal.

(a) IPE200 | Welded | γ_h=1.8   (b) HEB300 | Welded | γ_h=1.33
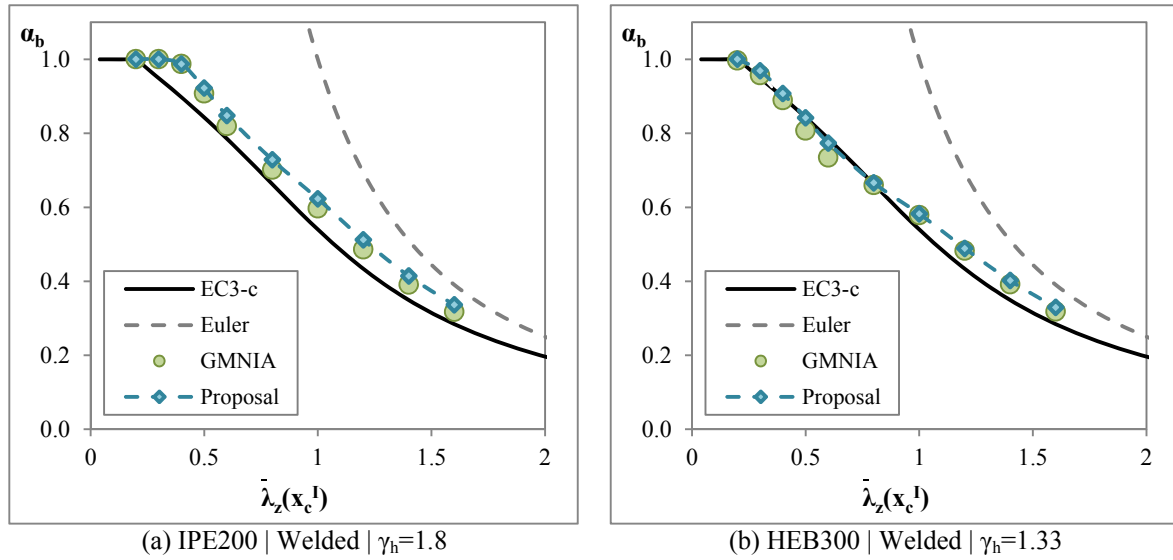
Figure 4.26: Resistance α_b against $\bar{\lambda}_z (x_c^I)$. Evaluation of the proposed method, out-of-plane buckling

4.4.3.2 Uncoupling of first and second order effects

a) Critical position

The parameters x_c^{II} and β take into account the combined effects of stability and cross-section resistance for a given slenderness, as discussed previously. A simplification is carried in the following by separating the effects of cross-section resistance from the effects of instability, i.e., in the Ayrton-Perry model, always consider $x_{c,lim}^{II}$ and β_{lim} according to the proposed methodology in Section 4.4.3.1. The Ayrton-Perry result is then limited by the cross-section resistance (given by x_c^I and corresponding β=0). This simplification is illustrated in *Figure 4.27* and results are shown in *Figure 4.29*. Excellent agreement is noticed and, as a result, this methodology will be considered. This avoids the calculation of a "plateau" slenderness and varying expressions along the beam length. Note that this only leads to similar results to the proposal in Section 4.4.3.1 because $x_{c,lim}^{II}$ is considered with the corresponding β_{lim}=1, both parameters corresponding to the same slenderness level.

(a) Considering expressions which vary along the slenderness

(b) Separating second order effects from first order effects
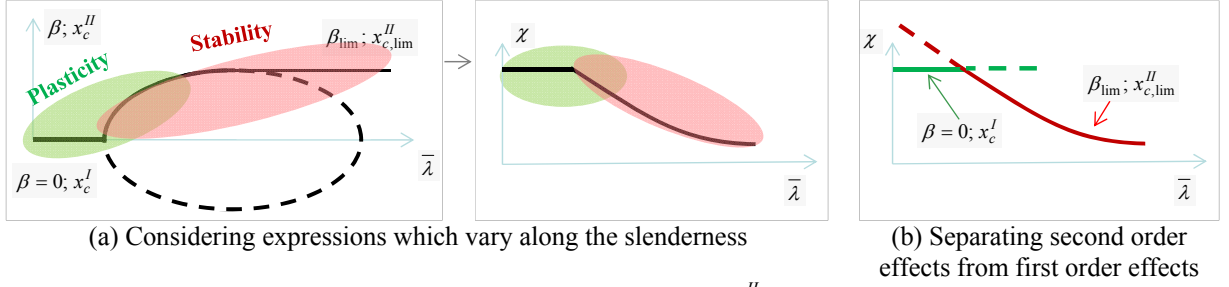
Figure 4.27: Simplification of x_c^{II} and β

Eq. (4.25) then becomes

$$\varepsilon(x_{c,\lim}^{II}) = 1 \rightarrow 1 = \chi(x_{c,\lim}^{II}) + \chi(x_{c,\lim}^{II}) \frac{1}{1 - \bar{\lambda}^2(x_{c,\lim}^{II})\chi(x_{c,\lim}^{II})} \underbrace{\underbrace{\frac{\alpha\left(\bar{\lambda}(x_{c,\lim}^{II}) - 0.2\right)}{\eta_{uniform}}}_{(x_{c,\lim}^{II})} \frac{1}{\beta_{\lim}}}_{\eta_{non-uniform}(x_{c,\lim}^{II})} \quad (4.43)$$

Eq. (4.43) matches clause 6.3.1, as long as $x_{c,lim}^{II}$ is considered. The values of α are obtained from Section 4.4.3.1. In addition, the cross section check at x_c^I needs to be carried out, i.e. $N_{Ed} \leq N_{Rk}(x_c^I)$.

$x_{c,lim}^{II}$ is summarized in Eq. (4.44):

$$x_{c,\lim}^{II}/L = \begin{cases} 1/(1 + \gamma_h), & In-Plane\ buckling \\ (1 + 4\gamma_h)/(10\gamma_h), & Out-of-Plane\ buckling \end{cases} \quad (4.44)$$

b) Introduction of an "over-strength factor"

An "over-strength" factor is now proposed. This concept was proposed in Taras (2010) for non-uniform bending moment distributions of prismatic beams. The "over-strength" factor is an intuitive parameter to qualitatively describe not only the lower spread of plasticity around the failure location, but also the increase in resistance for a given member with varying cross-section and forces relatively to the reference case of a prismatic member with constant forces and/or bending moment diagrams.

It will be seen in Chapter 5, in which the lateral-torsional buckling of tapered beams is treated, the advantages of performing this transformation in the analytical model, Eq. (4.25). To maintain consistency, a similar model is presented for the case of columns.

The "over-strength" factor can be defined as the ratio $\varphi = \alpha_{ult,k}(x_{c,lim}^{II})/\alpha_{ult,k}(x_c^I)$. When replaced in Eq.(4.43), it becomes

$$\varepsilon(x_{c,\lim}^{II}) = 1 \rightarrow 1 = \frac{\chi_{LT}(x_c^I)}{\varphi} + \frac{\chi_{LT}(x_c^I)}{\varphi} \frac{1}{1 - \varphi \overline{\lambda}_{LT}^2(x_c^I)\dfrac{\chi_{LT}(x_c^I)}{\varphi}} \alpha\left(\sqrt{\varphi}\,\overline{\lambda}(x_c^I) - 0.2\right) \quad (4.45)$$

The verification to flexural buckling is given by

$$\phi = 0.5 \times \left(1 + \eta + \varphi \times \overline{\lambda}^2(x_c^I)\right)$$

$$(4.46)$$

$$\chi(x_c^I) = \frac{\varphi}{\phi + \sqrt{\phi^2 - \varphi \times \overline{\lambda}^2(x_c^I)}} \leq 1$$

in which α and η are again obtained from Section 4.4.3.1 and η is determined with the slenderness $\sqrt{\varphi}\,\overline{\lambda}(x_c^I)$. Finally, regarding the definition of φ, for web-tapered columns subject to constant axial force a simple transformation may be performed based on the expressions for $x_{c,lim}^{II}$.

$$\varphi = \frac{\alpha_{ult,k}(x_{c,\lim}^{II})}{\alpha_{ult,k}(x_c^I)} = \frac{A(x_{c,\lim}^{II})f_y / N_{Ed}}{A(x_c^I)f_y / N_{Ed}} = \frac{A(x_{c,\lim}^{II})}{A(x_c^I)} \quad (4.47)$$

Provided that $x_{c,lim}{}^{II}/L=1/(\gamma_h+1)$, the depth of a hypothetical cross section at $x_{c,lim}{}^{II}$ is given by (see *Figure 4.28*)

$$h_{xcII,\lim} = \frac{2\gamma_h h_{\min}}{\gamma_h + 1} \qquad (4.48)$$

And φ_y becomes

$$\varphi_y = \frac{A(x_{c,\lim}^{II})}{A(x_c^I)} = \frac{\left(\dfrac{2\gamma_h h_{\min}}{\gamma_h+1}t_w\right)+\left(A_{\min}-h_{\min}t_w\right)}{\left(h_{\min}t_w\right)+\left(A_{\min}-h_{\min}t_w\right)} = \frac{\left(\dfrac{2\gamma_h h_{\min}}{\gamma_h+1}t_w\right)+\left(A_{\min}-h_{\min}t_w\right)}{A_{\min}}$$

(...) $\qquad (4.49)$

$$\varphi_y = 1 + \frac{h_{\min}t_w}{A_{\min}}\frac{\gamma_h-1}{\gamma_h+1}$$

$$h_{xcII,\lim} = \frac{2\gamma_h h_{\min}}{\gamma_h + 1}$$
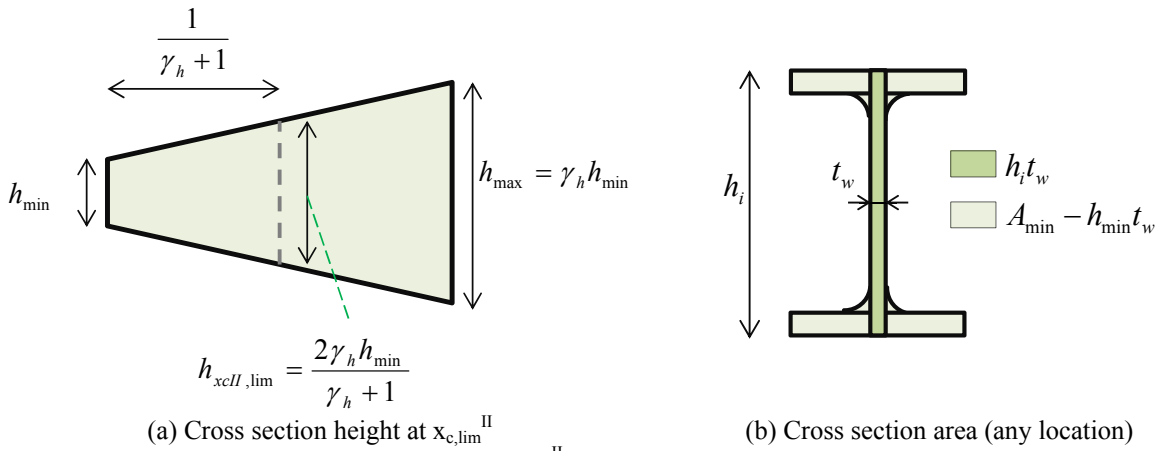
(a) Cross section height at $x_{c,\lim}{}^{II}$ (b) Cross section area (any location)
Figure 4.28: Definition of height at $x_{c,\lim}{}^{II}$ regarding in-plane buckling and cross section area

Carrying out a similar derivation considering the expression of $x_{c,lim}{}^{II}$ in Eq. (4.44) for out-of-plane buckling, φ_z is given by

$$\varphi_z = 1 + \frac{ht_w}{A_{\min}}\left[\frac{(1+4\gamma_h)(\gamma_h-1)}{10\gamma_h}\right] \qquad (4.50)$$

c) Results

Figure 4.29 illustrates results of the simplified methodology both for in-plane and out-of-plane flexural buckling. Note that both the "$x_{c,lim}{}^{II}$" and the "φ" yield exactly the same results as a simple transformation was carried out to obtain the over-strength factor φ. The resistance given by the simplified proposal is practically the same as for the proposal given in *Figure 4.23*. Actually, an improvement is noticed in terms of safety, as there is not such a restrictive decrease in the imperfection along the slenderness (due to β). The dotted orange line illustrates the proposal of *Figure 4.23*.

(a) 100x10 | Hot-Rolled | γ_h=6 | in-plane

(b) 100x10 | Welded | γ_h=4 | in-plane

(c) IPE200 | Welded | γ_h=1.8 | out-of-plane

(d) HEB300 | Welded | γ_h=3 | out-of-plane
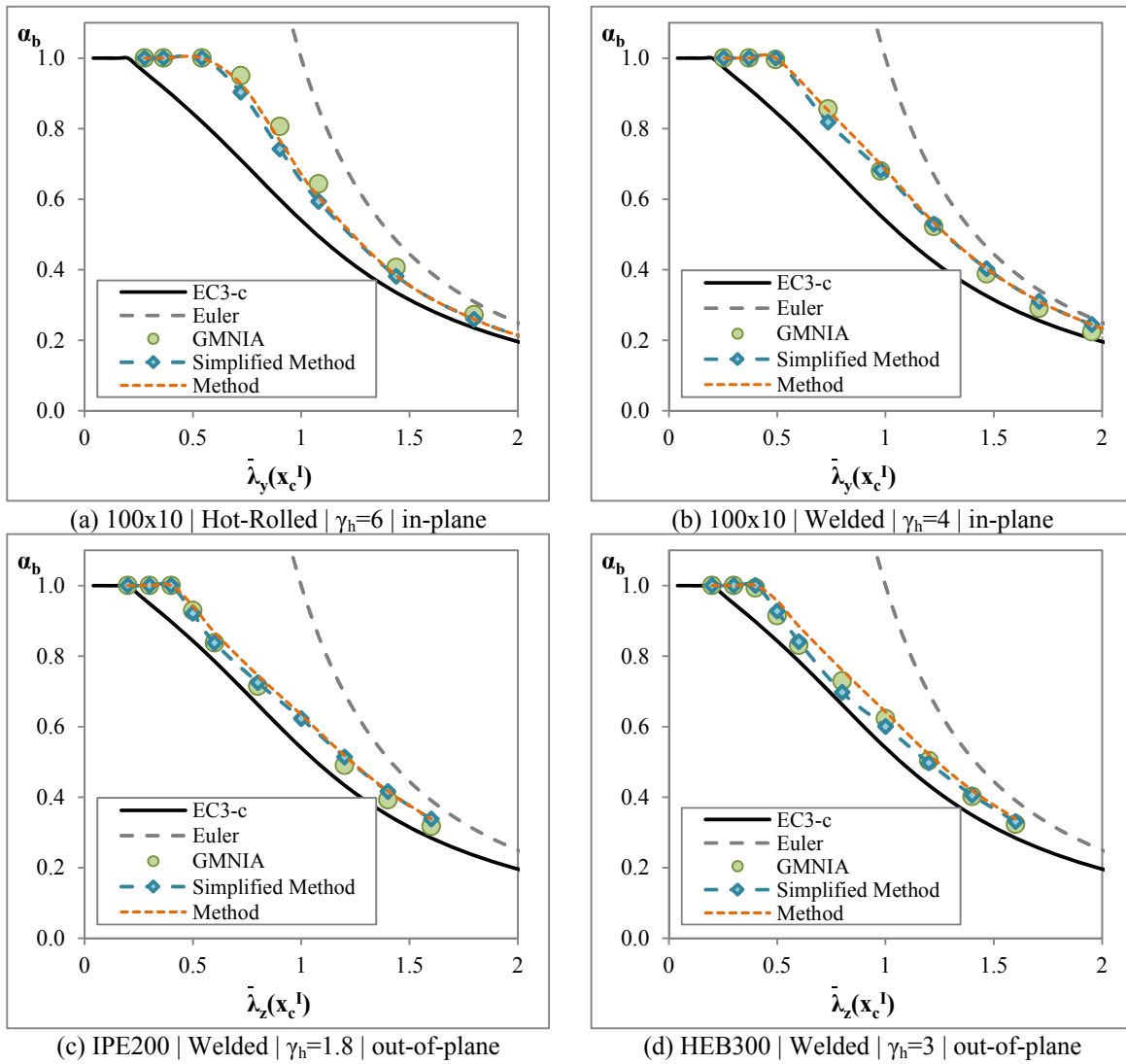
Figure 4.29: Resistance α_b against $\bar{\lambda}(x_c^I)$. Evaluation of the simplified proposal

4.4.4 Influence of cross section class

In a web-tapered member, due to the variation of the web, local instability effects are likely to occur. As a result, the critical location is not necessarily the calibrated location in Section 4.4.3. In fact, the maximum strain will probably occur in the web and not in the tip of the flanges as considered up to this point, once calibration was carried out considering the numerical models in which the web is restrained to local buckling. *Figure 4.30* illustrates a column composed of a (hot-rolled) *IPE200* regarding the smallest cross-section, with $\gamma_h=2$ and a relative slenderness of $\overline{\lambda}_z(x_c^I) = 0.4$, subject to out-of-plane buckling. Regarding the unrestrained model, it can be seen that the critical location is in a different location than for the restrained model, meaning that the proposed methodologies may not accurately describe the buckling behavior when local effects are present.

| (a.1) Principal strains | (a.2) Principal strains |

(b.1) Out-of-plane displacement of the web (b.2) Out-of-plane displacement of the web
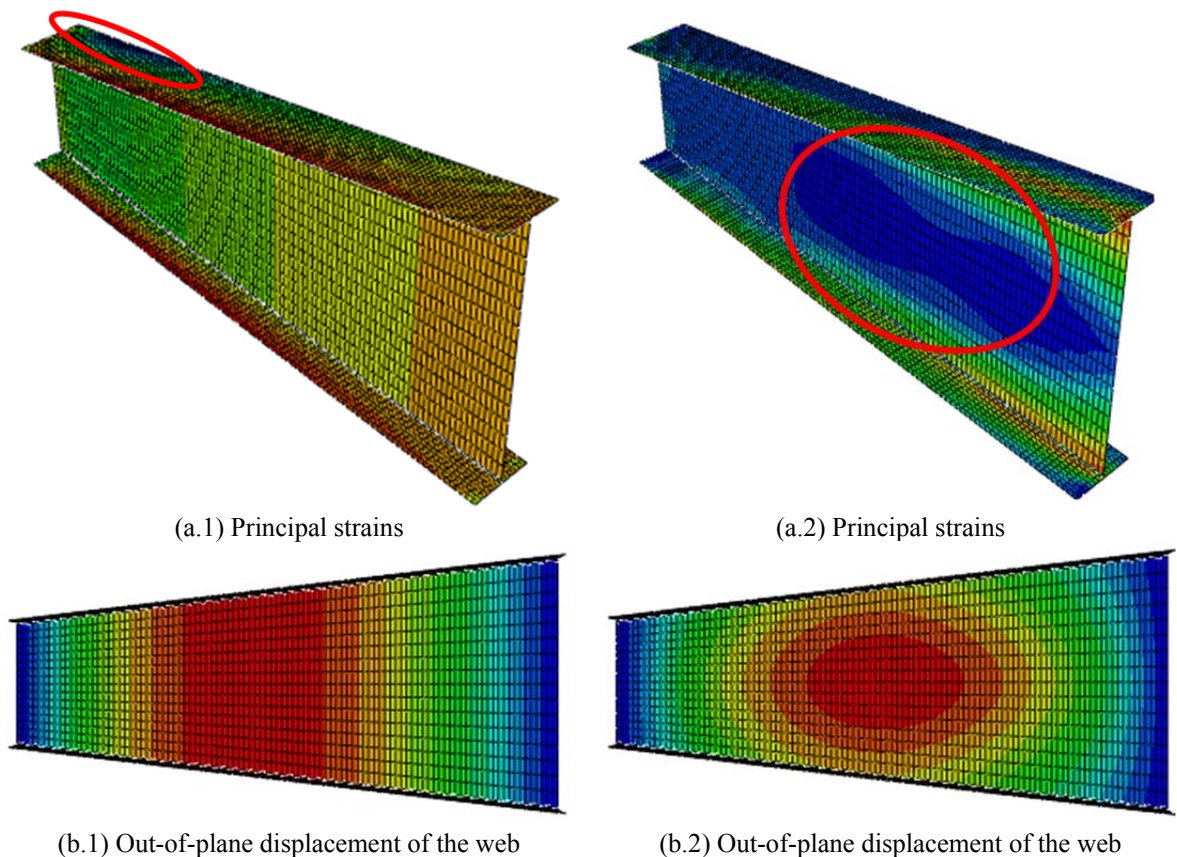
Figure 4.30: Analysis of contours: .1 – web restrained to local buckling; .2 – web unrestrained to local buckling

To overcome this, a simplification could be adopted such that the proposed design model is considered and the local effects are accounted for by the reduction of the cross section resistance, as currently done in EC3-1-1. It is described in the following.

The cross-section resistance for a given I-section is given by

$$N_{c,Rk} = \begin{cases} A f_y, & \text{Class 1, 2, 3} \\ A_{eff} f_y, & \text{Class 4} \end{cases}, \text{ clause 6.2.4 of EC3-1-1} \tag{4.51}$$

If the web in compression ($\psi=1$) is class 4, the area of the web $A_{c,eff}$ is to be reduced. $A_{c,eff}$ may be determined from clause 4.4 of EC3-1-5:

$$\overline{\lambda}_p = \frac{h_w / t_w}{28.4 \varepsilon \sqrt{k_\sigma}}, \quad \begin{cases} k_\sigma = 4 \\ \varepsilon = \sqrt{235 / f_y} \, [MPa] \end{cases}$$

$$\downarrow$$

$$\rho = \begin{cases} 1 & \text{if } \overline{\lambda}_p \le 0.673 \\ \dfrac{\overline{\lambda}_p - 0.055(3 + \psi)}{\overline{\lambda}_p^{\,2}}, & \psi = 1 \quad \text{if } \overline{\lambda}_p > 0.673 \end{cases} \tag{4.52}$$

$$\downarrow$$

$$A_{c,eff} = \rho A_c$$

For determination of the cross section class (in compression), the new limits proposed in the RFCS project Semi-Comp are considered:

$$c/t \le \begin{vmatrix} 28 \rightarrow \text{Class 1} \\ 34 \rightarrow \text{Class 2} \\ 38 \rightarrow \text{Class 3} \end{vmatrix} \\ c/t > 38 \rightarrow \text{Class 4} \tag{4.53}$$

In a first step, the first order utilization along the length of the column shall be determined, taking into account the cross section resistance at each location and respective class. The

location with the maximum utilization is the reference cross section, see also Greiner *et al.* (2011). For the analyzed column it is the smallest cross section, see *Figure 4.31*.
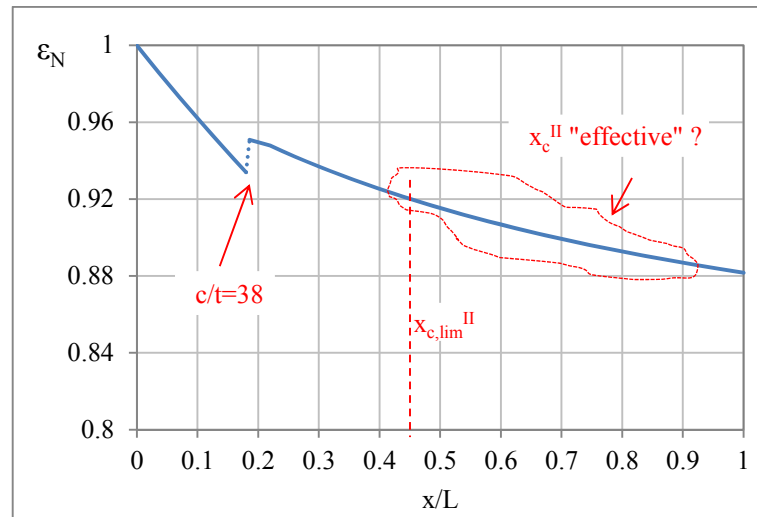
Figure 4.31: Utilization of the analyzed column

Then, for stability verification of the member, the simplified proposal given in Section 4.4.3.2 is considered. Two options are be possible:

- $x_{c,lim}{}^{II}$ approach – for the analyzed case it is $x_{c,lim}{}^{II}=0.45L$, which corresponds to $c/t=47.5$, higher than $c/t=38$. Somehow a reduction in the resistance is then considered, although this location does not represent the failure location of the column with the slender cross section;

- φ approach – for out-of-plane buckling it is given by Eq. (4.50) and leads to $\varphi_z=1.18$. However, note that, for this case, the "φ" approach does no longer coincide with the "$x_{c,lim}{}^{II}$" approach, as this factor reflects the ratio between the first order resistance multipliers regarding the gross cross-section. As a result, resistance will be over-estimated relatively to the "$x_{c,lim}{}^{II}$" approach. One must wonder if the "φ" approach should be considered for cross sections prone to local instability.

Results of the analyzed column are given in *Figure 4.32* for varying column lengths. For calculation of slenderness, the gross area is considered for N_{cr}, according to EC3-1-1, clause 6.3.1. As expected, the consideration of φ yields a higher level of resistance. On the other hand, considering $x_{c,lim}{}^{II}$ is quite conservative as the utilization of the cross-section at $x_{c,lim}{}^{II}$ is

higher than the utilization at the "effective" failure location, see also *Figure 4.31* and *Figure 4.30(a.2)*. The fact that the φ approach almost coincides with the numerical should be interpreted as coincidental regarding the analyzed case. A higher taper ratio would lead to higher differences as the "effective" failure location would move towards the higher cross section whereas $x_{c,lim}^{II}$ would move on the opposite direction.
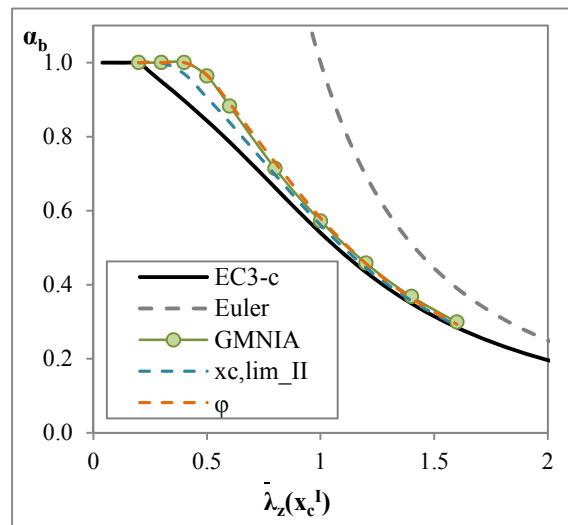
Figure 4.32: Results for the analyzed column considering the proposed methodologies and the web unrestrained

A wider parametric study would of course be needed to draw any conclusions on the conservativeness of any of the analyzed methodologies. Regardless of this, a more detailed study is required in the future to account correctly for the cross-section local buckling, whichever method is to be considered for calibration of a design proposal.

4.5 Example

A tapered column composed of a *IPE200* welded cross-section in the smallest end with a linearly varying height and a taper ratio of $\gamma_h=h_{max}/h_{min}=3$ is now analyzed (*Figure 4.33*) (web restrained to local buckling). The applied load is $N_{Ed}=$ 500 *kN* and the yield stress of $f_y=235$ *MPa*. The column has a length of *L=12.9 m*. In-plane buckling resistance is calculated using several methods.
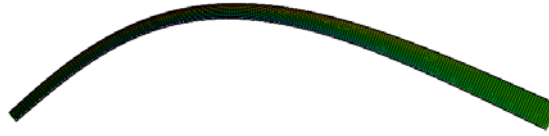
Figure 4.33: Analyzed tapered column, in-plane buckling mode

4.5.1 Elastic Critical Analysis

A numerical linear eigenvalue analysis LBA attains a critical load multiplier of α_{cr}=1.8501. For comparison, the critical load is also calculated by some of the methods described in *Table 1* and by the proposal given in Section 4.2.3. A negative difference illustrates a higher value of the critical load obtained in the literature relatively to the numerical value. Results are summarized in *Table 4.6*.

Table 4.6: Calculation of critical axial force of the tapered column

Method	Approach	α_{cr}=$N_{cr,tapered}$/N_{Ed}	Diff (%)
Hirt and Crisinel (2001)	$I_{y,eq}$ (...) = 33% $I_{y,max}$	2.0219	-9.3
Galambos (1998)	L_{eq} (...) = 52% L	1.7079	7.7
Rayleigh-Ritz (Eq. (4.13))	A= $N_{cr,tapered}$/ $N_{cr,min}$ (...) = 3.97	**1.8348**	**0.8**
LBA	Numerical	**1.8501**	-

4.5.2 Stability verification

In Section 4.5.2.1 the proposed verification procedure given in *Figure 4.23* is applied and in Section 4.5.2.2 the simplified procedure considering the "over-strength" factor approach is considered. Note that it will yield the exact results as the "$x_{c,lim}^{II}$" approach. The application of other methodologies is summarized in Section 4.5.2.3. A numerical GMNIA analysis leads to a maximum load factor of α_b=1.004.

The following cross section properties were considered in the numerical model. Firstly, the taper angle considering simplified minimum and maximum reference depths is obtained:

- h_{min}=200 *mm*; h_{max}=3*200=600 *mm*; α=0.9º

Because the flange thickness is not exactly t_f (but t_f') the depth of the web is kept and the total depth slightly increases.

- Smallest cross section h_w=183 mm; b=100 mm; t_f= 8.5 mm; t_f'= t_f/cosα= 8.501 mm; t_w=5.6 mm; h=200.002 mm

- Largest cross section h_w=583 mm; b=100 mm; t_f'=8.501 mm; t_w=5.6 mm; h=600.002 mm;

This leads into a correct taper ratio of γ_h=h_{max}/h_{min}= 600.002 / 200.002=3.0 ($\approx$2.99998). As mentioned previously, a small error is obtained when results are organized by taper ratio as, due to the change of the angle along a member length, the projected thickness slightly changes and, naturally, the taper ratio changes too. This was seen to be negligible concerning member stability design (small taper angles) and results may be grouped by taper ratio. Nevertheless, verification is performed in the following considering the same assumptions as for the numerical models.

4.5.2.1 Application of the proposed method

a) Calculation of slenderness at $x=x_c^I$ (smallest cross-section)

- $$\overline{\lambda}(x_c^I) = \sqrt{\frac{N_{Pl}(x_c^I)/N_{Ed}}{\alpha_{cr}}} = \sqrt{\frac{640.3/500}{1.8501}} = 0.832$$

b) Critical cross-section relative position, x_c^{II}/L

- $$a = 1.5 + \frac{0.6}{\gamma_h - 1} = 1.5 + \frac{0.6}{3-1} = 1.8 \ \text{and} \ b = \frac{1}{\gamma_h + 1} = 0.25 \left(\equiv x_{c,\lim}^{II}\right)$$

- $$2 - a = 0.2 \leq \overline{\lambda}(x_c^I) = 0.832 \leq 2 \ \ \Rightarrow$$

$$x_c^{II}/L = b\sqrt{1 - \frac{\left(\overline{\lambda}(x_c^I) - 2\right)^2}{a^2}} = 0.25\sqrt{1 - \frac{(0.832 - 2)^2}{1.8^2}} = 0.190$$

c) Calculation of slenderness at $x=x_c^{II}$

- $$N_{Pl}(x_c^{II}) = A(x_c^{II})f_y = 740.5 \ kN \ \ \Rightarrow$$

$$\overline{\lambda}(x_c^{II}) = \sqrt{\frac{N_{Pl}(x_c^{II})/N_{Ed}}{\alpha_{cr}}} = \sqrt{\frac{740.5/500}{1.8501}} = 0.895$$

d) Determination of imperfection factor, η

- Modified Eurocode-conform imperfection for uniform welded members (i.e. $\alpha=0.45$ instead of $\alpha=0.34$ and cut-off of $\eta \leq 0.27$, see Section 4.4.2):

$$\eta_{uniform} = \alpha\left(\overline{\lambda}(x_c^{II}) - 0.2\right) = 0.45(0.895 - 0.2) = 0.313 > 0.27 \quad \rightarrow \quad \eta_{uniform} = 0.27$$

- Additional Imperfection factor $\beta(x_c)$

$$2 - a = 0.2 \leq \overline{\lambda}(x_c) = 0.895 \leq 2 \quad \Rightarrow$$

$$\beta(x_c) = \sqrt{1 - \frac{\left(\overline{\lambda}(x_c^{II}) - 2\right)^2}{a^2}} = \sqrt{1 - \frac{(0.895 - 2)^2}{1.8^2}} = 0.789$$

- $\eta_{non-uniform} = \eta_{uniform} \times \beta(x_c^{II}) = 0.27 \times 0.789 = 0.213$

e) Reduction factor at x= x_c^{II}

- $\phi(x_c^{II}) = 0.5\left(1 + \eta + \overline{\lambda}^2(x_c^{II})\right) = 0.5\left(1 + 0.213 + 0.895^2\right) = 1.007$

- $\chi(x_c^{II}) = \dfrac{1}{\phi(x_c^{II}) + \sqrt{\phi^2(x_c^{II}) - \overline{\lambda}^2(x_c^{II})}} = \dfrac{1}{1.007 + \sqrt{1.007^2 - 0.895^2}} = 0.681 \leq 1$

f) Verification

- $N_{b,Rd} = \chi(x_c^{II})N_{Pl}(x_c^{II}) = 0.681 \times 740.5 = 504.2\ kN \leq N_{Pl}(x_c^{I})$

- $N_{b,Rd} \geq N_{Ed} \quad \rightarrow \quad 504.2 > 500 \rightarrow$ <u>Design check verified!</u>

$\alpha_b = N_{b,Rd} / N_{Ed} = 504.2/500 = 1.008$ (GMNIA, α_b=1.004)

4.5.2.2 Application of the proposed simplified method (φ approach)

a) Overstrength-factor, φ

- $\varphi_y = 1 + \dfrac{h_{min} t_w}{A_{min}} \dfrac{\gamma_h - 1}{\gamma_h + 1} = 1 + \dfrac{200\,mm \times 5.6\,mm}{2725\,mm^2} \dfrac{3-1}{3+1} = 1.206$

b) Determination of imperfection, η

- $\bar{\lambda}(x_c^I) = 0.832$

- $\eta_{uniform} = \alpha\left(\sqrt{\varphi}\,\bar{\lambda}(x_c^I) - 0.2\right) = 0.45\left(\sqrt{1.206} \times 0.895 - 0.2\right) = 0.321 > 0.27 \quad \rightarrow \quad \eta = 0.321$

c) Reduction factor

- $\phi = 0.5\left(1 + \eta + \varphi\bar{\lambda}^2(x_c^I)\right) = 0.5\left(1 + 0.27 + 1.206 \times 0.895^2\right) = 1.052$

- $\chi(x_c^I) = \dfrac{\varphi}{\phi + \sqrt{\phi^2 - \varphi \times \bar{\lambda}^2(x_c^I)}} = \dfrac{1.206}{1.052 + \sqrt{1.052^2 - 1.206 \times 0.895^2}} = 0.766 \leq 1$

d) Verification

- $N_{b,Rd} = \chi(x_c^I) N_{Pl}(x_c^I) = 0.766 \times 640.3 = 490.3\ kN$

- $N_{b,Rd} \geq N_{Ed} \quad \rightarrow \quad 490.3 < 500 \rightarrow$ <u>Design check not verified!</u>

$\alpha_b = N_{b,Rd} / N_{Ed} = 490.3/500 = 0.981$ (GMNIA, α_b=1.004)

4.5.2.3 Summary of results

Results are summarized in *Table 4.7* and *Table 4.8*. Firstly, from results of Section 4.5.2.1, the resistance calculated according to the proposed methodology is practically coincident with the GMNIA resistance (0.4% of difference). The simplified method of Section 4.4.3.2 yields slightly lower results giving a difference of 2.3% relatively to the numerical analysis.

Table 4.7 summarizes results considering the smallest cross-section for verification. Note that, in this case, the case corresponding to *α=0.34* leads to a smaller difference (10%) because current buckling curves for welded columns lead to unsafe results in this slenderness range. Therefore, the comparable correct difference is 15%, which corresponds to proposed buckling curve with *α=0.45* considering the cut-off of *η≤0.27*.

Finally, in *Table 4.8* the critical loads given by Galambos (1998); Hirt and Crisinel (2001) by Eq. (4.13) are also considered for application of the design procedure of *Figure 4.23*.

Table 4.7: Results – $x_c^{II}=x_{min}$ (minimum cross-section), Current procedure EC3 ($\beta=1$)

α (imperfection)	Cutt-off: $\alpha\left(\overline{\lambda}(x_c)-0.2\right)\le 0.27$	α_b	x_c^{II}	Diff (%)
0.34	x	0.903	0	10.1
0.45	√	0.853	0	15.0
GMNIA	-	1.004	0.17	-

Table 4.8: Results – Proposed method applied with other formulae for α_{cr}; Simplified method

Method		$\overline{\lambda}(x_c^I)$	φ or x_c^{II}	β	α_b	Diff (%)
Hirt and Crisinel (2001)		0.796	$x_c^{II}=0.185L$	$\beta(x_c^{II})=0.771$	1.035	-3.1
Galambos (1998)		0.866	$x_c^{II}=0.194L$	$\beta(x_c^{II})=0.805$	0.982	2.2
Rayleigh-Ritz (Eq. (4.13))		**0.835**	$x_c^{II}=0.191L$	$\beta(x_c^{II})=0.791$	**1.006**	**-0.2**
	Method	**0.832**	$x_c^{II}=0.190L$	$\beta(x_c^{II})=0.789$	**1.008**	**-0.4**
LBA	**Simplified Method** $\frac{\varphi}{\text{or } x_{c.lim}^{II}}$	0.832	$\frac{x_{c.lim}^{II}=0.25L}{\varphi=1.206}$	$\beta_{lim}=1$	**0.981**	**2.3**
GMNIA		-	-	-	1.004	-

4.6 Conclusions

In Chapter 4 an analytical derivation of non-prismatic columns was carried out and compared against numerical simulations. It was shown that, concerning non-uniform columns, Eurocode rules needed to be adapted in the following aspects:

• A practical approach for the determination of the design position needed to be developed;

• The column design formula had to be amended by an additional factor *β*, which specifically takes into the second-order behavior of tapered columns.

- The current imperfection factor of clause 6.3.1 for welded sections needed to be modified and re-calibrated.

In addition, the Rayleigh-Ritz method was considered for development of a simple formula for calculation of the major axis axial critical load of web-tapered columns.

A wide parametric study of more than 500 LBA and GMNIA simulations was carried out regarding linearly web-tapered columns with constant axial force.

After that, a proposal for the stability verification of these tapered columns was presented. It was noticed that, most of all, the consideration of the most stressed position is necessary in order not to achieve over-conservative levels of resistance. The above-mentioned factor β was developed based on the prior analytical formulation and calibrated with numerical results. In a second step, an alternative and simplified proposal was also presented, based on the separation of the first order effects from the second order effects of the member, also giving very accurate results. For this proposal, either the limit values of β and x_c^{II} previously calibrated or an "over-strength" factor are considered.

In addition, an analysis for tapered columns with class 4 cross-section was carried out. Although the developed design procedures could be considered with relatively acceptable loss in accuracy for the analysed example, a detailed and wider study is required to provide a mechanically consistent design model.

Finally, a new generalized imperfection for welded uniform columns was also calibrated in order to obtain improved results for the tapered cases.

Chapter 5

5 LATERAL-TORSIONAL BUCKLING OF TAPERED BEAMS

5.1 Introduction

In Chapter 5, the case of web-tapered beams is studied. In a first step, a second order analytical model based on a Ayrton-Perry approach is derived for the case of tapered beams with uniform bending moment and further extended to other bending moment distributions. Several consistent simplifications are carried out in order to build a simple but coherent design model for the stability verification of tapered beams subject to linear bending moment distributions and to parabolic bending moment. More than 3000 numerical simulations are carried out for calibration and analysis of the results. Throughout the chapter, specific issues such as the presence of shear or the codified imperfections for welded cross-sections are brought in and taken into account. Finally, it is noted that the proposed model is consistent with recently proposed design models for the stability verification of prismatic beams.

Throughout Chapter 5, whenever possible a parallelism is kept with Chapter 4, in which the flexural buckling of tapered columns is treated.

5.2 Theoretical background

5.2.1 Introduction

In this section, the second order theory formulae for lateral-torsional buckling of beams with linearly tapered web symmetrical to its centroid are derived. The following steps are taken:

- Firstly, in Section 5.2.2 the warping and uniform torsion component of a tapered beam (linearly tapered web and/or flanges) is presented;

- In Section 5.2.3 the second order theory differential equations regarding tapered beam-columns subject to constant N and M_y are obtained. Equations for flexural buckling out-of-plane, and torsional buckling are derived, the latter considering the derivation of Section 5.2.2;

- In Section 5.2.5, the derived equations of Section 5.2.3 are used to obtain a relationship considering the coupling of the degrees of freedom v and ϕ and, consequently, a relationship between the initial imperfections v_0 and ϕ_0. Those equations are then presented in a simpler format, i.e. as a function of the relevant critical loads, considering the applied load M_y only. Imperfections v_0 and ϕ_0 are finally considered;

- In Section 5.2.6, expressions for second order forces based on the preceding derivations are presented and a first yield criterion is used to find the resistance of the tapered beam at the most stressed cross-section.

The normal stresses of the tapered member are obtained considering the theory of prismatic bars. It is assumed that the error is negligible for small tapering angles (Gere and Timoshenko, 1991; Simões da Silva and Gervásio, 2007). This is then confirmed with the numerical results. Finally, the effect of shear deformations is not considered.

5.2.2 Torsion of tapered beams

Consider a beam with an I-shaped cross-section and a symmetrically tapered web and/or flanges subject both to uniform and non-uniform torsion components (*Figure 5.1*).
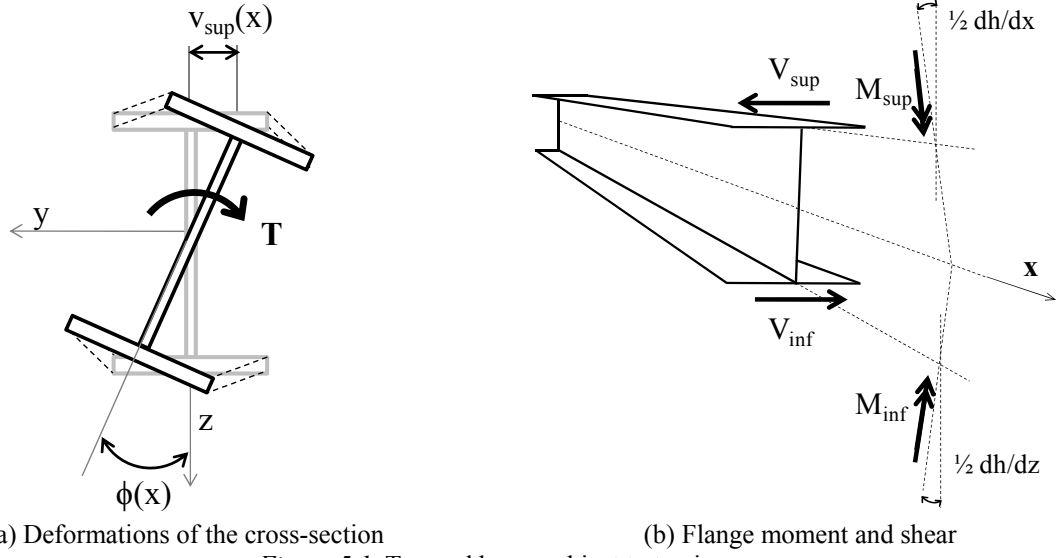
(a) Deformations of the cross-section (b) Flange moment and shear
Figure 5.1: Tapered beam subject to torsion

The uniform torsional moment component is given by

$$T_T(x) = GI_T(x)\phi'(x) \tag{5.1}$$

in which G is the shear modulus and I_T is the torsional constant.

Considering now $I_w = I_{fl,z}(h^2/2)$, the following relationships can be established:

$$\frac{v_{sup}(x)}{h(x)/2} = \tan(\phi(x)) \approx \phi(x) \quad \rightarrow \quad v_{sup}(x) = \phi(x)h(x)/2 \tag{5.2}$$

$$v_{sup}''(x) = -\frac{M_{sup}(x)}{EI_{fl,z}(x)} \quad \rightarrow \quad M_{sup}(x) = -E I_{fl,z}(x)v_{sup}''(x) = -E \frac{I_W(x)}{h^2(x)}(\phi(x)h(x))'' \tag{5.3}$$

$$V_{sup}(x) = M_{sup}'(x) \quad \rightarrow \quad V_{sup}(x) = -E\left(\frac{I_W(x)}{h^2(x)}(\phi(x)h(x))''\right)' \tag{5.4}$$

In the above, $I_{fl,z}$ denotes for the flange moment of inertia relatively to the *zz* axis.

The non-uniform torsional moment is given by

$$T_W(x) = h(x)\,V_{sup}(x) - M_{sup}(x)\,h'(x) \tag{5.5}$$

In Eq. (5.5), an additional warping component appears relatively to the prismatic beam case due to the inclination of the flanges given by $-2\left(\dfrac{1}{2}\dfrac{dh}{dx}\right)M_{sup}$, see *Figure 5.1(b).*

Finally, the resistance to torsion is given by the sum of the warping torsion component, T_w and the uniform torsion component, T_T:

$$T(x) = T_T(x) + T_W(x) = GI_T(x)\phi'(x) + h(x)\,V_{sup}(x) - M_{sup}(x)\,h'(x)$$
$$\downarrow$$
$$T(x) = GI_T(x)\phi'(x) - \underbrace{\left(E\left(\frac{I_W(x)}{h^2(x)}(\phi(x)\,h(x))''\right)'\right)}_{V_{sup}}h(x) + \underbrace{\left(E\frac{I_W(x)}{h^2(x)}(\phi(x)\,h(x))''\right)}_{M_{sup}}h'(x) \tag{5.6}$$
$$\downarrow$$
$$T(x) = G\big(I_T(x)\phi'(x)\big) + E\left[\left(\frac{I_W(x)}{h^2(x)}(\phi(x)\,h(x))''\right)h'(x) - \left(\frac{I_W(x)}{h^2(x)}(\phi(x)\,h(x))''\right)' h(x)\right]$$

The detailed derivation may be found in Kitipornchai and Trahair (1972).

5.2.3 Second order theory differential equations for tapered beam-columns

5.2.3.1 Introduction

The equilibrium of a column segment for arbitrary boundary conditions in its deformed configuration is given by the following, see Eq. (4.1) of Chapter 4.

$$E\big(I(x)\cdot v''\big)'' + \big(N(x)\cdot v'\big)' = 0 \quad \rightarrow \quad E\big(I(x)\cdot v''\big)'' = -\big(N(x)\cdot v'\big)' \tag{5.7}$$

Assume now that the acting axial force is constant and that the column is loaded by a fictitious lateral load of intensity –Nv'', statically equivalent to a lateral load of intensity (see also Timoshenko and Gere (1961))

$$-N\,v'' = -\int_A \sigma\, t\, ds\; v'' \tag{5.8}$$

in which σ=N/A.

For the case of a beam-column subject to axial force *N*, and bending moment about the major axis M_y, the normal stress acting on the deformed segment is given by

$$\sigma = \frac{N}{A} - \frac{M_y}{I_y} z \tag{5.9}$$

The sign conventions are given in Section 2.3.1, *Figure 2.4* of Chapter 2.

In Sections 5.2.3.2 and 5.2.3.3, the following relationships are considered

$$\int_A t\, ds = A; \quad \int_A z\, t\, ds = \int_A y\, t\, ds = 0; \quad \int_A y^2\, t\, ds = I_z; \quad \int_A z^2\, t\, ds = I_y \tag{5.10}$$

5.2.3.2 Equation for the deflection about minor axis

The out-of-plane deflection is given by a combination of the deflection *v* and of the rotation ϕ

$$\delta = v - \phi\, z \tag{5.11}$$

The lateral load defined in Eq. (5.8), for the case of the beam-column is given by

$$-\int_A \sigma\, t\, ds\, \delta'' = -\int_A \left(\frac{N}{A} - \frac{M_y}{I_y} z \right) t\, (v - \phi z)''\, ds \qquad (5.12)$$

After some manipulations and considering the expressions of Eq. (5.10), Eq. (5.12) becomes

$$-\int_A \left(\frac{N}{A} - \frac{M_y}{I_y} z \right) t\, (v - \phi z)''\, ds = -Nv'' - M_y \phi'' \qquad (5.13)$$

Finally, and analogous to Eq. (5.7) the differential equation for the deflection about minor axis of the tapered beam-column becomes

$$E\big(I_z(x) \cdot v''\big)'' = -Nv'' - M_y \phi'' \quad \rightarrow \quad E\big(I_z(x) \cdot v''\big)'' + Nv'' + M_y \phi'' = 0 \qquad (5.14)$$

5.2.3.3 Equation for torsion

The resistant torque per unit length is given by the derivative of Eq. (5.6):

$$-T'(x) = -G\big(I_T(x)\phi'(x)\big)'$$

$$+ E\left[\left(\frac{I_W(x)}{h^2(x)} (\phi(x)\, h(x))'' \right)' h(x) - \left(\frac{I_W(x)}{h^2(x)} (\phi(x)\, h(x))'' \right) h'(x) \right]' \qquad (5.15)$$

On the other hand, the acting torque causing compressive stresses in the deformed configuration of the member is given by (see Timoshenko and Gere, (1961))

$$m_x(x) = -\underbrace{\int_A \sigma t \left(w + \phi\, y\right)'' \times v\, ds}_{\substack{\text{Torque due to} \\ \text{in-plane component}}} + \underbrace{\int_A \sigma t \left(v - \phi\, z\right)'' \times w\, ds}_{\substack{\text{Torque due to} \\ \text{out-of-plane component}}} \qquad (5.16)$$

In Eq. (5.16), and analogous to Eq. (5.11) for the out-of-plane deflection, the in-plane deflection is given by a combination of the deflection w and of the rotation ϕ

$$\delta = w + \phi\, y \qquad (5.17)$$

The acting torque per unit length is then given by

$$m_x(x) = M_y v'' + N \underbrace{\frac{I_y(x) + I_z(x)}{A(x)}}_{i_s^2(x)} \phi'' \qquad (5.18)$$

Finally, the equilibrium of the acting and resistant torque leads to the differential equation regarding the twisting of the tapered beam-column

$$-T'(x) + m_x(x) = 0$$
$$\downarrow$$
$$-G\left(I_T(x)\phi'(x)\right)' + E\left[\left(\frac{I_W(x)}{h^2(x)}\left(\phi(x)\,h(x)\right)''\right)' h(x) - \left(\frac{I_W(x)}{h^2(x)}\left(\phi(x)\,h(x)\right)''\right) h'(x)\right]' \qquad (5.19)$$
$$+ M_y v'' + N\, i_s^2(x)\phi'' = 0$$

5.2.4 Determination of the critical moment of web-tapered beams (literature)

If the equations Eq. (5.14) and Eq. (5.19), respectively regarding out-of-plane buckling and twisting, are solved for $N=0$, the critical moment may be obtained.

In the following expressions from the literature (see Section 2.2) that may be used to obtain the critical moment of I-section tapered beams are described for the bending moment distributions treated in Chapter 5. Alternatively, numerical analysis (LBA) can be used. The latter will be considered for the analyses and calibration to be carried out.

a) Linear bending moment distribution

Andrade *et al*. (2005) propose the following expression for determination of the critical moment of web-tapered beams subject to a linear bending moment distribution ($\psi = M_{y,Ed,hmin}/M_{y,Ed,hmax}$):

$$M_{cr} = C_1 \left[\frac{\pi}{L} \sqrt{1 + a k_{\varpi,h\,\max}^2 + b k_{It,h\,\max}} \sqrt{EI_z^* I_{T,h\,\max}} \right] \qquad (5.20)$$

in which

$$\gamma_h = h_{\max} / h_{\min}$$

$$a = 1 - 1.021 \times \left(1 - \frac{1}{\gamma_h} \right) + 0.2927 \times \left(1 - \frac{1}{\gamma_h} \right)^2$$

$$b = -0.3815 \times \left(1 - \frac{1}{\gamma_h} \right)$$

$$I_{T,h\,\max} = \frac{2b}{3} \left(\frac{t_f}{\cos \alpha} \right)^3 + \frac{h_{\max} t_w^{\ 3}}{3}$$

$$I_z^* = \frac{1}{6} b^3 t_f \cos^3 \alpha$$

$$k_{\varpi,h\,\max} = \frac{\pi}{L} \sqrt{\frac{EI_{\varpi,h\,\max}^*}{GI_{T,h\,\max}}}, \quad \text{with} \quad I_{\varpi,h\,\max}^* = \frac{1}{24} h_{\max}^{\ 2} b t_f \cos^3 \alpha$$

$$k_{It,h\,\max} = \frac{h_{\max} t_w^{\ 3}}{3 I_{T,h\,\max}} \qquad (5.21)$$

α is the taper angle. C_1 is then given by

$$C_1 = \frac{1}{\sqrt{c + d(1-\psi) + f(1-\psi)^2}} \tag{5.22}$$

where

$$-\frac{1}{2} \le \psi \le 1:$$

$$c = 1$$

$$d = -1.2060 + \frac{0.2160}{\gamma_h} + 0.2275\,e^{-3/2\,k_{\omega,h\,\max}} - 0.2090\,\frac{e^{-3/2\,k_{\omega,h\,\max}}}{\gamma_h}$$

$$f = 0.3973 - \frac{0.1174}{\gamma_h} - 0.100\,e^{-3/2\,k_{\omega,h\,\max}} + 0.1070\,\frac{e^{-3/2\,k_{\omega,h\,\max}}}{\gamma_h}$$

$$-1 \le \psi < -\frac{1}{2}:$$

$$c = 1.4340 - \frac{0.3748}{\gamma_h} - 0.1828\,e^{-3/2\,k_{\omega,h\,\max}} + 0.2770\,\frac{e^{-3/2\,k_{\omega,h\,\max}}}{\gamma_h}$$

$$d = -1.6930 + \frac{0.6487}{\gamma_h} + 0.5275\,e^{-3/2\,k_{\omega,h\,\max}} - 0.5655\,\frac{e^{-3/2\,k_{\omega,h\,\max}}}{\gamma_h}$$

$$f = 0.5628 - \frac{0.2373}{\gamma_h} - 0.2208\,e^{-3/2\,k_{\omega,h\,\max}} + 0.2220\,\frac{e^{-3/2\,k_{\omega,h\,\max}}}{\gamma_h} \tag{5.23}$$

b) Uniformly distributed loading

In Galéa (1986), the elastic critical load of a web-tapered beam subject to a uniform bending moment distribution is obtained by determination of an equivalent height and moments of inertia. The critical load is then calculated using the formula for prismatic beams. For example, for the case of a simply supported beam, equivalent height and inertia are given by Eq. (5.24). For the case of other bending moment distributions, adequate coefficients for prismatic beams may be used. In the case of a uniformly distributed loading acting on the shear centre, $C_1=1.12$.

$$h_{eq} = h_{\max} \sqrt{0.283 + 0.434\gamma + 0.283\gamma^2}$$
$$I_{z,eq} \approx I_{z,\min} \qquad\qquad\qquad\qquad (5.24)$$
$$I_{T,eq} = \frac{I_{T,\max} + I_{T,\min}}{2}$$

5.2.5 Consideration of initial imperfections for tapered beams

5.2.5.1 Coupling of the degrees of freedom *v* and *φ*

The relevant equations for lateral-torsional buckling of tapered beams are Eq. (5.14) and Eq. (5.19), respectively regarding out-of-plane buckling and twisting. Note that if those are simplified for the case of a prismatic beam-column, the equations given in Eq. (2.6) of Chapter 2 regarding out-of-plane buckling and twisting are obtained.

In Taras (2010), the coupling of the degrees of freedom v and ϕ for prismatic beams is defined as

$$N_{cr,z}\,\overline{v}_0 = M_{cr}\,\overline{\phi}_0 \qquad\qquad (5.25)$$

in which $\overline{v}_0$ and $\overline{\phi}_0$ are the amplitudes of the initial lateral deflection and angle of twist respectively (see also Section 2.3.4.1).

Regarding tapered beams, in a first step, consider Eq. (5.14) in which $M_y=0$. The solution to this equation is the out-of-plane critical axial force of the tapered member $N_{cr,z,tap}$.

$$E\big(I_z(x)\cdot v''\big)'' + Nv'' + 0 = 0 \quad \rightarrow \quad E\big(I_z(x)\cdot v''\big)'' + N_{cr,z,Tap}\,v'' = 0 \qquad (5.26)$$

or

$$E\left(I_z(x) \cdot v''\right)'' = -N_{cr,z,Tap}\, v''$$

(5.27)

For the calculation of $M_{cr,Tap}$, both Eq. (5.14) and Eq. (5.19) are necessary with $N=0$:

$$E\left(I_z(x) \cdot v''\right)'' + 0 + M_y \phi'' = 0$$

(5.28)(a)

$$-G\left(I_T(x)\phi'(x)\right)'$$
$$+ E\left[\left(\frac{I_W(x)}{h^2(x)}(\phi(x)h(x))''\right)' h(x) - \left(\frac{I_W(x)}{h^2(x)}(\phi(x)h(x))''\right) h'(x)\right]'$$
$$+ M_y v'' + 0 = 0$$

(5.28)(b)

Eq. (5.28)(a) can then be written as

$$E\left(I_z(x) \cdot v''\right)'' = -M_{cr,Tap}\, \phi''$$

(5.29)

Combining Eq. (5.27) and Eq. (5.29) leads to

$$N_{cr,z,Tap}\, v'' = M_{cr,Tap}\, \phi''$$

(5.30)

Finally, for the case of initial imperfections, a similar format to Eq. (5.30) is obtained. As the functions for $v(x)$ and $\phi(x)$ are not known, it is not possible to further simplify Eq. (5.31).

$$N_{cr,z,Tap}\, v_0'' = M_{cr,Tap}\, \phi_0''$$

(5.31)

5.2.5.2 Differential Equations

Firstly Eq. (5.14) and Eq. (5.19) are simplified regarding the case of tapered beams. Then initial imperfections $v_0(x)$ and $\phi_0(x)$ are introduced. Substituting Eq. (5.27) in Eq. (5.14) for $N=0$ yields

$$M_y \phi'' - N_{cr,z,Tap} v'' = 0 \tag{5.32}$$

Analogous to Eq. (5.29), (5.28)(b) can be written as:

$$-G\left(I_T(x)\phi'(x)\right)' + E\left[\left(\frac{I_W(x)}{h^2(x)}\left(\phi(x)h(x)\right)''\right)' h(x) - \left(E\frac{I_W(x)}{h^2(x)}\left(\phi(x)h(x)\right)''\right)h'(x)\right]'$$
$$+ M_{cr,Tap} v'' + 0 = 0 \tag{5.33}$$

Introducing Eq. (5.30) in Eq. (5.33), yields

$$-G\left(I_T(x)\phi'(x)\right)' + E\left[\left(\frac{I_W(x)}{h^2(x)}\left(\phi(x)h(x)\right)''\right)' h(x) - \left(E\frac{I_W(x)}{h^2(x)}\left(\phi(x)h(x)\right)''\right)h'(x)\right]'$$
$$+ \frac{M^2_{cr,Tap}}{N_{cr,z,Tap}}\phi'' + 0 = 0 \tag{5.34}$$

Replacing Eq. (5.34) in Eq. (5.19) for $N=0$, leads finally to

$$-M_y v'' + \frac{M^2_{cr,Tap}}{N_{cr,z,Tap}}\phi'' = 0 \tag{5.35}$$

If imperfections $v_0(x)$ and $\phi_0(x)$ are introduced in the terms $v(x)$ and $\phi(x)$ of Eq. (5.14) and Eq. (5.19) and if the stiffness terms due to the curvature of the imperfect member are neglected

(see also Kaim (2004)), simplified equations regarding a tapered beam with initial imperfections are obtained:

$$\begin{cases} N_{cr,z,Tap} v'' - M_y \left(\phi'' + \phi_0'' \right) = 0 \\ - M_y \left(v'' + v_0'' \right) + \dfrac{M_{cr,Tap}^2}{N_{cr,z,Tap}} \phi'' = 0 \end{cases} \tag{5.36}$$

Introducing Eq. (5.31) in Eq. (5.36) the following system of equations is obtained

$$\begin{cases} N_{cr,z,Tap} v'' - M_y \phi'' = M_y \phi_0'' \\ - M_y v'' + \dfrac{M_{cr,Tap}^2}{N_{cr,z,Tap}} \phi'' = M_y \left(\dfrac{M_{cr,Tap}}{N_{cr,z,Tap}} \phi_0'' \right) \end{cases} \tag{5.37}$$

from which ϕ'' is obtained as follows

$$v'' = \frac{M_y \phi_0'' + M_y \phi''}{N_{cr,z,Tap}}$$

$$\downarrow$$

$$- M_y \left(M_y \phi_0'' + M_y \phi'' \right) + M_{cr,Tap}^2 \phi'' = M_y \left(M_{cr,Tap} \phi_0'' \right) \quad \rightarrow \quad \phi'' = \phi_0'' \frac{M_y M_{cr,Tap} + M_y^2}{M_{cr,Tap}^2 - M_y^2} \tag{5.38}$$

$$\rightarrow \phi'' = \phi_0'' \frac{M_y \left(M_{cr,Tap} + M_y \right)}{\left(M_{cr,Tap} - M_y \right)\left(M_{cr,Tap} + M_y \right)} \quad \rightarrow \quad \phi'' = \phi_0'' \frac{M_y}{M_{cr,Tap} - M_y}$$

and, consequently, v'' leads to

$$\phi'' = \phi_0'' \frac{M_y}{M_{cr,Tap} - M_y}$$

$$\downarrow$$

$$v'' = \frac{M_y \phi_0'' + M_y \left(\phi_0'' \dfrac{M_y}{M_{cr,Tap} - M_y} \right)}{N_{cr,z,Tap}} \quad \rightarrow \quad v'' = \frac{\phi_0''}{N_{cr,z,Tap}} \left(M_y + \frac{M_y^2}{M_{cr,Tap} - M_y} \right) \qquad (5.39)$$

$$\rightarrow v'' = \phi_0'' \frac{M_y}{N_{cr,z,Tap}} \left(\frac{M_{cr,Tap}}{M_{cr,Tap} - M_y} \right)$$

The obtained relationships are summarized in Eq. (5.40),

$$\phi'' = \phi_0'' \frac{M_y}{M_{cr,Tap} - M_y}$$

$$v'' = \phi_0'' \frac{M_y}{M_{cr,Tap} - M_y} \frac{M_{cr,Tap}}{N_{cr,z,Tap}} \qquad (5.40)$$

Note that Eq. (5.40) presents a similar format to Eq. (2.26) for prismatic members. Again, because for the case of prismatic beams the functions for ϕ_0'' and v_0'' may be simplified due to the sinusoidal mode shape, Eq. (2.26) may be presented as a function of the imperfection amplitudes and the corresponding result is also given by a discrete value.

5.2.6 Buckling check

5.2.6.1 Second order forces

The following expressions may be used to determine the second order internal forces M_z^{II} and M_ω^{II}, respectively the second order out-of-plane and warping moments.

$$M_z^{II} = -EI_z v''$$
$$M_\varpi^{II} = -EI_\omega \phi''$$

(5.41)

Or, using Eq. (5.40),

$$M_z^{II} = \left(-\frac{EI_z}{N_{cr,z,Tap}}\right)\phi_0'' \frac{M_y}{1 - \dfrac{M_y}{M_{cr,Tap}}}$$

(5.42)

$$M_\varpi^{II} = \left(-\frac{EI_\varpi}{M_{cr,Tap}}\right)\phi_0'' \frac{M_y}{1 - \dfrac{M_y}{M_{cr,Tap}}}$$

5.2.6.2 Consideration of e_0 according to EC3-1-1

In order to perform a buckling check considering the first order bending moment M_y and the second order forces, M_z^{II} and M_ω^{II}, consistent with the prismatic beam case presented in Taras (2010), the imperfection ϕ_0 is presented in terms of the amplitude $e_0=L/1000$, considered in EC3-1-1 for the derivation of buckling curves for uniform columns. For this, some manipulations are carried out and described in the following.

Firstly, *Figure 5.2* illustrates an arbitrary cross-section of the beam in its deformed configuration.
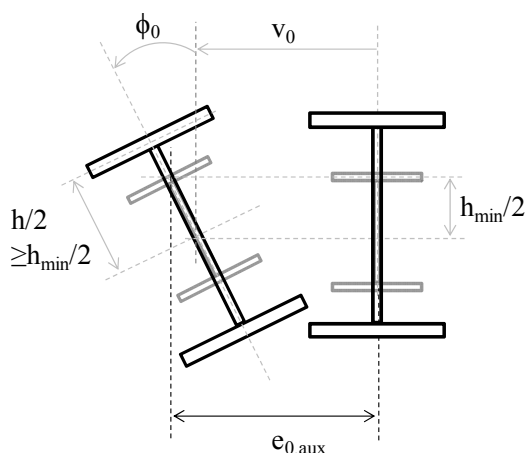
Figure 5.2: Deformed configuration of the tapered beam

The imperfection $e_{0,aux}(x)$ is an auxiliary parameter given by the value of the imperfection e_0 at $h=h_{min}$ and may be defined as

$$e_{0,aux}(x) = \phi_0(x)\frac{h_{min}}{2} + v_0(x) \quad \rightarrow \quad e''_{0,aux}(x) = \phi''_0(x)\frac{h_{min}}{2} + \frac{M_{cr,Tap}}{N_{cr,z,Tap}}\phi''_0(x) \qquad (5.43)$$

In order to introduce e_0 in Eq. (5.43), consider first $e_{0,aux}(x) = e_{0,aux} \cdot \delta_{cr,hmin}(x)$, in which $\delta_{cr,hmin}$ is the lateral displacement of the critical mode at $h=h_{min}$. Assuming now a weighing factor, which relates the displacements at h and h_{min}, given by Eq. (5.44) and illustrated in *Figure 5.3*, e_0 can be determined, see Eq. (5.45). The critical displacements $\delta_{cr,hmin}$ and $\delta_{cr,max}=1$ are obtained at the cross-section corresponding to the maximum critical displacement.

$$\xi = \frac{\overline{e}_{0,aux}}{\overline{e}_0} = \frac{\delta_{cr,h\,min}}{\delta_{cr,max}=1} = \delta_{cr,h\,min} \qquad (5.44)$$
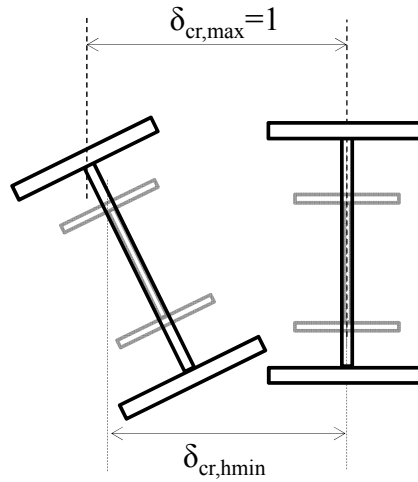
Figure 5.3: Weighing factor for determination of e_0

Eq. (5.43) becomes

$$\begin{cases} e''_{0,aux}(x) = \phi''_0(x)\left(\dfrac{h_{min}}{2} + \dfrac{M_{cr,Tap}}{N_{cr,z,Tap}}\right) \\ e''_{0,aux}(x) = \overline{e}_{0,aux}\, \delta''_{cr,h\,min}(x) = \xi\,\overline{e}_0\, \delta''_{cr,h\,min}(x) \end{cases} \rightarrow \quad \phi''_0(x) = \dfrac{\xi\,\overline{e}_0}{\dfrac{h_{min}}{2} + \dfrac{M_{cr,Tap}}{N_{cr,z,Tap}}}\,\delta''_{cr,h\,min}(x) \quad (5.45)$$

in which $\delta''_{cr,hmin}$ can be obtained numerically.

5.2.6.3 First yield criterion

The utilization ratio ε as defined in Section 4.3.1 for columns is given in Eq. (5.46) for the case of beams

$$\varepsilon(x) = \frac{M_y(x)}{W_y(x)f_y} + \frac{M_z^{II}(x)}{W_z(x)f_y} + \frac{M_\varpi^{II}(x)}{I_\varpi(x)/\varpi_{max}(x)f_y} \qquad (5.46)$$

Consider now: $\omega_{max}=h.b/4$ and $W_z=I_z/(b/2)$; the second order forces defined in Eq. (5.42); the relationship of Eq. (5.45) regarding the second derivative of the initial rotation $\phi_0{}''$ and the amplitude e_0; and

$$\chi_{LT}(x) = \frac{M_y(x)}{W_y(x)f_y}; \qquad \overline{\lambda}_z(x) = \sqrt{\frac{A(x)f_y}{N_{cr,z,Tap}}}; \qquad \overline{\lambda}_{LT}(x) = \sqrt{\frac{W_y(x)f_y}{M_{cr,Tap}}} \qquad (5.47)$$

Adopting a similar procedure as for columns, the utilization ratio becomes after some manipulations

$$\varepsilon = \frac{M_y}{W_y f_y} + \frac{M_y}{f_y\left(1 - \dfrac{M_y}{M_{cr,Tap}}\right)} \frac{\xi \, \bar{e}_0 \left(-\delta''_{cr,h\min}(x)\right)}{\dfrac{h_{\min}}{2} + \dfrac{M_{cr,Tap}}{N_{cr,z,Tap}}} \left(\frac{EI_z}{N_{cr,z,Tap}} \frac{1}{W_z} + \frac{EI_\varpi}{M_{cr,Tap}} \frac{\varpi_{\max}}{I_\varpi}\right) \times \left[\frac{W_y}{W_y}\right]$$

$\downarrow \ldots$

$$\varepsilon = \frac{M_y}{W_y f_y} + \frac{M_y/W_y}{f_y\left(1 - \dfrac{M_y}{M_{cr,Tap}}\right)} \frac{\xi \, \bar{e}_0 \left(-\delta''_{cr,h\min}(x)\right)}{\dfrac{h_{\min}}{2} + \dfrac{M_{cr,Tap}}{N_{cr,z,Tap}}} \frac{W_y}{W_z} \frac{EI_z}{N_{cr,z,Tap}} \left(1 + \frac{N_{cr,z,Tap}}{M_{cr,Tap}} \frac{h}{2}\right) \times \left[\frac{A}{A}\right]$$

$\downarrow \ldots$

$$\varepsilon = \chi_{LT} + \frac{\chi_{LT}}{1 - \bar{\lambda}_{LT}^2 \chi_{LT}} \frac{\xi \, \bar{e}_0 \left(-\delta''_{cr,h\min}(x)\right) EI_z}{N_{cr,z,Tap}} \left[\frac{W_y}{A} \frac{1 + \dfrac{N_{cr,z,Tap}}{M_{cr,Tap}} \dfrac{h}{2}}{\dfrac{h_{\min}}{2} + \dfrac{M_{cr,Tap}}{N_{cr,z,Tap}}}\right] \frac{A}{W_z}$$

$\downarrow \ldots$

$$\varepsilon = \chi_{LT} + \frac{\chi_{LT}}{1 - \bar{\lambda}_{LT}^2 \chi_{LT}} \frac{\xi \, \bar{e}_0 \left(-\delta''_{cr,h\min}(x)\right) EI_z}{N_{cr,z,Tap}} \left[\frac{\bar{\lambda}_{LT}^2}{\bar{\lambda}_z^2} \frac{1 + \dfrac{N_{cr,z,Tap}}{M_{cr,Tap}} \dfrac{h}{2}}{1 + \dfrac{M_{cr,Tap}}{N_{cr,z,Tap}} \dfrac{h_{\min}}{2}}\right] \frac{A}{W_z} \tag{5.48}$$

In Eq. (5.48) all terms are a function of x, except for the constants E, e_0, $N_{cr,z,Tap}$, $M_{cr,Tap}$, h_{min} and ξ. Finally, at x_c^{II} the utilization ratio attains a maximum of $\varepsilon(x_c^{II})=1$. $\varepsilon(x)$ may be again manipulated by multiplying the second term by :

$$\left[\frac{A(x_c^{II})}{W_z(x_c^{II})} \frac{W_z(x_c^{II})}{A(x_c^{II})}\right] \times \left[\frac{\bar{\lambda}_{LT}^2(x_c^{II})}{\bar{\lambda}_z^2(x_c^{II})} \frac{\bar{\lambda}_z^2(x_c^{II})}{\bar{\lambda}_{LT}^2(x_c^{II})}\right] \tag{5.49}$$

Eq. (5.48) finally becomes

$$\varepsilon(x) = \chi_{LT}(x) + \frac{\chi_{LT}(x)}{1 - \overline{\lambda}_{LT}^2(x)\chi_{LT}(x)} \left[\overline{e}_0 \frac{A(x_c^{II})}{W_z(x_c^{II})}\right]\left[\frac{\overline{\lambda}_{LT}^2(x_c^{II})}{\overline{\lambda}_z^2(x_c^{II})}\right] \times$$

$$\times \frac{\xi\left(-\delta_{cr,h\min}''(x)\right)EI_z(x)}{N_{cr,z,Tap}} \left[\frac{1 + \dfrac{N_{cr,z,Tap}}{M_{cr,Tap}}\dfrac{h(x)}{2}}{1 + \dfrac{M_{cr,Tap}}{N_{cr,z,Tap}}\dfrac{h_{\min}}{2}}\right] \qquad (5.50)$$

$$\times \left[\frac{A(x)}{W_z(x)} \frac{W_z(x_c^{II})}{A(x_c^{II})}\right]\left[\frac{\overline{\lambda}_{LT}^2(x)}{\overline{\lambda}_z^2(x)} \frac{\overline{\lambda}_z^2(x_c^{II})}{\overline{\lambda}_{LT}^2(x_c^{II})}\right]$$

At $x = x_c^{II}$, $\varepsilon(x_c^{II})$ is given by

$$\varepsilon(x_c^{II}) = 1 = \chi_{LT}(x_c^{II}) + \frac{\chi_{LT}(x_c^{II})}{1 - \overline{\lambda}_{LT}^2(x_c)\chi_{LT}(x_c)} \left[\overline{e}_0 \frac{A(x_c^{II})}{W_z(x_c^{II})}\right]\left[\frac{\overline{\lambda}_{LT}^2(x_c^{II})}{\overline{\lambda}_z^2(x_c^{II})}\right] \times$$

$$\times \frac{\xi\left(-\delta_{cr,h\min}''(x_c^{II})\right)EI_z(x_c^{II})}{N_{cr,z,Tap}} \left[\frac{1 + \dfrac{N_{cr,z,Tap}}{M_{cr,Tap}}\dfrac{h(x_c^{II})}{2}}{1 + \dfrac{M_{cr,Tap}}{N_{cr,z,Tap}}\dfrac{h_{\min}}{2}}\right] \qquad (5.51)$$

Considering

$$\eta = \overline{e}_0 \frac{A(x_c^{II})}{W_z(x_c^{II})} = \alpha_{LT}\left(\overline{\lambda}_z(x_c^{II}) - 0.2\right) \qquad (5.52)$$

Eq. (5.51) finally becomes

$$\varepsilon(x_c) = 1 \quad \rightarrow \quad 1 = \chi_{LT}(x_c^{II}) + \frac{\chi_{LT}(x_c^{II})}{1 - \overline{\lambda}_{LT}^2(x_c^{II})\chi_{LT}(x_c^{II})} \times$$

$$\times \underbrace{\left(\alpha_{LT}\left(\overline{\lambda}_z(x_c^{II}) - 0.2 \right) \left[\frac{\overline{\lambda}_{LT}^2(x_c^{II})}{\overline{\lambda}_z^2(x_c^{II})} \right] \right)}_{\eta_{uniform\ beams}\left(x_c^{II}\right)}$$

$$\underbrace{\times \underbrace{\frac{\xi\left(-\delta_{cr,h\min}''(x_c^{II})\right)EI_z(x_c^{II})}{N_{cr,z,Tap}} \underbrace{\left[\frac{1 + \dfrac{N_{cr,z,Tap}}{M_{cr,Tap}}\dfrac{h(x_c^{II})}{2}}{1 + \dfrac{M_{cr,Tap}}{N_{cr,z,Tap}}\dfrac{h_{\min}}{2}} \right]}_{Ponderatio\ n\ \ factor}}_{\beta\left(x_c^{II}\right)}}_{\eta_{non-uniform\ beams}\left(x_c^{II}\right)} \qquad (5.53)$$

Or, in a summarized format

$$\varepsilon(x_c) = 1 \quad \rightarrow \quad 1 = \chi_{LT}(x_c^{II}) + \frac{\chi_{LT}(x_c^{II})}{1 - \overline{\lambda}_{LT}^2(x_c^{II})\chi_{LT}(x_c^{II})} \times \underbrace{\eta_{uniform\ beams}(x_c^{II}) \times \beta(x_c^{II})}_{\eta_{non-uniform\ beams}\left(x_c^{II}\right)} \quad (5.54)$$

Eq. (5.53) is identical to the Ayrton-Perry formula. If $h_{max}=h_{min}$, i.e., uniform member, the term $\beta(x_c^{II})=1$ and a similar equation as derived in Taras (2010) for lateral-torsional buckling of uniform beams is obtained. Also, apart from the weighing factor due to the manipulation carried out in Eq. (5.45) in order to obtain the initial rotation ϕ_0'' as a function of e_0, the additional factor $\beta(x_c^{II})$ has a similar format as the factor $\beta(x_c^{II})$ presented for tapered columns in Chapter 4.

Finally, for a certain load multiplier α_b given by

$$\alpha_b = \chi_{LT}(x)\frac{M_{y,Rk}(x)}{M_{y,Ed}(x)} \tag{5.55}$$

the utilization ratio attains a maximum of $\varepsilon=1$ at the critical position of the beam, x_c^{II}. Similarly to the column case, an iterative procedure is needed to obtain x_c^{II} and α_b.

5.2.7 Interpretation of the utilization ratio *ε*

For application of the iterative procedure defined in Section 4.3.3, the considered values of α_{LT} will be adopted as the ones calibrated in Taras (2010). These are given in *Table 2.4.*

The variation of the utilization ratio ε of a non-uniform beam with $h_{min}=b=100$ *mm*, $h_{max}=300$ *mm*, $t_f=t_w=10$ *mm* and $L=9.2$ *m* is illustrated in *Figure 5.4*, concerning Eq. (5.50). For this, α_{cr} and $\delta''_{cr,hmin}$ are obtained numerically from a LBA analysis. The utilization ratio ε is divided into 2 terms – ε_M^{I} concerns first order forces, i.e., bending moment about strong axis, and ε_M^{II} concerns 2nd order forces, i.e., bending moment due to curvature of the member (about weak axis and warping moment). The sum of these terms leads to the total utilization ratio ε. For short members, ε_M^{I} is much higher compared to ε_M^{II} as cross-sectional resistance is more significant, and vice-versa. As a result, short members present a critical location x_c^{II} close to the first order critical location (x_c^{I}), i.e., the failure cross-section considering first order forces only. With the increase of the member length the second order failure location x_c^{II} deviates from x_c^{I}. For the example in *Figure 5.4*, the critical position x_c^{II} is located at about 35% of the member length ($x_c^{I}= L/2$).
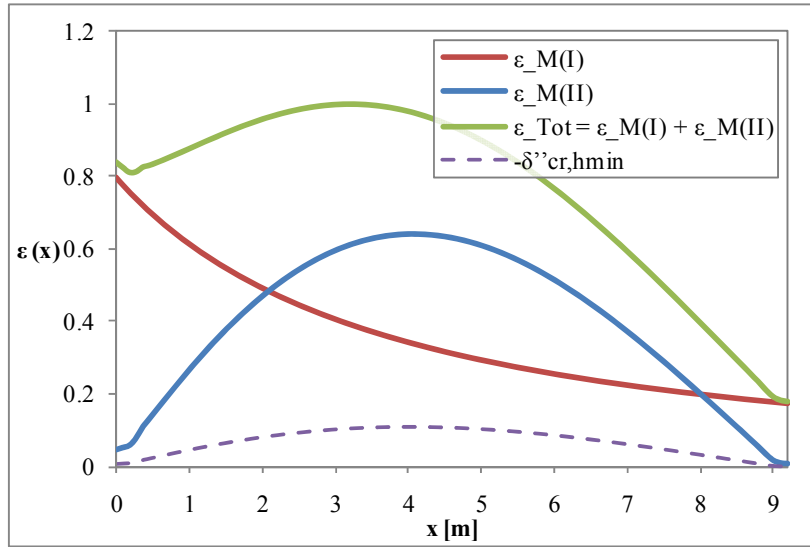
Figure 5.4: Curvature $\delta''_{cr,hmin}$ and utilization ratio ε

5.3 Evaluation of the analytical model

5.3.1 Parametric study

Table 5.1 summarizes the sub-set of cases to be compared with the advanced numerical simulations. The case of lateral-torsional buckling of linearly web-tapered beams subject to uniform bending moment is considered. About 100 numerical simulations with shell elements were carried out. Both GMNIA (Geometrical and Material Non-linear Analysis with Imperfections) numerical simulations and LBA are carried out to provide data for application of the analytical formulations. *Table 5.1* summarizes the parametric study, where the Taper Ratio is defined as $\gamma_h = h_{max}/h_{min}$.

Table 5.1: Parametric study – validation of the analytical model

Taper Ratio γ_h	Reference Cross-section (i.e. with h_{min}, at $x=x_{hmin}$)	Reference Beam Slenderness $\overline{\lambda}_{LT}(x_c^I \equiv x_{h\min}) = \sqrt{\dfrac{M_{y,Rk}(x_c^I)/M_{y,Ed}(x_c^I)}{\alpha_{cr}}}$
1 ... 6	100x100x10x10 ($h=b=100$ *mm*; $t_f=t_w=10$ *mm*)	0 ... 3

Table 5.2 summarizes the alternative procedures to obtain the resistance of the tapered beam:

Table 5.2: Considered procedures for stability verification

$\overline{\lambda}_{LT}$	α_{LT} and η (see Eq. (5.53))	α_b	Designation
General Method EC3			
$\alpha_{ult,k}=1$ (max. in-plane load multiplier) $\overline{\lambda}_{op}=\sqrt{\dfrac{\alpha_{ult,k}}{\alpha_{cr}}}$ $\equiv \overline{\lambda}_{LT}(x_{h\min})$ $\alpha_{cr}\rightarrow$ from LBA	. h/b≤2 → 0.21 (curve *a*) $\;\alpha_{LT}\left(\overline{\lambda}_{op}-0.2\right)$	$\chi_{op}\cdot\alpha_{ult,k}\equiv\chi_{op}$	GM_*a*
	. h/b>2 → 0.34 (curve *b*) $\;\alpha_{LT}\left(\overline{\lambda}_{op}-0.2\right)$		GM_*b*
	$.\,0.16\sqrt{\dfrac{W_{y,el}(x_{h\min})}{W_{z,el}(x_{h\min})}}\le 0.49$ (consistent with residual stress pattern adopted, $0.5f_y$) . Additional factor to η: $\eta^*=\eta\times\left(\dfrac{\overline{\lambda}_{LT}(x_{h\min})}{\overline{\lambda}_z(x_{h\min})}\right)^2$. $\eta_{\text{uniform beams}}(x_{\min})$ $\eta=\alpha_{LT}\left(\overline{\lambda}_z(x_{h\min})-0.2\right)$		GM_η*Taras*
Eq. (5.50)			
$\overline{\lambda}_{LT}(x_c^{II})$	$.\,0.16\sqrt{\dfrac{W_{y,el}(x_c^{II})}{W_{z,el}(x_c^{II})}}\le 0.49$. Additional factor to η: $\eta^*=\eta\times\left(\dfrac{\overline{\lambda}_{LT}(x_c^{II})}{\overline{\lambda}_z(x_c^{II})}\right)^2$. $\eta_{\text{uniform beams}}(x_c^{II})$ $\eta=\alpha_{LT}\left(\overline{\lambda}_z(x_c^{II})-0.2\right)$	$\chi_{LT}(x_c^{II})\cdot$ $M_{y,Rk}(x_c^{II})$ $/M_{y,Ed}(x_c^{II})$	EQU
GMNIA			
		Max. Load Factor	GMNIA

In *Table 5.2*, χ_{LT} (or χ_{op}) is obtained as follows

$$\begin{cases} \overline{\lambda}_{LT} \\ \eta \end{cases} \rightarrow \phi_{LT} = 0.5\left(1 + \eta + \overline{\lambda}_{LT}^{2}\right) \rightarrow \chi_{LT}\left(or \ \chi_{op}\right) = \frac{1}{\phi_{LT} + \sqrt{\phi_{LT}^{2} - \overline{\lambda}_{LT}^{2}}} \quad (5.56)$$

Note that, although the generalized imperfection given in *GM_η*Taras* (Taras, 2010) is not currently included in EC3-1-1, it is considered for comparison as the developed model leads to this approach for the case of prismatic beams, γ_h=1. The difference between *GM_η*Taras* and *EQU* is the consideration of the x_c^{II} and $\beta(x_c^{II})$ for the tapered case.

Finally, concerning nonlinear numerical calculations, the maximum load factor of GMNIA analysis corresponds to α_b load multiplier for the case of uniform bending moment, as the first order failure location is the smallest cross-section, i.e., x_c^{I}=x_{hmin}. The critical position x_c^{II} is also extracted from the numerical model corresponding to the element with the maximum strain at the maximum load factor, α_b.

Results are represented relatively to the location of the first order failure cross-section, which, for a constant bending moment distribution is $x_c^{I} \equiv x_{hmin}$. Because $M_{y,Rk}(x_{hmin})$=$M_{y,Ed}$, yields

$$\overline{\lambda}_{LT}(x_{h\min}) = \sqrt{\frac{M_{y,Rk}(x_{h\min})/M_{y,Ed}(x_{h\min})}{\alpha_{cr}}} = \frac{1}{\sqrt{\alpha_{cr}}};$$

$$\chi_{LT}(x_{h\min}) = \frac{\alpha_b}{\underbrace{M_{y,Rk}(x_{h\min})/M_{y,Ed}(x_{h\min})}_{=1}} = \alpha_b \quad (5.57)$$

5.3.2 Accuracy of analytical model

Figure 5.5 illustrates results regarding the application of Eq. (5.50) against GMNIA calculations for the taper ratios of γ_h=2 (*Figure 5.5(a)*), γ_h =4 (*Figure 5.5(b)*) and γ_h=6 (*Figure 5.5(c)*). Good agreement is achieved both for resistance and for the relative critical position. Regarding resistance, α_b, it is noticeable that from a certain level of slenderness $\overline{\lambda}_{LT}(x_c^{I}) \approx 1.4$ numerical results diverge from analytical results converging to a level of resistance of

$\alpha_b \approx M_{pl,z}(x_c^I)/M_{Ed}$. This happens because for this slenderness range the cross-section rotates so much that bending about the weak axis becomes relevant, i.e., the applied load about the strong axis acts about the weak axis on the critical cross-section, see also Taras (2010). Numerical results diverge from the analytical results as in the analytical model $\alpha_b \leq \alpha_{cr}$ (amplification factor $1 - M_y/M_{cr,Tap} \geq 1$, the Euler load is not exceeded). These are however non-practical levels of slenderness about the week axis of approximately $\overline{\lambda}_z \geq 6$. Nevertheless, regarding slenderness up to $\overline{\lambda}_{LT}(x_0) \approx 1.4$, maximum differences of 4% are noticed.

(a.1) Buckling curve representation, γ_h=2

(a.2) Critical location, γ_h =2

(b.1) Buckling curve representation, γ_h =4

(b.2) Critical location, γ_h =4

(c.1) Buckling curve representation, γ_h=6

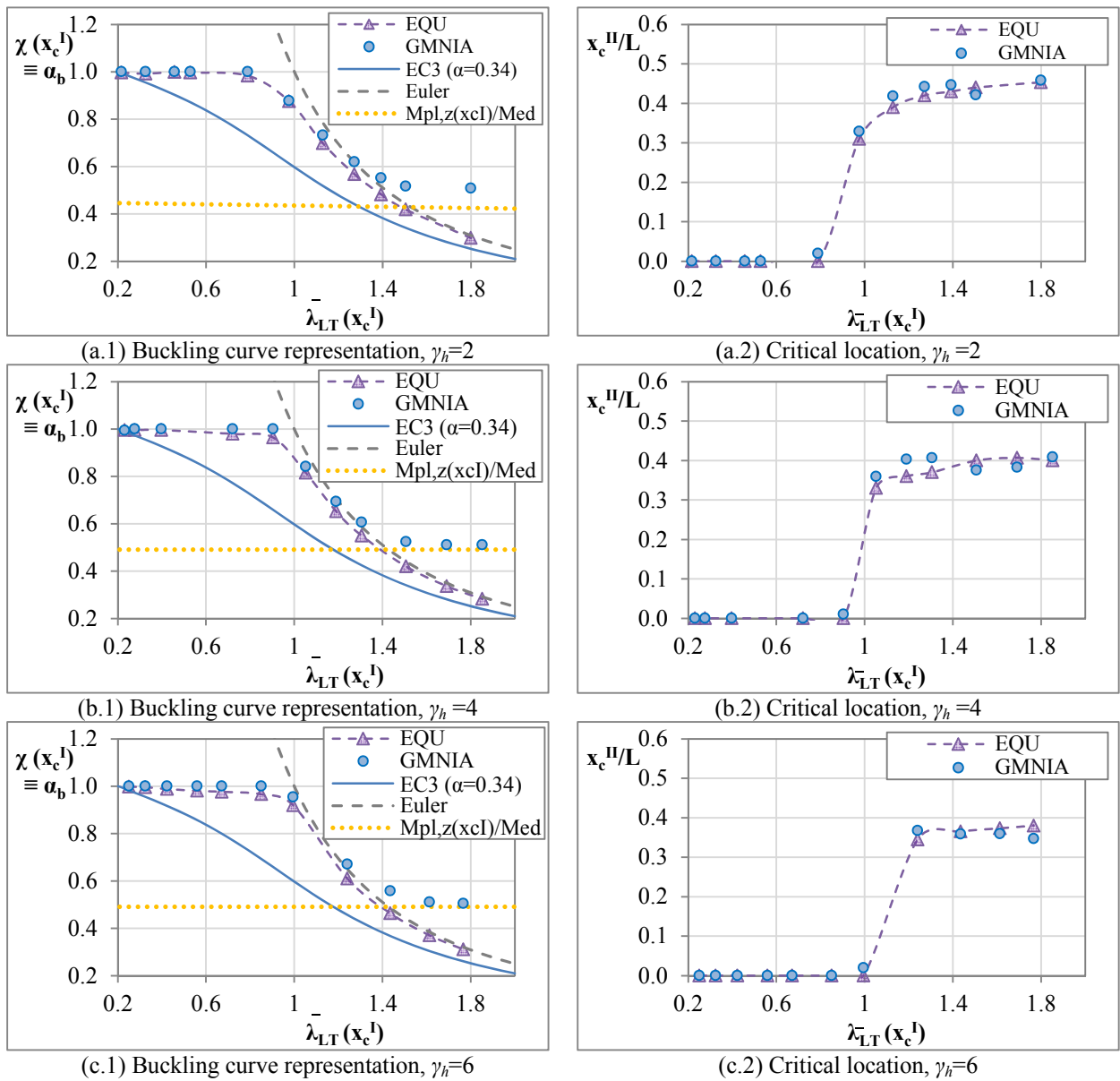(c.2) Critical location, γ_h=6

Figure 5.5: Analytical model resistance against GMNIA analysis

5.3.3 Influence of taper ratio

Figure 5.6 and *Figure 5.7* illustrate, for several taper ratios γ_h, results of Eq. (5.50) concerning respectively resistance and relative critical location.

Regarding *Figure 5.6*, it is noticeable the increase of both the resistance and of the plateau length with the increase of tapering. This increase is less significant for higher taper ratios. When comparing $\gamma_h=1$ (prismatic beam) with other values of γ_h, the influence of the tapering factor $\beta(x_c^{II})$ defined in Eq. (5.53) is also visible. This factor is illustrated in *Figure 5.8*. It is unity for prismatic beams and varies with the slenderness for tapered beams, therefore decreasing the generalized imperfection of uniform beams, $\eta_{uniform\ beams}(x_c^{II})$, also defined in Eq. (5.53). It accounts for the variation of the critical location due to the increase of second order effects relatively to the cross-section resistance. As a result, for low slenderness, it is 0 and for high slenderness it increases asymptotically to a certain limit. For the case of a prismatic beam with uniform bending moment, the increase of the second order relatively to the first order effects does not affect the location of the critical cross-section (it is always at mid-span) whereas when either a variation of the web height or of the bending moment distribution is present, this location will have to change due to the asymmetry of either the 1st or 2nd order utilization ratios (see again *Figure 5.4* for illustration of the utilization ratio).

As a result, in *Figure 5.7*, it can be seen that the relative critical location x_c^{II}/L reaches asymptotically a limit value for high slenderness (almost no plasticity effect). With the increase of γ_h, this location tends to decrease.
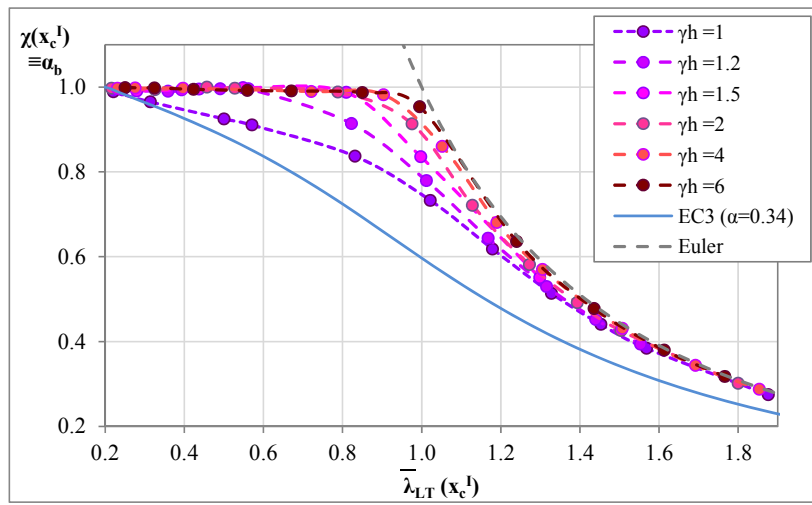
Figure 5.6: Buckling curve representation for all Taper Ratios (Eq. (5.50))
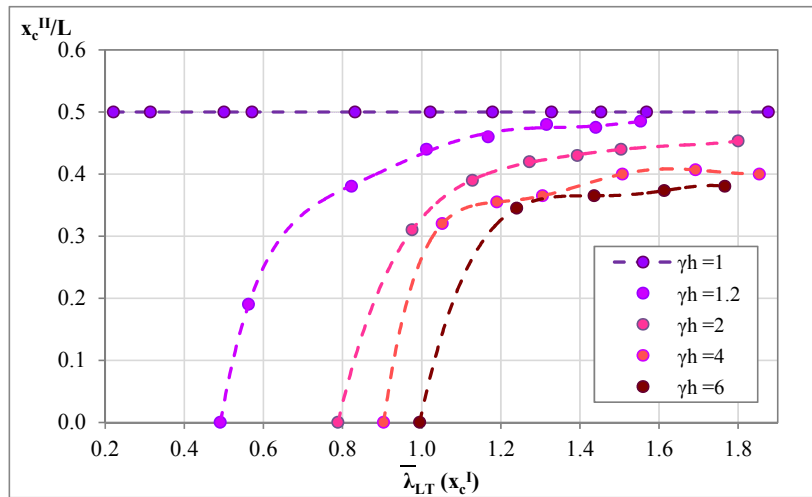

Figure 5.7: Critical location by Taper Ratio (Eq. (5.50))
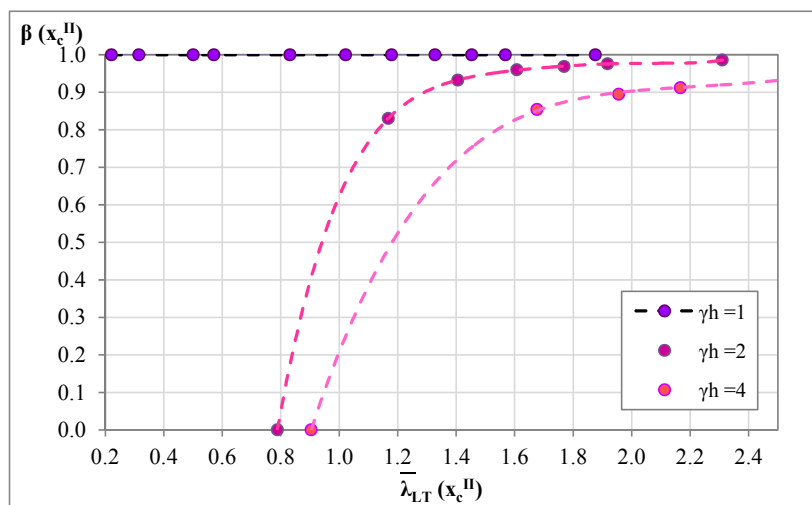
Figure 5.8: Imperfection factor $\beta(x_c^{II})$ (Eq. (5.50))

5.3.4 Buckling curve representation, x_c^I vs. x_c^{II} for $\gamma_h=3$

As carried out for columns in Section 4.3.4.5, here two representations of resistance are also considered and illustrated concerning a beam (*100x100x10x10*) with a taper ratio of $\gamma_h=3$: *Figure 5.9(a)* illustrates the slenderness $\bar{\lambda}(x_c^I)$ as a function of the reduction factor $\chi(x_c^I)\equiv\alpha_b$, and, therefore, resistance can be directly compared; *Figure 5.9 (b)* illustrates the slenderness $\bar{\lambda}(x_c^{II})$ as a function of the reduction factor $\chi(x_c^{II})$. These two forms of representation are compared in order to analyze if, when results of the reduction factor $\chi(x_c^{II})$ are considered, the buckling curve concerning the tapered elements $\gamma_h=3$ approximates to the buckling curve concerning uniform elements (represented as the red line). If this would happen, the calibration of an additional imperfection actor $\beta(x_c^{II})$ would be unnecessary. For the case of columns, a slight approximation to the uniform case was noticed, however not significant. In the case of tapered beams, that approximation is even less relevant.

(a) $\bar{\lambda}_{LT}(x_c^I)$ against $\chi(x_c^I)\equiv\alpha_b$ (b) $\bar{\lambda}_{LT}(x_c^{II})$ against $\chi(x_c^{II})$
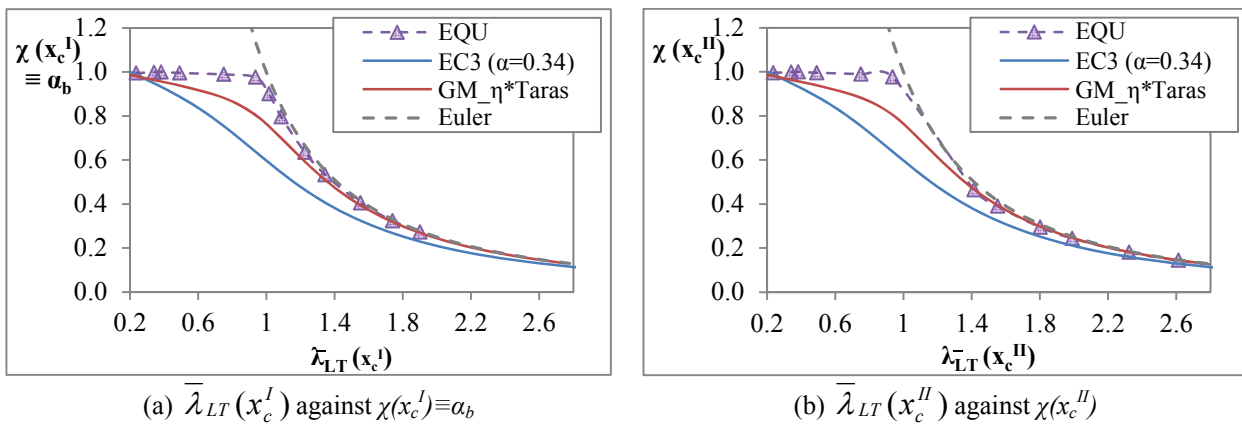
Figure 5.9: Buckling curve representation, $\gamma_h=3$

5.3.5 Comparison of Methodologies

Figure 5.10 illustrates, for $\gamma_h=3$, resistance calculated according to the methodologies described in Section 5.3.1. It is visible that Eq. (5.50) describes very well the tapering behavior. On the other hand, application of the General Method in EC3-1-1 leads to differences up to 26% and 34% respectively when curve *a* and *b* are used.
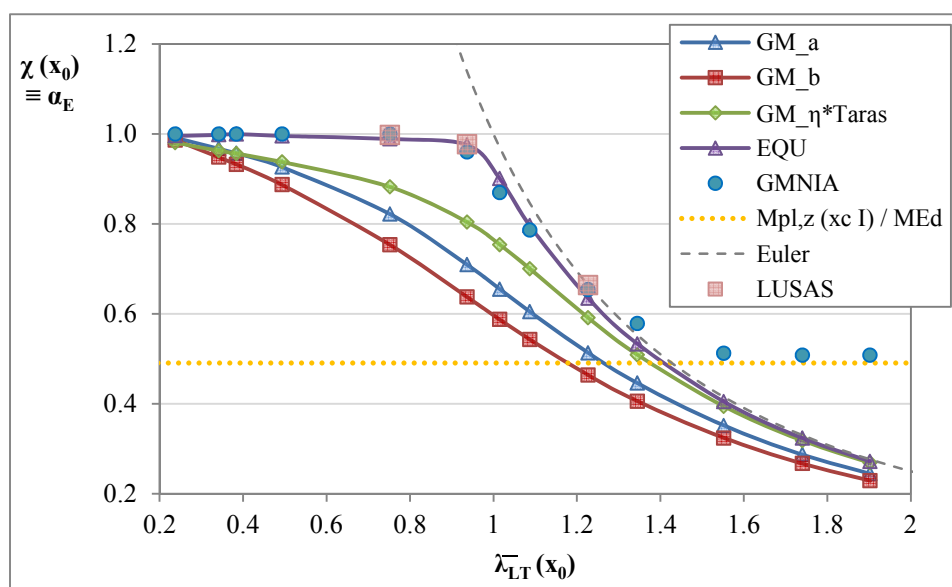
Figure 5.10: Comparison of Methodologies, γ_h=3

5.4 Design model for other bending moment distributions

5.4.1 Adequacy of the analytical model to other bending moment distributions

As already mentioned in Section 5.3.3, either the variation of the web or of the bending moment distribution leads to a variation in the utilization ratio causing the second order failure location to vary with the member length. In fact, the variation of the first order utilization due to variation of the web in a beam with uniform bending moment can be compared to a beam with a prismatic cross-section but with a varying uniform bending moment which leads to the same utilization. This assumption is valid as long as the correct critical moment is considered in the analytical model as, for the case of tapered beams, it takes into account the additional bi-moment due to the inclination of the flange. As a result, the developed model in Section 5.2 can be applied to other bending moment distributions as long as the correct M_{cr} (or α_{cr}) and the corresponding buckling mode shape is considered.

Figure 5.11 illustrates the utilization ratio of a prismatic beam with a *HEB300* cross-section a triangular bending moment distribution and a length of L=19.6 m ($\overline{\lambda}_z = 2.76$) and a

corresponding relative slenderness is $\overline{\lambda_{LT}}(x_c^I) = \sqrt{M_{pl}/M_{cr}} = 0.95$. The analytical model leads to a resistance of α_b=0.834 against a numerical resistance of α_b=0.870 (4% of difference on the safe side), as for the critical location, the analytical model leads to x_c^{II}/L=0.805 against a numerical failure location of x_c^{II}/L =0.817 (1.5% of difference).

Note that, for this case, with the increase of member length, the critical location would vary from x_c^{II}/L=1 ($\equiv x_c^I/L$) decreasing up to a limit value of x_c^{II}/L corresponding to a high slenderness level.
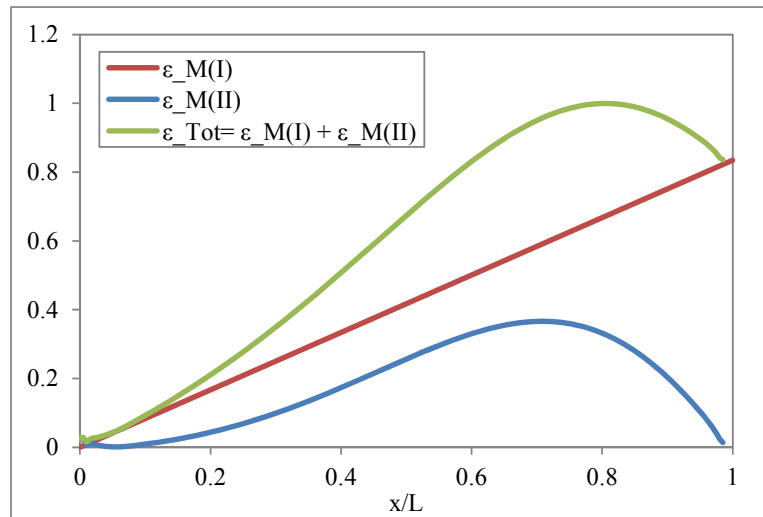
Figure 5.11: Application of the analytical model to other bending moment distributions. Utilization ratio ε

5.4.2 Influence of the bending moment distribution in tapered beams

Tapered members are usually adopted in order to optimize the load capacity at each cross-section according to the respective distribution of stresses. For the case of a uniform bending moment distribution, it is clear that the best member is the prismatic member in which all cross-sections are fully utilized, considering first order forces. Therefore, it is logical that, with the increase of the taper ratio the member capacity increases (in relative terms) as shown in *Figure 5.6* – i.e., for a same relative slenderness $\overline{\lambda}_{LT}^2(x_c^I)$, the reduction factor $\chi(x_c^I)$ is higher. However, when other bending moment distributions are considered, it is not that clear that a higher taper ratio will lead to a higher (relative) resistance. For example, for the case of

a triangular bending moment distribution, the cross-section utilization is optimized for higher taper ratios. These aspects must be accounted for in a design model.

Figure 5.12 illustrates the quantification of the "unused" resistance in a tapered beam with a linear bending moment distribution, ψ. For this calculation, the sum of the relative utilization is subtracted from the total capacity of the member. This calculation is better illustrated in *Figure 5.13*.
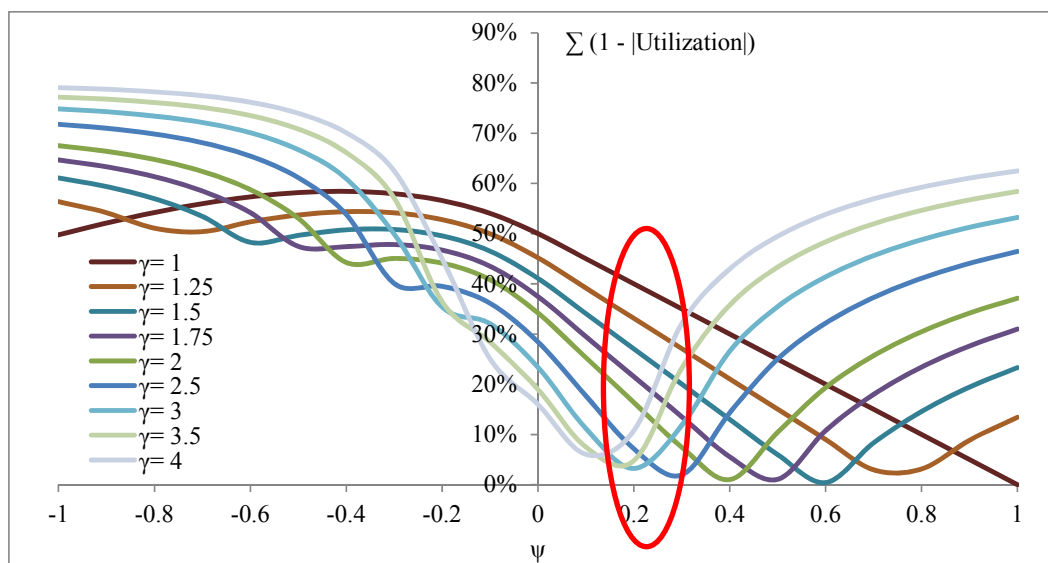
Figure 5.12: Quantification of the "unused" resistance
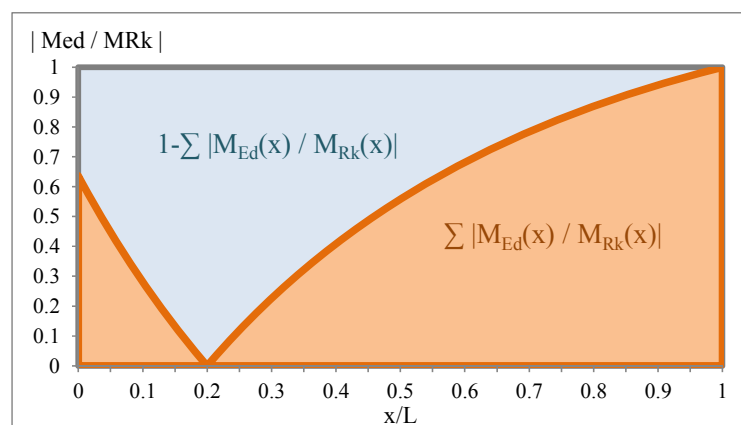
Figure 5.13: Determination of the "unused" resistance for a IPE200 (smallest cross-section), γ_h=2 and ψ=-0.25

Consider the bending moment distribution highlighted in *Figure 5.12*, corresponding to $\psi=0.2$. *Figure 5.14* illustrates this case for $1 \leq \gamma_h \leq 4$. A taper ratio of $\gamma_h \approx 3.1$ would lead to an optimized utilization for $\psi=0.2$.
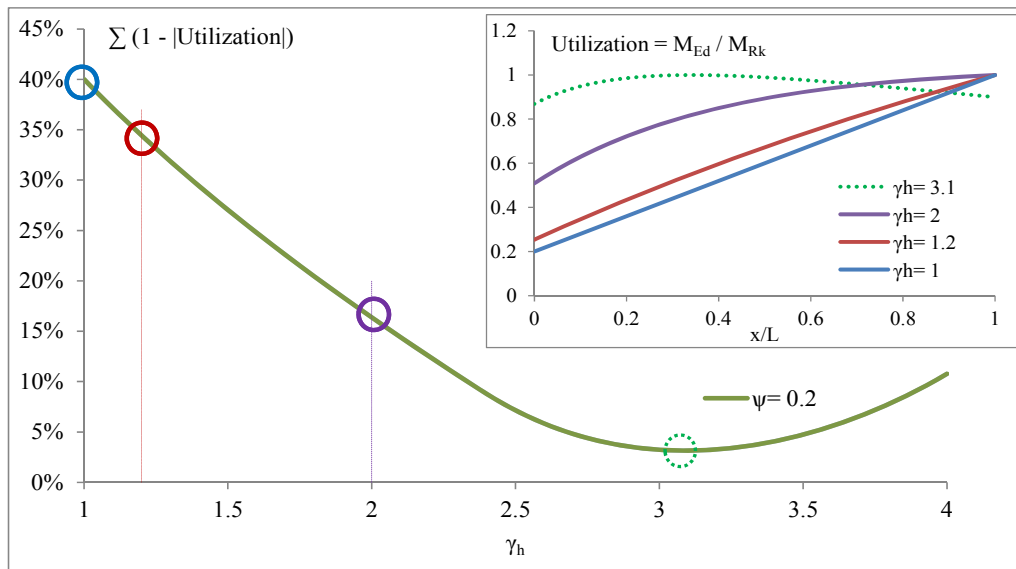
Figure 5.14: Analysis of the "unused" resistance of the beam for $\psi=0.2$

It is worth mentioning that *Figure 5.12* has the practical advantage of identifying the best taper ratio for a given bending moment distribution in a first step of the design procedure. Finally, regarding the first order failure cross-section it is again not clear how to identify its location in the beam, as it can be seen in *Figure 5.15*, in which the failure cross-section is determined considering plastic utilization.
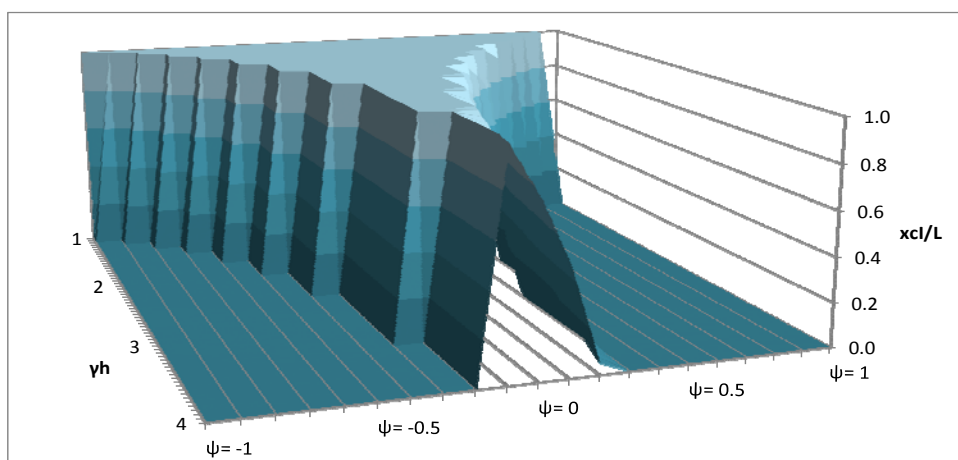
Figure 5.15: First order failure location for a *IPE200* (smallest cross-section)

For example, for the case of $\psi=0.3$, high taper ratios lead to a failure location at the smallest cross-section, whereas for low taper ratios, the failure location is at the largest cross-section, see *Figure 5.16*.
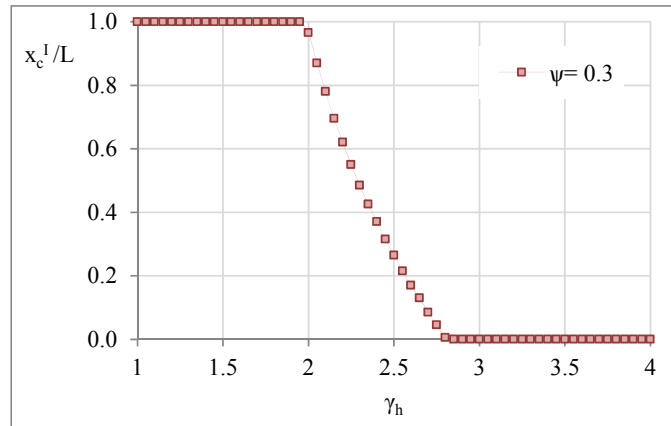
Figure 5.16: First order failure location for a *IPE200* (smallest cross-section), $\psi=0.3$

Note that, for simplification, in *Figure 5.12* to *Figure 5.16*, an elastic utilization was adopted to illustrate the behavior, i.e., $M_{y,Rk}=M_{y,el}$. In addition, due to the variation of the projected thickness $t_f{}'$ with the increase of member length (see *Figure 4.9*, Chapter 4), in order to obtain comparable results for the bending resistance organized by the taper ratio γ_h, the projected thickness $t_f{}'$ was assumed to be the same, i.e., member lengths such that $t_f{}'\approx t_f$ were adopted.

Another issue is the possible variation of the cross-section class along the member. The example of *Figure 5.17* illustrates a beam consisting of a *IPE200* (smallest cross-section) with $\gamma_h=3$ and $\psi=0.25$ in which the first order failure location varies according to the methodology adopted for calculation of the utilization. It was decided in this study to consider the Semi-Comp approach (Greiner *et al*., 2011), this way taking into account the plastic distribution in semi-compact cross-sections and avoiding discontinuities, see for example the yellow dots in *Figure 5.17* which illustrate that a first order failure location of $x_c{}^I/L=0.765$ would be obtained due to a jump from class 3 cross section to class 2 according to the current code provisions. A continuous utilization is obtained from the purple line in which the change from class 2 to

class 3 is considered according to Greiner *et al.* (2011). The red line illustrates the elastic utilization and the green line illustrates the plastic utilization.
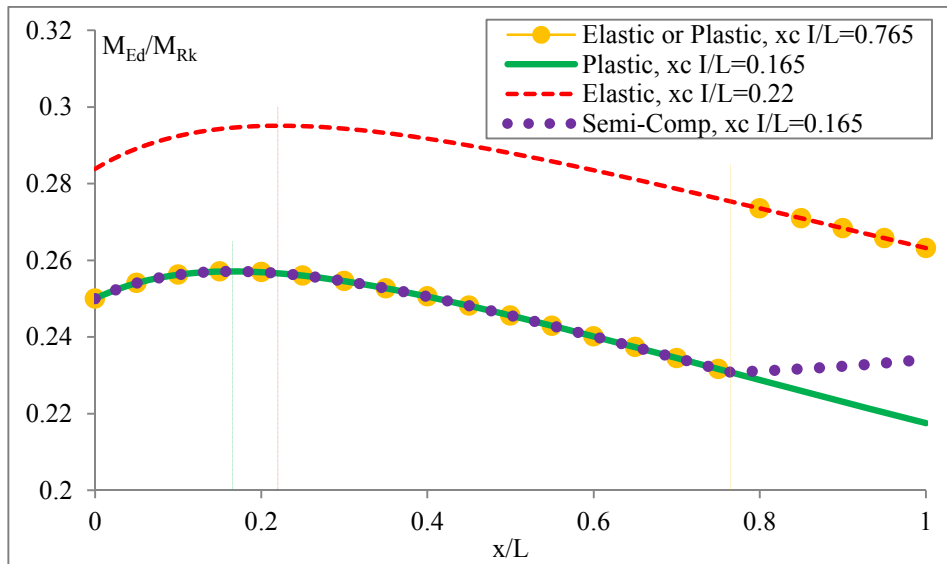
Figure 5.17: First order failure location according to several methodologies for cross-section classification

The first order failure location will be necessary for application of the model to be developed in the following. As a result, a simplified procedure is to determine the utilization ratio along a satisfactory number of locations along the beam (e.g. 10 locations, see Greiner *et al.*, 2011)), considering the adequate cross-section resistance at each position (elastic, plastic, or elasto-plastic, i.e., following the Semi-Comp approach). The position with the maximum utilization leads to first order failure cross-section.

5.4.3 Choice of a proper taper ratio definition

In order to account for the proportions of the cross-section, a suitable taper ratio shall be chosen. For example, for a given γ_h, two distinct smallest cross-sections, *HEB300* and *IPE200* present different utilizations. To analyze this, the diagrams of *Figure 5.12* were plotted in *Figure 5.18* for these two cross-sections and compared according to the taper ratios $\gamma_{h=}$ h_{max}/h_{min}; $\gamma_{I=} I_{y,max}/h_{y,min}$ and $\gamma_{w=} W_{y,el,max}/W_{y,elmin}$. The taper ratio γ_w was shown to be the best parameter to account for the cross-section shape of the tapered member. This parameter will be considered again for calibration in Sections 5.4.5.2 and 5.4.5.3. Nevertheless, for some

parameters in the formulae to be developed as well as for presentation of results, the ratio γ_h is also used.

(a) $\gamma_{h=} h_{max}/h_{min}$

(b) $\gamma_{I=} I_{y,max}/h_{y,min}$

(c) $\gamma_{w=} W_{y,el,max}/W_{y,elmin}$

(d) γ_I and γ_w against γ_h
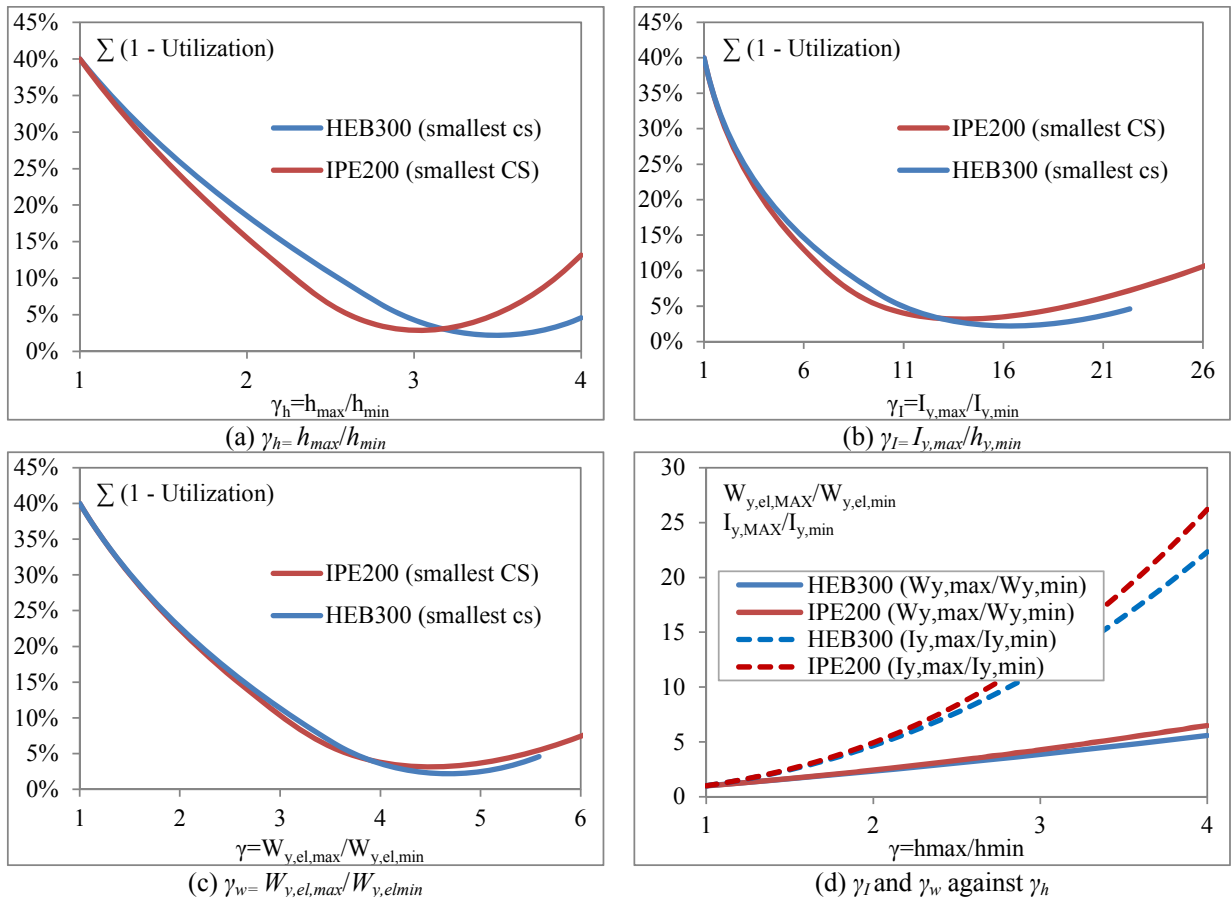
Figure 5.18: Choice of the taper ratio

5.4.4 Parametric study

Table 5.3 summarizes the sub-set of numerical cases to be considered for calibration of the design model, where the taper ratio is defined as $\gamma_h = h_{max}/h_{min}$. More than 3000 numerical simulations with shell elements were carried out. Both GMNIA numerical simulations and LBA were again carried out. A limit value in $\gamma_h = 4$ was here established, covering the relevant practical application range of tapered members (see also Section 1.1).

Table 5.3: Parametric study – calibration of the design model

Taper Ratio γ_h	Bending moment distribution	Reference Cross-section (i.e. with h_{min}, at $x=x_{hmin}$)	Fabrication procedure	$\bar{\lambda}_{LT}(x_c^I)$	Local web displacements
1 … 4	$-1 \leq \psi \leq 1$ UDL (uniformly distributed load)	IPE200 HEB300 100x100x10x10	Welded Hot-Rolled (res. Stresses $0.5f_y$)	0 … 3	Restrained Unrestrained

5.4.5 Development of a design model

5.4.5.1 Observed discontinuities of x_c^{II} for $\psi<0$

As a starting point of the problem, expressions for the second order critical location, $x_c^I \leq x_c^{II} \leq x_{c,lim}^{II}$, and the corresponding imperfection factor, $\beta(x_c^{II})$ should be calibrated. Regarding $\beta(x_c^{II})$, an elliptical expression varying from 0 in the "plateau" slenderness to 1 for a reasonable high slenderness could be calibrated without major difficulties, as long as the "plateau" slenderness and the "limit" slenderness is known. For the latter, a value of $\bar{\lambda}_{LT,lim} = 2$ can be considered (as already established in Chapter 4). For the first one, again, the parameter does not vary linearly with the increase of taper and bending moment distribution. Nevertheless, assuming that this slenderness is known, expressions for x_c^{II} need to be calibrated. This location should vary between x_c^I, calculated according to Section 5.4.2 and the location for $\bar{\lambda}_{LT,lim}$, see *Figure 5.19*. However, for certain cases a discontinuity is noticed, see *Figure 5.20(a)*. Although the first order utilization is maximum at *x/L=0*, see *Figure 5.20 (b)*, due to the shape of the second order forces utilization (approximately a sine function with different amplitudes in the positive and negative moment sides of the beam and with a inflection point at the node in which M_{Ed} is 0), a small increase in second order forces rapidly leads to a jump of the failure location to the positive moment side, leading to the observed discontinuity. As a result, and for practical reasons, a simplification is made in Section 5.4.5.2, in which the first and second order effects are uncoupled, as already carried out in Section 4.4.3.2 for tapered columns.

(a) $\psi=1$ (a) $\psi=0$
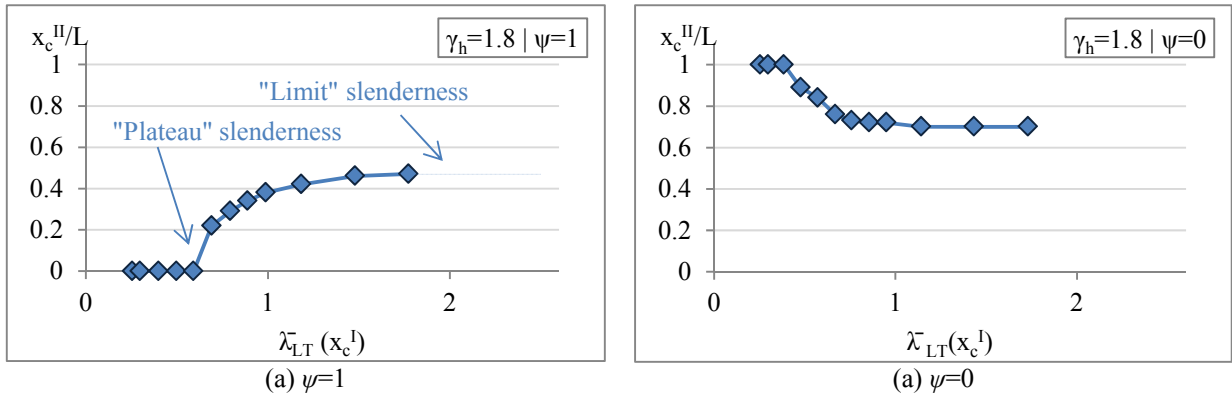
Figure 5.19: Second order failure location for a IPE200 (smallest cross-section), $\gamma=1.8$

(a) x_c^{II} (a) First and second order utilization
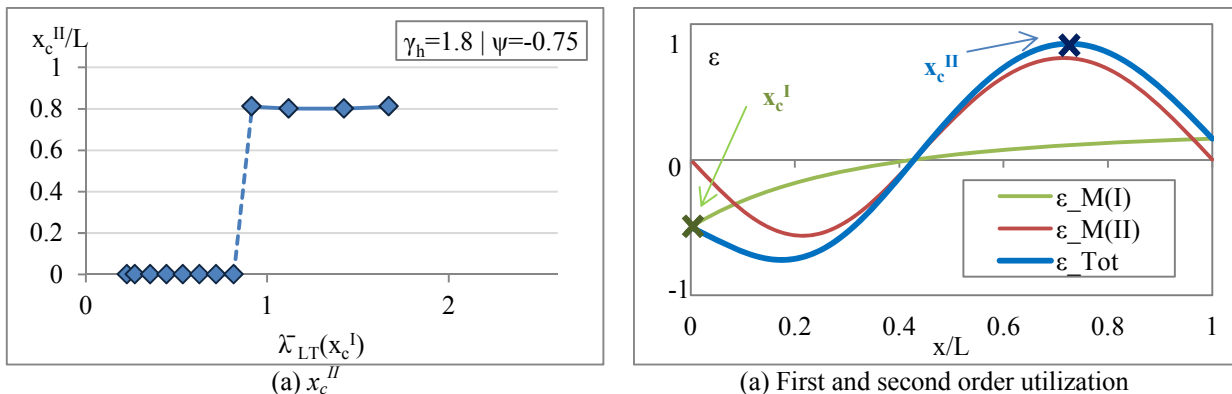
Figure 5.20: Second order failure location for a IPE200 (smallest cross-section), $\gamma_h=1.8$ and $\psi=-0.75$

5.4.5.2 Simplification and calibration of the parameters x_c^{II} and β

As discussed previously, when cross-section resistance governs, β is 0 (no imperfection effect) and x_c^{II} is x_c^{I}. On the other hand, for high slenderness, β increases and x_c^{II} converges to $x_{c,lim}^{II}$. Due to some bending moment distributions this transition may not always be continuous and a possible simplification is to separate the effects of cross-section resistance from the effects of instability, i.e., in the Ayrton-Perry model, always consider $x_{c,lim}^{II}$ and, accordingly, $\beta_{lim}=1$ (this limit was shown to be adequate and lead to safe estimations of resistance in Chapter 4). The Ayrton-Perry result is then limited by the cross-section resistance (given by x_c^{I} and corresponding $\beta=0$). Excellent agreement is noticed and, as a result, this methodology will be considered, see *Figure 5.21*.
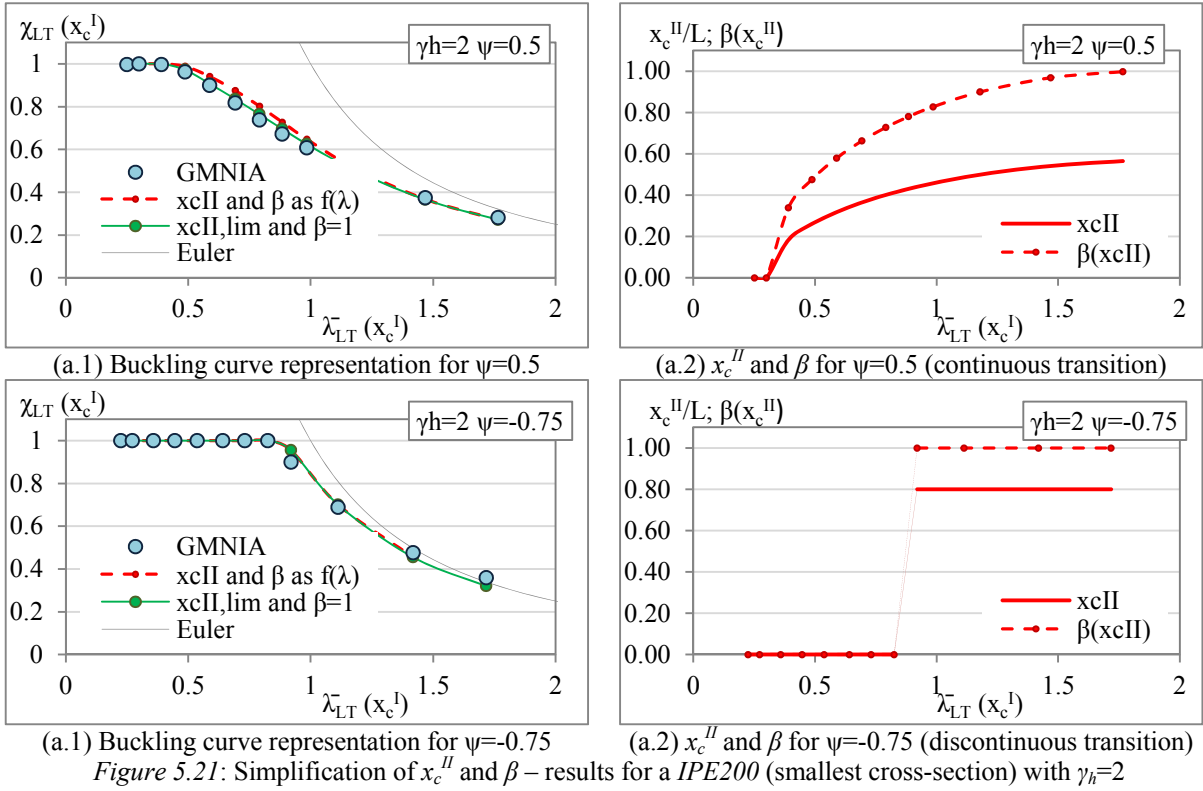
(a.1) Buckling curve representation for ψ=0.5   (a.2) x_c^{II} and β for ψ=0.5 (continuous transition)

(a.1) Buckling curve representation for ψ=-0.75   (a.2) x_c^{II} and β for ψ=-0.75 (discontinuous transition)

Figure 5.21: Simplification of x_c^{II} and β – results for a *IPE200* (smallest cross-section) with γ_h=2

Eq. (5.53) then becomes

$$\varepsilon(x_{c,\lim}^{II}) = 1 \rightarrow$$

$$1 = \chi_{LT}(x_{c,\lim}^{II}) + \frac{\chi_{LT}(x_{c,\lim}^{II})}{1 - \overline{\lambda}_{LT}^2(x_c^{II})\chi_{LT}(x_c^{II})} \times \underbrace{\left(\alpha_{LT}\left(\overline{\lambda}_z(x_{c,\lim}^{II}) - 0.2\right)\right)\underbrace{\left[\frac{\overline{\lambda}_{LT}^2(x_{c,\lim}^{II})}{\overline{\lambda}_z^2(x_{c,\lim}^{II})}\right]}_{\eta_{uniform\ beams}(x_{c,\lim}^{II})} \times \underbrace{\frac{1}{\beta(x_{c,\lim}^{II})}}_{}}_{\eta_{non-uniform\ beams}(x_{c,\lim}^{II})} \quad (5.58)$$

Calibration of $x_{c,lim}^{II}$ is now carried out. It can be fairly accurately described by a single expression for all cross-sections analysed, see Eq. (5.59) and *Figure 5.22*.

$$x^{II}_{c,\text{lim}} / L = \left(0.75 - 0.18\psi - 0.07\psi^2\right) + \left(0.025\psi^2 - 0.006\psi - 0.06\right)\left(\gamma_h - 1\right) \geq 0$$

(5.59)(a)

If $\quad \psi < 0 \quad and \quad \alpha \geq \alpha_{\text{lim}}$

$$x^{II}_{c,\text{lim}} / L = 0.12 - 0.03\left(\gamma_h - 1\right)$$

Where α and α_{lim} are given by

$$\alpha_{\text{lim}} = 1 + 1.214\left(\gamma_h - 1\right)$$
$$\alpha = |\psi|\gamma_w$$

(5.59)(b)

For a parabolic bending moment distribution, $x_{c,lim}{}^{II}$ becomes

$$x^{II}_{c,\text{lim}} / L = 0.5 + 0.0035\left(\gamma_h - 1\right)^2 - 0.03\left(\gamma_h - 1\right)^2 \leq 0.5$$

(5.59)(b)
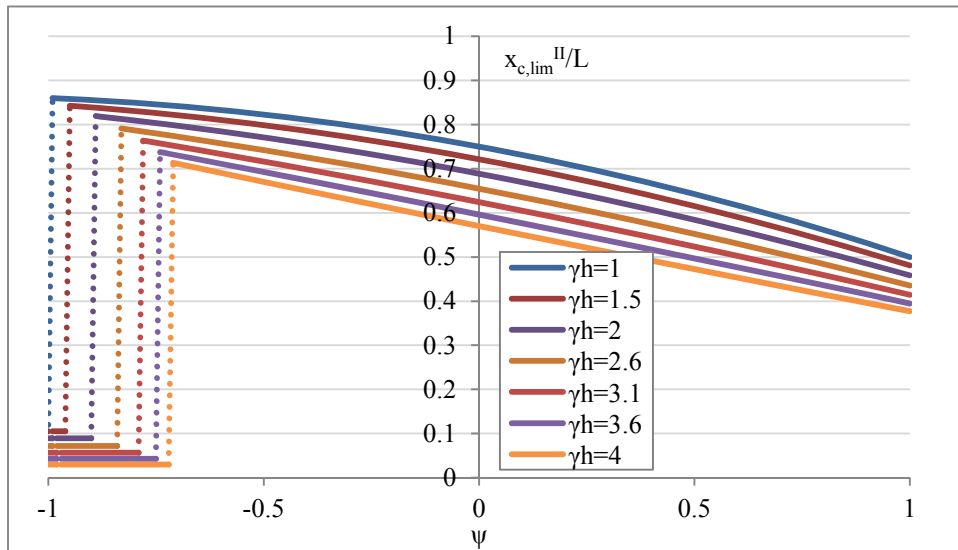
Figure 5.22: Calibration of $x_c{}^{II}$ for linear bending moment distributions for *IPE200* (smallest cross-section)

The observed discontinuity in *Figure 5.22* can be explained by the fact that for such high ratios between the minimum and maximum bending modulus, i.e., $\gamma_w = W_{y,el,max}/W_{y,el,min}$, the utilization ratio due to first order forces in the zone of minimum height has a very steep inclination. For this reason, the contribution of second order forces will not have much influence in the total utilization, resulting in a final failure location $x_c{}^{II}$ that is barely away

from x_c^I, as illustrated in *Figure 5.23*. This effect increases with the increase of the taper ratio and with the decrease of the absolute value of ψ. The parameters α and α_{lim} take this effect into account.
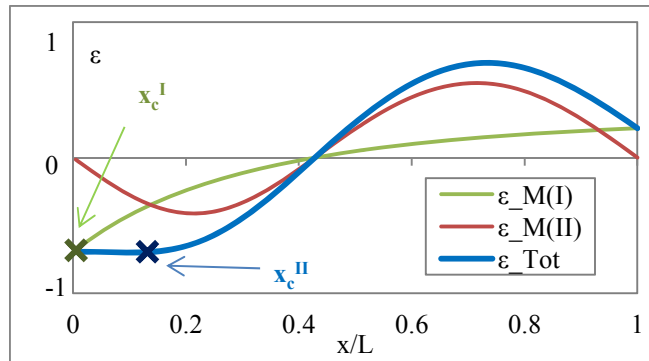
Figure 5.23: Critical location for a *IPE200* (smallest cross-section) with $\gamma_h=4$ and $\psi=-0.75$ and $\alpha \geq \alpha_{lim}$

5.4.5.3 Introduction and calibration of an "over-strength" factor

The "over-strength" factor approach was introduced in Chapter 4, section 4.4.3.2, and is here more detailed. The reason for considering an additional "over-strength" factor can be explained with the example of uniformly distributed loading in a prismatic beam. Note that, for this case, the second order failure location is coincident with the first order failure location, leading to the same load amplifier for both cases, $\alpha_{ult,k}(L/2)=M_{y,Rk}(L/2)/M_{y,Ed}(L/2)$. For this case, the increase in resistance of the parabolic bending moment case relatively to the uniform bending moment case is due to smaller size of the plastic zone that surrounds the failure location and as a result, due to a higher "supporting" action from the unyielded areas, see Taras (2010). For this reason, an "over-strength" factor was proposed in this research work for non-uniform bending moment distributions of prismatic beams. In order to maintain consistency with this approach, for the case of $\gamma_h=1$, an "over-strength" factor for a range of taper ratios and bending moment distributions is also considered here in the terms χ_{LT} and $\overline{\lambda}_{LT}$. Finally, the "over-strength" factor is an intuitive parameter to qualitatively describe not only the lower spread of plasticity around the failure location, but also the increase in (relative) resistance for a given beam with $\gamma_h \neq 1$ and $\psi \neq 1$ relatively to the reference case of $\gamma_h = \psi = 1$.

The "over-strength" factor can be defined as the ratio $\varphi = \alpha_{ult,k}(x_{c,lim}{}^{II}) / \alpha_{ult,k}(x_c{}^{I})$. When replaced in Eq. (5.58), it becomes

$$\varepsilon(x_{c,\lim}^{II}) = 1 \rightarrow$$

$$1 = \frac{\chi_{LT}(x_c^I)}{\varphi} + \frac{\dfrac{\chi_{LT}(x_c^I)}{\varphi}}{1 - \varphi\overline{\lambda}_{LT}^2(x_c^I)\dfrac{\chi_{LT}(x_c^I)}{\varphi}} \times \left(\alpha_{LT}\left(\overline{\lambda}_z(x_{c,\lim}^{II}) - 0.2\right)\right)\left[\frac{\varphi\overline{\lambda}_{LT}^2(x_c^I)}{\overline{\lambda}_z^2(x_{c,\lim}^{II})}\right] \qquad (5.60)$$

Note that the parameters $\overline{\lambda}_z(x_{c,\lim}^{II}) = f(A, I_z)$ and $\alpha_{LT} = f(W_{el,y}, W_{el,z})$ cannot be described as a function of φ. Although a simplification could be considered and, for example, the properties at $x = x_c^I$ or even at $x = L/2$ could be used instead of $x_{c,lim}{}^{II}$, in order to keep mechanical consistency, it was decided to consider $x_{c,lim}{}^{II}$ using the expressions of Eq. (5.59).

When plotted in the buckling curve, φ has the meaning illustrated in *Figure 5.24*. If it would not be limited by the cross-section resistance of the first order failure location, the full green line would have the path of the green dotted line up to $\chi(x_c^I) = \varphi$ (see orange dotted line). Note also that a higher φ is also related to a higher "plateau" slenderness, illustrating the lower influence of the imperfections in the member.

Finally, in *Figure 5.24*, the curve regarding the consideration of x_c^I (and no φ) is also illustrated, leading to resistance levels up to 20% lower than the numerical curve.
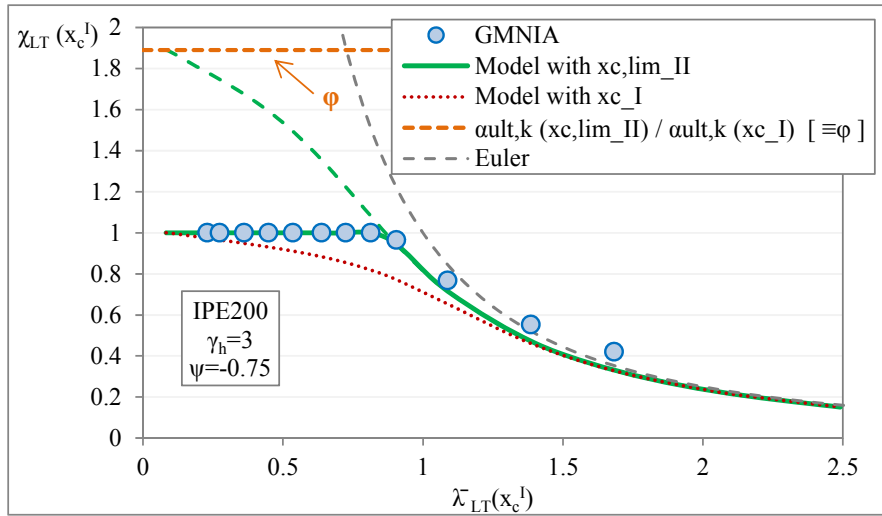
Figure 5.24:Interpretation of *φ*

In order to understand the variation of *φ* with *ψ* and *γ*, the numerical models of the cross-section *IPE200* (smallest cross-section) were considered for calculation of the *φ* factors that lead to the least error regarding the resistance. Each point regarding a given *ψ* and *γ*$_w$ corresponds to a range of slenderness that lead to a best fit value of *φ*. It is illustrated in *Figure 5.25*.
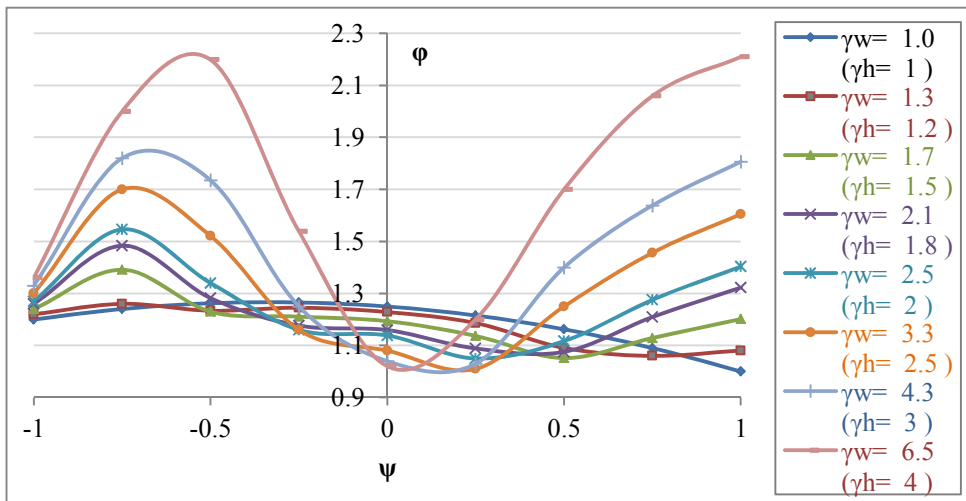
Figure 5.25:Numerical best fit *φ* values for *IPE200* (smallest cross-section)

If *Figure 5.25* is compared to *Figure 5.12* (in which only first order effects are considered) a parallelism can be noticed, illustrating that the *φ* factor can be somehow related to the amount of spare resistance in the beam including first and second order effects.

Three zones can be defined: for ψ values that are lower than the relative minimums in $\psi<0$; for ψ values that are higher than the relative minimums in $\psi>0$; and between those two relative minimums. As a result, for calibration of φ, three functions are considered according to the value of ψ relatively to ψ_{lim}. $|\psi_{lim}|$ is defined as the values of -ψ and +ψ that lead to an optimal member capacity (lowest φ) for a given γ_w respectively for negative and positive values of ψ, and can be approximated by Eq. (5.61)(a) as illustrated in *Figure 5.26*.

$$\psi_{\,\text{lim}} = \frac{1 + 120 \cdot a_\gamma + 600 \cdot a_\gamma{}^2 - 210 \cdot a_\gamma{}^3}{1 + 123 \cdot a_\gamma + 1140 \cdot a_\gamma{}^2 + 330 \cdot a_\gamma{}^3} \tag{5.61)(a}$$

in which

$$a_\gamma = -0.0005 \cdot (\gamma_w - 1)^4 + 0.009 \cdot (\gamma_w - 1)^3 - 0.077 \cdot (\gamma_w - 1)^2 + 0.78 \cdot (\gamma_w - 1) \tag{5.61)(b}$$

Note that the taper ratio γ_w is now considered in agreement with the evaluation carried out in 5.4.3 in which the curves of *Figure 5.18* were analyzed for three definitions of taper ratios.
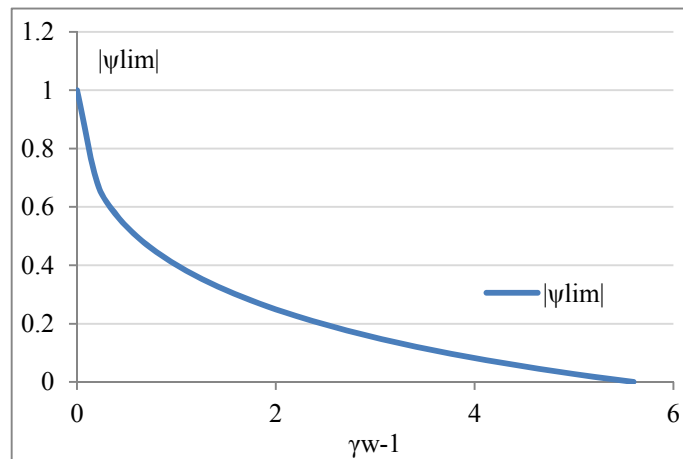
Figure 5.26: Values of ψ that lead to an optimal member capacity (lowest φ) for a given γ_w

Finally, an expression for φ, valid for $\gamma_h{\le}4$ and $\gamma_w{\le}6.5$ is given in Eq. (5.62).

$$\varphi = \begin{cases} A \cdot \psi^2 + B \cdot \psi + C \quad \geq 1, & if \ -1 \leq \psi \leq 1 \\ -0.0025\, a_\gamma{}^2 + 0.015\, a_\gamma + 1.05 & if \quad UDL \end{cases}, \quad \gamma_h \leq 4 \ and \ \gamma_w \leq 6.5 \qquad (5.62)$$

in which *A, B* and *C* are given in *Table 5.4*.

Table 5.4: Necessary parameters for determination of φ to be considered in Eq. (5.62)

	$\psi < -\psi_{lim}$	$-\psi_{lim} \leq \psi \leq \psi_{lim}$	$\psi > \psi_{lim}$
A	$-0.0665 \cdot a_\gamma{}^6 + 0.718 \cdot a_\gamma{}^5 - 2.973 \cdot a_\gamma{}^4$ $+5.36 \cdot a_\gamma{}^3 - 2.9 \cdot a_\gamma{}^2 - 2.1 \cdot a_\gamma - 1.09$	$\dfrac{-11.37 + 12090 \cdot a_\gamma - 8050 \cdot a_\gamma{}^2 + 1400 \cdot a_\gamma{}^3}{1 - 1058 \cdot a_\gamma + 705 \cdot a_\gamma{}^2 - 120 \cdot a_\gamma{}^3} + 11.22$	$0.008 \cdot a_\gamma{}^2 - 0.08 \cdot a_\gamma - 0.157$
B	$-0.1244 \cdot a_\gamma{}^6 + 1.3185 \cdot a_\gamma{}^5 - 5.287 \cdot a_\gamma{}^4$ $+9.27 \cdot a_\gamma{}^3 - 5.24 \cdot a_\gamma{}^2 - 2.18 \cdot a_\gamma - 2$	$+0.02 \cdot a_\gamma{}^6 - 0.133 \cdot a_\gamma{}^5 + 0.425 \cdot a_\gamma{}^4$ $-0.932 \cdot a_\gamma{}^3 + 1.05 \cdot a_\gamma{}^2 - 0.5 \cdot a_\gamma - 0.1$	$-0.033 \cdot a_\gamma{}^3 + 0.04 \cdot a_\gamma{}^2$ $+0.48 \cdot a_\gamma + 0.37$
C	$-0.0579 \cdot a_\gamma{}^6 + 0.6003 \cdot a_\gamma{}^5 - 2.314 \cdot a_\gamma{}^4$ $+3.911 \cdot a_\gamma{}^3 - 2.355 \cdot a_\gamma{}^2 + 0.02 \cdot a_\gamma + 0.3$	$0.02 \cdot a_\gamma{}^2 - 0.14 \cdot a_\gamma + 1.25$	$0.032 \cdot a_\gamma{}^3 - 0.092 \cdot a_\gamma{}^2$ $+0.06 \cdot a_\gamma + 0.8$

The functions defined in *Table 5.4* present a discontinuity at $\pm\psi_{lim}$. However, the differences are lower than 2% and shown to be negligible in the final resistance. Finally, *Figure 5.27* and *Table 5.5* illustrate the values of φ concerning linear bending moment distribution, within the defined limits of γ_w.

Figure 5.27:Graphic representation of φ according to Eq. (5.62)

Table 5.5: φ values according to Eq. (5.62)

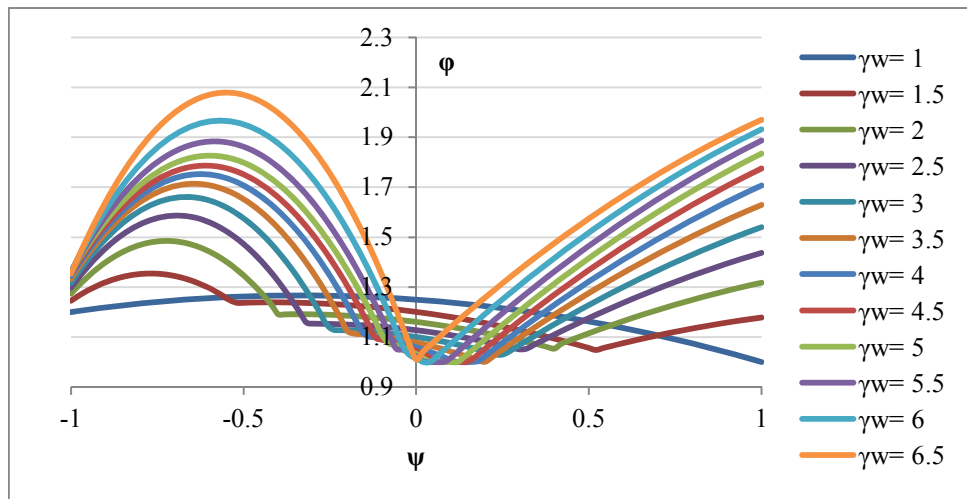| γ_w	Ψ (=$M_{y,Ed,hmin}$/$M_{y,Ed,hmax}$)								
	-1	**-0.75**	**-0.5**	**-0.25**	**0**	**0.25**	**0.5**	**0.75**	**1**
1	1.200	1.241	1.263	1.266	1.250	1.216	1.163	1.091	1.000
1.25	1.228	1.275	1.253	1.252	1.224	1.170	1.090	1.059	1.099
1.5	1.245	1.354	1.238	1.233	1.201	1.142	1.056	1.121	1.178
1.75	1.260	1.423	1.279	1.211	1.180	1.121	1.080	1.178	1.251
2	1.274	1.483	1.347	1.189	1.161	1.102	1.115	1.230	1.318
2.25	1.286	1.534	1.412	1.169	1.143	1.085	1.147	1.277	1.380
2.5	1.298	1.576	1.472	1.152	1.128	1.067	1.176	1.321	1.437
2.75	1.308	1.611	1.527	1.139	1.113	1.047	1.203	1.362	1.490
3	1.317	1.639	1.575	1.126	1.100	1.026	1.228	1.400	1.540
3.25	1.326	1.662	1.617	1.191	1.089	1.038	1.253	1.435	1.586
3.5	1.333	1.680	1.652	1.250	1.078	1.050	1.276	1.469	1.629
3.75	1.340	1.695	1.682	1.302	1.068	1.064	1.299	1.501	1.669
4	1.346	1.707	1.707	1.346	1.059	1.078	1.322	1.532	1.707
4.25	1.351	1.719	1.730	1.383	1.052	1.093	1.345	1.561	1.742
4.5	1.355	1.731	1.751	1.416	1.044	1.110	1.368	1.590	1.775
4.75	1.358	1.744	1.774	1.446	1.038	1.129	1.392	1.617	1.806
5	1.361	1.760	1.799	1.476	1.032	1.149	1.415	1.644	1.835
5.25	1.362	1.778	1.828	1.510	1.027	1.172	1.440	1.670	1.862
5.5	1.362	1.801	1.862	1.547	1.022	1.196	1.465	1.695	1.887
5.75	1.362	1.827	1.903	1.591	1.019	1.223	1.491	1.720	1.910
6	1.360	1.859	1.952	1.640	1.015	1.252	1.518	1.745	1.932
6.25	1.357	1.895	2.008	1.696	1.012	1.283	1.546	1.769	1.952
6.5	1.353	1.936	2.070	1.755	1.010	1.316	1.574	1.793	1.970

5.4.5.4 Introduction of a cut-off in the generalized imperfection η of welded I-sections

Again, for welded cross-sections, the generalized imperfection for welded beams is redefined. In Taras (2010), the imperfection factor α_{LT} was calibrated. Here, in addition, a limit value in the expression of $\eta = \alpha_{LT}\left(\bar{\lambda}_z(x_c^{II}) - 0.2\right)$ given by

$$\eta \leq \sqrt{\frac{W_{y,el}(x_c^{II})}{W_{z,el}(x_c^{II})}}\left(0.12\psi^2 - 0.23\psi + 0.35\right) \tag{5.63}$$

was shown to be adequate. In Eq. (5.63), ψ represents the ratio between the maximum and minimum bending moment. Results are given in Section 5.4.5.5, *Figure 5.29*.

5.4.5.5 Accuracy of the new formulation

a) Design Procedure

The verification of lateral-torsional buckling of web-tapered beams for which for $\gamma_h \leq 4$ and $\gamma_w \leq 6.5$, may be done as follows:

1. Determine the first order failure location, x_c^I, by calculating the utilization ratio $\varepsilon(x) = M_{y,Ed}(x)/M_{y,Rk}(x)$ at a satisfactory number of locations, e.g. 10. x_c^I is the location in which ε is maximum. $M_{y,Rk}(x)$ shall be determined considering $M_{y,pl}$ if the cross-section is class 1 or 2, $M_{y,3,Rd}$ if the cross-section is class 3 (Greiner *et al.*, 2011). Then calculate the cross-section resistance load multiplier $\alpha_{ult,k}(x_c^I) = M_{y,Rk}(x_c^I) / M_{y,Ed}(x_c^I)$.

2. Determine the critical load amplifier α_{cr} of the tapered beam. Finite element analysis may be performed for this.

3. Verify the stability resistance:

$$\chi_{LT}(x_c^I) \times \alpha_{ult,k}(x_c^I) = \alpha_b \geq 1$$

From which:

$$\chi_{LT}(x_c^I) = \frac{\varphi}{\phi_{LT} + \sqrt{\phi_{LT}^2 - \varphi \times \bar{\lambda}_{LT}^2(x_c^I)}} \leq 1$$

$$\phi_{LT} = 0.5 \times \left(1 + \varphi \times \eta \times \frac{\bar{\lambda}_{LT}^2(x_c^I)}{\bar{\lambda}_z^2(x_{c,\lim}^{II})} + \varphi \times \bar{\lambda}_{LT}^2(x_c^I) \right)$$

And

$$\bar{\lambda}_{LT}(x_c^I) = \sqrt{\alpha_{ult,k}(x_c^I)/\alpha_{cr}} \ .$$

η and α_{LT} are obtained from

	Hot-rolled	Welded
α_{LT}	$0.16\sqrt{\dfrac{W_{y,el}(x_{c,\lim}^{II})}{W_{z,el}(x_{c,\lim}^{II})}} \leq 0.49$	$0.21\sqrt{\dfrac{W_{y,el}(x_{c,\lim}^{II})}{W_{z,el}(x_{c,\lim}^{II})}} \leq 0.64$
η	$\alpha_{LT} \times \left(\bar{\lambda}_z(x_{c,\lim}^{II}) - 0.2\right)$	$\alpha_{LT} \times \left(\bar{\lambda}_z(x_{c,\lim}^{II}) - 0.2\right)$ $\leq \sqrt{\dfrac{W_{y,el}(x_{c,\lim}^{II})}{W_{z,el}(x_{c,\lim}^{II})}}\left(0.12\psi^2 - 0.23\psi + 0.35\right)$

$\bar{\lambda}_z(x_{c,\lim}^{II})$ is obtained from

$$\overline{\lambda}_z(x_{c,\lim}^{II}) = \sqrt{N_{Rk}(x_{c,\lim}^{II}) \Big/ \dfrac{\pi^2 E I_z(x_{c,\lim}^{II})}{L^2}}$$

$x_{c,lim}{}^{II}$ and φ are obtained from Eq. (5.59) and Eq. (5.62), respectively.

b) Results

Four examples regarding hot-rolled cross-sections are illustrated in *Figure 5.28*. Regarding all results, maximum differences of 10% relatively to the numerical models are observed.

(a.1) Buckling curve representation, *IPE200*

(a.2) Buckling curve representation, *IPE200*

(b.1) Buckling curve representation, *HEB300*

(b.2) Buckling curve representation, *HEB300*
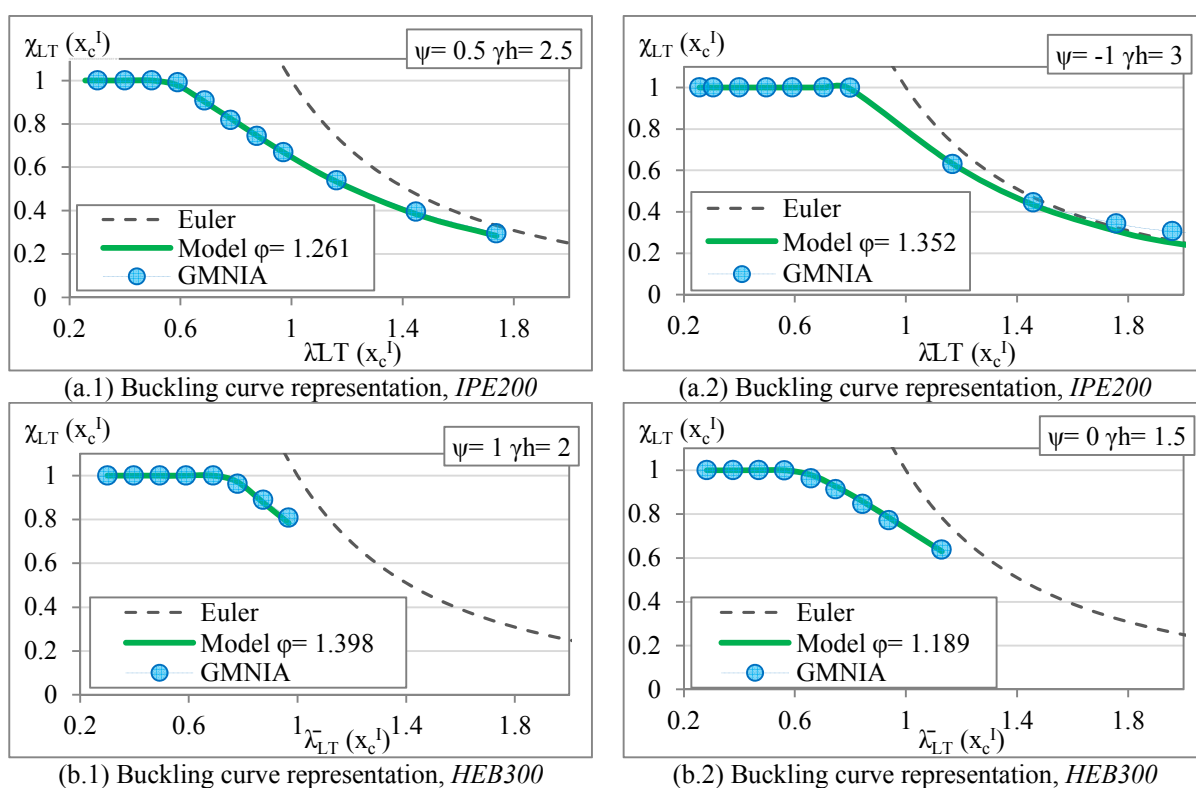
Figure 5.28:Results for hot-rolled cross-sections

c) Welded cross-sections

Figure 5.29 illustrates the results for welded cross-sections considering a limiting value of the generalized imperfection η. For calibration of the cut-off, it was noticed that it varies with the bending moment distribution.

(a) Buckling curve representation, *HEB300*   (b) Buckling curve representation, *HEB300*
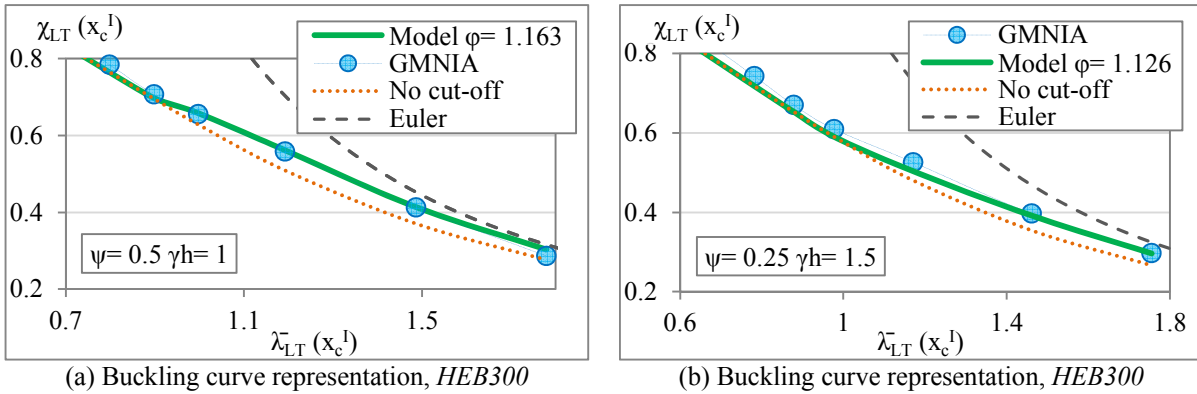
Figure 5.29: Results for welded cross-sections

d) Interaction with shear

In tapered members, the interaction with shear may not be negligible for low slenderness. Consider, for example, a tapered beam (*IPE200* smallest cross-section), with γ_h=2.5 and a uniformly distributed loading. Not taking into account local buckling of the web (plastic resistance), the utilization ratio of a beam with a length of *L*=2 m is illustrated in *Figure 5.30*. For this case, first order failure is governed by the presence of shear in the smallest cross-section. Verification to shear resistance and bending and shear interaction should be performed according to EC3-1-1 in addition to the stability verification. For this, the equations Eq. (2.49) and (2.50) of Chapter 2 should be satisfied.

(a) Buckling curve representation   (b) First order utilization ratios: ε(M) – due to bending moment; ε(V) – due to shear stress; ε(M+V) – due to bending and shear interaction;
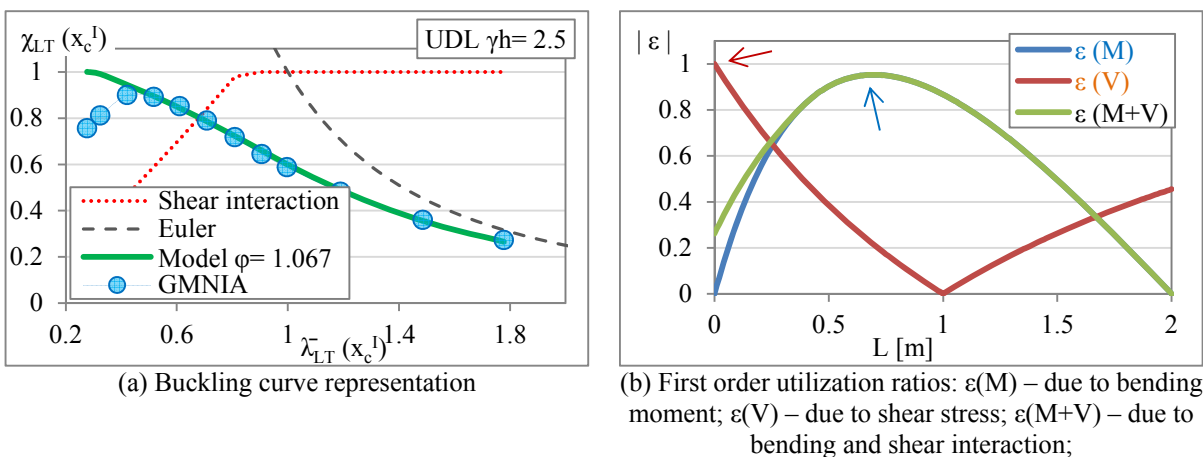
Figure 5.30: Influence of shear stresses for a *IPE200*, γ_h=2.5, UDL

φ factors were calibrated taking into account the models in which the web is not allowed to exhibit local deformations. Accordingly, a plastic resistance in the models was considered. This was adopted in order not to consider possible shear buckling in the calibration of φ. φ factors can be considered in the models with the unrestrained web, as long as the adequate resistance level is considered. Nevertheless, as already observed in Chapter 4, when the φ factor calibrated for plastic capacity is considered, a slight unconservatism is noticed. (*Figure 5.31(a)*).

However, for some cases, in the presence of shear buckling, see *Figure 5.31*, the calibrated φ factors may not be sufficient for the stability verification of the beam. In further studies, the reduction of resistance due to shear buckling will be analyzed and taken into account.

(a) Web prevented from buckling (b) Web unrestrained
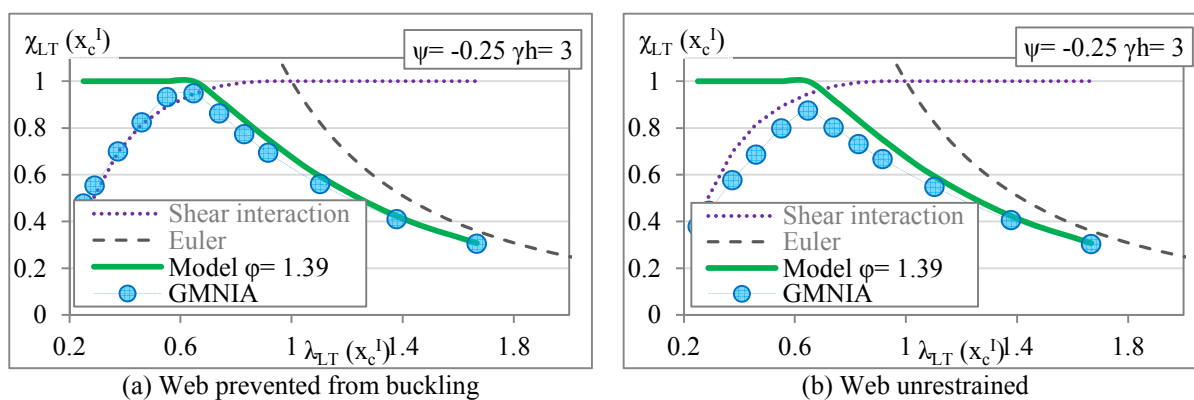
Figure 5.31: Buckling curve representation for *IPE200*; ψ=-0.25; γ_h=3

e) Comparison to other methodologies

In EC3-1-1, the General Method may be applied to verify the lateral-torsional buckling stability of non-uniform members. The determination of the overall reduction factor, χ_{op}, shall be carried out as follows:

- The minimum between χ for flexural buckling and χ_{LT}, considering clauses 6.3.1 and 6.3.2 respectively;

- An interpolated value between χ and χ_{LT}, in the case of bending and axial force interaction.

It was proven in Section 2.4.2.3 that, for the case of prismatic beams, the General Method leads to clause 6.3.2 if χ_{LT} is considered. Nevertheless, because χ_{LT} may not be the minimum between χ and χ_{LT}, the curve for flexural buckling is also considered in the analysis. For calculation of χ_{LT}, it is possible to consider either clause 6.3.2.2 (general case) or 6.3.2.3 (LTB curves for rolled sections or equivalent welded sections, denoted as special case).

Table 5.6 presents the possible buckling curves according to the application of the General Method (clause 6.3.4) as described in *Table 5.2*. In addition, the buckling curves derived in Taras (2010) for prismatic beams are also considered for consistent comparison with the tapered case derived here. Note that existing procedures do not account for the second order failure location x_c^{II}. As a result, x_c^{I} is considered for determination of cross-section properties.

*Table 5.6:*Possible buckling curves for web-tapered beams

Clause	Hot rolled	Welded
6.3.1 $\chi_z(x_c^{I})$ (flexural buckling)	h/b≤1.2 → curve *c* (consistent with the residual stress pattern adopted)	curve *c*
6.3.2.2 $\chi_{LT}(x_c^{I})$ (general case LTB)	h/b≤2 → curve *a* h/b>2 → curve *b*	h/b≤2 → curve *c* h/b>2 → curve *d*
6.3.2.3 $\chi_{LT,mod}(x_c^{I})$ (special case LTB)	h/b≤2 → curve *b* h/b>2 → curve *c*	h/b≤2 → curve *c* h/b>2 → curve *d*
$\chi_{LT,,\eta*Taras}$	$0.16\sqrt{\dfrac{W_{y,el}(x_c^{I})}{W_{z,el}(x_c^{I})}} \le 0.49$	$0.21\sqrt{\dfrac{W_{y,el}(x_c^{I})}{W_{z,el}(x_c^{I})}} \le 0.64$

The example of *Figure 5.32* describes the inaccuracy obtained by the consideration of any of the curves that were calibrated or derived for the specific case of prismatic hot-rolled beams:

- *Figure 5.32(a)* illustrates resistance when curve *c* for flexural buckling is considered. An improvement of 10% is obtained with the proposed method;

- In *Figure 5.32(b)* it is visible how curve *a* may become unsafe when the General Case for calculation of the lateral-torsional buckling reduction factor is considered. Nevertheless, x_c^{I} is located at the higher cross-section such that curve *b* could be considered. In comparison with curve *a*, it would actually lead to a better solution for this case;

- As already mentioned, for a non-uniform bending moment distribution, resistance is not necessarily higher than the resistance obtained for the prismatic beam. For this example of $\Psi=0$, $\varphi=1.25$ for $\gamma_h=1$ and $\varphi=1.064$ for $\gamma_h=3$. If the General Method of clause 6.3.4 is applied with the special case of clause 6.3.2.3 for calculation of the lateral-torsional buckling reduction factor, and a correction factor of $k_c=0.75$ (for $\Psi=0$) is considered, 18% and 28% increase in resistance is achieved respectively for curves *c* and *b*, see *Figure 5.32(c)*. In Rebelo *et al.* (2008) it was shown that the resistance obtained by special case of clause 6.3.2.3 generally leads to higher resistance than the general case of clause 6.3.2.2. For the case of tapered members this is even more evident because of the wrong consideration of the k_c factors developed for prismatic beams. This is however a possible and probable choice by the designer because of the possibility of accounting for the bending moment distribution in the determination of χ_{LT} and, as a result, of χ_{op};

- Finally, in *Figure 5.32(d)*, the design method which was specifically developed for prismatic beams in Taras (2010) is also analyzed. Because this method is analytically consistent with the buckling behavior of prismatic beams subject to lateral-torsional buckling and is also the solution of the proposed method here for the case of $\gamma_h=1$, it is also illustrated here. 2 cases are analyzed. Firstly the consideration of x_c^I instead of x_c^{II} as well as $\varphi=1$ instead of the calibrated $\varphi=1.064$ yields lower results. Note that, for other (tapered) cases with higher φ (which can be greater than $\varphi=2$) the difference would even be more noticeable. On the other hand, if the φ factor developed for the triangular bending moment distribution of prismatic beams is wrongly considered ($\varphi_{prismatic,\Psi=0}$ =1.25) in the tapered beam, the dotted blue line is obtained. The examples of *Figure 5.4(c)* and *(d)* illustrate the need to calibrate adequate φ factors / failure locations for tapered beams subject to non-uniform bending moment distributions and that rules for prismatic members should not be used to verify the stability of non-uniform members, for as reliable as those may be.

(a) Curve *c* for flexural buckling

(b) Curves *a* and *b* according to the General Case of clause 6.3.2.2

(c) Curves *b* and *c* according to the Special Case of clause 6.3.2.4

(d) Curves proposed in Taras (2010) for prismatic beams with φ=1 (uniform bending moment) and φ=1.25 (Ψ=0)
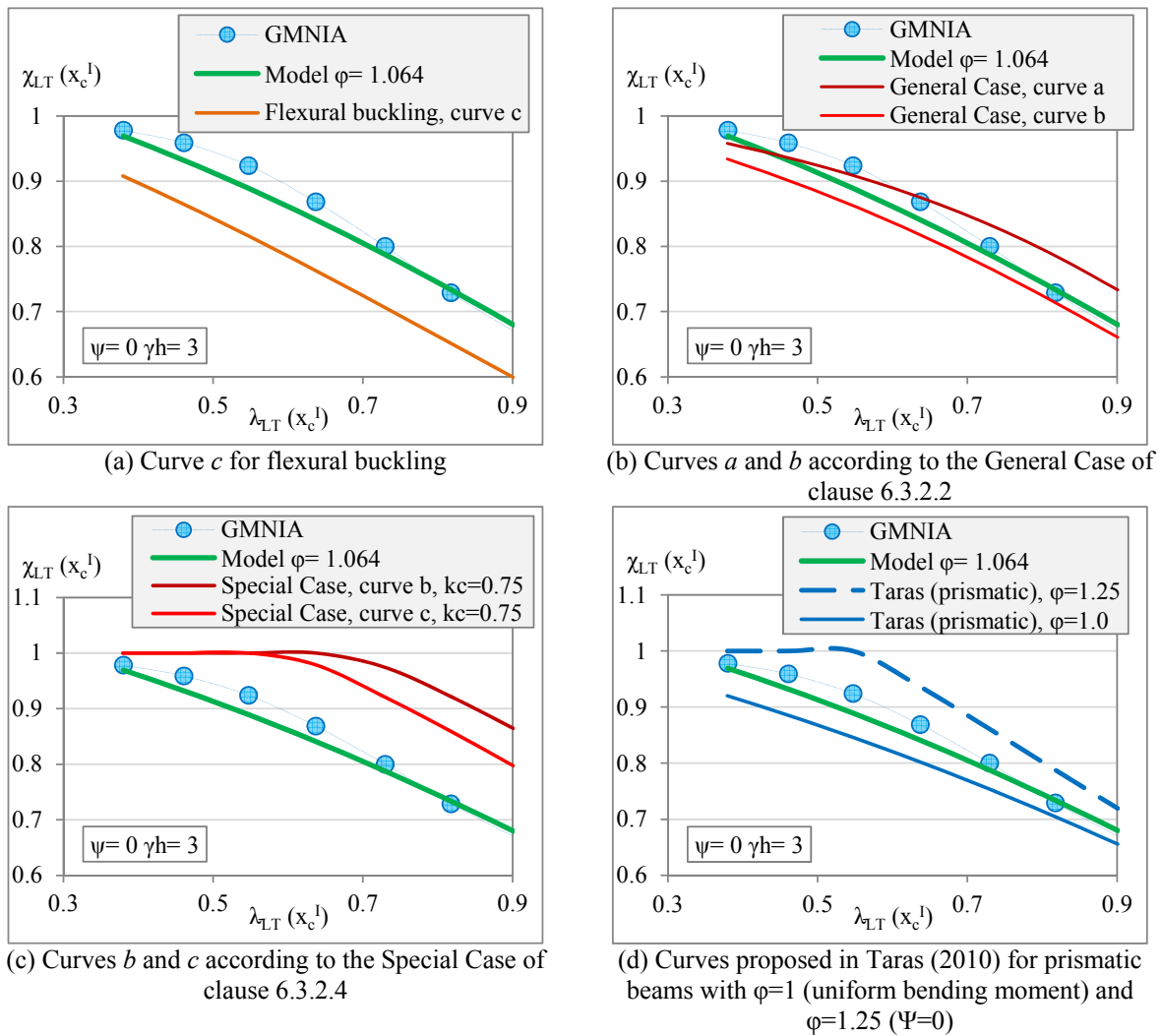
Figure 5.32: Comparison of methodologies – Buckling curve representation for *HEB300 ψ=0; γ_h=3*

Regarding welded cross-sections, *Figure 5.33* illustrates an example in which curve *c* is considered both for lateral-torsional buckling (considering clause 6.3.2.2, general case) and for flexural buckling. Note that the curve for lateral-torsional buckling may be *c* or *d* for welded cross-sections. Differences of 37% regarding curve *c* are visible in *Figure 5.33*. Although it is not illustrated, considering curve *d* would lead to a drop in the resistance level up to 45%.
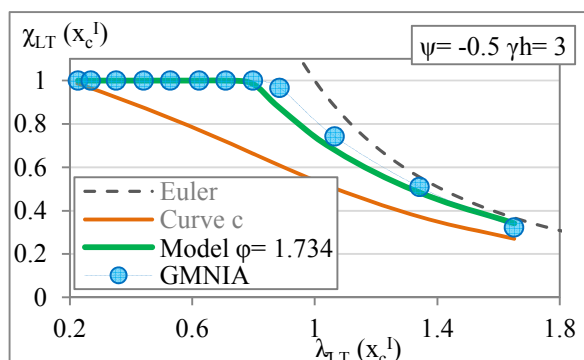
Figure 5.33: Comparison of methodologies; $\psi=-0.25$; $\gamma_h=3$ (welded cross section)

5.4.5.6 Statistical analysis

Finally, a statistical evaluation of all cases and methodologies considered for this study is carried out. Only members with a practical slenderness level of $\overline{\lambda}_{LT}(x_c^I) \leq 1.5$ and whose plastic resistance is not affected by the presence of shear are considered for this purpose, covering a total of 2808 cases. *Figure 5.34* to *Figure 5.36* illustrate the numerical resistance against the resistance obtained by the proposed methodology (*Figure 5.34*); and obtained by clause 6.3.4 using (i) the general case for determination of χ_{op} (*Figure 5.35*) and (ii) the special case for determination of χ_{op} (*Figure 5.36*). It is evident the improvement the proposed methodology relatively to the other cases. *Figure 5.35(a)* illustrates that curve *a* can lead to differences between approximately 20% on the unsafe side and 25% on the safe side. On the other hand, curve *c*, commonly considered for application of clause 6.3.4 for the case of tapered beams may lead to a loss in resistance up to 40%, see *Figure 5.35(c)*. The application of curve *c* in the special case is shown in *Figure 5.36* in which a high spread of results is visible.
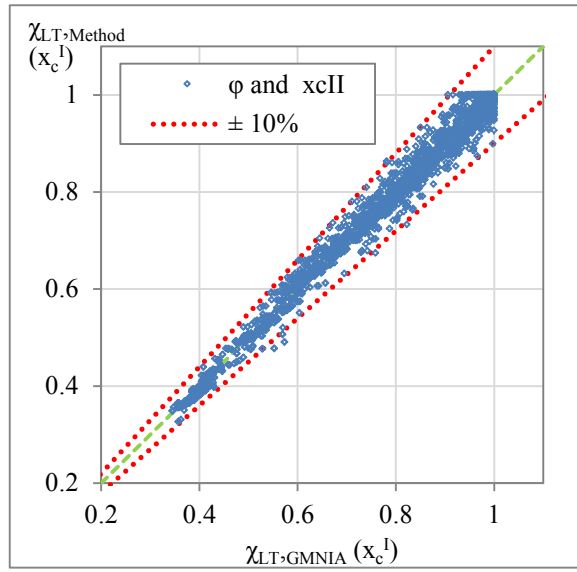
Figure 5.34:Resistance obtained by the proposal against the numerical models

(a) Curve *a*

(b) Curve *b*

(c) Curve *c*   (d) Curve *d*
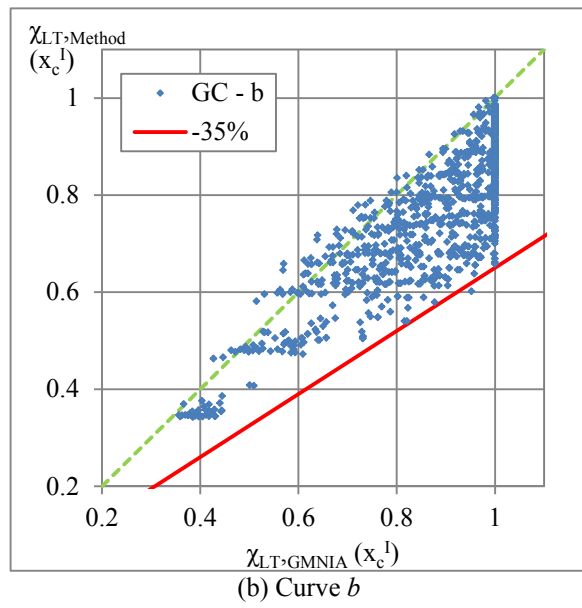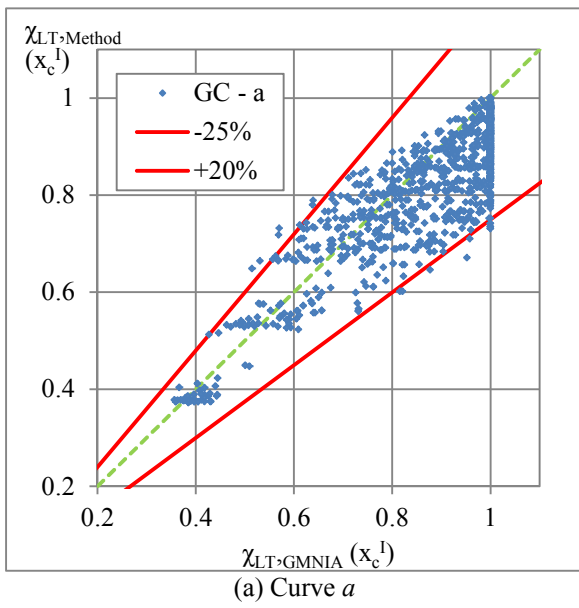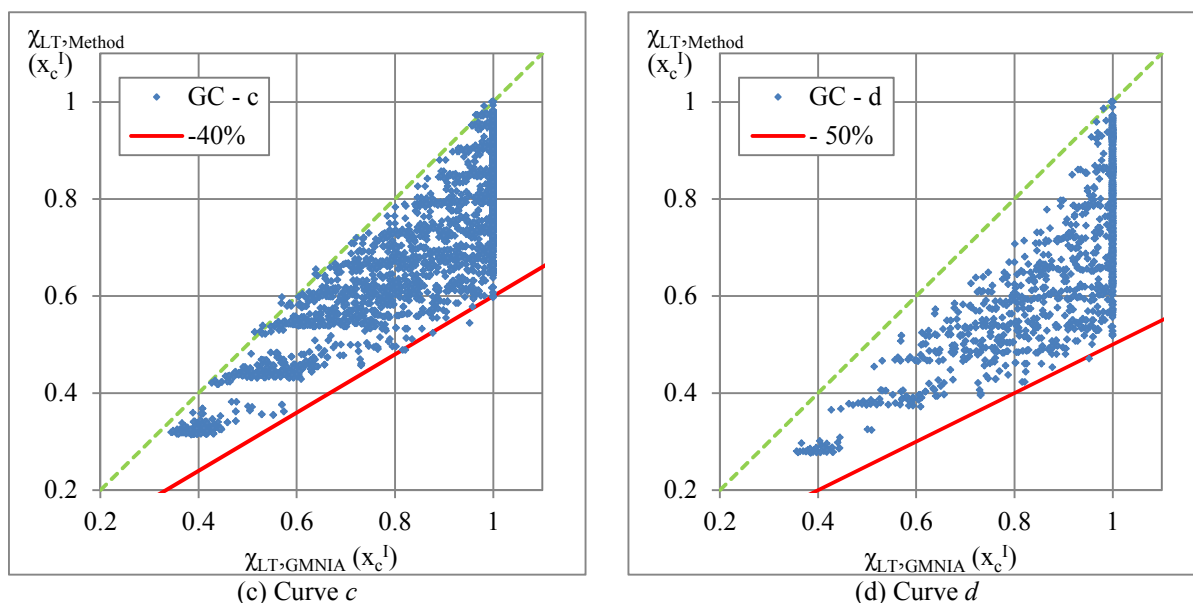
Figure 5.35:Resistance obtained by the General Method (considering the general case of clause 6.3.2.2 for the reduction factor determination) against the numerical models
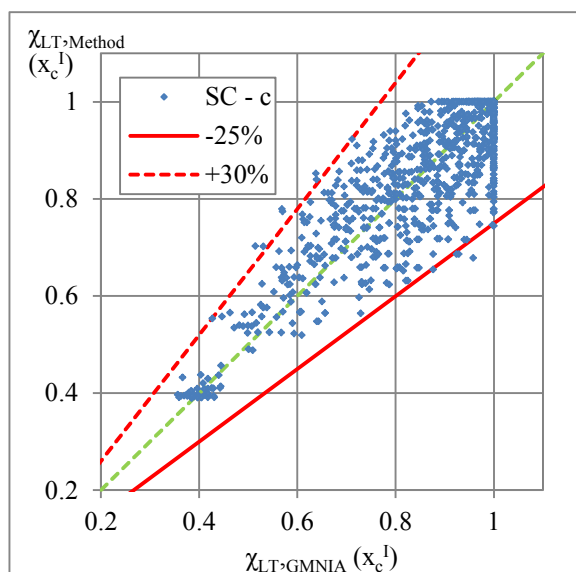
Figure 5.36:Resistance obtained by the General Method (considering the speciall case of clause 6.3.2.3 for the reduction factor determination) against the numerical models – curve *c*

Finally, following a similar procedure as in Rebelo *et al*. (2008) and Simões da Silva *et al*. (2008), statistical indicators of the ratio $\chi_{LT,Method}\,(x_c^I)$ / $\chi_{LT,GMNIA}\,(x_c^I)$ are given in

Table 5.7 to *Table 5.9*. In

Table 5.7, the various methodologies considered here are analyzed according to fabrication procedure. Again, the lower spread and the average value of the proposal relatively to the other methodologies, show the accuracy of the calibrated method. In addition, an

improvement is observed with the introduction of a cut-off in the generalized imperfection for the welded cases. If all cases are analyzed *Table 5.8* indicates that, if the transformation of variables considered in Eq. (5.60) is not adopted, i.e.,

$$\frac{\chi_{LT}(x_c^{I})}{\varphi} \to \chi_{LT}(x_{c,\lim}^{II}) \quad \text{and} \quad \varphi\bar{\lambda}_{LT}^{2}(x_c^{I}) \to \bar{\lambda}_{LT}^{2}(x_{c,\lim}^{II}) \tag{5.64}$$

an adequate accuracy level is also reached. Although this alternative approach avoids the calculation of a φ factor as the second order failure location is always considered in the terms χ_{LT} and $\bar{\lambda}_{LT}$, it does not take into account the increase in resistance of the uniformly distributed load case for γ_h=1, as already referred. It also does not lead to the design method developed in Taras (2010) for the other bending moment distributions of γ_h=1 (as the calibrated $x_{c,lim}^{II}$ do not exactly match φ for those cases, once a direct transformation would be too complex to carry out as done for web tapered columns subject to <u>constant</u> axial force). In addition a cross-section resistance check at x_c^{I} would still have to be performed (this check is implicit in the *"φ"* approach). Nevertheless, it could be a suitable and simpler alternative to avoid the determination of φ. *Table 5.8* also presents a simplification relatively to the proposed method in which the terms determined with $x_{c,lim}^{II}$ are now obtained with x_c^{I}. Although this simplification leads to a loss in mechanical consistency, this would avoid the use of Eq. (5.59) for calculation of $x_{c,lim}^{II}$.

Finally, *Table 5.9* gives statistical results of the proposed design model according to the various subsets of cross-section; fabrication procedure; modeling of the web stiffness; taper ratio and bending moment distribution. Uniformity in results is visible, regardless of the subset analyzed. A safety factor may be afterwards established in order to account for the higher ratios of $\chi_{LT,Method}(x_c^{I}) / \chi_{LT,GMNIA}(x_c^{I})$.

In

Table 5.7 to *Table 5.9*, *CoV* is the coefficient of variation given by the ratio between the standard deviation and the mean.

Table 5.7: Statistical evaluation of the ratio $\chi_{LT,Method}\,(x_c^I)\,/\,\chi_{LT,GMNIA}\,(x_c^I)$ according to the methodology

Methodology	n	Mean	St. Dev.	CoV (%)	Min.	Max.
Hot-rolled						
Proposal with φ and $x_{c,lim}^{II}$	2455	1.00	0.02	2.5	0.86	1.10
General Case - curve a	1024	0.92	0.08	8.19	0.70	1.16
General Case - curve b	1024	0.87	0.09	9.93	0.63	1.05
General Case - curve c	2455	0.83	0.09	11.28	0.57	1.01
General Case - curve d	1024	0.75	0.12	15.77	0.49	1.00
Special Case - curve b	1024	1.02	0.08	7.61	0.77	1.37
Special Case - curve c	1024	0.98	0.08	7.83	0.71	1.26
η^* Taras with $\varphi \geq 1$	2455	0.98	0.06	6.39	0.73	1.13
η^* Taras with $\varphi=1$	2455	0.91	0.06	6.10	0.73	1.03
Welded						
Proposal with φ and $x_{c,lim}^{II}$	353	0.99	0.03	2.65	0.89	1.09
Proposal with φ and $x_{c,lim}^{II}$ - no cut-off in η	353	0.97	0.04	3.86	0.88	1.08
General Case - curve a	353	0.97	0.09	9.74	0.75	1.28
General Case - curve b	353	0.91	0.09	9.60	0.68	1.16
General Case - curve c	353	0.85	0.09	10.53	0.62	1.05
General Case - curve d	353	0.76	0.10	13.13	0.54	0.99
Special Case - curve c	353	1.03	0.09	9.03	0.77	1.37
Special Case - curve d	353	0.96	0.09	9.26	0.69	1.21
η^* Taras with $\varphi \geq 1$	353	0.94	0.07	7.87	0.71	1.08
η^* Taras with $\varphi=1$	353	0.88	0.06	7.36	0.70	1.06

Table 5.8: Statistical evaluation of the ratio $\chi_{LT,Method}\,(x_c^I)\,/\,\chi_{LT,GMNIA}\,(x_c^I)$ regarding all n=2808 cases

Methodology	n	Mean	St. Dev.	CoV (%)	Min.	Max.
Proposal with φ and $x_{c,lim}^{II}$	2808	1.00	0.03	2.5	0.86	1.10
Proposal with φ and x_c^I (instead of $x_{c,lim}^{II}$)	2808	1.00	0.03	2.7	0.86	1.16
Proposal with $x_{c,lim}^{II}$ only (instead of φ)	2808	1.01	0.03	2.67	0.84	1.15
General Case - curve c	2808	0.83	0.09	11.20	0.57	1.05

Table 5.9: Statistical evaluation of the ratio $\chi_{LT,Method} (x_c^I) / \chi_{LT,GMNIA} (x_c^I)$ – analysis of the proposal by sub-sets

Sub-set / case	n	Mean	St. Dev.	CoV (%)	Min.	Max.
Smallest cross-section						
100x100x10x10	266	1.00	0.03	2.68	0.90	1.07
HEB300	758	1.00	0.02	2.36	0.93	1.10
IPE200	1784	1.00	0.03	2.56	0.86	1.10
Fabrication procedure						
Hot Rolled	2455	1.00	0.02	2.47	0.86	1.10
Welded	353	0.99	0.03	2.65	0.89	1.09
Modeling of web stiffness						
Web prevented from local buckling	1447	1.00	0.02	2.46	0.86	1.09
Web free to local buckling	1361	1.00	0.03	2.56	0.86	1.10
γ						
$\gamma_h=1$	517	1.00	0.02	1.97	0.93	1.07
$1<\gamma_h\leq2$	1350	1.00	0.02	2.14	0.92	1.07
$2<\gamma_h\leq3$	615	1.00	0.03	3.20	0.86	1.10
$3<\gamma_h\leq4$	326	0.99	0.03	3.22	0.86	1.10
Bending moment distribution						
$-1\leq\Psi<-0.5$	582	1.00	0.02	2.15	0.86	1.09
$-0.5\leq\Psi<0$	516	1.01	0.03	2.84	0.89	1.10
$0\leq\Psi<0.5$	551	1.01	0.03	2.72	0.92	1.09
$0.5\leq\Psi<1$	655	0.99	0.02	2.51	0.89	1.07
$\Psi=1$	340	0.99	0.02	1.75	0.92	1.02
UDL	164	1.00	0.02	2.31	0.91	1.06

5.5 Example

5.5.1 Introduction

A tapered beam composed of a *IPE200* welded cross-section in the smallest end with a linearly varying height and a taper ratio of $\gamma_h=h_{max}/h_{min}=3$ is now analyzed, see *Figure 5.37*. The applied bending moment is $M_{y,Ed}=50$ *kNm* with $\psi=0.75$ and the yield stress of $f_y=235$ *MPa*. The beam has a length of $L=2.72$ *m* and a taper angle of $\alpha=4.21°$. The safety of the beam is verified in the following in order to illustrate application of the proposed methodology.
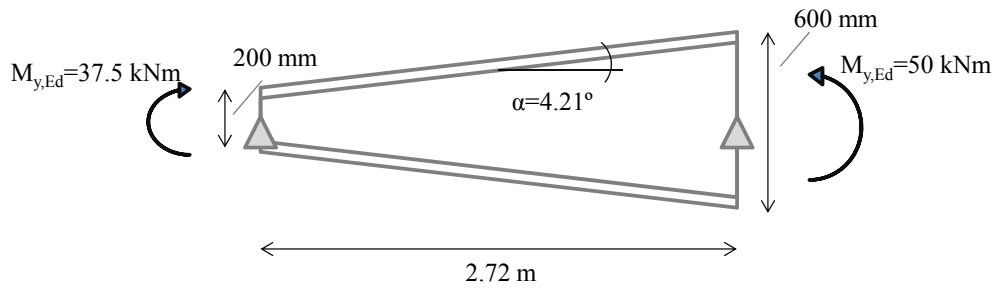
Figure 5.37: Analyzed tapered beam

A numerical linear eigenvalue analysis LBA attains a critical load multiplier of α_{cr}=2.022 ($M_{cr,Tap}$=101.1 kNm), whereas a GMNIA analysis attains an ultimate load multiplier of α_b=1.167 ($M_{b,Rd,Tap}$=58.4 kNm), see *Figure 5.38*.
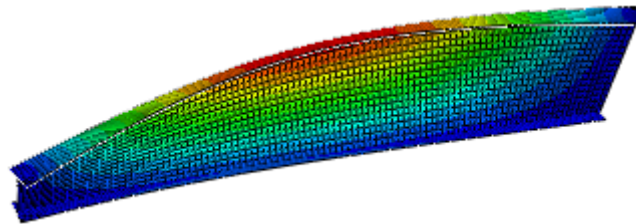
Figure 5.38: Lateral-torsional buckling mode displacement

The following cross section properties were considered in the numerical model (see the example of Chapter 4). Firstly, the taper angle considering simplified minimum and maximum reference depths is obtained:

- h_{min}=200 *mm*; h_{max}=3*200=600 *mm*; α=4.21º

Because the flange thickness is not exactly t_f, the depth of the web is kept and the total depth slightly increases.

- Smallest cross section h_w=183 *mm*; b=100 *mm*; t_f= 8.5 *mm*; t'_f= t_f/cosα= 8.523 *mm*; t_w=5.6 *mm*; h=200.046 *mm*

- Largest cross section h_w=583 *mm*; b=100 *mm*; t'_f=8.523 *mm*; t_w=5.6 *mm*; h=600.046 *mm*;

This leads into a correct taper ratio of γ_h=h_{max}/h_{min}= 600.046 / 200.046=3.0 ($\approx$2.9995).

5.5.2 Determination of the first order resistance

The utilization at each section is illustrated in *Figure 5.36* and shall be obtained at, at least 10 cross sections, considering the following expression

$$\varepsilon_M(x) = \frac{M_{y,Ed}(x)}{M_{3,y,Rd}(x)} \tag{5.65}$$
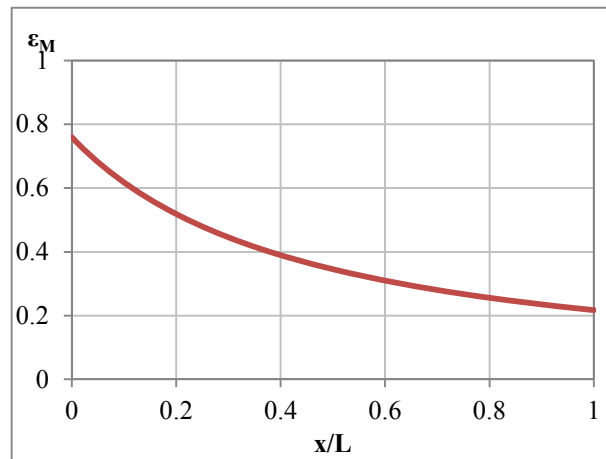
Figure 5.39: First order utilization

It is seen that the first order failure location x_c^I is at the smallest cross section. The utilization ratio at this section is given by

$$\varepsilon_M(x_c^I) = \frac{M_{y,Ed}(x_c^I)}{W_{pl,y}(x_c^I)f_y} = \frac{37.5}{49.38} = 0.759 \tag{5.66}$$

as illustrated in *Figure 5.36*. Note that, for the analysed case, the cross section class is always 1 or 2. For example, for the higher cross section, the cross section class is given by

$$\frac{c}{t} = \frac{600.046 - 8.523 - 8.523}{5.6} = \frac{583}{5.6} = 104.1 \leq 124 \qquad (5.67)$$

Because c/t=104.1≤124 (Table 5.2 of EC3-1-1) the highest cross section class is 2.

In addition, the cross sections should be verified against the presence of shear. This should also be carried out along the member length. However, because the maximum effect of shear will occur at the smallest cross section which also coincides with the first order failure cross section due to bending, it is enough to verify this cross section. Shear is verified according to clause 6.2.6 of EC3-1-1 (see also Chapter 2).

$$\begin{cases} V_{Ed} = \dfrac{(50 - 37.5)\ kNm}{2.72\ m} = 4.6\ kN \\[3mm] V_{pl,Rd} = \dfrac{h_w t_w f_y / \sqrt{3}}{\gamma_{M0}} = \dfrac{0.583 \cdot 0.0056 \cdot 135677}{1} = 139.04\ kN \end{cases} \qquad (5.68)$$

Because $V_{Ed} \leq 50\%\ V_{pl,Rd}$, interaction of bending and shear does not need to be accounted for (clause 6.2.8 of EC3-1-1).

Shear is then verified. Nevertheless, note that, according to clause 6.2.6(6), when h_w/t_w>72 shear buckling resistance for webs without intermediate stiffeners should be verified according to section 5 of EN 1993-1-5. This would be the case of this example, in which h_w/t_w=104.1 for the maximum height. Because the web is restrained to local buckling in the numerical models, this does not occur. In real situations this aspect shall however be taken into consideration.

5.5.3 Stability verification according to the proposed method

The procedure is summarized in Section 5.4.5.5.

a) Calculation of slenderness at $x=x_c^I$ (smallest cross-section)

- First order resistance multiplier: $\alpha_{ult,k}(x_c^I) = 1/\overline{\lambda}(x_c^I) = 1/\varepsilon(x_c^I) = 1/0.759 = 1.317$

- $\overline{\lambda}(x_c^I) = \sqrt{\dfrac{\alpha_{ult,k}(x_c^I)}{\alpha_{cr}}} = \sqrt{\dfrac{1.317}{2.022}} = 0.807$

b) Determination of auxiliary terms

- Second order failure location, $x=x_{c,lim}{}^{II}$, Eq. (5.69)

$$\gamma_w = \frac{W_{y,el,\max}}{W_{y,el,\min}} = \frac{8.052 \cdot 10^{-7}\, m^3}{1.850 \cdot 10^{-7}\, m^3} = 4.353$$

$$x_{c,\lim}^{II} / L = \left(0.75 - 0.18\psi - 0.07\psi^2\right) + \left(0.025\psi^2 - 0.006\psi - 0.06\right)\left(\gamma_h - 1\right) = 0.475 \geq 0$$

- Over-strength factor, φ, Eq. (5.61)

$$\gamma_w = \frac{W_{y,el,\max}}{W_{y,el,\min}} = \frac{8.052 \cdot 10^{-7}\, m^3}{1.850 \cdot 10^{-7}\, m^3} = 4.353$$

$$a_\gamma = -0.0005 \cdot \left(\gamma_w - 1\right)^4 + 0.009 \cdot \left(\gamma_w - 1\right)^3 - 0.077 \cdot \left(\gamma_w - 1\right)^2 + 0.78 \cdot \left(\gamma_w - 1\right) = 2.026$$

$$|\psi_{\lim}| = \frac{1 + 120 \cdot a_\gamma + 600 \cdot a_\gamma^2 - 210 \cdot a_\gamma^3}{1 + 123 \cdot a_\gamma + 1140 \cdot a_\gamma^2 + 330 \cdot a_\gamma^3} = 0.125$$

$$\psi > \psi_{\lim} \rightarrow \begin{cases} A = 0.008\, a_\gamma^2 - 0.08 a_\gamma - 0.157 = -0.286 \\ B = -0.033\, a_\gamma^3 + 0.04 a_\gamma^2 + 0.48 a_\gamma + 0.37 = 1.232 \\ C = 0.032\, a_\gamma^3 - 0.092\, a_\gamma^2 + 0.06 a_\gamma + 0.8 = 0.810 \end{cases}$$

$$\varphi = A \cdot \psi^2 + B \cdot \psi + C = 1.573 \geq 1$$

c) Generalized imperfection

- Imperfection factor, α_{LT}

$$\alpha_{LT} = 0.21 \sqrt{\frac{W_{y,el}(x_{c,\lim}^{II})}{W_{z,el}(x_{c,\lim}^{II})}} = 0.21 \sqrt{\frac{4.421 \cdot 10^{-4}\, m^3}{2.842 \cdot 10^{-5}\, m^3}} = 0.828 > 0.64 \rightarrow \alpha_{LT} = 0.64$$

- Slenderness, $\overline{\lambda}_z(x_{c,\lim}^{II})$

$$\overline{\lambda}_z(x_{c,\lim}^{II}) = \sqrt{N_{Rk}(x_{c,\lim}^{II}) \Big/ \frac{\pi^2 EI_z(x_{c,\lim}^{II})}{L^2}} = \sqrt{\big((3.79 \cdot 10^{-3}\, m^2) \times f_y\big) \Big/ \frac{\pi^2 E \times (1.421 \cdot 10^{-6}\, m^4)}{2.72^2}}$$

$$\overline{\lambda}_z(x_{c,\lim}^{II}) = 1.50$$

Generalized imperfection, η

$$\eta = \alpha_{LT}\left(\overline{\lambda}_z(x_{c,\lim}^{II}) - 0.2\right) = 0.829 \leq \sqrt{\frac{W_{y,el}(x_{c,\lim}^{II})}{W_{z,el}(x_{c,\lim}^{II})}}(0.12\psi^2 - 0.23\psi + 0.35) = 0.966$$

$$\eta = 0.829$$

c) Verification

- Reduction factor

$$\phi_{LT} = 0.5 \times \left(1 + \varphi \times \eta \times \frac{\overline{\lambda}^2_{LT}(x_c^I)}{\overline{\lambda}^2_z(x_{c,\lim}^{II})} + \varphi \times \overline{\lambda}^2_{LT}(x_c^I)\right) = 1.202$$

$$\chi_{LT}(x_c^I) = \frac{\varphi}{\phi_{LT} + \sqrt{\phi_{LT}^2 - \varphi \times \overline{\lambda}_{LT}^2(x_c^I)}} = 0.850 \leq 1$$

- Verification

$$\chi_{LT}(x_c^I) \times \alpha_{ult,k}(x_c^I) = \alpha_b = 0.850 \times 1.317 = 1.12 \geq 1$$

$$(M_{b,Rd} = M_{y,Ed} \times \alpha_b = 50 \times 1.12 = 55.98\ kNm)$$

→The beam is verified!

d) Summary

The beam attains a maximum load factor of α_b=1.12. When compared to the GMNIA resistance (α_b=1.167), a difference of 4.0% on the safe side is achieved.

5.6 Final remarks

In this chapter, an analytical derivation of linearly web-tapered beams subject to uniform bending moment was carried out and compared against numerical simulations. Differences up to 4% were noticed relatively to numerical results. The model was then shown to be adequate for non-uniform bending moment distributions.

In a second step, a design model was developed in line with recent proposals for prismatic beams. The calibration of the second order failure location x_c^{II} and of an "over-strength" factor φ was carried out in order to be considered in the Ayrton-Perry equation. From the statistical evaluation it was seen that the model gives differences up to 10% whereas the application of, for example, the buckling curve c of EC3-1-1 may lead to differences of 40% on the safe side. On the other hand, the application of the same buckling curve c considering the Special Case procedure of clause 6.3.2.3 can lead to results that are 25% unsafe.

In addition, a cut-off in the generalized imperfection of welded cross-sections was calibrated in order to improve the adequacy of the design method to the behavior of the member along the slenderness range.

It was also seen that some variations to the proposed method may be further performed: (i) either the $x_{c,lim}^{II}$ could be replaced by x_c^{I} so that only φ needs to be determined; or (ii) φ could be replaced by $x_{c,lim}^{II}$ avoiding the calculation of φ. Although some disadvantages were shown for each of these alternatives, more simple procedures would be obtained.

Finally, it was shown that the presence of shear buckling may have an influence in the resistance obtained by the proposed method, such that additional checks should be performed. This will be considered in a next step of the research. The same applies to local buckling due to bending as already stated in Chapter 4.

Chapter 6

6 ON THE VERIFICATION OF TAPERED MEMBERS AND FRAMES UNDER AXIAL COMPRESSION AND UNIAXIAL BENDING

6.1 Introduction

In EC3-1-1, the safety verification of a tapered beam-column may be performed either by the General Method; by a second order analysis considering all relevant imperfections followed by a cross section check or by a numerical analysis taking account of all relevant nonlinear geometrical and material effects. These alternatives were discussed in the previous chapters and some aspects may be highlighted again here:

- The verification of a member by a full nonlinear analysis is, for the time being, not the preferred alternative. On the other hand, the consideration of in-plane (local and global) imperfections for the determination of the in-plane load multiplier $\alpha_{ult,k}$ of the General Method, may result in a need to perform those complex numerical analyses as there are yet no analytical stability verification procedures for non-uniform members. Similarly, the determination of the imperfections to consider in a second order analysis to be followed by a cross section check is also unclear;

- The General Method requires the in-plane resistance of the member considering second order in-plane effects and imperfections. Besides the discussion in Section 2.4.2.5 regarding the definition of $\alpha_{ult,k}$, it was proved that, for the case of columns (even prismatic), considering the in-plane imperfection does not lead to the out-of-plane ultimate resistance, resulting in a loss of resistance up to 20%. As a result, for the stability verification of a beam-column it is decided here to consider the most general approach in which $\alpha_{ult,k}$ is given purely by the cross-sectional resistance. In-plane effects are accounted for separately;

- For prismatic members, it was seen that the consideration of the minimum between the lateral-torsional reduction factor and the out-of-plane reduction factor results in a discontinuity in the *M-N* interaction curve, for high bending moment relatively to axial force or vice versa, depending on the mode of "minimum" reduction factor. As a result, an interpolation between the lateral-torsional and the out-of-plane modes is mechanically more consistent, although an adequate interpolation needs to be developed. The same applies to non-prismatic members;

- The consideration of the existing buckling curves a_0 to d to tapered beams or columns is not only incorrect as it may lead to a spread in the safety level of -40% on the safe side to 30% on the unsafe side. If a generalized slenderness approach is to be considered, the developed buckling curves for tapered columns (Chapter 4) and tapered beams (Chapter 5) should be applied.

As a result, in Chapter 6, the several possibilities for the stability verification of tapered beam-columns are brought into discussion. Firstly, possible member stability procedures (both in-plane and out-of-plane) are presented based on a direct adaptation of EC3-1-1 rules: both the interaction formulae format and a generalized slenderness approach format are considered, although focus is given on the latter as in reality, the interaction formulae was not intended for verification of non-uniform members. Still regarding the generalized slenderness approach, possible interpolation procedures are analyzed. The General Method of clause 6.3.4 is again shown to lead to inconsistent and unreliable resistance levels, in what concerns member design. Finally, in the context of the global structure, some of the methods of analysis presented in Section 2.5 are analyzed so that in-plane stability may or may not be checked by adequate verification formulae. Framed structures are considered for this discussion.

Only global instability failure modes are analyzed here, i.e., the cross section plastic capacity may be fully attained and accordingly, the numerical models do not develop local buckling deformations. In addition, only the "over-strength" factor approaches developed in Chapters 4 and 5 are considered for the following analysis, although similar procedures could be considered with the "critical location" proposals.

Some general aspects are now mentioned regarding some limitations of the General Method but that may be overcome:

- The determination of $\alpha_{ult,k}$ must be reevaluated as already discussed;

- At the moment, the General Method does not account for out-of-plane loading, which when compared to the interaction formulae is a negative aspect. If such a procedure is judged to be better (i.e. than the interaction format), it may be further developed to include out-of-plane loading;

- Although the General Method is focused here only for the stability verification of out-of-plane buckling, it is not necessarily limited to it (if correctly adapted). Studies on the generalized slenderness concept have been carried out concerning in-plane buckling of prismatic members (Greiner and Ofner, 2005; Ofner and Greiner, 2005) and, in fact, a proposal for the in-plane stability verification of prismatic beam-columns was developed leading in many times to more accurate results than the interaction formulae itself (Taras, 2010).

6.2 Member stability verification – possible adaptations of EC3-1-1 rules

6.2.1 Interaction formulae

The interaction formulae of clause 6.3.3 for the stability verification of <u>prismatic</u> beam-columns are presented in Eq. (2.42) and Eq. (2.43) of this thesis. For uniaxial bending and class 1, 2 or 3 cross section they are given by

$$\frac{N_{Ed}}{\chi_y \, N_{Rk}/\gamma_{M1}} + k_{yy} \frac{M_{y,Ed}}{\chi_{LT} \, M_{y,Rk}/\gamma_{M1}} \le 1.0 \tag{6.1}$$

$$\frac{N_{Ed}}{\chi_z \, N_{Rk}/\gamma_{M1}} + k_{zy} \frac{M_{y,Ed}}{\chi_{LT} \, M_{y,Rk}/\gamma_{M1}} \le 1.0 \tag{6.2}$$

in which N_{Ed} and $M_{y,Ed}$ are the design values of the compression force and the maximum moment about the yy axis along the member. The interaction factors k_{yy} and k_{zy} may be determined either by Annex A (Method 1) or Annex B (Method 2) of the same code. Finally, besides the verification of Eq. (6.1) and Eq. (6.2), an additional cross section check is required at the extremes of the member.

The adaptation of the interaction formulae to the verification of tapered member naturally leads to some questions as there is not an analytical background specifically developed for the tapered beam-column case as it was performed for prismatic members. Nevertheless, an adjustment can be fairly easily analyzed especially when considering Method 2.

In a tapered beam-column the following verifications shall be performed:

- Out-of-plane stability verification;
- In-plane stability verification;
- Cross section verification at the most heavily loaded cross section, i.e., with the highest first order utilization.

In the following, possible alternatives for each of these verifications are discussed and results are analyzed further in Section 6.3.2.1.

6.2.1.1 Cross section verification

The first order failure location of tapered beam-columns varies with varying levels of axial force relatively to the applied bending moment leading. Putting aside the fact that cross section class may vary with varying height of the beam-column, consider the example of *Figure 6.1* which illustrates results of a member composed of a (hot-rolled) *IPE200* cross section with a taper ratio of γ_h=2.5 and subject to uniformly distributed loading and constant axial force. The beam attains a maximum utilization at about 35% of the member length ($x_{c,M}^I/L$). With increasing axial force the maximum utilization location, $x_{c,MN}^I$, moves towards the smallest cross section, which is the first order failure location of the column, $x_{c,N}^I$, as the axial force is constant.

For illustration, $M_{y,Ed}$ corresponds to the maximum applied bending moment along the member, irrespective of the utilization – for the example of *Figure 6.1* (uniformly distributed loading) the pairs (N_{Ed}; $M_{y,Ed}(L/2)$) are considered. If, for example, the utilization at $x_{c,MN}^I$ is considered for representation at each point of the curve, no direct information regarding the load that actually leads to first order failure can be obtained, as each point corresponds to a different cross section location. Therefore, the first option is preferred and adopted along the examples of Chapter 6.

(a) Interaction cross section resistance curve and analyzed cases

(b) First order (plastic) utilization
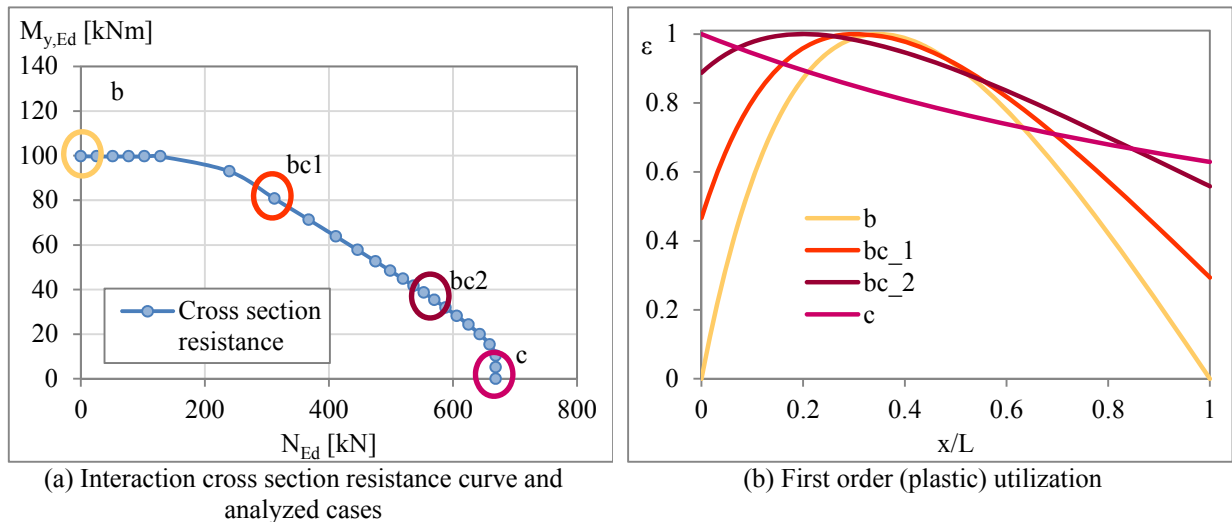
Figure 6.1 First order failure location with varying axial force relatively to the bending moment

As a result, and also as referred in Chapter 5, cross section verification should be performed in a sufficient number of locations in order to find the cross section with the highest first order utilization. For example, for a class 1 or 2 I-section at an arbitrary location of the beam-column subject both to major axis bending and axial force, the utilization ratio may be determined from (see also Eq. (2.44))

$$\varepsilon(x) = \frac{N_{Ed}(x)}{N_{pl,Rd}(x)} + (1 - 0.5a)\frac{M_{y,Ed}(x)}{M_{pl,y,Rd}(x)} \le 1.0 \qquad (6.3a)$$

Also, if $N_{Ed} \leq 0.25 N_{pl,Rd}$ and $N_{Ed} \leq 0.5 h_w t_w f_y / \gamma_{M0}$, the axial force does not need to be taken into account and the utilization is given by

$$\varepsilon(x) = \frac{M_{y,Ed}(x)}{M_{pl,y,Rd}(x)} \leq 1.0 \tag{6.3b}$$

Another interesting aspect that can be observed from *Figure 6.1* and that may lead to some questions is the vertical plateau around the high axial force zone. This can be explained because, for high axial force relatively to bending moment, the first order failure location of the beam-column approaches the first order location of the column (smallest cross-section) $x_{c,MN}^I \rightarrow x_{c,N}^I$. For the particular cases of bending moment distributions in which there is no applied bending moment at the smallest cross section, for high axial force, the utilization of the axial force at the smallest cross section is higher than the utilization of the combined loading at the immediate adjacent cross sections. Note that this only happens because the member is tapered. As a result, the failure location is the smallest cross section in which only axial force is present, leading to the vertical plateau of *Figure 6.1*.

Finally, a comparison between the first order resistance obtained by Eq. (6.3) and by performing a plastic distribution of stresses (analytical approach) is illustrated in *Figure 6.2*, for the same example of *Figure 6.1*, showing that results are very similar. For the analyses to be carried out throughout Chapter 6, Eq. (6.3) is considered.
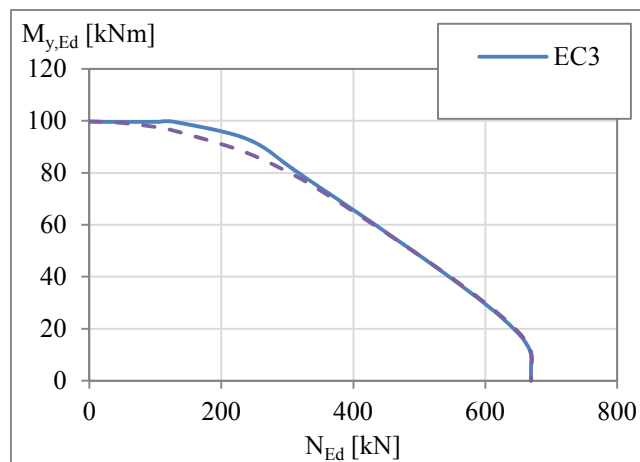

Figure 6.2 Comparison between EC3-1-1 cross section resistance and analytical plastic resistance regarding combined bending and axial force

6.2.1.2 Possible adaptation of the interaction formulae to tapered members

Eq. (6.1) and Eq. (6.2) shall now be adapted to the case of tapered beam-columns:

$$\frac{N_{Ed}(x_?^I)}{\chi_y(x_?^I)\,N_{Rk}(x_?^I)\big/\gamma_{M1}} + k_{yy}\,\frac{M_{y,Ed}(x_?^I)}{\chi_{LT}(x_?^I)M_{y,Rk}(x_?^I)\big/\gamma_{M1}} \leq 1.0 \tag{6.4}$$

$$\frac{N_{Ed}(x_?^I)}{\chi_z(x_?^I)\,N_{Rk}(x_?^I)\big/\gamma_{M1}} + k_{zy}\,\frac{M_{y,Ed}(x_?^I)}{\chi_{LT}(x_?^I)M_{y,Rk}(x_?^I)\big/\gamma_{M1}} \leq 1.0 \tag{6.5}$$

The first question that arises is related the correct location to take into consideration in the given interaction formulae. The expression in EC3-1-1

   "N_{Ed}, $M_{y,Ed}$ *are the design values of the compression force and the maximum bending moments about the yy (...) axis along the member*",

shall be replaced by

   "N_{Ed}/N_{Rk}, $M_{y,Ed}/M_{y,Rk}$ *are the design values of the maximum first order utilization due to the compression force and due to the maximum bending moments about the yy (...) axis along the member*".

For the case of prismatic beam-columns this location is always the location of maximum bending moment utilization as the axial force is constant; however, for tapered beam-columns, it may not be the case. However, according to the definitions of Chapter 4 and 5, $F_{Ed}/(\chi F_{Rk})=1/(\chi \alpha_{ult,k,F})$ is a constant value along the member length (F represents either the axial force or the bending moment). As a result, it is irrelevant which location is chosen and is here recommended (for simplicity reasons) the consideration of the first order failure location of the axial force acting alone ($x_{c,N}^I$) for the utilization term regarding axial force; and the first order failure location of the bending moment acting alone ($x_{c,M}^I$) for the utilization term regarding the bending moment. This leads to

$$\frac{N_{Ed}(x_{c,N}^{I})}{\chi_y(x_{c,N}^{I})\,N_{Rk}(x_{c,N}^{I})\big/\gamma_{M1}} + k_{yy}\,\frac{M_{y,Ed}(x_{c,M}^{I})}{\chi_{LT}(x_{c,M}^{I})M_{y,Rk}(x_{c,M}^{I})\big/\gamma_{M1}} \le 1.0 \qquad (6.6)$$

$$\frac{N_{Ed}(x_{c,N}^{I})}{\chi_z(x_{c,N}^{I})\,N_{Rk}(x_{c,N}^{I})\big/\gamma_{M1}} + k_{zy}\,\frac{M_{y,Ed}(x_{c,M}^{I})}{\chi_{LT}(x_{c,M}^{I})M_{y,Rk}(x_{c,M}^{I})\big/\gamma_{M1}} \le 1.0 \qquad (6.7)$$

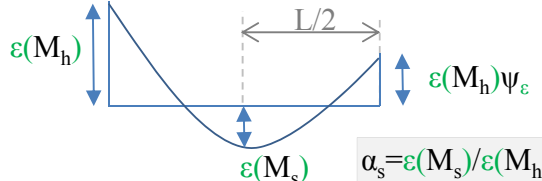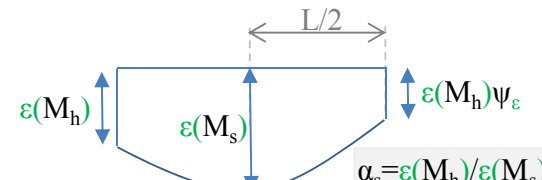### 6.2.1.3 Interaction factors k_{yy} and k_{zy}

The interaction factors given in Annex A (Method 1) and Annex B (Method 2) of EC3-1-1 are directly adapted to the tapered beam-column case in the following. Method 1 is composed of two sets of formula in which the transition between the consideration of torsional deformations or not is implicit. In addition, a more complex transition between cross-section resistance failure (for the low slenderness range) and instability failure is also accounted for. However, this method contains too many parameters in a sense that it is not flexible for an adaptation for tapered beam-columns. A possible application of the method to non-uniform members would bring many questions and probably would not lead to a satisfactory result as, from the beginning, this method was specifically developed for prismatic members. A more detailed analysis and even calibration of new interaction factors would therefore be required to attain satisfactory results. It is not the purpose of this study and, as a result, only Method 2 is considered for a straightforward application/adaptation of the interaction formulae to the case of tapered beam-columns. Because I-sections are susceptible to torsional deformations, according to Method 2, the interaction factors to be considered are summarized in *Table 6.1*. The terms $N_{Ed}/(\chi N_{Rk})$ are the same as considered in the interaction equation. Regarding the relative slenderness, for the slenderness $\overline{\lambda}_y$ or $\overline{\lambda}_z$, the question again arises on which location is to be considered: (i) at $x_{c,N}{}^{I}$; or (ii) at $x_{c,N,i}{}^{II}$, i.e. $\overline{\lambda}_i(x_{c,N,i}^{II}) = \sqrt{\varphi_i}\,\overline{\lambda}(x_{c,N}^{I})$. One could think that the location should be the same as the one considered for $N_{Ed}/(\chi N_{Rk})$ (alternative (i)); however, because that slenderness is related to a "plateau" level, alternative (ii) is probably more suitable. A sensitive analysis concerning the parametric study to be analyzed further in Chapter 6 showed that this aspect hardly influences the value of the interaction factor and, as a result, no deeper study is given to this subject.

Table 6.1 Possible interaction factors for web-tapered beam-columns according to Method 2

k_{yy}	
	$C_{my} \times \left(1 + \underbrace{\left(\overline{\lambda}_y(x^?_{c,N}) - 0.2 \right)}_{\leq 0.8 \geq 0} \dfrac{N_{Ed}(x^I_{c,N})}{\chi_y(x^I_{c,N}) N_{Rk}(x^I_{c,N})/\gamma_{M1}} \right)$
k_{zy}	$1 - \dfrac{\overbrace{0.1\overline{\lambda}_z(x^?_{c,N})}^{\leq 0.1}}{C_{m,LT} - 0.25} \dfrac{N_{Ed}(x^1_{c,N})}{\chi_z(x^1_{c,N}) N_{Rk}(x^1_{c,N})/\gamma_{M1}}$
	$\text{for } \overline{\lambda}_z(x?) < 0.4:$
	$0.6 + \overline{\lambda}_z(x?) \leq 1 - \dfrac{0.1\overline{\lambda}_z(x^?_{c,N})}{C_{m,LT} - 0.25} \dfrac{N_{Ed}(x^1_{c,N})}{\chi_z(x^1_{c,N}) N_{Rk}(x^1_{c,N})/\gamma_{M1}}$

Finally, regarding the equivalent uniform moment factors $C_{m,y}$ and $C_{m,LT}$, Table B.3 of EC3-1-1 can be adopted provided that the diagram to be considered is the <u>bending moment first order utilization diagram</u> instead of the bending moment diagram itself, see *Table 6.2*.

Table 6.2 Adaptation of the equivalent uniform moment factors C_m for prismatic members

Moment **utilization** diagram	Range		C_{my} and C_{mLT}
	$0 \leq \alpha_s \leq 1$	$-1 \leq \psi_\varepsilon \leq 1$	$0.2 + 0.8\,\alpha_s \geq 0.4$
	$-1 \leq \alpha_s < 0$	$0 \leq \psi_\varepsilon \leq 1$	$0.1 - 0.8\,\alpha_s \geq 0.4$
		$-1 \leq \psi_\varepsilon < 0$	$0.1(1-\psi_\varepsilon) - 0.8\,\alpha_s \geq 0.4$
	$0 \leq \alpha_s \leq 1$	$-1 \leq \psi_\varepsilon \leq 1$	$0.95 + 0.05\,\alpha_h$
	$-1 \leq \alpha_s < 0$	$0 \leq \psi_\varepsilon \leq 1$	$0.95 + 0.05\,\alpha_h$
		$-1 \leq \psi_\varepsilon < 0$	$0.95 + 0.05\,\alpha_h(1+2\,\psi_\varepsilon)$

In a tapered beam subject to a linear bending moment distribution, the diagram of the utilization can be fairly well compared to the diagram of a prismatic beam subject both to

uniformly distributed loading and end moments. The C_m factor may be obtained from the respective C_m factor due to that diagram. For the case of a tapered beam-column subject to uniformly distributed loading the error would be higher. *Figure 6.3* illustrates these two examples.
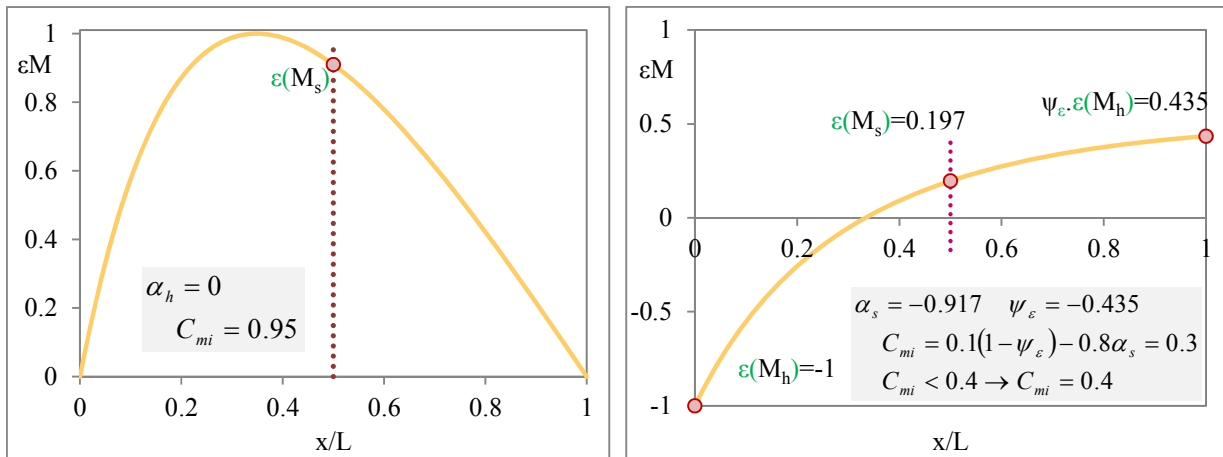
(a) IPE200 (rolled) | γ_h=2.5 | UDL
(b) IPE200 (rolled) | γ_h=3 | ψ=-0.5
Figure 6.3 Determination of C_m factors for tapered beam-columns (plastic utilization ε)

6.2.2 Generalized slenderness approaches for out-of-plane stability verification

6.2.2.1 The general method in its current format

For application of the general method of clause 6.3.4 of EC3-1-1, the following steps are taken (see Section 2.4):

a) Determination of the generalized slenderness given by $\overline{\lambda}_{op} = \sqrt{\alpha_{ult,k}/\alpha_{cr}}$:

   o α_{cr} may be obtained numerically;

   o $\alpha_{ult,k}$ may be obtained numerically and should account for the in-plane imperfections;

b) Calculation of the generalized reduction factor, χop:

o Minimum between the reduction factor χ_z and χ_{LT}, both calculated with $\overline{\lambda}_{op}$. For web-tapered beam-columns and taking into account the assumptions for the residual stress pattern of the hot-rolled cases ($0.5f_y$), the buckling curves to consider are:

	For χ_z	For χ_{LT} (general case)
Rolled I-section	c	$h/b \leq 2 \rightarrow$ a $h/b > 2 \rightarrow$ b
Welded I-section	c	$h/b \leq 2 \rightarrow$ c $h/b > 2 \rightarrow$ d

o As no clear guidelines are given for an interpolation between χ_z and χ_{LT} in the code nor it is recommended by ECCS TC8 (2006), this alternative is not considered;

c) Verification: $\chi_{op}\alpha_{ult,k}/\gamma_{M1} \geq 1$.

6.2.2.2 Modification of the General Method – general aspects

It was seen that the consideration of in-plane local imperfections in the determination of $\alpha_{ult,k}$ could be mechanically inconsistent with the column buckling case. As a result the more general approach in which $\alpha_{ult,k}$ is obtained by the cross section resistance of the beam-column is also considered and treated in the following. It will, as expected, lead to higher levels of resistance.

Additionally, an in-plane verification shall be performed considering one of the alternatives of Section 6.2.1 regarding Eq. (6.4). The subscript "op" is here replaced by "ov", as referred in Chapter 2. In general, both alternatives will be referred to as a "generalized slenderness" concept.

a) Determination of the generalized slenderness given by $\overline{\lambda}_{ov} = \sqrt{\alpha_{ult,k}/\alpha_{cr}}$

• α_{cr} may be obtained numerically;

• $\alpha_{ult,k}$ is here given by the load multiplier that leads to the cross-section resistance of the first order failure location of the column, $x_{c,MN}{}^I$, see Eq. (6.3). To obtain $\alpha_{ult,k}$ the pair of loads $(N_{Ed}(x_{c,MN}{}^I), M_{y,Ed}(x_{c,MN}{}^I))$ shall be increased proportionally until the condition $\varepsilon=1$

of Eq. (6.3) is met. The cross section resistance multiplier is given by $\alpha_{ult,k}=M_{y,Ed,MAX}(x_{c,MN}{}^I)/M_{y,Ed}(x_{c,MN}{}^I)=N_{Ed,MAX}(x_{c,MN}{}^I)/N_{Ed}(x_{c,MN}{}^I)$. For the cases that Eq. (6.3b) applies, naturally the first condition is considered and $\alpha_{ult,k}=M_{y,Ed,MAX}(x_{c,MN}{}^I)/M_{y,Ed}(x_{c,MN}{}^I)$.

b) Calculation of the generalized reduction factor, χ_{ov}

Apart from the determination of $\alpha_{ult,k}$, the generalized reduction factor χ_{ov} shall be obtained from a generalized slenderness $\overline{\lambda}_{ov}$. With the variation of the ratio M/N, or ϕ (see Eq. (2.62)), the slenderness $\overline{\lambda}_{ov}$ varies between $\overline{\lambda}_{LT}$ for $\phi=0$ (beam) up to $\overline{\lambda}_z$ for $\phi=\infty$ (column), see the orange dots of *Figure 6.4*.
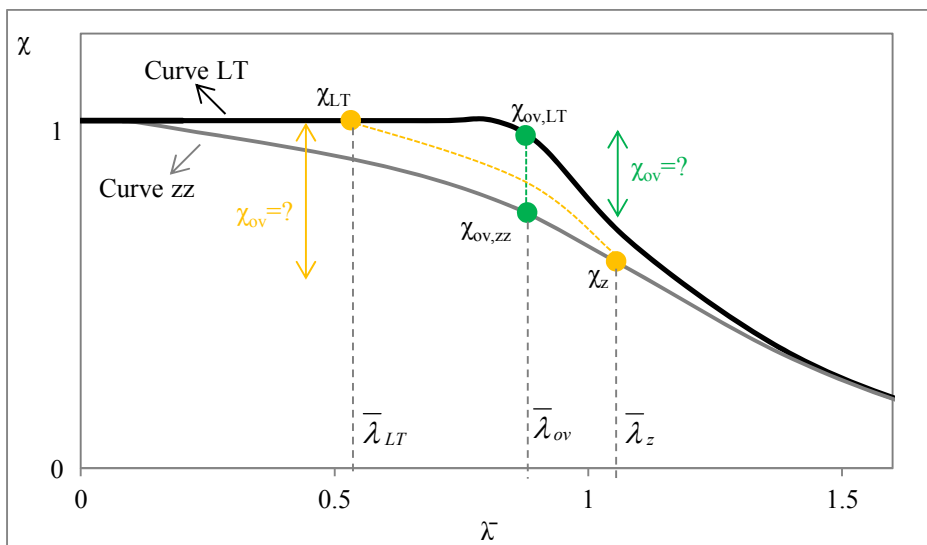
Figure 6.4 Determination of χ_{ov}

According to the general method in EC31-1, the reduction factor χ_{ov} shall be calculated with the generalized slenderness $\overline{\lambda}_{ov}$ considering the imperfection factors for lateral-torsional buckling or flexural buckling, respectively $\chi_{ov,LT}$ and $\chi_{ov,zz}$. This corresponds to the green dots of *Figure 6.4* (vertical line). Furthermore, if an interpolation between those reduction factors is to be carried out, $\chi_{ov,Interpol}$ is then found somewhere in the vertical green line. However, if this approach is analyzed, it can be right away observed that $\overline{\lambda}_{ov,zz} = \overline{\lambda}_{ov,LT} = \overline{\lambda}_{ov}$ correspond

to different member lengths. For example, if the generalized slenderness of the beam-column (with a given length) is considered to evaluate $\chi_{ov,zz}$, the generalized slenderness assumes the role of flexural buckling slenderness. A column with such slenderness does not present the same length as the analyzed beam-column, even for the case of prismatic members, as illustrated in the scheme of *Figure 6.5*. A similar conclusion would be achieved for the case of $\overline{\lambda}_{ov,LT} = \overline{\lambda}_{ov}$. It is clear that, irrespective of considering the "minimum" of χ_{ov} or the "interpolation" between $\chi_{ov,LT}$ and $\chi_{ov,zz}$, the resistance of the beam-column is based on the properties of members that have different lengths and, therefore, different member behaviours. This is even more evident for the case of tapered members that will exhibit different taper angles with the variation of the member length. As a result, a more consistent approach is to determine the value of χ_{ov} based on the actual $\overline{\lambda}_{LT}$ and $\overline{\lambda}_z$ respectively of the beam and column with the real member length of the beam-column. This corresponds to the orange line of *Figure 6.4*.
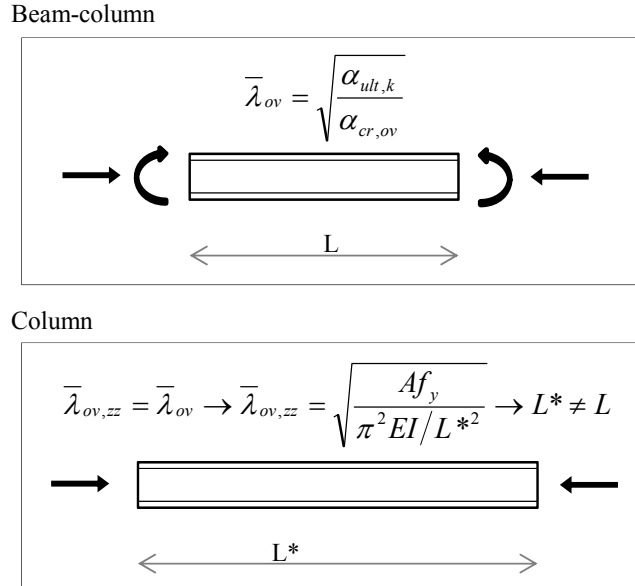

Figure 6.5 Column with a member length corresponding to $\overline{\lambda}_z = \overline{\lambda}_{ov}$

In order to distinguish from the 2 analyzed approaches, the approach in *Figure 6.4* corresponding to the green line is denoted as "$\overline{\lambda}_{ov}$ approach" whereas the corresponding to the

orange line is denoted as "$\overline{\lambda}_{real}$ approach". Still regarding the $\overline{\lambda}_{ov}$ approach, if the reduction factors $\chi_{ov,LT}$ and $\chi_{ov,zz}$ were to be obtained the following would have to be considered, see *Table 6.3*:

Table 6.3 Procedure for reduction factor determination according to a $\overline{\lambda}_{ov}$ approach

	For $\chi_{z,op}$ (see Chapter 4)	For χ_{LT} (see Chapter 5)
η	$\eta_z = \alpha_z \left(\sqrt{\varphi_z}\, \overline{\lambda}_{ov,zz} - 0.2 \right)$	$\eta_{LT} = \alpha_{LT} \left(\overline{\lambda}_z \left(x^{II}_{c,\lim,M} \right) - 0.2 \right)$
ϕ	$\phi_z = 0.5 \times \left(1 + \eta_z + \varphi_z \times \overline{\lambda}_{ov,zz}{}^2 \right)$	$\phi_{LT} = 0.5$ $\times \left(1 + \eta_{LT} \times \left(\dfrac{\sqrt{\varphi_{LT}} \times \overline{\lambda}_{ov,LT}}{\overline{\lambda}_z \left(x^{II}_{c,\lim,M} \right)} \right)^2 + \varphi_{LT} \times \overline{\lambda}_{ov,LT}{}^2 \right)$
χ	$\chi_{op,zz} = \dfrac{\varphi_z}{\phi_z + \sqrt{\phi_z{}^2 - \varphi_z \times \overline{\lambda}_{ov,zz}{}^2}} \leq 1$	$\chi_{LT} = \dfrac{\varphi_{LT}}{\phi_{LT} + \sqrt{\phi_{LT}{}^2 - \varphi_{LT} \times \overline{\lambda}_{ov,LT}{}^2}} \leq 1$

Table 6.3 highlights the $\overline{\lambda}_z$ parameter that must correspond to the slenderness $\overline{\lambda}_z$ of a beam with $\overline{\lambda}_{LT} = \overline{\lambda}_{ov,LT} = \overline{\lambda}_{ov}$, in order to coincide with the proposed buckling curves for tapered beams in Chapter 5. In other words, the length of a fictitious beam with a lateral-torsional slenderness with a value of $\overline{\lambda}_{ov}$ would have to be achieved – as it is known, obtaining a member length from the value of the lateral-torsional buckling slenderness is not simple, even for prismatic members and, should not be provided for a practical design procedure. As a result, a "$\overline{\lambda}_{real}$ approach" is preferred not only due to a higher mechanical background but also because it leads to a more simple procedure.

c) Verification: $\chi_{ov}\alpha_{ult,k}/\gamma_{M1} \geq 1$

6.2.2.3 Possible forms of interpolation

As already referred in Chapter 2, Greiner and Ofner (2005); Ofner and Greiner (2005); and Taras and Greiner (2006) present GMNIA results regarding prismatic members that, when plotted in a buckling curve representation, may fall below the lowest of the column flexural buckling or lateral-torsional buckling curves. One must then reflect if the "interpolation" term

is adequate as the χ_{ov} values corresponding to intermediate ϕ (beam-columns) are not always between the extreme cases of $\phi=0$ and $\phi=\infty$, i.e., beams and columns. Nevertheless, some possible approaches for an "interpolation" or "transition" between χ_{LT} and χ_z are presented in the following, based on the "$\overline{\lambda}_{real}$ approach":

1. Suggested interpolation in EC3-1-1 (clause 6.3.4 – general method) based on a linear cross section interaction – $\underline{GM\_cs}$ interpolation:

$$\frac{N_{Ed}(x_{c,N}^I)}{\chi_{op}N_{Rk}(x_{c,N}^I)} + \frac{M_{y,Ed}(x_{c,M}^I)}{\chi_{op}M_{y,Rk}(x_{c,M}^I)} = \frac{N_{Ed}(x_{c,N}^I)}{\chi_z(x_{c,N}^I)N_{Rk}(x_{c,N}^I)} + \frac{M_{y,Ed}(x_{c,M}^I)}{\chi_{LT}(x_{c,M}^I)M_{y,Rk}(x_{c,M}^I)}$$

(6.8)

$$\rightarrow \chi_{op} = ...$$

2. Interpolation based on the relative position of $\overline{\lambda}_{ov}$ to $\overline{\lambda}_z$ and $\overline{\lambda}_{LT}$ – $\underline{\lambda}$ interpolation (*Figure 6.6*). This alternative corresponds to a line in the buckling curve representation.
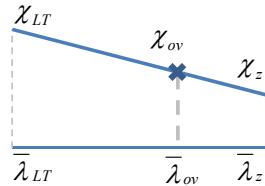

Figure 6.6 λ interpolation

3. Interpolation that would lead to exact application of the adjusted interaction formulae (equation 6.62 of EC3-1-1), as described in Sections 6.2.1.2 and 6.2.1.3 – $\underline{kzy}$ interpolation. Note that this case is only considered here in order to evaluate the χ_{ov} given by the interaction formula in the buckling curve representation. In addition, at a point, a slightly modification of χ_{LT} is analyzed such that it may lead to slightly different results than the ("original") interaction formula.

$$\frac{1}{\chi_{op}\alpha_{ult,k}} = \frac{N_{Ed}(x_{c,N}^I)}{\chi_z(x_{c,N}^I)N_{Rk}(x_{c,N}^I)} + k_{zy}\frac{M_{y,Ed}(x_{c,M}^I)}{\chi_{LT}(x_{c,M}^I)M_{y,Rk}(x_{c,M}^I)} \rightarrow \chi_{op} = ...$$

(6.9)

Results provided by these alternatives and possible variations are given and discussed in Section 6.3. It will be shown that a deeper study is needed in order to establish a procedure which correctly takes into account the weight between lateral and lateral-torsional buckling.

6.3 Out-of-plane buckling of tapered beam-columns

6.3.1 Parametric study

The parametric study concerning 273 beam-columns which will fail in out-of-plane buckling (with or without lateral-torsional buckling) is summarized in

Table 6.4. Results of the various methods described in 6.2 are given in Section 6.3.2. The cases were chosen such that:

- Torsional deformations may or may not occur;
- The first order failure location is not always at the smallest cross section with the varying ratio M/N;
- Buckling curves for the different fabrication procedures could be analyzed;
- Different slenderness for the same cases could be analyzed;
- In-plane buckling would not lead to failure but could lead instead to a decrease of the in-plane load multiplier $\alpha_{ult,k}$ if this is obtained according to the general method in EC3-1-1.

Table 6.4 Parametric study

	cs / fabrication	γ_h	Bending moment	$\bar{\lambda}_z (x_{h\,min})$	$x_{c,M}^I / L$	φ_{LT}	χ_{LT} $(x_{c,M}^I)$	χ_z $(x_{c,N}^I)$	χ_y $(x_{c,N}^I)$
1	IPE200 *hr*	2.5	UDL	1.2	0.35	1.07	0.624	0.466	1
2	IPE200 *hr*	3	Ψ =-0.5	2.5	0	1.74	0.772	0.136	1
3	IPE200 *hr*	3	Ψ =-0.5	1.2	0	1.74	1	0.474	1
4	IPE200 *hr*	1.2	Ψ =-0.25	2	1	1.25	0.782	0.197	0.918
5	HEB300 *hr*	2	Ψ =0.25	1	1	1.08	0.802	0.563	0.993
6	HEB300 *hr*	1.5	Ψ =0	1.5	1	1.19	0.874	0.318	0.813
7	HEB300 *hr*	1.5	Ψ =0	0.7	1	1.19	1	0.750	0.995
8	HEB300 *hr*	2	Ψ =1	1	0	1.4	1	0.563	0.993
9	IPE200 *w*	1.5	Ψ =-0.5	0.6	1	1.26	1	0.792	1
10	IPE200 *w*	1.2	Ψ =0	0.9	1	1.22	0.951	0.618	1
11	IPE200 *w*	1.5	Ψ =-0.5	1.2	1	1.26	0.910	0.498	1
12	IPE200 *w*	1.2	Ψ =0	1.7	1	1.22	0.690	0.299	0.922
13	IPE200 *w*	3	Ψ =-0.5	2	0	1.74	0.885	0.233	1
14	IPE200 *hr*	2.5	UDL	0.5	0.35	1.07	0.931	1	1

6.3.2 Results and discussion

6.3.2.1 Adaptation of the interaction formulae

Figure 6.7 compares the procedure presented in Section 6.2.1, regarding Eq. (6.7) with the numerical results. Differences of 10% and 14% on the safe side are achieved respectively for *Figure 6.7(a)* and *(b)*.
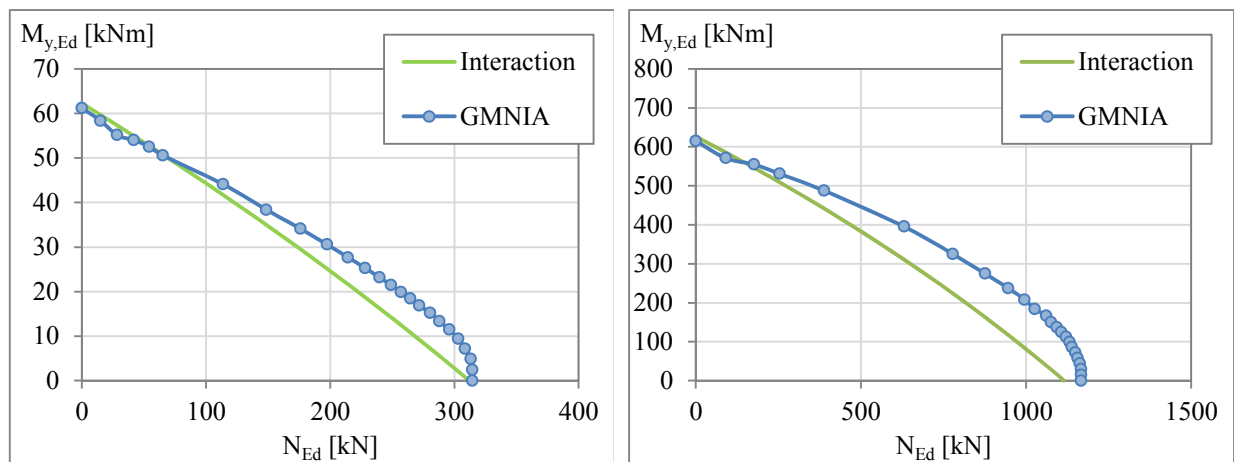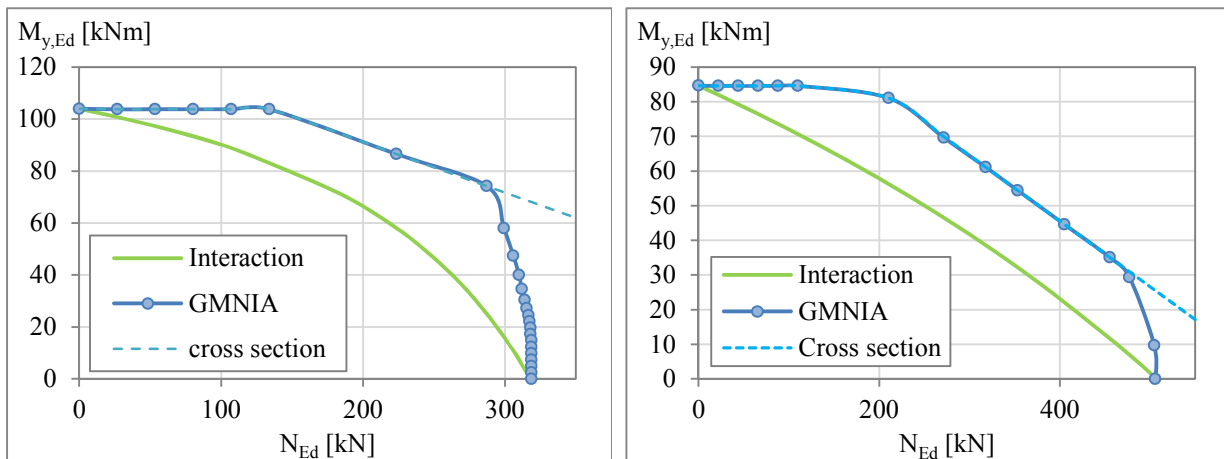

(a) #1 IPE200 *hr* | γ_h=2.5 | UDL | $\bar{\lambda}_z(x_{h\min})=1.2$ (b) #6 HEB300 *hr* | γ_h=1.5 | Ψ =0 | $\bar{\lambda}_z(x_{h\min})=1.5$

Figure 6.7 Interaction curve representation concerning interaction formulae results

Notice now the examples of *Figure 6.8* that correspond to a beam column such that $\chi_{LT}(x_{c,M}^I)$=1. Because web-tapered sections present higher ratios *h/b*, these present low torsional rigidity and fail mostly in flexural buckling. On the other hand, the examples of *Figure 6.8* are mainly beam-columns such that the reduction factor is χ_{LT}=1 and with very low slenderness, $\bar{\lambda}_{LT}$, sufficiently smaller than the plateau slenderness, see *Figure 6.9*. If, in addition the bending moment is much higher relatively to the axial force, flexural buckling is negligible relatively to the bending moment effect and, as a result, cross section capacity prevails. The interaction factor k_{zy} does not properly take advantage of this behavior for the case of tapered members which often present a higher slenderness plateau.

(a) #3 IPE200 hr | γ_h=3 | Ψ =-0.5 | $\bar{\lambda}_z(x_{h\,\text{min}})=1.2$ (b) #9 IPE200 w | γ_h=1.5 | Ψ =-0.5 | $\bar{\lambda}_z(x_{h\,\text{min}})=0.6$

Figure 6.8 Interaction curve representation concerning interaction formulae results
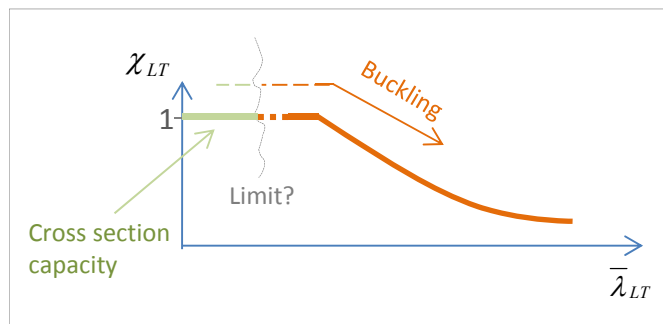

Figure 6.9 Instability in a tapered beam-column with a high lateral-torsional slenderness plateau

In general, the consideration of the analyzed adapted interaction approach for tapered beam-columns leads to a resistance level between 80% and 103% of the GMNIA resistance, with an average of 93% and a coefficient of variation of CoV=5.66%. In Figure 6.10, to have a common basis, the generalized reduction factors are compared: $\chi_{ov}^{GMNIA}=\alpha_b^{GMNIA}/\alpha_{ult,k}$ and $\chi_{ov}^{interaction}=\alpha_b^{interaction}/\alpha_{ult,k}$, in which α_b is the resistance multiplier obtained numerically or by the interaction approach and $\alpha_{ult,k}$ is the cross section resistance multiplier.

Finally, note that this study was only carried out to give an overview of an "interaction type" buckling check. Although adequate interaction factor k_{zy} accounting for specific buckling behavior of tapered members could improve results,further improvements of the interaction factors would possibly require too many differentiations in the end not leading to a practical approach.
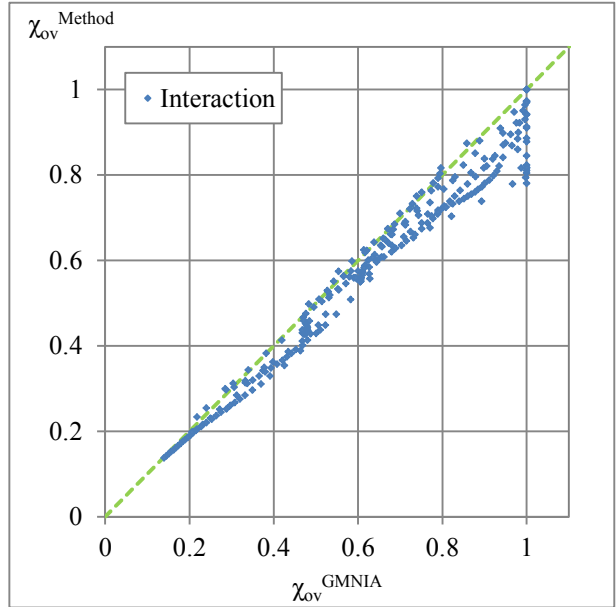
Figure 6.10 Results given by the interaction approach

6.3.2.2 General method

The consideration of the in-plane second order effects and imperfections for $\alpha_{ult,k}$ may lead to a decrease of the capacity of the member when applying the General Method. *Figure 6.11* illustrates the in-plane flexural buckling (numerical GMNIA in plane) and the cross section resistance regarding cases #5 and #6. For lower slenderness the GMNIA in plane curve moves towards the cross section resistance curve.
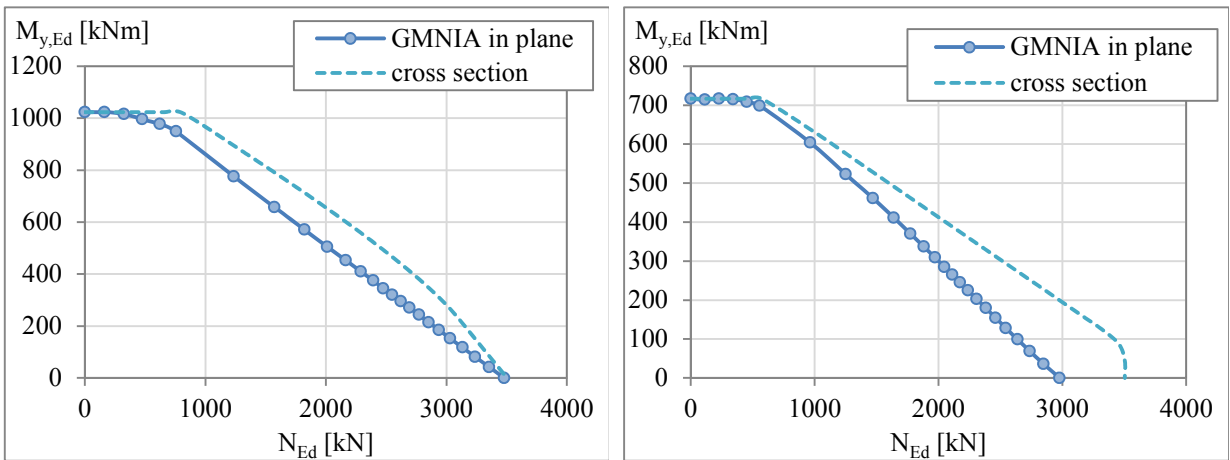
(a) #5 HEB300 *hr* | γ_h=2 | Ψ =0.25 | $\bar{\lambda}_z(x_{h\,min}) = 1$ (b) #6 HEB300 *hr* | γ_h=1.5 | Ψ =0 | $\bar{\lambda}_z(x_{h\,min}) = 1.5$

Figure 6.11 In-plane flexural buckling vs. cross section capacity

Figure 6.12 illustrates the same cases when the General Method is considered. Results are given regarding curves *a*, *b* and *c*. *GM num* and *GM CS* illustrate the cases in which $\alpha_{ult,k}$ is obtained from the GMNIA in plane analysi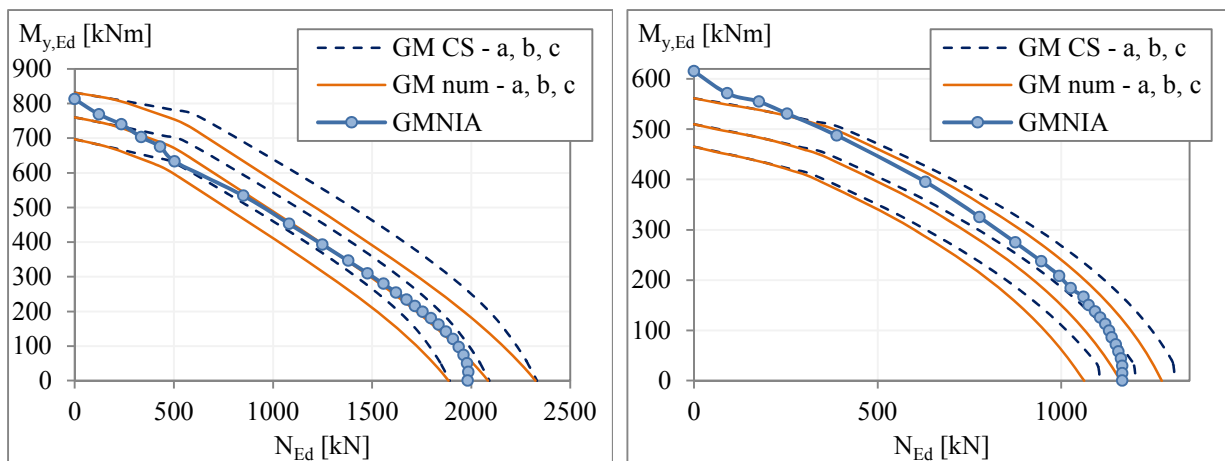s and from the cross section resistance, respectively. Differences between the two approaches for the given example can go up to 8%, such that for *Figure 6.12(a)*, the maximum differences are observed in the intermediate area of the interaction curve whereas for *Figure 6.12(a)* they are observed in the high axial force area.

(a) #5 HEB300 *hr* | γ_h=2 | Ψ =0.25 | $\bar{\lambda}_z (x_{h\,min}) = 1$ (b) #6 HEB300 *hr* | γ_h=1.5 | Ψ =0 | $\bar{\lambda}_z (x_{h\,min}) = 1.5$

Figure 6.12 Results of the general method considering different assumptions for $\alpha_{ult,k}$

Focusing now on the level of safety given by the general method, from *Figure 6.12* it can also be seen that the safety provided by the method may be either too conservative (up to 25%) or too unconservative (up to 20%). This is because there is not a clear decision on which curve to adopt. The examples of *Figure 6.13* show that this assumption may lead to an over-conservative resistance level: up to 30% for *Figure 6.13(a)* (case #12) and up to 45% for *Figure 6.13(b)* (case #13). Resistance given by the analyzed interaction formula is also presented for comparison leading to maximum (safe sided) differences of 12% and 10% for case #12 and #13, respectively.

Regarding welded cross sections, the curves to consider are either *c* (for flexural buckling); or *c* or *d* for lateral-torsional buckling. The analyzed sections are *IPE200* (smallest cross section)

with increasing height along the member, i.e., only in one extreme of the member curve *c* would apply for lateral-torsional buckling. Nevertheless, the argument that for the case #13 the first order failure location is $x_{c,M}^{I}=0$, could be used in order to justify the use of curve *c* (this argument has no analytical background). Results given by curve *c* are therefore also presented.

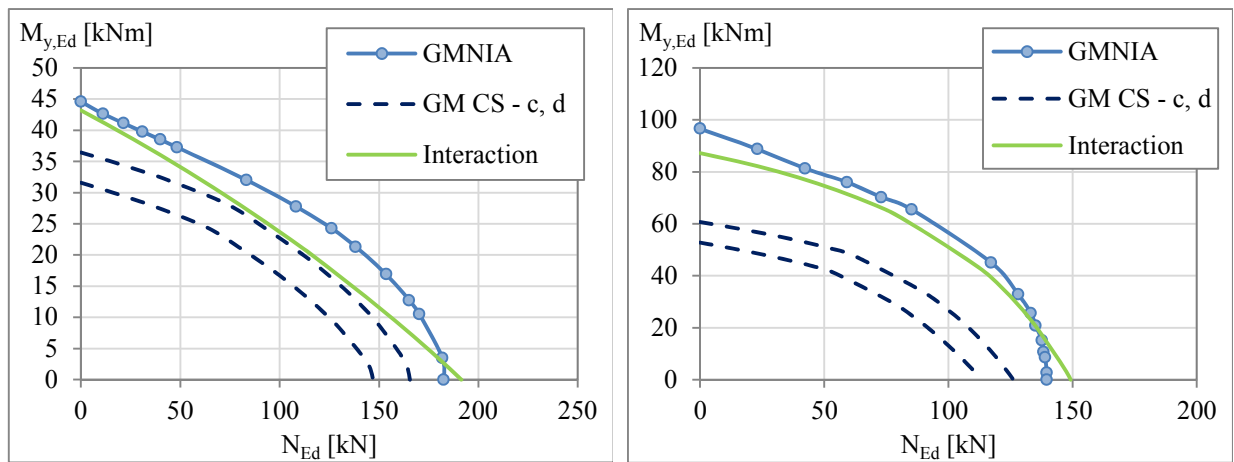(a) #12 IPE200 *w* | γ_h=1.2 | Ψ =0 | $\bar{\lambda}_z (x_{h\,min}) = 1.7$ (b) #13 HEB300 *hr* | γ_h=1.5 | Ψ =0 | $\bar{\lambda}_z (x_{h\,min}) = 1.5$

Figure 6.13 Results of the general method leading to over-conservative level of resistance

Results of the general method are plotted against numerical results in *Figure 6.14* (flexural buckling curve – *c*) and *Figure 6.15* (extreme possibilities for the lateral-torsional buckling curve – *a* and *d*). The points in *Figure 6.14* and *Figure 6.15* are obtained as the points from *Figure 6.10.*
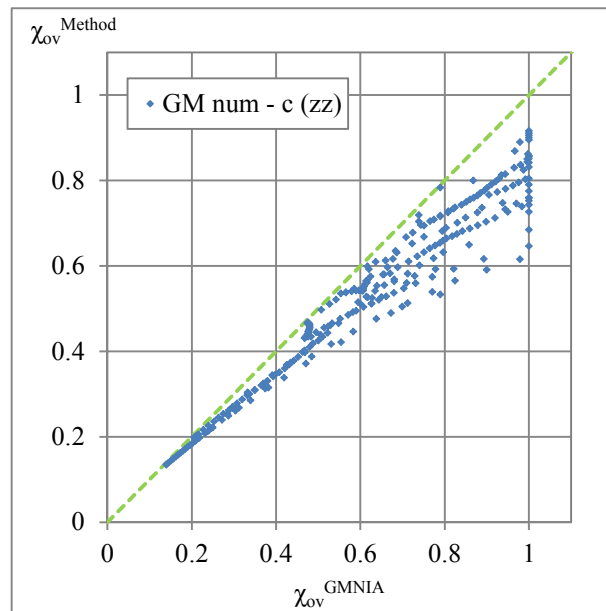
Figure 6.14 Results of the general method for out-of-plane flexural buckling – curve *c*
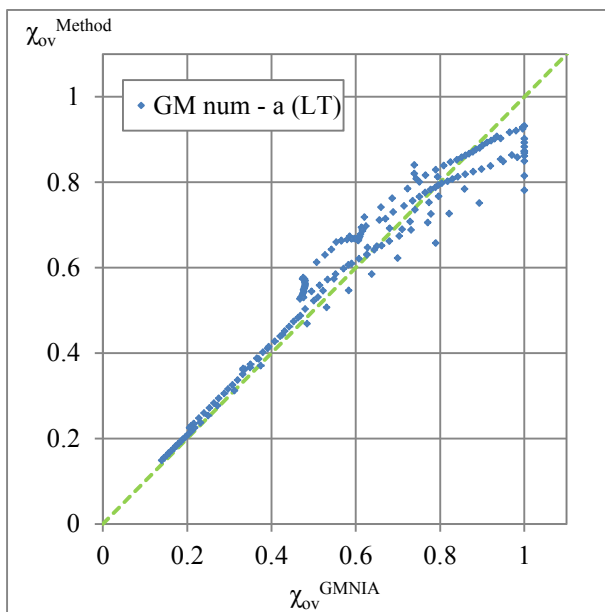
(a) Curve *a* (hot-rolled cases)
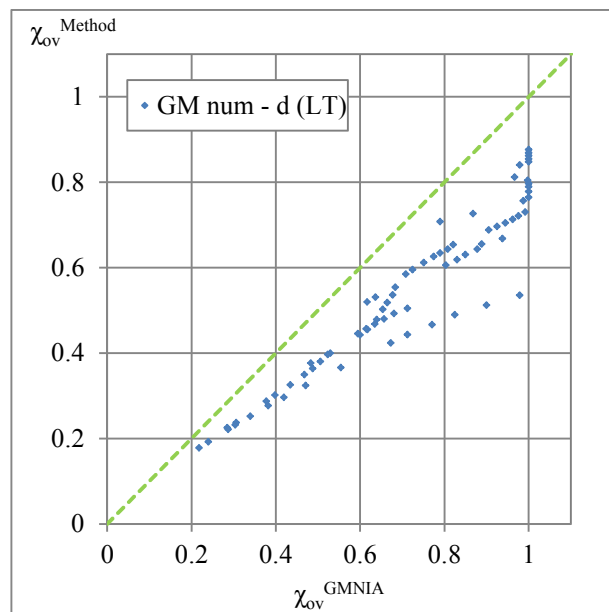
(b) Curve *d* (welded cases)

Figure 6.15 Results of the general method for lateral-torsional buckling

Finally, *Table 6.5* summarizes statistical results for the general method. For comparison, the interaction approach is also presented. Comparing the analyzed verification procedures, the interaction approach leads to a best approximation to the numerical results. As for the General Method, curve *c* gives a decrease in resistance of more than 30%. Curve *d* and curve *a* may be

excluded from the beginning, respectively for the excessive conservatism (resistance is 45% lower than the numerical results) or lack of it (resistance is 20% higher for curve *a*). In summary, any of the curves *a, b, c* or *d* present a high weight of cases whose ratio $\chi_{ov}^{Method}/\chi_{ov}^{GMNIA}$ falls below 0.9 (safe) and above 1.03 (unsafe) when compared to the interaction approach.

Table 6.5: Statistical evaluation concerning the ratio $\chi_{ov}^{Method}/\chi_{ov}^{GMNIA}$ for the analyzed methodologies

Case	Methodology	n	Mean	St. Dev.	CoV (%)	Min.	Max.	% cases <0.9	% cases >1.03
All	6.3.3 mod	273	0.93	0.053	5.66	0.78	1.07	26.7	2.2
	GM - c (zz)	273	0.87	0.067	7.77	0.63	0.99	67.0	0.0
Hot-Rolled	GM - curve a (LT)	198	1.04	0.086	8.30	0.78	1.21	8.1	59.6
	GM - curve b (LT)	198	0.95	0.074	7.80	0.71	1.09	23.7	10.6
Welded	GM - curve c (LT)	75	0.85	0.066	7.73	0.63	0.99	77.3	0.0
	GM - curve d (LT)	75	0.76	0.068	8.92	0.55	0.90	100.0	0.0

6.3.2.3 Modified General Method – overview of the analyzed possibilities

In this section, results of the parametric study are evaluated. At the same time that the possible "interpolation" alternatives between χ_z and χ_{LT} presented in Section 6.2.2.3 are analyzed, the shape of the real χ_{ov} (GMNIA) and its relative position in the buckling curve are evaluated, in order to try to understand the physical behavior and a possible starting point for an adequate "interpolation" procedure.

Case #5 is firstly illustrated in *Figure 6.16*, in which results are plotted over the buckling curve and the *M-N* interaction curve.

(a) Buckling curve representation

(b) Buckling curve representation (zoomed)

(c) Interaction curve representation
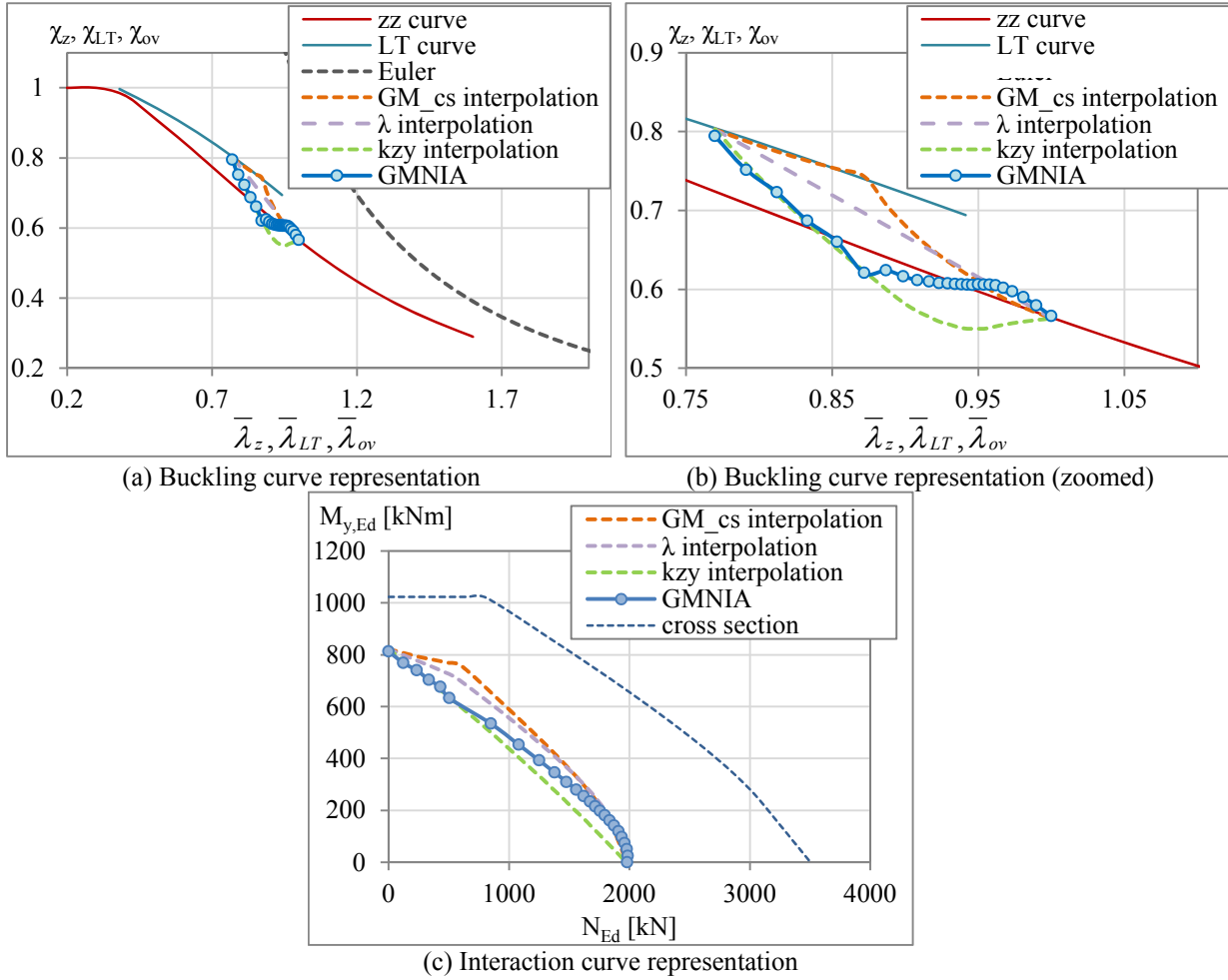
Figure 6.16 Results of the analyzed methodologies for case #5: #5 HEB300 *hr* | γ_h=2 | Ψ =0.25 | $\bar{\lambda}_z\,(x_{h\,\min}) = 1$

When *Figure 6.16(a)* and *(b)* is analyzed it is noticed that both the *GM_cs* and the λ interpolation lead to unsafe levels of resistance. This can be confirmed in *Figure 6.16(c)*. Firstly, regarding the *GM_cs* interpolation, it actually follows an opposite path from the GMNIA points. This can be easily explained: the interpolation provided by Eq. (6.8) may be arranged as

$$\chi_{op} = \frac{\phi+1}{\dfrac{\phi}{\chi_z(x_{c,N}^I)} + \dfrac{1}{\chi_{LT}(x_{c,M}^I)}}, \quad \phi = \frac{M_{y,Rk}(x_{c,M}^I)\big/M_{y,Ed}(x_{c,M}^I)}{N_{Rk}(x_{c,N}^I)\big/N_{Ed}(x_{c,N}^I)} \tag{6.10}$$

It is clear that it represents a *1/x* type function (of ϕ) such that for ϕ=0 (beam) it leads to χ_{LT} and for ϕ=∞ it leads to χ_z. The transition is therefore nonlinear but nevertheless smooth along

ϕ. When plotted over the interaction curve (see *Figure 6.17*) the same shape of the curve corresponding to the cross section resistance ($\alpha_{ult,k}$) must be obtained but varying between $\chi_z{}^*N$ and $\chi_{LT}{}^*M_y$. For the analyzed case, it is then seen that χ_{ov} (given by the ratio between the buckling – orange line, and cross section resistance – blue line) will hardly decrease for high bending moment which confirms the shape in *Figure 6.16(b)* (buckling curve representation).
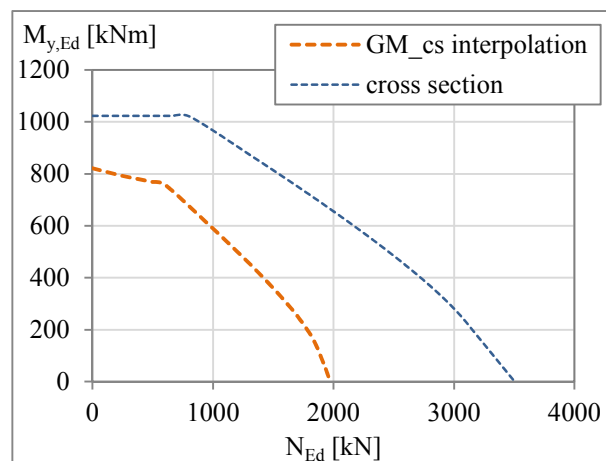
Figure 6.17 Case #5 – Relationship between the *GM_cs* interpolation and the cross section resistance

Considering now the λ interpolation, it is given by a linear interpolation between χ_z and χ_{LT} based on the relative position of the generalized slenderness to the out-of-plane and lateral-torsional slenderness. The interpolation is directly visualized in the buckling curve representation and as a result may many times lead to an unsafe value of χ_{ov}.

The *kzy* interpolation (i.e., interaction format based interpolation) leads exactly to the interaction approach. It is seen that for high axial force the interaction factor does not correctly follow the GMNIA curve, becoming linear (see *Figure 6.16(c)*).

Focus now on case #2. Results are shown in *Figure 6.18*.

(a) Buckling curve representation (zomed)   (b) Interaction curve representation

Figure 6.18 Results of the analyzed methodologies for case #2: IPE200 *hr* | γ_h=3 | Ψ =-0.5 | $\bar{\lambda}_z(x_{h\min})$ = 2.5

Firstly, regarding the *GM_cs* interpolation, for this case it presents quite accurate results. By comparing this methodology to the cross section resistance curve in the interaction curve representation it is then understandable that the transition is much smoother when plotted over the buckling curve format. Because χ_z is much lower than χ_{LT}, the bi-linearity of the cross section capacity interaction curve will not be felt as pronounced in the final $\chi_{ov}=\alpha_b^{Method}/\alpha_{ult,k}$. However, when observing *Figure 6.19* a small angle can still be noticed.
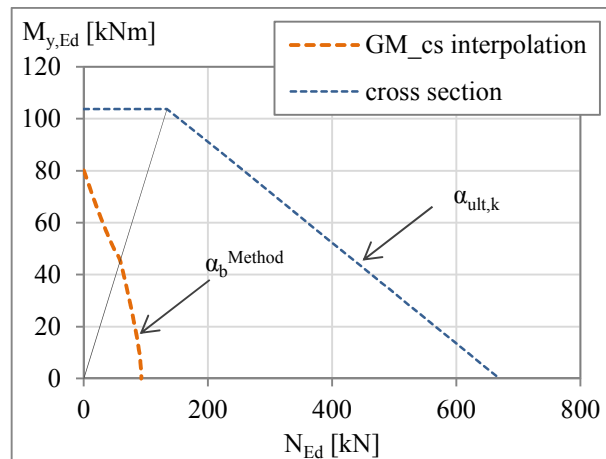
Figure 6.19 Case #2 – Relationship between the *GM_cs* interpolation and the cross section resistance

Regarding the λ approach, for this case the curvature of the buckling curve in between χ_z and χ_{LT} is such that the difference between the line corresponding to χ_{ov}^{Method} and the χ_{ov}^{GMNIA}

leads to an actual violation of the condition $N_{Ed} \leq \chi N_{Rk}$. This may then be observed in the interaction curve representation. While in the interaction approach it is assured that the utilization due to the bending moment and due to the axial force are not higher than unity (otherwise the buckling check would not be verified), in a generalized slenderness approach this cannot be checked because $\alpha_{ult,k}$ contains the information of the <u>combination</u> of the axial force and bending moment acting together (not accounted by the respective reduction factors). As a result, an additional check would have to be performed. However, because the k_{zy} interpolation is in fact no more than the interaction formula represented in terms of χ_{ov}, that additional check is not required for this alternative. Finally, it is obvious that a <u>linear</u> λ interpolation cannot be considered.

Consider case #3 previously analyzed for the interaction approach. Due to the low lateral-torsional buckling slenderness, for high bending moment, cross section capacity will prevail. Results concerning the generalized slenderness approach are illustrated in *Figure 6.20* regarding the *kzy* interpolation, i.e., the interaction approach is illustrated in the buckling curve format. The resultant χ_{ov} curve starts decreasing from $\phi=0$ (beam) and, as a result, it is incorrectly illustrating that buckling starts occurring as soon as axial force is present ($\phi>0$). However, if advantage is taken from the lateral-torsional buckling curve that is not reduced (i.e. $\chi_{LT}*\varphi_{LT}$ instead of χ_{LT}) only for the purpose of interpolating χ_{ov}, an improvement can be achieved, see *kzy* interpolation* curve in *Figure 6.20*. After obtaining the new χ_{ov}, the condition $\chi_{ov} \leq 1$ shall be satisfied. Note that this alternative is just a simplification and means that for some cases the resultant χ_{ov} could be slightly unconservative. However, because this interpolation is related to the member over-strength factor φ_{LT}, if φ_{LT} is small (but higher than 1), then resultant χ_{ov} will be closer to the original interpolation approach. For the analyzed case, $\varphi_{LT}=1.74$.

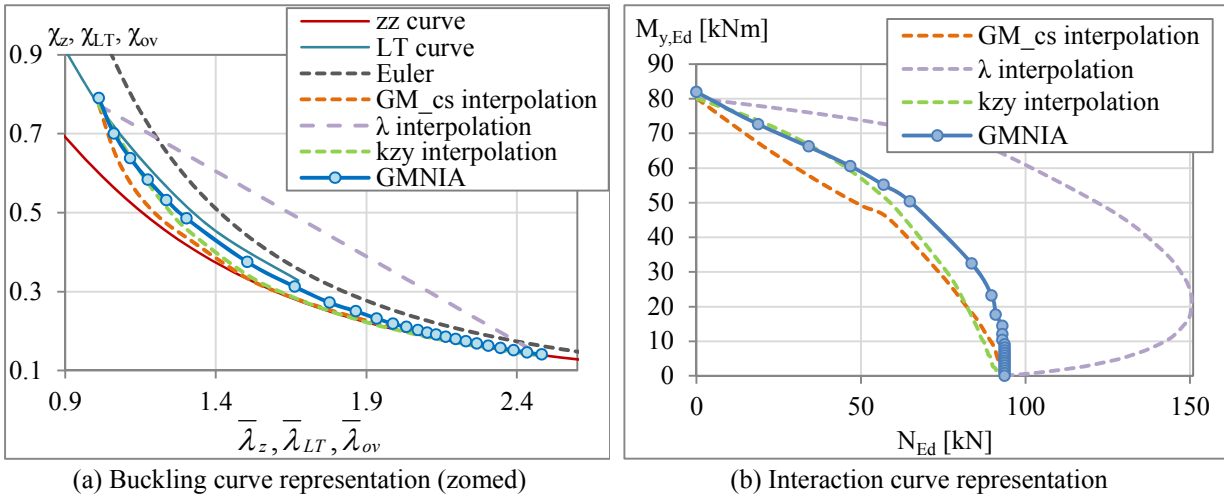(a) Buckling curve representation (zoomed) (b) Interaction curve representation
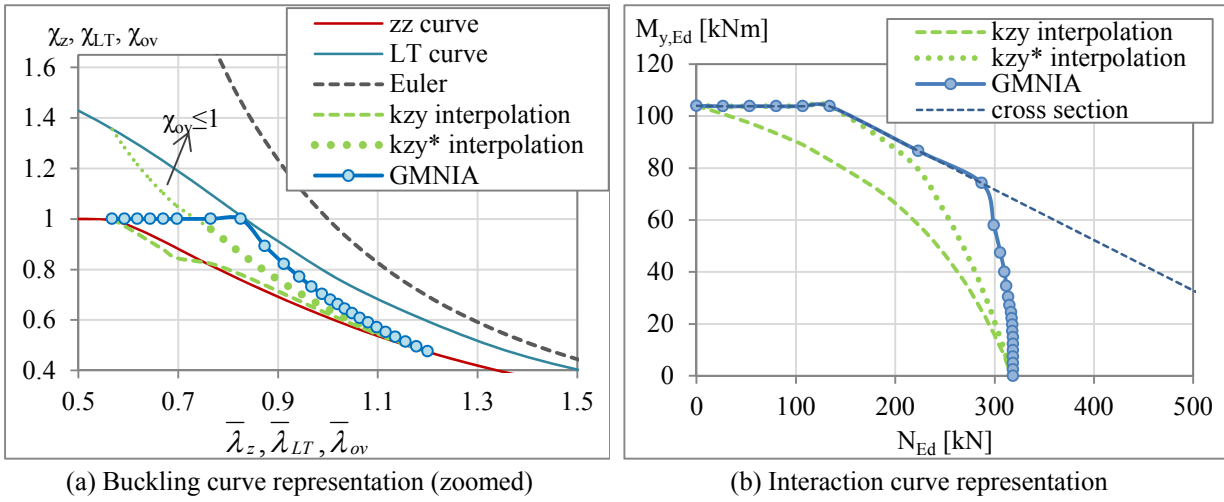
Figure 6.20 Results of the analyzed methodologies for case #3: IPE200 *hr* | γ_h=3 | Ψ =-0.5 | $\bar{\lambda}_z (x_{h\min}) = 1.2$

Figure 6.21 illustrates results for the *kzy* interpolation for case #9. From this case the interaction factor k_{zy} does not provide (mechanically) satisfactory results. The consideration of $\chi_{LT}*\varphi_{LT}$ does not give a satisfactory answer here. As already mentioned, for this case the cross section failure governs here and the interaction formula is not able to provide a smooth transition between instability and cross section resistance failure.

(a) Buckling curve representation (zoomed) (b) Interaction curve representation

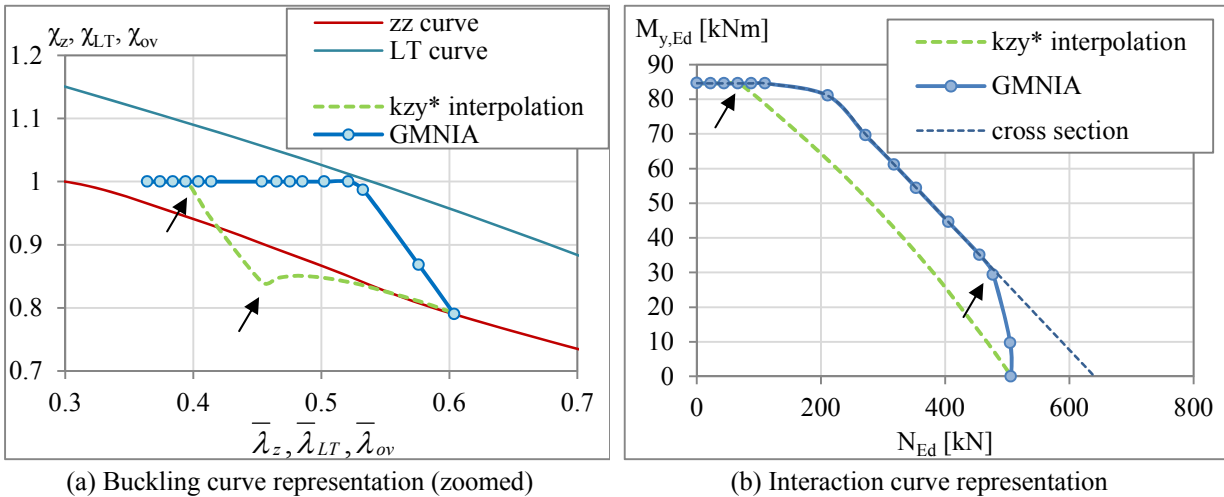*Figure 6.21* Results of the *kzy** interpolation for case #9: IPE200 *w* | γ_h=1.5 | Ψ =-0.5 | $\bar{\lambda}_z (x_{h\min}) = 0.6$

One last case is analyzed. Case #14 ($\bar{\lambda}_z (x_{h\min})$=0.5) presents flexural buckling and lateral-torsional buckling over-strength factors of, respectively φ_z=1.26 and φ_{LT}=1.07. For this case of

uniformly distributed loading the over-strength factor is low when compared to the over-strength factor for lateral-torsional buckling. This causes the buckling curve for flexural buckling to be higher for than the buckling curve for lateral-torsional buckling for the lower slenderness range, see *Figure 6.22*. As a result, χ_{ov} will vary from a lower χ_{ov} (corresponding to χ_{LT}) up to χ_z. Case #1 ($\overline{\lambda}_z(x_{h\,min})$=1.2) is also illustrated for comparison.
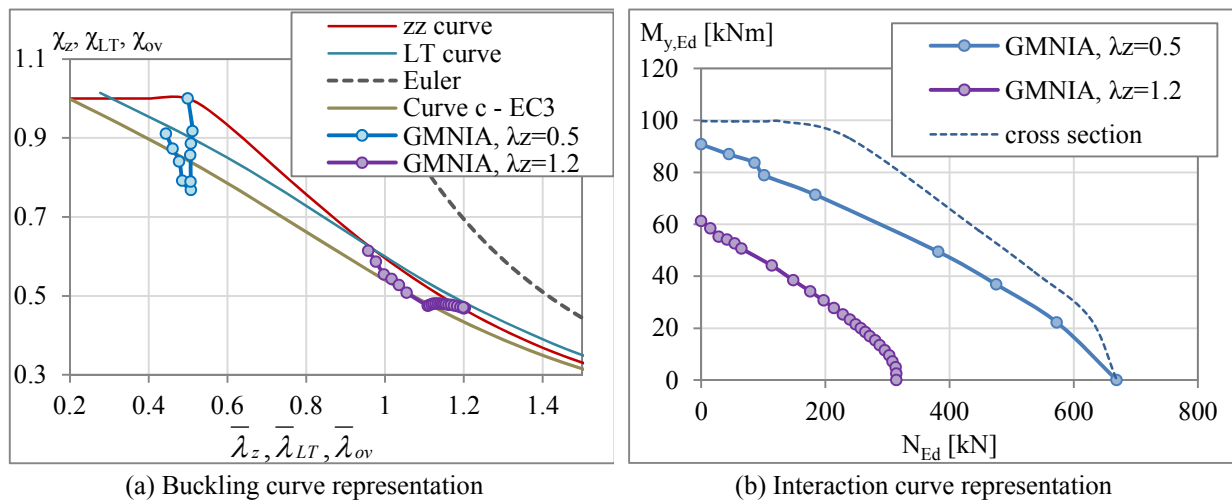
(a) Buckling curve representation   (b) Interaction curve representation
Figure 6.22 Results for case #14: IPE200 *hr* | γ_h=2.5 | UDL

Figure 6.22 also illustrates that with the increase of the member length, the χ_{ov} curve has a tendency be smoother. This is because with the increase of distance from the cross section capacity curve, the ratio $\chi_{ov}= \alpha_b^{Method}/\alpha_{ult,k}$ decreases and the bi-linear variation of the cross section capacity (associated to $\alpha_{ult,k}$) has a lower effect in the final result.

Still regarding *Figure 6.22*, case #14 may be given as a counterexample to illustrate that the consideration of in-plane local effects according to the General Method does not always give an answer to the unconservativeness of χ_{op} relatively to the minimum of the buckling curves. Of course this is not as noticeable if the existing code curves are used because these are already conservative (but nevertheless inaccurate to use in tapered members). For this case it would be curve *c*, which is seen to be safe relatively both to the flexural buckling and lateral-torsional buckling developed curves for this tapered member, see again *Figure 6.22*.

Considering then curve *c*, *Figure 6.23* illustrates the interaction curves depending on the calculation of $\alpha_{ult,k}$ – i.e., considering local in-plane imperfections or not – which for this slenderness level are very close. As previously mentioned, the inclusion of in-plane imperfections should provide safe results, however (for this case) some results (slightly) on the unsafe side are still achieved. Note also that this is a case in which the bending moment distribution will have more effect in the out-of-plane capacity and that is why the generalized reduction factor reduces significantly up to a certain ϕ level. This would be a case in which the provided EC3-1-1 definition for $\alpha_{ult,k}$ would work. This confirms (see also Section 2.4.2.5) that the consideration of in-plane local imperfections in the upper bound of the member resistance, in the end does not seem to always solve the targeted problem of providing a safe resistance level if the minimum buckling curve is considered. Besides this aspect and also because of the high conservativeness it brings to the cases in which in-plane instability has higher effect, $\alpha_{ult,k}$ should be obtained from the cross section resistance and this problem should be overcome by a more grounded approach.
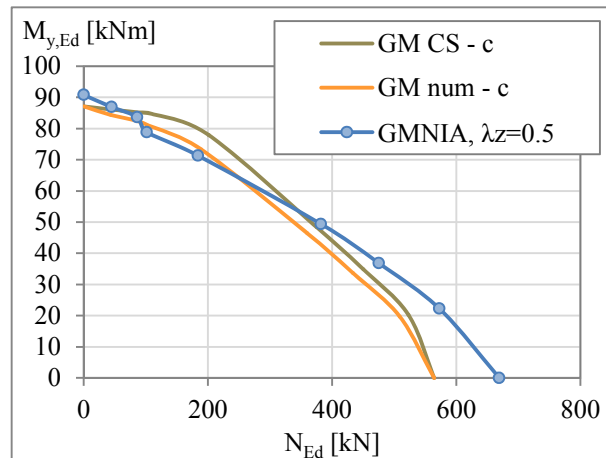
Figure 6.23 M-N interaction curve considering different assumptions for $\alpha_{ult,k}$

In summary, from the previous analyses it is possible to conclude that an interpolation (or transition) between the flexural and lateral-torsional buckling modes is not a straight forward procedure and that some of the alternative interpolation schemes may sometimes be unsafe. The third type of interpolation (k_{zy} interpolation) has the advantage of establishing the lateral and lateral-torsional buckling limits, for N_{Ed} and for $M_{y,Ed}$ respectively and always gives safe

results. This alternative coincides with the adapted interpolation formula. Regarding generalized slenderness procedure, a slenderness interpolation would be the simplest approach but could only be developed provided that a nonlinear function suitable to the buckling behavior of each member is considered. For this a wider parametric study must be carried out.

Other examples of the parametric study are finally analyzed. *Figure 6.24*, *Figure 6.25*, *Figure 6.26* and *Figure 6.27* illustrate respectively the GMNIA and cross section resistance cases #2 and #3; cases #6 and #7; cases #9 and #11 and cases #10 and #12. The following comments are given:

- With the increase of the member length, the relative distance between $\bar{\lambda}_z$ and $\bar{\lambda}_{LT}$ increases leading to a lower effect of the in-plane bending moment in the out-of-plane resistance. At the same time, the influence of the cross section resistance becomes lower and due to this, χ_{ov} which is given by the ratio between the ultimate load and the cross section resistance becomes less affected by the latter and the appearance in the buckling curve format is therefore smoother;

- At low slenderness cross section capacity may be critical and therefore $\chi_{ov}=1$ (see mainly *Figure 6.24* and *Figure 6.26*). So far, none of the presented alternatives were able to consider this aspect;

- If buckling starts occurring for high bending moment relatively to axial force, for the low slenderness range the difference in the inclination of χ_{ov} may be more visible because of the shape of the cross section resistance variation. This difference occurs at the value of ϕ in which the axial force starts having an effect on the cross section capacity (a visible change of slope in the cross section resistance interaction curve – see the grey lines in *Figure 6.25* and *Figure 6.26*). As a result, a possible type of interpolation could be developed such that it is given by a certain function up to the referred ϕ; and by other function from that limit. See also case #5 (*Figure 6.16*);

- Finally, it may also be observed that with increasing slenderness the zones with higher axial force approach the flexural buckling curve more quickly (lower effect of the in-plane bending moment), which could eventually be used to develop an interpolation function for this zone. In general, all figures below illustrate this. See also case #14

(*Figure 6.22*). Although they are not illustrated, cases #4 and #13 (high slenderness examples) also present this behavior.
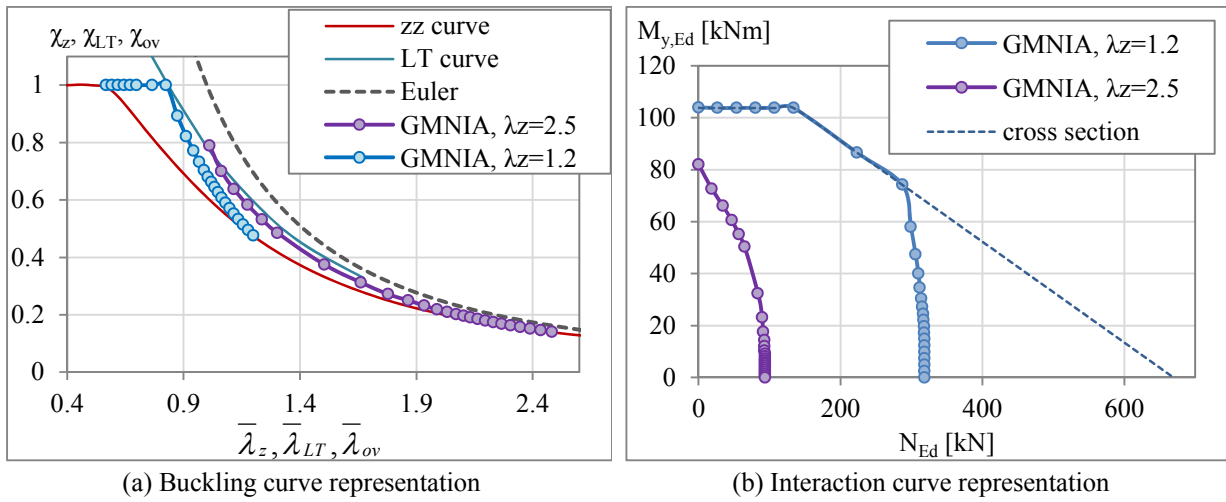
(a) Buckling curve representation   (b) Interaction curve representation
Figure 6.24 Results for cases #2 and #3: IPE200 *hr* | γ$_h$=3 | Ψ =-0.5
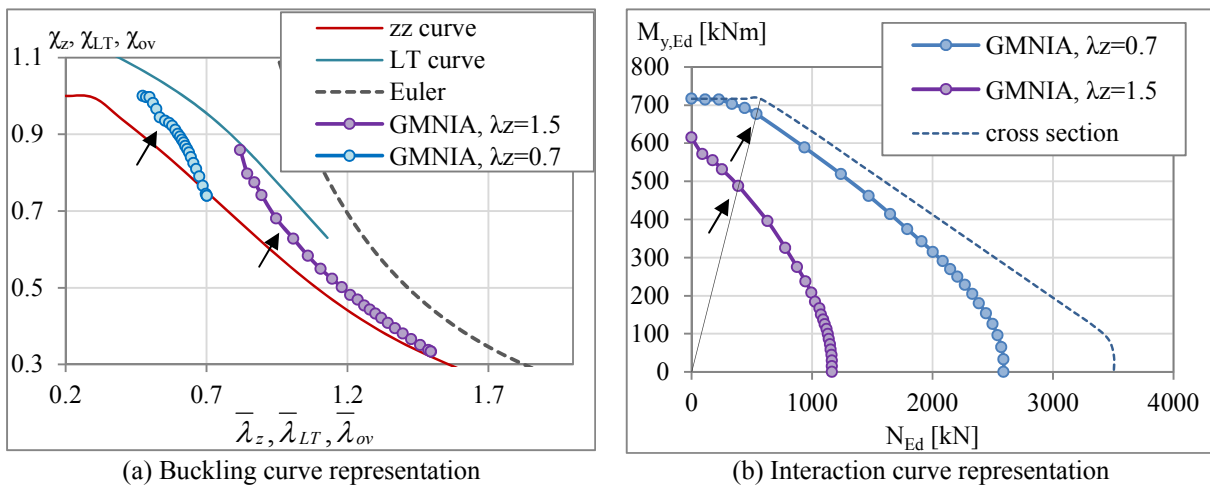
(a) Buckling curve representation   (b) Interaction curve representation
Figure 6.25 Results for cases #6 and #7: HEB300 *hr* | γ$_h$=1.5 | Ψ =0
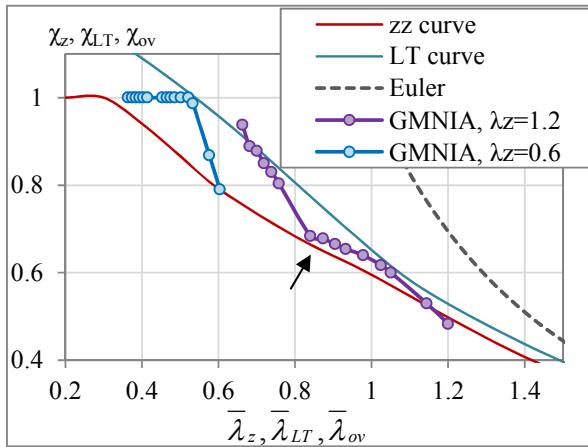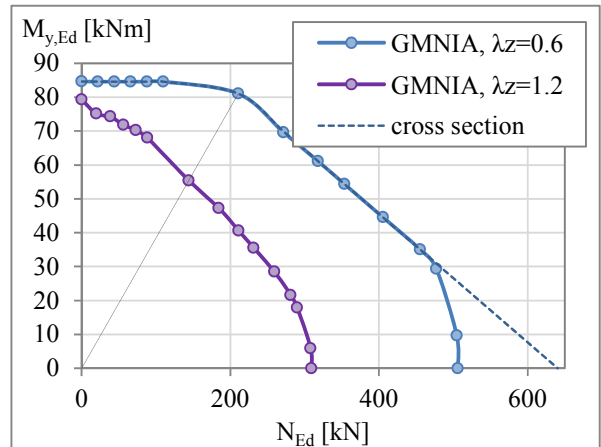
(a) Buckling curve representation (b) Interaction curve representation

Figure 6.26 Results for cases #9 and #11: IPE200 w | γh=1.5 | Ψ =0.5
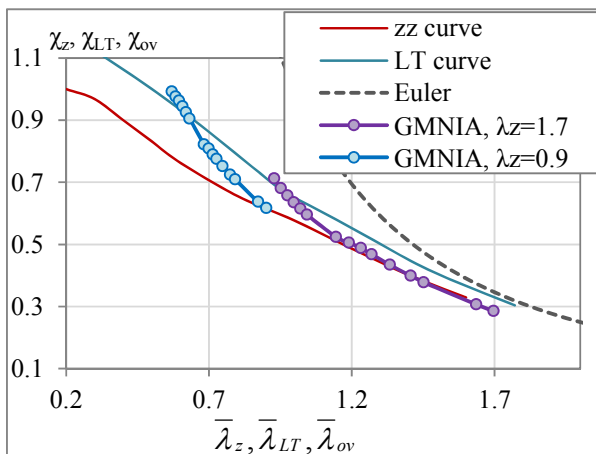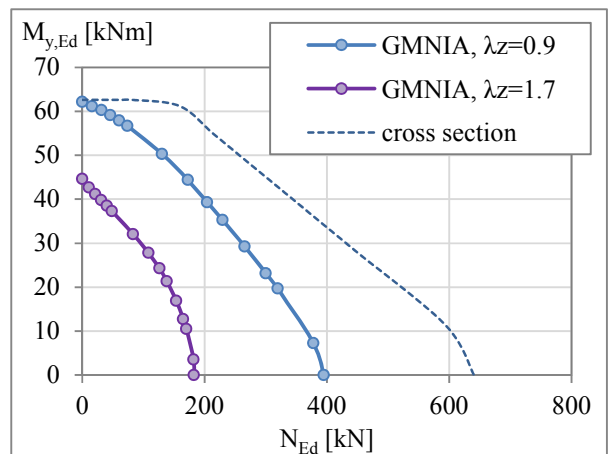
(a) Buckling curve representation (b) Interaction curve representation

Figure 6.27 Results for cases #10 and #12: IPE200 w | γ_h=1.2 | Ψ =0

6.4 Stability verification of frames composed of tapered members

6.4.1 Introduction and scope

In Chapter 4 and Chapter 5 design procedures for respectively flexural buckling of columns and lateral-torsional buckling of beams were developed for the case of isolated members with fork conditions. However, members in real structures often do not exhibit these idealized boundary conditions. Due to this, several procedures exist on how to tackle the problem, either by considering all the relevant imperfections in the structural analysis or by extracting

the member from the real structure by adequate buckling lengths in order to perform its stability verification separately from the global structure. These methods were discussed in Section 2.5 and are brought into this section for the design of structural systems (focus on frames) with tapered members.

As a starting point, only straight tapered members buckling out-of-plane between points that are braced in both flanges (i.e. in which both lateral and torsional deformation is prevented) are considered. Partial bracing is not contemplated in this analysis. As a result, for the considered cases, the buckling lengths may be assumed to be approximately equal to the member length, i.e., an approximation to fork conditions. Note that, even if the buckling lengths of tapered members with other boundary conditions are determined, either numerically or by approximate formulae, throughout the analytical derivations of Chapter 4 and 5, the member verification methodologies were developed on the basis of a second order location which is not the same when the buckling mode is different from the standard simply supported case. This is true even for prismatic members. Of course if member imperfection amplitudes are adapted to be relative to the length of the "equivalent" simply supported member and because resistance is brought into a <u>relative</u> slenderness scale, the buckling curves may actually be similar. Nevertheless more attention needs to be given to this subject before outlining any conclusions. As a result, only simply supported "isolated" members are considered at this point.

In summary, in the scope of the present study, some of the possibilities of structural analysis and member verification (see also Section 2.5) are now presented for the case of frames with tapered members, assuming that, as a starting point, isolated member verification procedures are provided. The possibilities for these design procedures were discussed in the previous sections of Chapter 6 and are summarized in *Table 6.6*. The developed reduction factors in Chapter 4 and Chapter 5 are naturally considered in the procedures. In Section 6.4.2.2, these procedures are combined with the structural methods of analysis such that in-plane stability verification may alternatively be covered by the account of in-plane global and local imperfections in the second order analysis.

Table 6.6: Potential member stability design procedures to be developed

In-plane stability verification	Out-of-plane stability verification
Interaction approach: • Considering k_{yy} interaction factor (from EC3-1-1 Annex B) – to be validated;	**Interaction approach**: • Considering k_{zy} interaction factor (from EC3-1-1 Annex B) – is it realistic and worth improving for for the case of tapered members?
Or	Or
Generalized slenderness approach?	**Generalized slenderness approach (modified general method)**: • $\alpha_{ult,k}$ is determined according to the most stressed cross section considering first order effects only; • A proper interpolation procedure needs to be developed;

6.4.2 Possible methods of structural analysis and subsequent stability verification

Consider the simply supported frame of *Figure 6.28*, prevented from out-of-plane and torsional deformations at the end of each rafter and column.
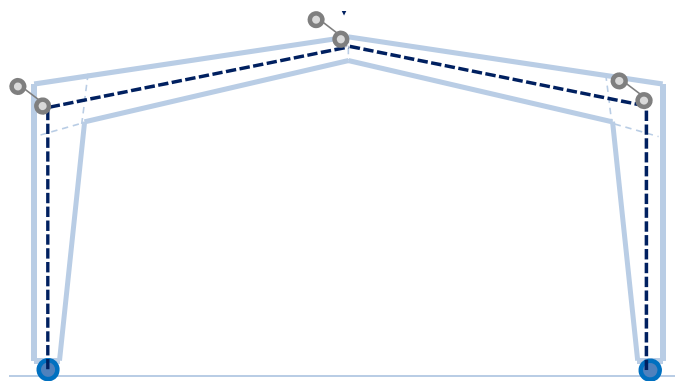

Figure 6.28 Frame with tapered columns and tapered rafters

In Section 6.4.2.1 the definition of the local and global imperfections is analyzed whereas in Section 6.4.2.2, methods for the structural analysis of the frame are combined with the member stability procedures summarized in *Table 6.6*.

6.4.2.1 Definition of imperfections

Assuming elastic global analysis and that α_{cr} of the frame is $\alpha_{cr}<10$, second order analysis needs to be performed. The sway imperfections ϕ are obtained from clause 5.3.2 of EC3-1-1. Local imperfections shall be obtained from Table 5.1 of EC3-1-1 or *Table 1.1* of this thesis repeated here in *Table 6.7* for sake of simplicity.

Table 6.7: Design values of initial bow imperfection e_0/L (Table 5.1 of EC3-1-1)

Buckling curve acc. to EC3-1-1, Table 6.1	Elastic analysis e_0/L	Plastic analysis e_0/L
a_0	1/350	1/300
a	1/300	1/250
b	1/250	1/200
c	1/200	1/150
d	1/150	1/100

Because non-uniform members, either tapered or with non-uniform loading do not exactly exhibit a sinusoidal shape for the buckling mode, it is questionable whether the local member imperfections should be modeled with a bow shape or not. In addition, the amplitudes presented in *Table 6.7* were calibrated for specific buckling curves that are different than, for example, the buckling curve calibrated for members with welded cross sections subject to flexural buckling in-plane (Chapter 4). As a result, the definition of local imperfections is not clear. Some comments are given in the following:

- In-plane imperfection factors for in-plane flexural buckling of linearly web-tapered columns are given in Chapter 4, *Figure 4.24*. Regarding members with hot-rolled cross sections, the flexural in-plane imperfection factor is $\alpha=0.34$ (curve b). e_0/L is then given by $e_0/L=1/250$ in *Table 6.7*; On the other hand, the imperfection factor for columns with welded cross-sections buckling in-plane was re-calibrated in Chapter 4 leading to a value of $\alpha=0.45$. As a result, e_0/L needs to be calibrated. Because $1/250 \leq e_0/L \leq 1/200$, on the safe side it could be considered $e_0/L=1/200$;

- As referred in Chapter 4, the imperfections should have the in-plane flexural eigenmode shape of the simply supported column in order to lead to the most unfavorable results. As a result, the consideration of bow imperfections (or equivalent forces) for non-uniform members should be validated in the future;

- Finally, for other members with a non-linear variation of the axis or that are composed by different types of cross sections distributed along the length, such as the rafters of *Figure 1.10(a)* (see *Figure 6.29*), no procedure was developed in the scope of this work regarding the flexural buckling imperfection factors to be considered. In fact, according to the analytical derivation of Chapter 4, the imperfection factors for columns with prismatic cross sections may be used independently of the variation function of the taper, but provided that the centroid axis is linear (the influence of the taper is then accounted for by a proper second order failure location, $x_{c,N}^{II}$ or, alternatively, over-strength factor, φ). That is not the case of the examples in *Figure 6.29*, in which the centroid axis is not linear. In addition, for the cross section of the haunch on the left extreme of the rafter of *Figure 6.29(b)* the code does not provide flexural buckling imperfection factors. For the case of in-plane buckling, curve *c* is probably satisfactory and safe; however, because these configurations are usually considered in practice, a buckling curve should be calibrated (or confirmed) in the future.

(a)   (b)

Figure 6.29 Different taper configurations

6.4.2.2 Methods of analysis

a) In-plane and out-of-plane member verification procedure exists (Level 2)

If proper in-plane verification procedure is available, only *P*-Δ and global (ϕ) imperfections are required in the frame analysis. The verification is then performed as follows:

1. Out-of-plane verification check (for each member):
   - Determine χ_z and χ_{LT} considering the buckling length equal to the member length;
   - Obtain the second order forces from *P*-Δ effects and imperfections (ϕ);

- Perform the out-of-plane check considering the second order forces and either an interaction or generalized slenderness approach.

2. In-plane verification:
   - Determine χ_y considering the buckling length equal to the member length;
   - Consider χ_{LT} from step no. 1;
   - Obtain the second order forces from P-Δ effects and imperfections (ϕ);
   - Perform the in-plane check considering the second order forces and either an interaction or generalized slenderness approach;

3. Perform a cross section check (considering the calculated second order forces) at a sufficient number of sections, e.g. 10 sections per member.

b) Only out-of-plane member verification procedure is provided (Level 1 and Level 3)

Considering that only out-of-plane member stability may be checked individually, the global and local in-plane second order effects and imperfections of the frame need to be accounted for in the structural analysis. For this, the second order analysis of the frame must contemplate the imperfections of *Figure 6.30*. This example illustrates the combination of level 1 and 3 of analysis, see also Section 2.5.2.5 a).
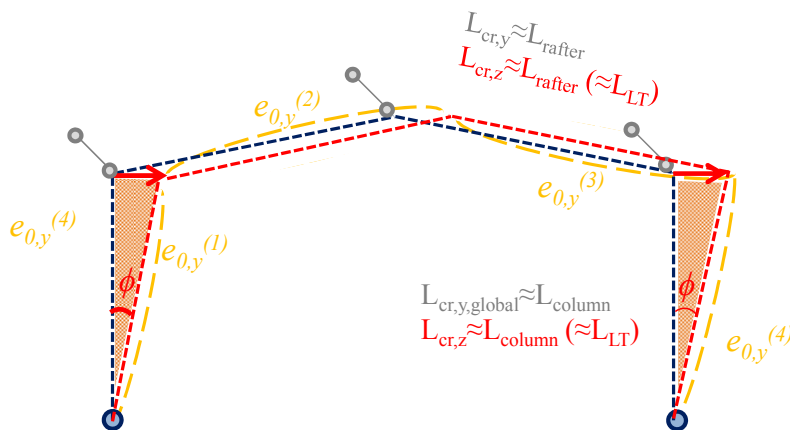
Figure 6.30 In-plane global and local imperfections

Finally, after definition of the local and global in-plane imperfections, following then a similar procedure as in *Figure 2.25*, the verification of the frame is perfomed as follows:

1. Out-of-plane verification check (for each member):

   o Determine χ_z and χ_{LT} considering the buckling length equal to the member length;

   o Obtain the second order forces from P-Δ effects and imperfections (ϕ) <u>only</u>;

   o Perform the out-of-plane check considering the second order forces and either an interaction or generalized slenderness approach.

2. In-plane verification:

   o Obtain the second order forces from P-Δ and P-δ effects and imperfections (ϕ and $e_{0,y}$);

   o To include the torsional effects, reduce $M_{y,Rk}$ by χ_{LT} $M_{y,Rk}$ (to be in line with the interaction formula 6.61 of EC3-1-1), considering χ_{LT} of each member;

   o Perform a cross section check (considering the calculated second order forces and the reduced moment capacity) at a sufficient number of sections, e.g. 10 sections per member.

6.5 Final remarks

In this chapter, the stability verification of web-tapered beam-columns was discussed.

Firstly, regarding out-of-plane buckling of beam-columns it was seen that the General Method, which is the current alternative for the stability verification of such members, not only does not provide clear guidelines of which curve to be considered, but also may lead to a high (and random) spread regarding the level of safety. Because of this, based on the results of Chapter 4 (for columns) and 5 (for beams), simple adaptations of both the interaction formulae of clause 6.3.3 and the general method of clause 6.3.4 were analyzed:

• The interaction formula is applied considering the utilization of the forces N_{Ed}/N_{Rk} and $M_{y,Ed}/M_{y,Rk}$ at an arbitrary position and the respective reduction factors at the same position. For simplicity reasons it is recommended to consider $x_{c,N}^{I}$ and $x_{c,M}^{I}$, respectively. The interaction approach leads to results that are mostly on the safe side. Maximum differences of 20% relatively to the numerical results are achieved;

- A "modified" General Method is considered such that the generalized slenderness is calculated with the cross section resistance load multiplier for $\alpha_{ult,k}$. Several alternatives for the interpolation between the flexural buckling and lateral-torsional buckling reduction factors calculated with the generalized slenderness were analyzed. It was seen that a deeper analysis needs to be carried out to provide a proper interpolation procedure considering the stability behavior of the member and also to provide limits between the stability and cross section resistance for the low slenderness range.

Regarding the verification of non-uniform members, the General Method (modified or not) should give a quite accurate answer. However the fact that in the end a proper interpolation may not be as simple to develop and further give accurate results for each and any possible combination of loading / taper ratio and that the General Method as given in the code was shown more than once to not be accurate and mechanically solid, leads to the question of whether a new generalized slenderness model built analogous to the analytical models developed in Chapters 4 and 5 would be worth developing by considering the relevant first and second order force utilizations – this shall be analyzed in a next step of the research.

Finally, in Section 0 the possible design procedures were analyzed in the context of frame analysis and, in line with Chapter 2, the possibilities for the global structural verification were described.

Chapter 7

7 CONCLUSIONS AND FURTHER WORK

7.1 Summary of the design proposals for tapered columns and beams

Sections 7.1.1 and 7.1.2 summarize the design proposals of Chapters 4 and 5 respectively.

7.1.1 Flexural buckling of web-tapered columns

In Chapter 4, proposals were made for in-plane and out-of-plane flexural buckling of linearly web-tapered columns subject to constant axial force. The verification of the column is determined according to clause 6.3.1 of EC3-1-1 however considering the properties at a calibrated limit second order failure location, $x_{c,lim}^{II}$, or alternatively a calibrated over-strength factor φ. These are summarized respectively in Table 7.1 and
Table 7.2, both for in-plane and out-of-plane flexural buckling.

Table 7.1 Proposed verification procedures for web-tapered I-section beams – $x_{c,lim}^{II}$ approach

	Out-of-plane flexural buckling	In-plane flexural buckling
$\alpha_{ult,k}(x_c^I)$	$N_{Rk}(x_c^I)/N_{Ed}$ – for N_{Ed}=const. is the smallest cross section	
α_{cr}	$\approx N_{cr,z,hmin}/N_{Ed}$ (approximately the Euler load of an equivalent column with the smallest cross section)	Numerically e.g. or $N_{cr,y,Tap}$ by proposed exp.: $A \cdot N_{cr,min}$, $\quad A = \gamma_I^{0.56}\left(1 - 0.04 \cdot \tan^{-1}(\gamma_I - 1)\right)$
$x_{c,lim}^{II}$	$(1+4\gamma_h)/(10\gamma_h)$	$1/(1+\gamma_h)$
$\overline{\lambda}(x_c^{II})$	$\sqrt{\alpha_{ult,k}(x_c^{II})\big/\alpha_{cr}} = \sqrt{N_{Rk}(x_{c,lim}^{II})/N_{Ed}\big/\alpha_{cr}}$	
α	Hot-rolled: 0.49 Welded: 0.64	Hot-rolled: 0.34 Welded: 0.45
η	$\alpha_z\left(\overline{\lambda}(x_{c,lim}^{II}) - 0.2\right)$ If welded, $\eta_z \leq 0.34$	$\alpha_y\left(\overline{\lambda}(x_{c,lim}^{II}) - 0.2\right)$ If welded, $\eta_z \leq 0.27$
ϕ	$0.5 \times \left(1 + \eta + \overline{\lambda}^2_z(x_{c,lim}^{II})\right)$	
$\chi(x_c^I)$	$1\big/\phi + \sqrt{\phi^2 - \overline{\lambda}^2(x_{c,lim}^{II})} \leq 1$	
Verification	$\chi(x_{c,lim}^{II})\times\alpha_{ult,k}(x_{c,lim}^{II}) \geq 1$; $\alpha_{ult,k}(x_c^I) \geq 1$	

Table 7.2 Proposed verification procedures for web-tapered I-section columns – φ approach

	Out-of-plane flexural buckling	In-plane flexural buckling
$\alpha_{ult,k}(x_c^I)$	See *Table 7.1*	
α_{cr}	See *Table 7.1*	See *Table 7.1*
$\overline{\lambda}(x_c^I)$	$\sqrt{\alpha_{ult,k}(x_c^I)\big/\alpha_{cr}}$	
φ	$1 + \dfrac{h t_w}{A_{min}}\left[\dfrac{(1+4\gamma_h)(\gamma_h - 1)}{10\gamma_h}\right]$	$1 + \dfrac{h_{min} t_w}{A_{min}}\dfrac{\gamma_h - 1}{\gamma_h + 1}$
α	See *Table 7.1*	See *Table 7.1*
η	$\alpha_z\left(\sqrt{\varphi_z}\,\overline{\lambda}(x_c^I) - 0.2\right)$ If welded, $\eta_z \leq 0.34$	$\alpha_y\left(\sqrt{\varphi_y}\,\overline{\lambda}(x_c^I) - 0.2\right)$ If welded, $\eta_y \leq 0.27$
ϕ	$0.5 \times \left(1 + \varphi \times \eta + \varphi \times \overline{\lambda}^2(x_c^I)\right)$	
$\chi(x_c^I)$	$\varphi\big/\phi + \sqrt{\phi^2 - \varphi \times \overline{\lambda}^2(x_c^I)} \leq 1$	
Verification	$\chi(x_c^I)\times\alpha_{ult,k}(x_c^I) \geq 1$	

7.1.2 Lateral-torsional buckling of web-tapered beams

In Chapter 5, proposals were made for lateral-torsional buckling of linearly web-tapered beams. The stability verification of the beam is based on an Ayrton-Perry model in which specific parameters regarding the lateral-torsional buckling mode derive from the model,

relatively to the Ayrton-Perry model for flexural buckling. Analogous to the column case, the verification is finally determined based on the properties of the (mode specific) second order limit failure location $x_{c,lim}^{II}$. Several possibilities for calibration of a procedure were analyzed. *Table 7.3* summarizes the procedure in which both $x_{c,lim}^{II}$ and an over-strength factor φ are considered In addition to *Table 7.3,* verification to shear should be performed.

Table 7.3 Proposed verification procedure for web-tapered I-section beams $- x_{c,lim}^{II}$ and φ combined approach

	Lateral-torsional buckling
$\boldsymbol{\alpha_{ult,k}(x_c^{\,I})}$	$M_{y,Rk}(x_{c,M}^{\,I})/M_{y,Ed}(x_{c,M}^{\,I})$ – the minimum along the beam, e.g. 10 sections
$\boldsymbol{\alpha_{cr}}$	Numerically e.g. or by expressions for M_{cr} from the literature, see Section 5.2.4. The multiplier α_{cr} shall afterwards be obtained with respect to the applied load.
$\overline{\boldsymbol{\lambda_{LT}}}\boldsymbol{(x_c^{\,I}\,)}$	$\sqrt{\alpha_{ult,k}(x_c^{\,I})\big/\alpha_{cr}}$
$\boldsymbol{x_{c,lim}^{\,II}}$	See *Table 7.4*
$\boldsymbol{\varphi_{LT}}$	For ψ: $\quad A\cdot\psi^2 + B\cdot\psi + C \quad \geq 1$ For UDL: $\quad -0.0025a_\gamma^{\,2} + 0.015a_\gamma + 1.05$ See *Table 7.5* for A,B,C and a_γ
$\boldsymbol{\alpha_{LT}}$	Hot-rolled: $\quad 0.16\sqrt{\dfrac{W_{y,el}(x_{c,\lim}^{II})}{W_{z,el}(x_{c,\lim}^{II})}} \leq 0.49$ Welded: $\quad 0.21\sqrt{\dfrac{W_{y,el}(x_{c,\lim}^{II})}{W_{z,el}(x_{c,\lim}^{II})}} \leq 0.64$
$\boldsymbol{\eta_{LT}}$	$\alpha_{LT}\times\left(\overline{\lambda}_z(x_{c,\lim}^{II})-0.2\right)$ If welded, $\eta_{LT} \leq \sqrt{\dfrac{W_{y,el}(x_{c,\lim}^{II})}{W_{z,el}(x_{c,\lim}^{II})}}\left(0.12\psi^2 - 0.23\psi + 0.35\right)$
$\overline{\boldsymbol{\lambda}}_z(\boldsymbol{x_{c,lim}^{\,II}}\,)$	$\sqrt{N_{Rk}(x_{c,\lim}^{II})\big/N_{cr,z,h\,min}}$
$\boldsymbol{\phi_{LT}}$	$0.5\times\left(1 + \varphi\times\eta\times\dfrac{\overline{\lambda}^{\,2}_{LT}(x_c^{\,I})}{\overline{\lambda}^{\,2}_z(x_{c,\lim}^{II})} + \varphi\times\overline{\lambda}^{\,2}_{LT}(x_c^{\,I})\right)$
$\boldsymbol{\chi_{LT}(x_c^{\,I})}$	$\varphi\big/\phi + \sqrt{\phi^2 - \varphi\times\overline{\lambda}^{\,2}_{LT}(x_c^{\,I})} \leq 1$
Verification	$\chi_{LT}(x_c^{\,I})\times\alpha_{ult,k}(x_c^{\,I}) \geq 1$

Table 7.4 Calculation of $x_{c,lim,M}^{II}/L$ for lateral-torsional buckling of tapered I-beams

For ψ	$\left(0.75 - 0.18\psi - 0.07\psi^2\right) + \left(0.025\psi^2 - 0.006\psi - 0.06\right)\left(\gamma_h - 1\right) \geq 0$
	If $\psi < 0$ and $\quad |\psi|\gamma_w \geq 1 + 1.214\left(\gamma_h - 1\right), \quad x_{c,\lim}^{II}/L = 0.12 - 0.03\left(\gamma_h - 1\right)$
For UDL	$0.5 + 0.0035\left(\gamma_h - 1\right)^2 - 0.03\left(\gamma_h - 1\right)^2 \leq 0.5$

Table 7.5 Calculation of φ for lateral-torsional buckling of tapered I-beams

a_γ	$-0.0005 \cdot (\gamma_w - 1)^4 + 0.009 \cdot (\gamma_w - 1)^3 - 0.077 \cdot (\gamma_w - 1)^2 + 0.78 \cdot (\gamma_w - 1)$		
ψ_{lim}	$1 + 120 \cdot a_\gamma + 600 \cdot a_\gamma^2 - 210 \cdot a_\gamma^3 \big/ 1 + 123 \cdot a_\gamma + 1140 \cdot a_\gamma^2 + 330 \cdot a_\gamma^3$		
φ_{LT}	$\psi < -\psi_{lim}$	$-\psi_{lim} \le \psi \le \psi_{lim}$	$\psi > \psi_{lim}$
A	$-0.0665 \cdot a_\gamma^6 + 0.718 \cdot a_\gamma^5 - 2.973 \cdot a_\gamma^4$ $+5.36 \cdot a_\gamma^3 - 2.9 \cdot a_\gamma^2 - 2.1 \cdot a_\gamma - 1.09$	$\dfrac{-11.37 + 12090 \cdot a_\gamma - 8050 \cdot a_\gamma^2 + 1400 \cdot a_\gamma^3}{1 - 1058 \cdot a_\gamma + 705 \cdot a_\gamma^2 - 120 \cdot a_\gamma^3} + 11.22$	$0.008 \cdot a_\gamma^2 - 0.08 \cdot a_\gamma - 0.157$
B	$-0.1244 \cdot a_\gamma^6 + 1.3185 \cdot a_\gamma^5 - 5.287 \cdot a_\gamma^4$ $+9.27 \cdot a_\gamma^3 - 5.24 \cdot a_\gamma^2 - 2.18 \cdot a_\gamma - 2$	$+0.02 \cdot a_\gamma^6 - 0.133 \cdot a_\gamma^5 + 0.425 \cdot a_\gamma^4$ $-0.932 \cdot a_\gamma^3 + 1.05 \cdot a_\gamma^2 - 0.5 \cdot a_\gamma - 0.1$	$-0.033 \cdot a_\gamma^3 + 0.04 \cdot a_\gamma^2$ $+0.48 \cdot a_\gamma + 0.37$
C	$-0.0579 \cdot a_\gamma^6 + 0.6003 \cdot a_\gamma^5 - 2.314 \cdot a_\gamma^4$ $+3.911 \cdot a_\gamma^3 - 2.355 \cdot a_\gamma^2 + 0.02 \cdot a_\gamma + 0.3$	$0.02 \cdot a_\gamma^2 - 0.14 \cdot a_\gamma + 1.25$	$0.032 \cdot a_\gamma^3 - 0.092 \cdot a_\gamma^2$ $+0.06 \cdot a_\gamma + 0.8$

7.2 Conclusions

In this thesis an overview of the stability verification rules for non-uniform members was carried out. Firstly, existing approaches throughout the literature were described and the given procedures in EC3-1-1 were then analyzed.

There are mainly three levels of member stability verification available in EC3-1-1. The interaction formula is suitable to the most simple cases of prismatic members with well-defined boundary conditions and symmetrical cross-sections. Regarding non-uniform members, the General Method of clause 6.3.4 is supposed to give answers to the stability level of such members. Alternatively, either a second order analysis of the system considering the relevant second order effects and imperfections or even a numerical analysis accounting for all the material and geometrical nonlinearities can be performed although these options add too much complexity to the problem.

In Chapter 2, these possibilities are analyzed and the General Method is explored firstly for prismatic members and secondly for tapered members. Even when dealing with prismatic members the following gaps are observed:

- When the General Method is derived for the flexural buckling of columns it does not coincide with clause 6.3.1 due to the consideration of in-plane member imperfections in

the definition of the resistance load multiplier, $\alpha_{ult,k}$. . Even when there are in-plane member second order effects present, these do not have such a weight in the final buckling resistance;

- For determination of the reduction factor, the General Method gives the possibility of considering either the minimum or an interpolated value between the reduction factors for flexural buckling and lateral-torsional buckling, determined with the generalized slenderness of the combined load case. If the minimum between the reduction factors for out-of-plane flexural bucking and lateral-torsional buckling is adopted (instead of an interpolated value), discontinuities are observed for the extremes of the interaction M-N curves. Although a interpolation of those reduction factors was derived based on the definitions of $\alpha_{ult,k}$ of clause 6.3.4, a more detailed study is needed to account for the proper behavior of the beam-column when considering a mode interpolation, as the referred derivation does not always seem to be correct for intermediate ϕ ($\approx M/N$) values;

- The account for second order local member effects and imperfections in the value of $\alpha_{ult,k}$ was discussed and seen to be inappropriate in a way that in-plane imperfections do not affect so significantly the out-of-plane capacity of the member.

Regarding non-uniform members many difficulties arise such as the choice of the cross-section class or the critical location for verification. But the main and pertinent question is the choice of one of the buckling curves according to EC3-1-1, which are organized by the ratio depth/width. In a tapered member, this ratio varies and consequently the buckling curve may vary.

On the structural level, the possibilities for the structural analysis combined with the analyzed stability member check procedures were then described and interpreted. Again, many difficulties were noticed whether second order effects are accounted for by a proper global buckling length or a modeled imperfection, instead of by commonly used stability member check procedures.

As a result, and because the latter are widely used in practical design, in this thesis member stability rules for web tapered columns and beams were developed. Proper generalized imperfections were calibrated respectively in Chapter 4 and 5 based on an Ayrton-Perry formulation, making it possible to achieve consistency with the prismatic rules for steel members. Three options are possible:

- Account for the real behavior of the column (subject to flexural buckling) or the beam (subject to lateral-torsional buckling) with varying length (or slenderness) and, as a result, account for the weight between cross-section resistance and imperfection. An additional imperfection factor β and a second order failure location x_c^{II} need to be determined for stability check;

- Separation of the first and second order effects. The factor β_{lim} and $x_{c,lim}^{II}$ are the ones calibrated for sufficient high slenderness in which instability effects are dominant. A limitative value given by the first order failure (cross-section) resistance needs to be then considered;

- Transformation of the previous into an "over-strength" factor which is an indicator of the increase of resistance relatively to the basic case of a prismatic member with a constant stress level along the member length.

For the calibration of the new parameters, the generalized imperfections for prismatic members with welded cross sections were adjusted to truthfully follow the adopted residual stress pattern widely accepted and considered for the development of stability rules in EC3.

The developed rules for tapered columns coincide with the rules for prismatic columns when $\gamma_h=1$, whereas for beams, the developed rules coincide with the mechanically consistent proposals for prismatic beams given in previous proposals from the literature (Taras, 2010).

In addition, for tapered columns, the Rayleigh-Ritz method was considered to obtain the flexural buckling critical load of web-tapered columns leading to differences lower than 8% for the relevant range of taper ratio, $\gamma_h \leq 4$.

Finally, in Chapter 6, the developed rules for flexural buckling of tapered columns and lateral-torsional buckling of beams were applied to the case of beam-columns. Two approaches are

possible, both regarding in-plane and out-of-plane buckling verification. These are either the interaction or generalized slenderness concept:

- Regarding the first, the interaction formulae were developed specifically for prismatic members such that, in order to be extended to tapered members some improvements of the interaction factors would have to be carried out – especially in order to avoid significant gaps between instability and cross section failure. Nevertheless, maximum differences of 20% on the safe side were achieved relatively to the numerical GMNIA analysis;

- Regarding the latter, some types of logical interpolation procedures were analyzed and inadequacies were seen for all the alternatives. A generalized slenderness concept was then seen not to be as straight forward as envisaged in the code, even if the minimum of the referred flexural and lateral-torsional buckling reduction factors in accordance with the analyzed non-uniform member would be used. Although it is a useful concept to account for all the possible member non-uniformities as it relativizes those in a slenderness which could be used with the defined imperfection factors for uniform members, this was seen to not be quite as simple. As a result, wider parametric studies should be carried out in order to develop adequate interpolation rules for the most commonly applied non-uniform members.

- In the end, it was seen that either adequate interpolation rules may be developed or interaction factors may be improved, respectively regarding the generalized slenderness or interaction concept.

Finally, provided that a member check is available, it is brought into the structural analysis regarding portal frames prevented from out-of-plane global displacements. In order to avoid in-plane member check, local in-plane imperfection amplitudes e_0/L would have to be calibrated based on the new imperfection factors derived in Chapter 4 for welded cross sections although, on the safe side, amplitudes for curve c could be used. Finally, it was seen that, if adequate member verification procedures are developed, the verification of plane frames with tapered members would be brought to the same level of complexity as for frames with prismatic members.

7.3 Future research

Throughout the chapters of this thesis some limitations were noted and are to be considered in a further continuation of this study:

- The consideration of local effects (due to bending and due to shear) in the tapered member verification are of major importance and as a result, an additional check shall be investigated, probably by the determination of a failure location due to local effects in which the cross section resistance shall be reduced by the effective resistance;

- The account of partial restraints must be considered in the basic cases of beams and columns as these greatly improve the out-of-plane stability resistance and are commonly provided in, for example, roof structure supports or side walls;

- Application and validation of the proposed methodologies to the case of web-tapered beam-columns, correctly taking into account the in-plane and out-of-plane buckling modes, regardless of the (interaction or generalized slenderness) approach to be considered. In addition, regarding the account for member in-plane buckling effects, these may alternatively be considered by the calibration of adequate amplitude imperfections e_0/L to be considered in the structural analysis;

- Validation of the application of the developed rules for other boundary conditions. Relevant issues are necessarily attached to this subject such as the amplitude of the imperfections to be considered for calibration of the design rule or the change of the (real) second order failure location. The analytical accuracy of such simplifications to the existing design rules should be evaluated and, if necessary, proper adaptations should be provided;

- Verification of any non-uniform member subject to any boundary conditions and loading, which can be further attained by the development of a general approach based on the distribution of the compression force in the flange (as instability is mainly due to the buckling of the flange in compression). To this distribution – which may be fairly described by the utilization of forces along the member – an adequate "over-strength" factor (or "compressed flange utilization factor") is to be associated. For this, new factors need to be calibrated for several types of common "stress utilization" functions.

The work developed in this thesis aims at contributing to many of the issues that are currently present for the stability verification of non-uniform members. Because tapered members are frequently employed in practical applications, e.g., portal frames, these were considered as the starting point of a wider study to be continued in the future.

7.4 Publications

The following publications have so far resulted from the work presented in this thesis:

a) Journals

Simões da Silva, L., Rebelo, C., Nethercot. D, Marques, L., Simões, R. and Vila Real, P., "Statistical evaluation of the lateral-torsional buckling resistance of steel I-beams - Part 2: Variability of steel properties", Journal of Constructional Steel Research, 65 (4), pp. 832-849 (2009);

Simões da Silva, L., Marques, L., and Rebelo, C., "Numerical validation of the General Method in EC3-1-1 for prismatic members", Journal of Constructional Steel Research, 66 (4), pp. 575-590 (2010).

Marques, L., Taras, A., Simões da Silva, L. Greiner, R. and Rebelo, C., "Development of a consistent design procedure for tapered columns", Journal of Constructional Steel Research, 72 (May 2012), pp. 61-74 (2012).

b) Conference Proceedings

Marques, L., Simões da Silva, L., Rebelo, C. and Simões, R., "Influência da variabilidade do aço na resistência de vigas à encurvadura lateral", in Simões da Silva, L., Caetano, E., Piloto, P. Martins, C e Abecasis, T., (eds.), Construção Metálica e Mista VI, pp. II-679-87, cmm Press, Porto (2007).

Marques, L., Simões da Silva, L. and Rebelo, C., "Numerical validation of the general method in EC3-1-1: lateral and lateral-torsional buckling of non-uniform members", in ECCS European Convention for Constructional Steelwork (eds.), Proceedings of Eurosteel 2008 – 5th European Conference on Steel and Composite Structures – Volume A, pp. 753-8, Graz, Austria (2008);

Marques, L., Simões da Silva, L. and Rebelo, C., "Numerical validation of the general method in EC3-1-1: lateral, lateral-torsional and bending and axial force interaction" , ASCCS 2009 9th International Conference on Steel Concrete Composite and Hybrid Structures, School of Civil Engineering, University of Leeds, Leeds, UK, July 8-10 (2009).

Marques, L., Simões da Silva, L., e Rebelo, C., "Métodos avançados de análise por elementos finitos para verificação da estabilidade de estruturas metálicas", VII CMM, VII Congresso em Construção Metálica e Mista, Instituto Superior Técnico, Lisboa, Portugal,19-20 November (2009).

Simões da Silva, L., Marques, L., and Rebelo, C., "Application of the general method for the evaluation of the stability resistance of non-prismatic members", ICASS'09 Sixth International Conference on Advances in Steel Structures, Department of Civil and Structural Engineering, The Hong Kong Polytechnic University, Hong Kong, China, December 16-18 (2009).

Marques, L., Taras, A., Simões da Silva, L. Greiner, R. and Rebelo, C., "Análise numérica do comportamento de colunas de secção variável". CMNE 2011, Coimbra, 14-17 June (2011).

Marques, L., Simões da Silva, L. Greiner, R. and Rebelo, C., "Flexural buckling behavior of non-uniform members". ICSAS 2011 7th International Conference on Steel & Aluminium Structures, Kuching, Sarawak, Malaysia, 13 – 15 July.

Marques, L., Taras, A., Simões da Silva, L. Greiner, R. and Rebelo, C., "Development of a consistent procedure for the stability verification of non-uniform columns". 6th European Conference on Steel and Composite Structures, Budapest, Hungary, 31 August – 2 September (2011).

Simões da Silva, L., Marques, L. and Martins, J. P., "Stability and Design of Thin-Walled Steel Shells". International Conference on Thin-Walled Structures, Timisoara, Romania, 5 – 7 September (2011).

Marques, L., Simões da Silva, L., Greiner, R., e Rebelo, C., "Verificação da encurvadura lateral de vigas de secção variável". VIII CMM, VIII Congresso em Construção Metálica e Mista, Centro Cultural Vila Flor, Guimarães, Portugal,24-25 November (2011).

Marques, L., Simões da Silva, L. and Rebelo, C., "Numerical analysis of the stability behavior of web-tapered beam-columns". 10th International Conference on Advances in Steel Concrete Composite and Hybrid Structures, Singapore, 2 – 4 July (2012).

Marques, L., Simões da Silva, L. Greiner, R. and Rebelo, C., "stability verification of web-tapered beams: development of a consistent procedure". Nordic Steel Construction Conference 2012, Oslo, Norway, 5 – 7 September (2012) (accepted for publication).

REFERENCES

Abaqus (2010). v.6.10, Dassault Systems/Simulia, Providence, RI, USA.

Andrade A., Dinis P.B., Providência P. and Camotim D. (2007b). "Vigas em I com Alma Linearmente Variável: Cálculo de Momentos Críticos Elásticos e Verificação da Segurança", Métodos Numéricos e Computacionais em Engenharia (CMNE 2007 + XXVIII CILAMCE), J.C. Sá *et al*. (Eds.), 214, Porto, June 13-15.

Andrade A., Providência P., Dinis P.B. Camotim D. (2010b) "European Provisions for the Design of Web-Tapered I-Beams - An Appraisal of the EC3 'General Method' ", Proceedings of 4th International Conference on Steel & Composite Structures (ICSCS'10), B. Uy *et al*. (Eds.), University of Western Sydney, Sydney, pp. 241-243, July 21-23.

Andrade A., Camotim D. and Dinis P.B. (2007a). "Lateral-torsional buckling of singly symmetric web-tapered thin-walled I-beams: 1D model vs. shell FEA", Computers and Structures 85(17-18) 1343-1359.

Andrade A., Dinis P.B., Providência P. and Camotim D. (2007c). "On the design of web-tapered I-section beams; Proceedings of 5th International Conference on Advances in Steel Structures (ICASS 2007), Singapore, 2007, Vol. III, 316-321.

Andrade A., Providência P. and Camotim D. (2006). "Buckling formulae for doubly symmetric web-tapered I-section cantilevers acted by a tip load", Proceedings of International Colloquium on Stability and Ductility of Steel Structures (SDSS 06 − Lisboa, 6-8/9), D. Camotim, N. Silvestre e P.B. Dinis (eds.), IST Press, 323-330 (Vol. 1), 2006.

Andrade A., Providência P. and Camotim D. (2010a). "Elastic Lateral-Torsional Buckling of Restrained Web-Tapered I-Beams", Computers & Structures, Vol. 88, nº 21-22, 1179-1196.

Andradre A., Camotim D., Providência P. (2005). "Critical moment formulae for doubly symmetric web-tapered I-section steel beams acted by end moments", Proceedings of the 4th European Conference on Steel and Composite Structures, Eurosteel 2005, pp. 1.2-135-1.2-143, Maastricht, The Netherlands.

Ayrton W.E. and Perry J. (1886). "On Struts", The Engineer, 62, pp. 464-465, 513-515.

Baptista A.M., Muzeau J.P. (1998). "Design of Tapered Compression Members According to Eurocode 3", Journal of Constructional Steel Research 46 (1-3), pp. 146-148.

Beer H. and Schulz G. (1970). "Bases théoriques des courbes européenes de flambement", Construction Métallique 3, pp. 5-12.

Beer H. and Schulz G. (1969). "Die Traglast des planmäβig mittig gedrückten Stabes mit Imperfektionen", VDI-Zeitschrift, 21, pp. 1537-1541, 1683-1687, 1767-1772.

Bleich F. (1932). Stahlhochbauten ihre theory, berechnung und bauliche gestaltung", Berlin, Verlag von Julius Springer.

Boissonnade N., Greiner R., Jaspart J. P., and Lindner J. (2006). "Rules for member stability in DIN EN 1993-1-1, Background documentation and design guidelines", ECCS (European Convention for Constructional Steelwork) / Publication no. 119, Brussels.

Boissonnade N., Jaspart J. P., Muzeau J. P., and Villette M. (2003). "New Interaction Formulae for Beam-Columns in Eurocode 3: The French- Belgian Approach", Journal of Constructional Steel Research 60 (3-5), pp. 421-431.

Boissonnade N. (2002). "Mise au point d'un élément fini de type poutre à section variable et autres applications à la construction métallique", PhD Thesis, Blaise Pascal University, Clermont-Ferrand, France.

Bradford M.A. (1988). "Stability of tapered I-beams". Journal of Constructional Steel Research, 9, pp. 195-216.

Braham M. (1997) "Elastic lateral torsional buckling of web lapered I-beams subjected to end moments". Proceedings of the Steel Structures and Bridges Conference, Brno, May.

Braham M. and Hanikenne D. (1993). "Lateral buckling of web tapered beams: An original design method confronted with a computer simulation", Journal of Constructional Steel Research, 27(1-3), 23-36.

British Standard Institution (1985). "Structural Use of Steelwork in Building. BS 5950 – Part I", London, BSI.

Butler D.J. and Anderson G.B. (1963). "The elastic buckling of tapered beam-columns" Welding Research Supplement, January 1963, pp. 29-36.

CBCA (no date). Centro Brasileiro de Construção em Aço, Revista Arquitectura & Aço #13. http://www.cbca-acobrasil.org.br, accessed June 16th, 2010.

CEN (2002). "Eurocode, EN-1990, Eurocode: Basis of Structural Design", European Committee for Standardization, Brussels, Belgium.

CEN (2005). "Eurocode 3, EN-1993-1-1:2005, Eurocode 3: Design of steel structures – Part 1-1: General Rules and Rules for Buildings", European Committee for Standardization, Brussels, Belgium.

CEN (2006). "Eurocode 3, EN-1993-1-5:2006, Eurocode 3: Plated structural elements", European Committee for Standardization, Brussels, Belgium.

CEN (2007). "Eurocode 3, EN-1993-1-6:2007, Eurocode 3: Strength and stability of shell structures", European Committee for Standardization, Brussels, Belgium.

Chen W.F. and Lui E.M. (1987). "Structural stability – Theory and implementation", Elsevier Science Publishing Co., New York.

ECCS (1978). "European Recommendations for Steel Construction", Brussels.

ECCS TC8 (2006)."Resolution of ECCS/TC8 with respect to the general method in EN 1993-1-1", Technical Committee 8 – Structural Stability.

ENV 1993-1-1:1992 (1992). "Eurocode 3: Design of steel structures - Part 1-1: General rules and rules for buildings", Brussels.

Ermopoulos J. (1997). "Equivalent buckling length of non-uniform members", Journal of Constructional Steel Research, 42 (2), pp. 141-158.

Galambos T.V. (1998) (editor). "Guide to Stability Design Criteria for Metal Structures, Fifth Edition", John Wiley & Sons Inc.

Galéa Y. (1986). "Deversement des barres à section en I bissymétriques et hauteur d´âme bilinéairement variable", Construction Métallique 23(2), pp. 50-54.

Gere J.M., Timoshenko S.P. (1991). "Mechanics of Materials", 3rd edition, Chapman & Hall.

Greiner R. (2003). "Concepts for the numerically-based buckling check of steel structures", Conference Paper, ISBN 80-01-02747-3, Prague.

Greiner R. and Lechner A. (2007). "Comparison of General Method with traditional methods – Part 2 – Example of a sway frame with the free unrestrained corners", ECCS TC8 Stability, TC8-2007-013.

Greiner R. and Lindner J. (2006). Interaction formulae for members subjected to bending and axial Compression in EUROCODE 3 – the Method 2 Approach", Journal of Constructional Steel Research 62 (8), pp. 757-770.

Greiner R. and Ofner R. (2005). "Buckling design of steel structures based on overall load cases according to Eurocode 3", Eurosteel Conference, Maastricht 2005, pp. 1.4-1 – 1.4-8.

Greiner R. and Ofner R. (2007). "Comparison of General Method with traditional methods – Example of a sway frame with lateral restraints", ECCS TC8 Stability, TC8-2007-006.

Greiner R., Kettler M., Lechner A., Jaspart J.P. Weynand K. Ziller, C. and Örder, R. (2011). "SEMI-COMP+: Valorisation Action of Plastic Member Capacity of Semi-Compact Steel Sections – a more Economic Design", RFS2-CT-2010-00023, Background Documentation, Research Programme of the Research Fund for Coal and Steel – RTD.

Greiner R., Salzgeber G. and Ofner R. (2000). "New lateral-torsional buckling curves – numerical simulations and design formulae", ECCS TC8 Stability, TC8-2000-014.

Hirt M.A. and Crisinel. M (2001). "Charpentes Métaliques – Conception et Dimensionnement des Halles et Bâtiments", Traité de Génie Civil, vol. 11, Press Polytechniques et Universitaires Romandes, Lausanne.

Horne M.R., Shakir-Khalil H. and Akhtar S. (1979). "The stability of tapered and haunched beams". Proceedings of the Institution of Civil Engineers, Vol. 67, N° 2, September 1979, pp. 677-694.

Ibañez J.R. and Serna M.A. (2010) "Equivalent moment approach for elastic lateral-torsional buckling of tapered beams", International Journal of Structural Stability and Dynamics, Vol. 10, No. 3, 387-409.

Kaehler R.C., White D.W. and Kim Y.D. (2010) "Frame Design Using Web-Tapered Members", Design Guide 25,Metal Building Manufacturers Association and AISC, Chicago, IL.

Kaim P. (2004). "Spatial buckling behavior of steel members under bending and compression", PhD Thesis, Fakultät für Bauingenieurwesen der Technischen Universität Graz, Graz, Austria.

Kim Y.D. (2010), "Behavior and Design of Metal Building Frames with General Prismatic and Web-Tapered Steel I-Section Members," PhD Thesis, School of Civil and Environmental Engineering, Georgia Institute of Technology, Atlanta, USA.

Kitipornchai S. and Trahair, N.S. (1972). "Elastic Stability of Tapered I-Beams", Journal of the Structural Division – Proceedings of the American Society of Civil Engineers ST3, pp. 713-729.

Lee G. C., Morrell M. L., and Ketter R. L. (1972). "Design of Tapered Members", Weld Res. Counc. Bull. No. 173, June, pp. 1-32.

Lindner J. (2004). "Comments on paper TC8-2004-021: Second draft of the background documentation". ECCS TC8 Stability, TC8-2004-021.

MIMOA (no date). Mi modern architecture, http://www.mimoa.eu/, accessed March 31th, 2012.

Müller C. (2003). "Zum Nachweis ebener Tragwerke aus Stahl gegen seitliches Ausweichen", PhD Thesis, RWTH Aachen, Germany.

Nahverkehrsdrehscheibe Graz-Hauptbahnhof (02-02-2012). www.nvd-graz-hbf.info/, accessed March 31st, 2012.

Naumes J. (2009). "Biegeknicken und Biegedrillknicken von Stäben und Stabsystemen auf einheitlicher Grundlage", PhD thesis, RWTH Aachen, Germany.

Ofner R. (1997). "Traglasten von Stäben aus Stahl bei Druck und Biegung", PhD thesis, Fakultät für Bauingenieurwesen der Technischen Universität Graz, Graz, Austria.

Ofner R. and Greiner R. (2005). "Buckling check of steel members based on numerical simulations of overall load cases", Eurosteel Conference, Maastricht 2005, pp. 1.4-25 – 1.4-32.

Optima Cube (no date). www.optimacube.com, accessed March 31st, 2012.

Petersen C. (1993). "Stahlbau", Vieweg Verlag, Wiesbaden.

Prawell S.P., Morell M.L. and Lee G.C. (1974). "Bending and buckling strength of tapered structural members" Welding Research Supplement, 1974, pp. 75-84.

Raftoyiannis I. and Ermopoulos J. (2005). "Stability of tapered and stepped steel columns with initial imperfections", Engineering Structures 27(2005), pp. 1248-1257.

Rebelo C., Simões da Silva L. and Simões R. (2006). "Statistical evaluation of the reliability of beam-column stability checks in EC3", Proceedings of SDSS'06, Lisboa, Portugal, 6-8 September.

Rebelo C., Lopes N., Simões da Silva L., Nethercot D. and Vila Real P. (2009). "Statistical evaluation of the lateral-torsional buckling resistance of steel I-beams - Part 1: Variability of the Eurocode 3 design model", Journal of Constructional Steel Research 65 (4), pp. 818-831.

Rondal J. and Maquoi R. (1979). "Formulation d'Ayrton-Perry pour le flambement des barres métaliques", Construction Métallique, 4, pp. 41-53, 1979.

Rotter J.M. and Schmidt, H. (2008). "Buckling of Steel Shells European Design Recommendations", 5th Edition, ECCS Press – P125, Brussels.

Salter J.B., Anderson D. and May I.M. (1980). "Tests on tapered steel columns". The Structural Engineer, Vol. 58A, N°6, June 1980, pp. 189-193.

Salzgeber G. (2000a) "Lateral Torsional Buckling of Beam-Columns under N+My+Mz - Derivation of an elastic second order solution with mode-related imperfections", March 2000 (not published).

Salzgeber G. (2000b) "LT-Buckling effect on the strong axis buckling mode", Report 2000-005 ECCS TC8.

Simões da Silva L. and Gervásio H. (2007). "Manual de Dimensionamento de Estruturas Metálicas: Métodos Avançados", cmm Press, Coimbra, Portugal.

Simões da Silva L., Gervásio H. and Simões R. (2010b). "Design of Steel Structures – , Part 1-1: General Rules and Rules for Buildings", ECCS.

Simões da Silva L., Marques L. and Rebelo C., (2010a). "Numerical validation of the General Method in EC3-1-1 for prismatic members", Journal of Constructional Steel Research 66 (4), pp. 575-590.

Simões da Silva L., Rebelo C., Nethercot D., Marques L., Simões R., and Vila Real P. (2009). "Statistical evaluation of the lateral-torsional buckling resistance of steel I-beams - Part 1: Variability of steel properties", Journal of Constructional Steel Research 65 (4), pp. 832-849.

Simões da Silva L., Marques L. and Martins, J.P., (2011). "Stability and Design of Thin-Walled Steel Shells". International Conference on Thin-Walled Structures, Timisoara, Romania, 5 – 7 September, pp. 87-98.

Snijder B., Greiner R. and Jaspart J. P. (2006). "Fields and limits of the application of the General Method", ECCS TC8 Stability, TC8-2006-015.

Standards Australia (1998) "AS4100-1998, Steel Structures", 1998.

Steel Construct (no date). www.steelconstruct.com, accessed June 16th, 2010.

Tal Projecto (no date). http://www.talprojecto.pt, accessed March 31th, 2012.

Taras A. and Greiner R. (2006). "On the variety of buckling curves", Proceedings of SDSS'06, Lisboa, Portugal, 6-8 September, pp. 1101–1108.

Taras A. (2010). "Contribution to the development of consistent stability design rules for steel members", PhD Thesis, Technical University of Graz, Graz,Austria.

Timoshenko S.P. and Gere J.M. (1961). "Theory of Elastic Stability", McGraw-Hill Book Company Inc., New York/Toronto/London.

Trahair N.S. (1993) "Flexural-Torsional Buckling of Structures", E & FN SPON, London.

Vandermeulen T. (2007). "Le déversement des poutres métalliques en I à hauteur d'âme linéairement variable sous moments d'extrémité", Diploma Work, ArGEnCo Department, University of Liège, Belgium.

Veer (no date). www.veer.com, accessed June 16th, 2010.

Ziemian R.D. (editor) (2010). "Guide to stability design criteria for metal structures – sixth edition", John Wiley & Sons Ltd.